



TECHNISCHE
UNIVERSITÄT
WIEN

DISSERTATION

Continuous and Discrete Approximations of Cross-Diffusion and Chemotaxis Systems

Ausgeführt zum Zwecke der Erlangung des akademischen Grades
eines Doktors der Naturwissenschaften unter der Leitung von

Univ.Prof. Dr. rer. nat. Ansgar Jüngel

E101 - Institut für Analysis und Scientific Computing, TU Wien

eingereicht an der Technischen Universität Wien
Fakultät für Mathematik und Geoinformation
von

Oliver Leingang, MSc

Matrikelnummer: 00705235
Wiedner Hauptstrasse 8-10, 1040 Wien

Diese Dissertation haben begutachtet:

1. **Prof. Dr. Josipa Pina Milišić**
FER (Faculty of Electrical Engineering and Computing), University of Zagreb,
Kroatien
2. **Prof. Dr. Michael Winkler**
Institut für Mathematik, Universität Paderborn, Deutschland

Wien, am 30. Juli 2019



Die approbierte gedruckte Originalversion dieser Dissertation ist an der TU Wien Bibliothek verfügbar.
The approved original version of this doctoral thesis is available in print at TU Wien Bibliothek.

Kurzfassung

Die kontinuierliche und diskrete strukturerhaltende Approximation von Chemotaxis- und Kreuzdiffusionssystemen wird für zwei verschiedene Modelle diskutiert: für das Keller–Segel-System und das Poisson–Maxwell–Stefan-System. Beide makroskopischen Systeme verfügen über reichhaltige mathematische Strukturen, z.B. freie Energie- und Entropiefunktionale. Eine numerische Approximation sollte diese Eigenschaften nützen und widerspiegeln. Ein Teilaspekt dieser Arbeit ist daher, durch die Übersetzung kontinuierlicher Techniken ins Diskrete, strukturerhaltende Schemata zu entwickeln. Weiters werden neue analytische und numerische Ergebnisse für die beiden Kreuzdiffusionssysteme bewiesen bzw. illustriert. Insbesondere werden drei Resultate präsentiert: Es wird ein viriales Argument für das Keller–Segel-System im semidiskreten Fall bewiesen, die Konvergenz eines regularisierten Keller–Segel-Systems zum ursprünglichen System gezeigt und ein strukturerhaltendes Galerkin-Schema entwickelt sowie die Konvergenz dessen zur kontinuierlichen Lösung eines Poisson–Maxwell–Stefan-Systems bewiesen. Die Arbeit und die Ergebnisse können wie folgt zusammengefasst werden:

Die Existenz von schwachen Lösungen und oberen Schranken für den Blow-up-Zeitpunkt von zeitdiskreten parabolisch-elliptischen Keller–Segel-Systemen am zweidimensionalen Euklidischen Raum wird bewiesen. Durch die Verwendung einer diskreten Version des klassischen virialen Arguments erhalten wir die gleichen Grenzen für den Blow-up Zeitpunkt wie im bekannten kontinuierlichen Fall. Insbesondere können wir dies für die wichtigsten impliziten Zeitdiskretisierungen zeigen, d.h. die impliziten Euler-, BDF- und Runge-Kutta-Methoden. Diese theoretischen Ergebnisse werden durch numerische Simulationen mithilfe einer Upwind-Finite-Elemente-Methode in Kombination mit einer Zeitdiskretisierung zweiter Ordnung veranschaulicht.

Darüber hinaus untersuchen wir den Limes eines Keller–Segel-Systems mit regularisierender Kreuzdiffusion zum ursprünglichen System. Insbesondere ist der zusätzliche Kreuzdiffusionsterm bekannt dafür, den Blow-up des ursprünglichen Systems zu verhindern. Der Limes des verschwindenden Kreuzdiffusionsparameters wird dabei im parabolisch-elliptischen und parabolisch-parabolischen Fall rigoros bewiesen. Für unterschiedliche Parameter werden dabei zwei verschiedene Techniken eingesetzt, um den Limes zu bilden. Im Fall von sublinearer Signalproduktion wird die Existenz von globalen schwachen Lösungen in der Zeit sowie die Konvergenz der Lösungen zu denen des klassischen parabolisch-elliptischen Keller–Segel-Systems bewiesen. Für den Fall einer superlinearen Signalproduktion bestimmen wir Konvergenzraten für glatte

Lösungen, die lokal in der Zeit sind (da hier ein Blow-up nicht ausgeschlossen ist). Der Beweis basiert auf sorgfältigen Abschätzungen in Sobolev-Räumen und einer Variante des Gronwall-Lemmas. Numerische Simulationen in zwei Raumdimensionen veranschaulichen die theoretischen Ergebnisse und quantifizieren die Form der Zellaggregation in Abhängigkeit des Kreuzdiffusionsparameters.

Abschließend wird eine volldiskrete Galerkin-Methode eines thermodynamisch konsistenten, transienten Maxwell–Stefan-Systems für die Teilchendichten, gekoppelt mit der Poisson-Gleichung für ein elektrisches Potential, untersucht. Das System modelliert die Diffusionsdynamik eines isothermen und ionisierten Flüssigkeitsgemisches mit verschwindender baryzentrischer Geschwindigkeit. Die Gleichungen werden auf einer beschränkten Umgebung untersucht, wobei die Analyse verschiedene molare Massen berücksichtigt. Die Galerkin-Methode bewahrt die Gesamtmasse, die Nichtnegativität der Teilchendichten, ihre Schranken, und sie erfüllt das zweite Gesetz der Thermodynamik in dem Sinne, dass die diskrete Entropieproduktion nicht negativ ist. Weiters wird die Existenz von Lösungen für das Galerkin-System und die Konvergenz einer Teilfolge zu einer Lösung des kontinuierlichen Systems bewiesen. Numerische Simulationen zeigen die empfindliche Abhängigkeit der Teilchendichten und der Konvergenzrate zum Gleichgewicht von den molaren Massen.

Abstract

The continuous and discrete structure-preserving approximation of chemotaxis and cross-diffusion systems is discussed for two different models: the Keller–Segel system and the Poisson–Maxwell–Stefan system. Both models feature rich mathematical structures, e.g. free energy and entropy functionals, and a numerical approximation should reflect and use these properties. Hence, one aspect of this thesis is to follow the approach to design structure-preserving schemes by translating continuous arguments to the discrete realm. In particular, three results are shown: A virial argument for the Keller–Segel system in the semi-discrete case is proved, a regularized Keller–Segel system is shown to converge to the original system, and a fully discrete structure-preserving Galerkin scheme is developed and the convergence to the continuous solution of a Poisson–Maxwell–Stefan system is proved. The thesis and results can be subsumed as follows:

The existence of weak solutions and upper bounds for the blow-up time to time-discrete parabolic-elliptic Keller–Segel systems on the two-dimensional whole Euclidean space are proved. For various time discretizations, including the implicit Euler-, BDF-, and Runge-Kutta methods, the same bounds for the blow-up time as in the well-known continuous case are derived by discrete versions of the virial argument. The theoretical results are illustrated by numerical simulations using an upwind finite-element method combined with second-order time discretizations.

In addition, we investigate the limit of a cross-diffusion regularization of the Keller–Segel system. The additional cross-diffusion term is known to prevent the usual blow-up behavior of this system. The limit of the vanishing cross-diffusion parameter is proved rigorously in the parabolic-elliptic and parabolic-parabolic cases. Two different techniques are used to pass to the limit, depending on the parameter setting in question. When the signal production is sublinear, the existence of global-in-time weak solutions as well as the convergence of the solutions to those of the classical parabolic-elliptic Keller–Segel equations are proved. For superlinear signal production terms, convergence rates in the cross-diffusion parameter are proved for local-in-time smooth solutions (since finite-time blow up is possible). The proof is based on careful estimates in Sobolev spaces and a variant of the Gronwall lemma. Numerical simulations in two space dimensions illustrate the theoretical results and quantify the shape of the cell aggregation bumps as a function of the cross-diffusion parameter.

Finally, a fully discrete Galerkin scheme for a thermodynamically consistent transient Maxwell–Stefan system for the mass particle densities, coupled to the Poisson

equation for the electric potential, is investigated. The system models the diffusive dynamics of an isothermal ionized fluid mixture with vanishing barycentric velocity. The equations are studied in a bounded domain, while different molar masses are allowed. The Galerkin scheme preserves the total mass, the nonnegativity of the particle densities, their boundedness, and it satisfies the second law of thermodynamics in the sense that the discrete entropy production is nonnegative. The existence of solutions to the Galerkin scheme and the convergence of a subsequence to a solution to the continuous system is proved. Numerical simulations show the sensitive dependence of particle densities and equilibration rate on the molar masses.

Acknowledgements

As there is nothing more exciting in life than a room (or a page) full of people, I would like to thank everyone who made this thesis possible for various reasons.

First of all, I would like to thank my supervisor Prof. Ansgar Jüngel for the opportunity to work with him and his research group. His guidance, patience, and inspiring discussions about our scientific topics and life in general were extremely valuable to me. As a true mentor, he created a welcoming, interesting and supportive work environment that allowed me to learn and thrive.

Out of the members of this environment, I am grateful to Anita Gerstenmayer, Marcel Braukhoff and Gaurav Dhariwal for mathematically proofreading parts of this manuscript. In addition, I want to thank Anna Lena Bankel for linguistically proofreading parts of the thesis and using endurance against stubbornness. I also would like to express my gratitude for the fruitful research collaboration with Prof. Shu Wang of the Beijing University of Technology.

Special thanks go to my colleagues Anita, Esther, Gaurav, Gerhard, Marcel, Philipp and Tobias for scientific discussions and their support. Furthermore, I want to thank Frau Khaladj for handling any administrative task fast and reliably during my time at the TU Wien.

In addition, I would like to address Annalisa, Bea, Carina, Flo Katha, Kirian, Mani, Michi and Stefan who have brightened up my day at our lunch and coffee breaks or elsewhere, even when the estimates did not.

I also wish to thank Lena for our ruthless, inciting and inspiring discussions where no shades remain untouched and no regrets are ever felt.

Last but not least, I am grateful for the support of my parents Heidemarie and Franz; their different natures allowed me to reach and enjoy my goals in life.



Die approbierte gedruckte Originalversion dieser Dissertation ist an der TU Wien Bibliothek verfügbar.
The approved original version of this doctoral thesis is available in print at TU Wien Bibliothek.

Eidesstattliche Erklärung

Ich, Oliver Leingang, erkläre an Eides statt, dass ich die vorliegende Dissertation selbstständig und ohne fremde Hilfe verfasst, andere als die angegebenen Quellen und Hilfsmittel nicht benutzt bzw. die wörtlich oder sinngemäß entnommenen Stellen als solche kenntlich gemacht habe.

Wien, am 30. Juli 2019



Die approbierte gedruckte Originalversion dieser Dissertation ist an der TU Wien Bibliothek verfügbar.
The approved original version of this doctoral thesis is available in print at TU Wien Bibliothek.

Contents

1	Introduction	1
1.1	Cross-Diffusion and Chemotaxis	2
1.2	Structure Preserving Schemes	3
1.3	The Keller–Segel System	4
1.3.1	The Model Equations	5
1.3.2	Structures and Qualitative Properties	6
1.3.3	Mathematical Challenges and State of the Art	8
1.4	A Poisson–Maxwell–Stefan System	12
1.4.1	The Model Equations	12
1.4.2	Structures and Qualitative Properties	14
1.4.3	Mathematical Challenges and State of the Art	15
1.5	Main Results and Outline	17
1.6	Notation	19
2	The Semi-Discrete Virial Argument for the Keller–Segel System	21
2.1	Key Idea: The Virial Identity	21
2.2	Implicit Euler Scheme	23
2.3	Higher-Order Schemes	31
2.3.1	BDF-2 Scheme	32
2.3.2	BDF-3 Scheme	34
2.3.3	Runge-Kutta Schemes	36
2.4	Numerical Examples	42
2.4.1	Numerical Scheme	42
2.4.2	Numerical Results	44
2.4.3	Convergence Rate	45
2.4.4	Numerical Blow-up	46
2.5	Discussion and Outlook	49
3	Vanishing Cross-Diffusion Regularization in a Keller–Segel System	53
3.1	Key Idea: Entropy and Gronwall Inequalities	54
3.2	The Parabolic-Elliptic Case	56
3.3	The Parabolic-Parabolic Case	63
3.4	Numerical Simulations	70
3.5	Discussion and Outlook	75

4	A Structure Preserving Scheme for a Poisson–Maxwell–Stefan System	83
4.1	Key Idea: A Discrete Boundedness-by-Entropy Method	84
4.2	Main Results	86
4.3	Modeling	89
4.4	Auxiliary Results	91
4.4.1	Expressions for the Diffusion Fluxes	91
4.4.2	Inversion of $\rho \mapsto w$	93
4.5	Existence of a Discrete Solution	95
4.6	Convergence of the Scheme	98
4.7	Numerical Simulations	104
4.7.1	Discretization and Iteration Procedure	104
4.7.2	Numerical Examples	106
4.8	Discussion and Outlook	110
A	Appendix: Some Auxiliary Results	115
B	Appendix: A Nonlinear Gronwall Inequality	119
	Bibliography	121
	Curriculum Vitae	133

1 Introduction

The aim of this thesis is to establish and discuss new results concerning the broad topic of cross-diffusion and chemotaxis models, regarding structure preserving numerical and continuous approximations for cross-diffusion and chemotaxis models. In particular, I will present a semi-discrete version of a virial argument and the convergence of a cross-diffusion regularization for the Keller–Segel (KS) system. Furthermore, a fully-discrete scheme in entropy variables for a Poisson–Maxwell–Stefan (PMS) system is introduced and the convergence of this scheme is proven. The results are mainly based on the publications [86, 87] (A. Jüngel, O. Leingang) and the submitted work of [88] (A. Jüngel, O. Leingang, S. Wang). In addition, some supplemental remarks and numerical simulations to further illustrate the topic at hand and set the findings in context are included. In short, we will analyze the following two models:

The Keller–Segel System

The (Patlak)–Keller–Segel model describes the evolution of agents, mostly cells, that produce an (chemo)attracting substance and release it into the environment to attract other agents [95, 115]. This can lead to self-organization of the agents, and various modifications of this model are used to describe physical and biological aggregation processes. The formation of a multicellular organism in the life cycle of the slime mold amoebae *Dictyostelium discoideum* is an important example showcasing such a phenomenon in nature.

The Poisson–Maxwell–Stefan System

The second model, the Poisson–Maxwell–Stefan system, describes the dynamics of a charged fluid mixture in the diffusive regime [108, 134]. The fluid mixture can consist of various subcomponents with different qualitative physical properties. The interplay between the properties of the components leads to interesting and significant effects like up-hill diffusion. In addition, the repulsive or attracting force of an electric field acting on the charged components is important in various applications, for instance in sedimentation, dialysis, electrolysis and ion exchange.

I will now continue with a brief introduction to cross-diffusion and chemotaxis systems, followed by some remarks on structure preserving schemes. The remainder

of this chapter is dedicated to the background, the state of the art of the specific equations in question, and an overview of main results presented in this thesis.

1.1 Cross-Diffusion and Chemotaxis

Two important concepts in physics in order to describe the movement of fluids are the notion of bulk flow and diffusion flow. The first one describes the movement of the entire body of a substance according to a pressure gradient. Diffusion on the other hand, is the movement within the body, without net movement of the substance, due to the gradient in the concentration of the substance. Hence, the gradient of the substance induces a flux inside the substance. In particular, the substance moves/diffuses from an area of high concentration to an area of low concentration. If more than one substance is present, say A and B, also the gradient of substance A can induce a flux in substance B. This phenomena is called cross-diffusion. The Keller–Segel and the Poisson–Maxwell–Stefan system are both examples of quasilinear partial differential systems, or more specific, cross-diffusion equations. We remark here that, although chemotaxis is technically not emerging from a diffusion process, we still subsume it, in view of a mathematical framework, as cross-diffusion; see [142] for a general discussion of cross-diffusion and its effects. Both models act on the macroscopic level, i.e. analyse the substance as a continuum instead of individual particles, and can describe rich dynamics in physics, chemistry and biology. In particular, the macroscopic scale allows us to study complex phenomena in a qualitative manner, using the rich toolbox of modern mathematics. Hence, the field has seen an remarkable development with respect to mathematical results in recent years, e.g. in population dynamics, ion transport, tumor-growth, or multi-component models; see [84] for a parade of examples and results. Cross-diffusion systems have been shown to describe a series of effects which are missing in simple diffusion systems. One of these effects is up-hill diffusion, where, in contrast to the usual diffusion dynamics, the quantity in question can flow from a region of lower concentration to a region of higher concentration [17, 47, 99]. Another important phenomenon is chemotaxis, a fundamental guidance mechanism for cells and other organisms. In short, the flux of a species depends on the gradient of a chemical substance, the chemoattractant. This can lead to the self-organization of rather simple agents to form a more complex organism. Although originally used to describe the aggregation of bacteria and other singular cells [49, 119], a generalized concept of chemotaxis has already spread to other areas in science and is applied to models that explore the evolution of cancer, ecology or crime [114]. Of course, the rather simple systems also have limitations for certain modeling domains [149]. As we will discuss later in more detail, the elegant description of chemotaxis on the macroscopic level has led to an enormous amount of research in mathematics and is continuing to do so, also embedded and coupled to other systems, like the Navier–Stokes equations [147]. In many cases, the math-

ematical treatment can guarantee the existence of solutions and characterize their longtime behavior.

Remark 1.1. *Curiously enough, there also is a chemotaxis model, that attempts to investigate the reason for the vast amount of chemotaxis models [114, p.12].*

The payoff for such diverse dynamics are mathematical difficulties in the analysis, such as the lack of a maximum or comparison principle. Nevertheless, the rather recent development of specialized techniques for these systems has paved the way for the analysis of cross-diffusion systems. One example for such a technique is the boundedness-by-entropy method [83]. In particular, the approach allows in many cases to prove the existence of solutions and a L^∞ bound for solutions. This is done using a semi-discrete approximation procedure; we will discuss a fully discrete argument for the Poisson–Maxwell–Stefan system in Chapter 4.

1.2 Structure Preserving Schemes

Like most physical models, both the Keller–Segel as well as the Poisson–Maxwell–Stefan system come with innate properties of the quantities involved. For example, if the solution corresponds to the density of a physical quantity, we expect that the solution is nonnegative. The model could also specify an upper bound for the density in the case of a population cap or other properties, such as the conservation of mass. We also find that models inhere an additional structure specific to them, e.g. solutions stay constant or decay along an energy or entropy functional. In essence, rather than trying to fulfill these desired properties or constraints via a very fine grid or shorter time steps, a structure-preserving scheme is designed to capture the assumptions of the model in a more tailored and efficient way. I will now give a quick introduction and argument for structure preserving schemes in general.

Preserving Modeling Assumptions

The above mentioned structures and constraints are often built into the model via physical assumptions and are reflected in the corresponding continuous mathematical formulation. In particular, the roles of conservation laws and thermodynamical entropies in modern modeling already encode functional inequalities into the model. A violation of these properties and structures renders the outcome of a model unphysical and often useless, since the assumptions play a vital role in the modeling of the system. In conclusion, a physical approximation via numerical or continuous schemes should obey these constraints. But even the discretization of a simple ODE system can lure solutions into a qualitative behavior that may look convincing on screen but is simply not true. An example for the Lotka–Volterra model can be found in [69, Chapter I], where the numerical approximation fails to capture the well-known closed orbits of this model.

Using All the Information: Analysis goes Numerics

In several cases, the mathematical analysis of a system already reveals structures and therefore sheds light on the behavior of the solution. This additional knowledge is unused in the numerics if it is not built into the scheme. One strategy to derive structure preserving schemes is to mimic or translate the continuous arguments already used to prove the behavior in the continuous case to the discrete case. Parts of this thesis are therefore *continuing the program to “translate” mathematical techniques from continuous to discrete situations* [89, 90, 91]. See also [48] for a first step towards a general framework for entropy-structure-preserving methods and [55] for another approach via discretizing the entropy/energy functional. The hope is that such an approach leads to a more efficient and more stable numerical scheme. Of course, the idea of structure preserving schemes is not new and found already numerous applications, see [35, 55]. In particular, structure preserving schemes for ODEs are already established as one of the go-to-techniques to make simulations more stable or to retain a known qualitative behavior of solutions.

1.3 The Keller–Segel System

The (Patlak)–Keller–Segel system [95, 115] describes the collective behavior of bacteria or amoebae that are attracted by a chemical substance they produce themselves. In a simplified situation, this behavior can be described by the evolution of the cell density $\rho(x, t)$ and the density of the chemoattractant $c(x, t)$ in the form of the system (1.1) below. In particular, the solution of the Keller–Segel system shows a distinct qualitative behavior depending on the initial mass of the cells, i.e. the L^1 norm of ρ_0 . If certain conditions, depending on the domain and the initial conditions, are fulfilled, the cell density ρ will start to aggregate over time and eventually a blow-up of the density function will manifest itself. At least in the radial symmetric case, blow-up profiles can be described with a delta distribution [72, 143]. If the initial mass of ρ is not big enough, no aggregation takes place; the cells simply diffuse. This dichotomy can model an important part in the life cycle of the slime mold amoebae *Dictyostelium discoideum*. When singular cells of the slime mold are starving, they produce a chemoattractant that signals other cells that they should aggregate and start the next step in their life cycle: the formation of a multicellular organism. Similar to the possible blow-up in the model, such an evolution is only possible if enough cells are present [59]. This effect, and related asymptotic behavior such as stationary states, has led to an enormous amount of research and inspired new models in other areas of applications. See [4, 73, 76] for a survey from a mathematical point of view. Our approach for this system can be stated as follows: first, we want to translate a specific blow-up argument in the parabolic-elliptic case, called the virial argument, to the discrete case. The hope is that such a scheme can be used to numerically

resolve the blow-up in a computationally cheaper way and in turn allows us to compute a more accurate estimate for the blow-up/aggregation time. We are setting the first step in this direction and will discuss the existence of solutions and the preservation of the virial argument in the semi-discrete case for various discretizations in time. In addition, we want to prove the convergence of a regularized system to the original Keller–Segel system. This regularized system shows interesting properties: the additional cross-diffusion prevents the blow-up of the cell density, but not the aggregation.

1.3.1 The Model Equations

While there are many versions of the Keller–Segel model, in this thesis we will use the following:

$$\begin{aligned}\partial_t \rho &= \operatorname{div}(\nabla \rho - \rho \nabla c), \\ \varepsilon \partial_t c &= \Delta c - \beta c + \rho^\alpha, \quad x \in \Omega, \quad t > 0,\end{aligned}\tag{1.1}$$

where $\Omega \subseteq \mathbb{R}^d$ is an open domain and $\alpha > 0$, $\varepsilon, \beta \geq 0$. In addition, we assume nonnegative initial conditions $\rho(x, 0) = \rho_0(x)$, and if $\varepsilon > 0$, $c(x, 0) = c_0(x)$, with $x \in \Omega$. If $\Omega \subset \mathbb{R}^d$ is bounded, we also imply no-flux boundary conditions

$$\nabla \rho \cdot \nu = \nabla c \cdot \nu = 0 \quad \text{on } \partial\Omega, \quad t > 0,$$

where ν denotes the exterior unit normal vector on $\partial\Omega$. Depending on the parameter ε , this system is also called parabolic-parabolic KS (Keller–Segel model), for $\varepsilon > 0$, or parabolic-elliptic KS, for $\varepsilon = 0$. For $\alpha = 1$, we will call this model the classical Keller–Segel system. One can view the parabolic-elliptic KS as the limit of a rescaled version of the parabolic-parabolic case, where it is assumed that the diffusion of the chemoattractant c is much faster than the movement of the cells. Various derivations of the model can be found in a range of works: a slightly informal, but informative continuum mechanic point of view can be found in [110], a diffusive limit of a kinetic system is described in [4] and a derivation from an interacting stochastic many-particle system is presented in [135]. We will cite literature concerning this system in the following subsection tailored to our results. For the moment, we mention here that for the classical Keller–Segel system (1.1), i.e. $\alpha = 1$, local-in-time smooth solutions exist [4, 111, 138] and can experience blow up of the L^∞ norm, depending on the initial datum and the domain in question [9, 10, 22, 38, 82, 111, 138, 146].

In addition, we will investigate a Keller–Segel system with a cross-diffusion regularization proposed in [75],

$$\begin{aligned}\partial_t \rho_\delta &= \operatorname{div}(\nabla \rho_\delta - \rho_\delta \nabla c_\delta), \\ \varepsilon \partial_t c_\delta &= \Delta c_\delta - \beta c_\delta + \delta \Delta \rho_\delta + (\rho_\delta)^\alpha, \quad x \in \Omega, \quad t > 0,\end{aligned}\tag{1.2}$$

where $\delta, \alpha, \beta > 0$, $\varepsilon \geq 0$, together with initial conditions $\rho_\delta(x, 0) = \rho_0(x)$, and if $\varepsilon > 0$, $c_\delta(x, 0) = c_0(x)$, with $x \in \Omega$. In the bounded case, we prescribe homogeneous Neumann boundary conditions, i.e.

$$\nabla \rho_\delta \cdot \nu = \nabla c_\delta \cdot \nu = 0 \quad \text{on } \partial\Omega, \quad t > 0.$$

In contrast to the Keller–Segel system (1.1), under reasonable assumptions on α and the domain, global-in-time solutions for the system with additional cross-diffusion (1.2) exist; see [75]. This is just one example of a variety of modifications for the classical Keller–Segel system that can prevent the blow-up in the classical KS system, as we will see in Subsection 1.3.3.

Remark 1.2. *Informal discussion: The system (1.1) consists of a conservation of mass equation for ρ and a diffusion equation for c . Heuristically, we see a competition between the diffusive term $\operatorname{div}(\nabla \rho)$ and a cross-diffusion term with opposite sign proportional to the gradient of the chemoattractant, i.e. $-\operatorname{div}(\rho \nabla c)$, in the first equation. The second equation is a simple diffusion equation for c but with a source term depending on ρ . In short, cells move towards a higher concentration of c , but also spread out in a random-like fashion. At the same time, the production of c is higher where the cell density ρ is higher. This feedback can lead to an aggregation behavior, followed by a blow-up of the solutions as mentioned above. The parameter β measures the signal degradation rate and α the (cell-dependent) production rate of the chemoattractant c .*

1.3.2 Structures and Qualitative Properties

Since we are interested in preserving structures and the qualitative behavior of solutions, let us go through some specific features of the KS (1.1) and the regularized system (1.2). In order to illustrate the main points, we assume the existence of smooth solutions on an open domain $\Omega \subset \mathbb{R}^d$. In the case that $\Omega = \mathbb{R}^d$, we assume in addition that the solutions decay fast enough at infinity. We will detail the assumptions in the specific chapters 2 and 3, tailored to our arguments. First of all, in harmony with the nature of our equation, we have that a solution (ρ, c) of (1.1) and ρ_δ of (1.2) is nonnegative if (ρ_0, c_0) is nonnegative. In addition, the total mass of the

cells is not changing over time, i.e.

$$M := \|\rho_0\|_{L^1(\Omega)} = \|\rho(t)\|_{L^1(\Omega)} = \|\rho_\delta(t)\|_{L^1(\Omega)} \quad \text{for all } t > 0.$$

Remark 1.3. *The nonnegativity for c_δ in the parabolic-parabolic case holds at least locally in time. However, the situation in the parabolic-elliptic case is unclear.*

The Virial Inequality and Blow-up

Next, we restrict ourselves to the classical parabolic-elliptic KS on the whole plane, i.e. $\Omega = \mathbb{R}^2$, $\varepsilon = 0$, $\alpha = 1$ and $\beta \geq 0$ and define the second moment of ρ by $I(t) := \int_{\Omega} |x|^2 \rho(x, t) dx$. One can use the system (1.1) and the Poisson equation structure of the second equation, to derive the following inequality

$$\frac{dI(t)}{dt} \leq -\frac{M}{2\pi}(M - 8\pi) + \frac{\sqrt{\beta}}{\pi} M^{3/2} \sqrt{I(0)}, \quad (1.3)$$

along solutions (ρ, c) of the system (1.1). See [22] for the derivation of this estimate. This approach via the second moment is called virial method or virial argument and is usually used in dispersive equations like the nonlinear Schrödinger equation; see [139]. In the case $\beta = 0$, this expression becomes an identity. Now, if $t > T^*$,

$$T^* := \frac{2\pi I(0)}{M(M - 8\pi - 2\sqrt{\beta}MI(0))}, \quad (1.4)$$

$M > 8\pi$ and $I(0)$ small is enough, we infer that $I(t) < 0$, contradicting $\rho(\cdot, t) \geq 0$. Hence, this inequality allows us to identify an upper bound for the maximal lifespan of a solution and whether a (weak) solution (ρ, c) can exist for all $t > 0$ or not.

In order to get a better understanding of the mathematical structure, we can rewrite the system (1.1) into one single equation:

$$\partial_t \rho = \operatorname{div}(\nabla \rho - \rho(\nabla B_\beta * \rho)), \quad \rho(\cdot, 0) = \rho_0 \quad \text{in } \mathbb{R}^2. \quad (1.5)$$

Here B_β denotes the Bessel potential if $\beta > 0$, and the Newton potential if $\beta = 0$ (see Appendix A for the definitions). This nonlocal or long-range interaction leads to the well-known blow-up dichotomy in the parabolic-elliptic case of (1.1). First, let us consider the case without degradation: $\beta = 0$. If the initial mass satisfies $M < 8\pi$, no aggregation takes place and the solutions exist for all time. On the other hand, if the mass is supercritical, $M > 8\pi$, and the second moment $I_0 := \int_{\mathbb{R}^2} |x|^2 \rho_0 dx$ is finite, the solutions will blow up in finite time [10]. In the limit case $M = 8\pi$, a blow-up takes place in infinite time with constant second moment [9]. We remark that the critical space is $L^{d/2}(\mathbb{R}^d)$ in space dimensions $d \geq 3$; see [38]. When the signal degrades, $\beta > 0$, a similar criteria holds: the solutions exist for all time for

subcritical initial masses $M < 8\pi/\beta$, and they blow up in finite time for supercritical masses $M > 8\pi/\beta$ and sufficiently small second moment I_0 [22]. The blow-up time T_{\max} can be estimated from above by T^* defined in (1.4).

Free Energy Functionals

In the case $\alpha = 1$, we can define the free energy functional

$$\mathcal{F}[\rho] := \int_{\Omega} \rho(\log \rho - 1) - \rho c + \frac{1}{2} |\nabla c|^2 + \frac{\beta}{2} c^2 dx$$

which is nonincreasing along solutions (ρ, c) of the system (1.1). To be more precise, the system and integration by parts lead to the following identity

$$\frac{d}{dt} \mathcal{F}[\rho] = -\varepsilon \|c_t\|_{L^2(\Omega)}^2 - \int_{\Omega} \rho |\nabla(\log \rho - c)|^2 dx,$$

see [138] for the corresponding calculations. This identity also hints that the system (1.1) can be seen as the gradient flow of the free energy functional [7]. From an analysis point of view, the energy is a Lyapunov functional. In particular, it provides us with a priori estimates and is used to show global-in-time existence in certain situations.

For the regularized version, (1.2), we have a similar structure at hand:

$$\mathcal{F}^{\delta}[\rho_{\delta}] := \int_{\Omega} \rho_{\delta}(\log \rho_{\delta} - 1) + \frac{\varepsilon}{2\delta} (c_{\delta})^2 dx,$$

this time depending on δ . Now, at least formally for smooth solutions $(\rho^{\delta}, c^{\delta})$ of the corresponding system (1.2), we have

$$\frac{d}{dt} \mathcal{F}_{\delta}[\rho_{\delta}] = - \int_{\Omega} \left(4|\nabla \sqrt{\rho_{\delta}}|^2 + \frac{1}{\delta} (|\nabla c_{\delta}|^2 + (c_{\delta})^2) \right) dx + \frac{\beta}{\delta} \int_{\Omega} \rho_{\delta} c_{\delta} dx. \quad (1.6)$$

If β is equal to zero, we have again a Lyapunov functional, and hence the functional is nonincreasing along solutions. In the case $\beta > 0$, we can still absorb the right hand side and derive a priori estimates. This is the main ingredient for the global-in-time existence shown in [75].

1.3.3 Mathematical Challenges and State of the Art

Although the Keller–Segel system is rather simple, the solution can show complex (long time) behavior and the analysis is challenging, because we are dealing with a quasilinear cross-diffusion system. In general, classical approaches out of the parabolic toolbox, like maximum principle, are not available for this class of sys-

tems. The reformulated problem (1.5) reveals the prototypical nonlocal nature of the system, which is a challenging topic from an analytic and numerical point of view; see [94] for an overview of applications. Since the difficulties and approaches to this problem depend strongly on the setting, we will restrict our literature survey and the corresponding remarks to the two cases treated in Chapter 2 and Chapter 3.

The Parabolic-Elliptic Case on the Plane:

In this case, we deal with the system (1.1) and assume $\alpha = 1$, $\beta \geq 0$ and $\varepsilon = 0$ for $\Omega = \mathbb{R}^2$. As already mentioned above, there are clean and simple blow-up criteria via the virial inequality (1.3) and the existence of weak solutions for all time in the case $M < 8\pi$ [10]. In particular, the virial argument builds on a symmetry in the cross-diffusion term of (1.5), the conservation of mass and the nonnegativity of the solution. The preservation of these three properties in a discrete setting at once is quite challenging. Most of the numerical approximations use additional tools to stabilize the scheme, which in turn destroys one of the three properties mentioned above. We start with some general numerical results concerning this system. A detailed numerical study of the collapse phenomenon for the parabolic-parabolic case has been performed in [19]. The asymptotic profile of blow-up solutions in the parabolic-elliptic model was studied in [40]. Numerical blow-up times were computed, for instance, in [52] using a kind of H^2 norm indicator; in [19] using the moving-mesh method; and in [50] using discontinuous Galerkin approximations.

Since the literature on the analysis and numerical approximation of Keller–Segel models is enormous, we will only review in the following the papers concerned with the analysis of numerical schemes and the blow-up behavior of the discrete solutions, in particular those possessing structure-preserving features. We do not claim completeness and refer to the introduction of [1] for more references. Most of the numerical schemes for the Keller–Segel model utilize the implicit Euler method for the time discretization and aim to preserve some properties of the continuous equations, like (local) mass conservation, positivity (nonnegativity, to be precise) preservation, or energy dissipation. These schemes use (semi-implicit) finite-difference methods [29, 125]; an upwind finite-element discretization [122]; an Eulerian-Lagrangian scheme based on the characteristics method [131]; a Galerkin method with a diminishing flux limiter [137]; an implicit-explicit moving mesh method [133]; and finite-volume methods [53, 152]. A finite-volume scheme was also studied in [1], but with a first-order semi-exponentially fitted time discretization. Finally, a mass-transport steepest descent scheme was analyzed in [8]. All these schemes are based on first-order discretizations.

Only few results are concerned with higher-order time integrators. In [104], a semi-implicit finite-difference scheme with BDF2 time discretization is analyzed. Strongly $A(\theta)$ -stable Runge-Kutta finite-element discretizations were analyzed in [112], and the convergence of the discrete solution was shown. However, mass conservation or

positivity preservation was not verified. As A -stable time integrators are computationally very costly, often splitting methods are used. A third-order strong stability preserving (SSP) Runge-Kutta time discretization for the advection term and the second-order Krylov IIF (implicit integration factor) method for the reaction-diffusion term, together with a positivity-preserving discontinuous Galerkin approximation in space, was suggested in [150], but without any analysis.

A number of papers are concerned with the preservation of the nonnegativity of the cell density. An example is [32], where a semi-discrete central-upwind scheme was proposed. Moreover, in [33], a hybrid finite-volume finite-difference method was combined with SSP explicit Runge-Kutta schemes (for the parabolic-parabolic case) or the explicit Euler scheme (for the parabolic-elliptic case). Clearly, a CFL condition is needed to ensure the stability of the explicit schemes. Another approach was used in [141] for a related tumor-angiogenesis model, where a Taylor series method in time allows for higher-order but still explicit schemes. Furthermore, the authors of [67] propose an energy dissipating and positivity preserving discontinuous Galerkin scheme. The semi-implicit finite difference scheme of [104], with first order in time discretization, preserves the mass and the positivity.

We remark that there do not exist SSP implicit Runge-Kutta or multi-step methods of higher order [64, Section 6]. Moreover, SSP for such methods is guaranteed only under some finite time step condition [11, 132] (also see the recent work [96]). In view of these results, positivity preservation of our higher-order schemes cannot be expected.

We do not aim to preserve the free energy of the Keller–Segel system, since such schemes usually destroy the symmetry property needed for the blow-up argument; see Remark 2.4 for details. An exception is the work [8] for a modified version of the Keller–Segel model in one dimension, where the virial blow-up argument could be used for an implicit Euler steepest descent scheme, which also provides the decay of the gradient-flow energy. Some estimates on the discrete free energy in an implicit Euler finite-volume approximation were shown in [152]. A scheme that dissipates the free energy numerically was suggested in [26] using a gradient-flow formulation of the energy functional with respect to a quadratic transportation distance. It is shown in [125] that the dissipation of the discrete free energy may fail in an upwind finite-difference scheme. The dissipation of the discrete entropy in a finite-volume modified Keller–Segel system was proved in [5].

Blow-up and Existence in a Bounded Domain:

We continue this survey with the general case of (1.1) and (1.2) on a bounded open domain $\Omega \subset \mathbb{R}^d$. We start with some blow-up results, this time concerning only the bounded case with the classical setting of $\alpha = 1$, $\beta = 1$ and $\delta = 0$. In particular, for $d = 2$, we can observe a similar behavior as in the unbounded case from above. In the parabolic-elliptic case, if the initial mass $M := \|\rho_0\|_{L^1(\Omega)}$ is small enough, $M < 4\pi$

for a general domain and $M < 8\pi$ for radial symmetric initial condition, we have global-in-time smooth solutions. If $M > 8\pi$, and ρ_0 is concentrated enough i.e. the second moment is small, the solution will blow up in the L^∞ norm [6, 111, 138]. The condition on the second moment implies that the initial density is highly concentrated around some point. It is necessary in the sense that there exists a set of initial data with total mass larger than 8π such that the corresponding solutions are global [3]. In the parabolic-parabolic case, again in two space dimensions and with finite second moment, the solutions exist globally in time if $M < 8\pi$ [25]. However, in contrast to the parabolic-elliptic case, the threshold value for M is less precise [129], and solutions with large mass can exist globally. In dimensions $d \geq 3$, a related critical phenomenon occurs: the solutions in the parabolic-elliptic case exist globally in time if $\|\rho^0\|_{L^{d/2}(\Omega)}$ is sufficiently small, but they blow up in finite time if the total mass is large compared to the second moment [38]. In the parabolic-parabolic case, global solutions in time exist and diffuse to a constant steady state, provided the critical norm of ρ_0 , the $L^{d/2}$ norm, is small enough [145]. In general, we see the blow-up in higher dimensions for arbitrary initial mass [146].

Approaches to Exclude a Blow-up:

In the case $\alpha = 1$, the system (1.2) becomes the cross-diffusion system introduced and analyzed in [75]. In [28], a similar set of equations is analyzed, this time with a nonlinear cross-diffusion term $\delta\Delta\rho^n$ with $n > 1$. It turns out that the additional cross-diffusion allows us to prove the global existence of solutions for $\delta > 0$ and prevents the finite-time blow-up usually expected for this system. Of course, other modifications can be made to prevent a blow-up of the cell density: one can introduce nonlinear cell diffusion [20], nonlinear cell diffusion and a nonlinear chemoattractant sensitivity function [34, 36, 81, 151], volume filling [42], limit the flux [118] or consider a nonvanishing growth-death model [12, 144] to avoid the blow-up of the cell density. If $\alpha < 2/d$, $\delta = 0$, we also have global existence of classical solutions, see [103]. In the case $\alpha > 2/d$, $\delta = 0$, and $\varepsilon = 0$, solutions of a slightly different equation blow up, if the initial mass is big enough [148]. See [4] and [28, 75] for an overview of these modifications.

Known Results for the Regularized System (1.2):

In the case $\alpha = 1$, the system features global-in-time weak solutions [75]. For the case $\varepsilon = 0$, $\alpha = 1$ and $d \leq 3$, the equations can be reformulated to fit into the framework of [97], where an L^∞ bound is shown but no existence result is presented. A numerical study was performed for the regularized parabolic-elliptic case in [5]. In particular, it demonstrated that intermediate states of the solution exist; see Chapter 3 for a continuation of this observation. A finite element scheme for the parabolic-parabolic case was analyzed in [68], but without highlighting the role of the parameter δ .

1.4 A Poisson–Maxwell–Stefan System

The Maxwell–Stefan equations describe the dynamics of a fluid mixture in the diffusive regime. They have numerous applications, for instance in sedimentation, dialysis, electrolysis and ion exchange. The system itself was already derived in the 19th century by Maxwell using gas theory [108]. In most situations, a component in a fluid diffuses down the gradient of its concentration, i.e. according to Fick’s law. This is not always the case; experiments show that in multicomponent fluids the diffusion flux of any component is strongly coupled to that of the other components, i.e. cross-diffusion appears, to take into account the drag/friction force between the components. This can lead to the already mentioned phenomena of uphill diffusion, where the flux goes from regions of low concentration to regions of high concentration; see [47] for the original experiment, [17] for a mathematical discussion and [99] for a new survey of this topic. While Maxwell–Stefan models have been investigated for several decades from a modeling and simulation viewpoint in the engineering literature (e.g. [58]), the mathematical and numerical analysis started more recently [15, 63]. The global existence of weak solutions under natural conditions was proved in [31, 93] for neutral mixtures. The main tool for proving these results is the boundedness-by-entropy method, introduced in [83]. In case of ion transport, the electric charges and the self-consistent electric potential need to be taken into account. Usually, this is done in the context of Nernst–Planck models [27, 29], where the diffusion flux only depends on the density gradient of the i th component, and thus without any cross-diffusion effects. In certain cases, e.g. in an infinitely diluted mixture, we can view the Nernst–Planck equations as a specific instant of the Maxwell–Stefan equations for ions [65]. At this point in time, to our knowledge, no mathematical results are available in the literature for such Poisson–Maxwell–Stefan models. As stated above, we want to translate the continuous idea, in this case the boundedness-by-entropy method, to the discrete world. In particular, we will derive a structure-preserving fully discrete Galerkin scheme and prove its convergence to the continuous problem. This provides us also, for the first time, with a global existence result for Poisson–Maxwell–Stefan systems.

1.4.1 The Model Equations

In order to write down this model, we have to define several quantities and restrict ourself to a particular setting. We consider an ionized fluid mixture consisting of n components on a bounded domain $\Omega \subset \mathbb{R}^d$, with the partial mass density ρ_i , partial flux J_i , and molar mass M_i of the i th species. The evolution of the particle densities ρ_i is governed by the partial mass balance equations

$$\partial_t \rho_i + \operatorname{div} J_i = r_i(x), \quad i = 1, \dots, n, \quad (1.7)$$

where r_i are the production rates satisfying $\sum_{i=1}^n r_i(x) = 0$ and $\sum_{i=1}^n J_i = 0$. The variables are functions of the spatial variable y and time t . The molar concentrations are defined by $c_i = \rho_i/M_i$ and $x_i = c_i/c_{\text{tot}}$ are the molar fractions, where $c_{\text{tot}} = \sum_{i=1}^n c_i$ denotes the total concentration and we have set $x = (x_1, \dots, x_n)$. The partial fluxes J_i and the gradients of the molar fractions x_i are related by the (scaled) Maxwell–Stefan equations

$$-\sum_{j=1}^N k_{ij}(\rho_j J_i - \rho_i J_j) = D_i := \nabla x_i + (z_i x_i - (z \cdot x)\rho_i)\nabla\Phi, \quad i = 1, \dots, n, \quad (1.8)$$

where $k_{ij} = k_{ji} = 1/(c_{\text{tot}}^3 M_i M_j D_{ij})$ are the rescaled (reciprocal) Maxwell–Stefan diffusivities, D_i is the driving force, z_i the electric charge of the i th component, and Φ the electric potential. The numbers $D_{ij} = D_{ji}$ are the Maxwell–Stefan diffusivities and can be interpreted as inverse drag coefficients. We refer to Section 4.3 for details on the modeling in our situation. A derivation of the Maxwell–Stefan system itself from the Boltzmann equation can be found in [17, 58], including a non-isothermal setting [79]. These equations are coupled to the (scaled) Poisson equation

$$-\lambda\Delta\Phi = \sum_{i=1}^n z_i c_i + f(y), \quad (1.9)$$

where λ is the scaled permittivity, and $f(y)$ is a fixed background charge. The equations are solved in a bounded domain $\Omega \subset \mathbb{R}^d$ ($d \geq 1$) and supplemented by the boundary conditions

$$J_i \cdot \nu = 0 \quad \text{on } \partial\Omega, \quad i = 1, \dots, n, \quad (1.10)$$

$$\Phi = \Phi_D \quad \text{on } \Gamma_D, \quad \nabla\Phi \cdot \nu = 0 \quad \text{on } \Gamma_N, \quad (1.11)$$

where Γ_D models the electric contacts, $\Gamma_N = \partial\Omega \setminus \Gamma_D$ is the union of insulating boundary segments, and ν denotes the exterior unit normal vector to $\partial\Omega$. This means that the mixture cannot leave the container Ω and an electric field is applied at the contacts Γ_D . The initial conditions are given by

$$\rho_i(\cdot, 0) = \rho_i^0 \quad \text{in } \Omega, \quad i = 1, \dots, n.$$

We assume that the total mass is constant initially, $\sum_{i=1}^n \rho_i^0 = 1$, which implies from (1.7) that the total mass is constant for all times, $\sum_{i=1}^n \rho_i(t) = 1$, expressing total mass conservation.

A Poisson–Maxwell–Stefan Cross-Diffusion System:

Observe that (1.8) defines a linear system in the diffusion fluxes. Since $\sum_{i=1}^n D_i = 0$, the kernel of that system is nontrivial, and we need to invert the relation between the fluxes J_i and the driving forces D_i on the orthogonal component of the kernel. It was shown in [93, Section 2] that we can write (1.8) as $D' = -A_0 J'$, where $D' = (D_1, \dots, D_{n-1})$, $J' = (J_1, \dots, J_{n-1})$, and $A_0 \in \mathbb{R}^{(n-1) \times (n-1)}$ is invertible but not positive definite nor symmetric, see Section 4.4.1 for details, and is given by

$$(A_0)_{ij} = \begin{cases} \sum_{\ell=1, \ell \neq i}^{n-1} (k_{i\ell} - k_{in}) \rho_\ell + k_{in} & \text{if } i = j, \\ -(k_{ij} - k_{in}) \rho_i & \text{if } i \neq j. \end{cases}$$

The n th components are recovered from $D_n = -\sum_{i=1}^{n-1} D_i$ and $J_n = -\sum_{i=1}^{n-1} J_i$. Thus, (1.7)-(1.11) can be written compactly as a cross-diffusion system coupled to a Poisson equation, i.e.

$$\begin{aligned} \partial_t \rho' &= \operatorname{div}(A_0^{-1}(\rho) D'(\rho, \Phi)) + r'(x), & \rho_n &= 1 - \sum_{i=1}^{n-1} \rho_i, \\ D_i &= \nabla x_i + (z_i x_i - (z \cdot x) \rho_i) \nabla \Phi, & i &= 1, \dots, n-1, \\ -\lambda \Delta \Phi &= \sum_{i=1}^n z_i c_i + f(y), & & \text{in } \Omega, \end{aligned} \quad (1.12)$$

where $\rho' = (\rho_1, \dots, \rho_{n-1})$, with the mixed boundary conditions

$$\begin{aligned} A_0^{-1} D' \cdot \nu &= 0 \quad \text{on } \partial\Omega, \quad i = 1, \dots, n-1, \\ \Phi &= \Phi_D \quad \text{on } \Gamma_D, \quad \nabla \Phi \cdot \nu = 0 \quad \text{on } \Gamma_N, \end{aligned} \quad (1.13)$$

with $A_0^{-1} D' \cdot \nu$ and $\operatorname{div}(A_0^{-1} D')$ defined in the Section 1.6.

1.4.2 Structures and Qualitative Properties

The assumptions from above imply that a solution $\rho \in \mathbb{R}^n$ of (1.12)-(1.13) is supposed to be nonnegative and every component ρ_i is constrained from above by one, i.e. $\rho_i \in [0, 1]$, $i = 1, \dots, n$. If these bounds are satisfied, we know, by the reformulation of the system, that the total mass is conserved over time and in particular,

$$\|\rho\|_{L^1(\Omega)} = \|\rho_0\|_{L^1(\Omega)} = |\Omega| \quad \text{for all } t > 0.$$

Entropy Inequality:

Next, we introduce the entropy

$$H(\rho) = \int_{\Omega} h(\rho) dy, \quad h(\rho) = c_{\text{tot}} \sum_{i=1}^n x_i \log x_i + \frac{\lambda}{2} |\nabla(\Phi - \Phi_D)|^2,$$

see Section 4.3 for more details. Using a transformation $\rho \mapsto w(\rho)$, so-called entropy variables, we can formally compute that

$$\frac{dH}{dt} + \int_{\Omega} \nabla w : B \nabla w dy = \int_{\Omega} \sum_{i=1}^n r_i(x) \frac{\partial h}{\partial \rho_i} dy, \quad (1.14)$$

if Φ_D is constant and $\nabla w : B \nabla w = \sum_{i,j=1}^{n-1} B_{ij} \nabla w_i \cdot \nabla w_j$. This transformation is well-known in nonequilibrium thermodynamics, where w_i is called the electrochemical potential and B is the mobility or Onsager matrix. The matrix B in our case is symmetric and positive definite; see Section 4.4. This implies that the entropy production (the diffusion term) is nonnegative, which expresses the second law of thermodynamics. Thus, if the right-hand side is nonpositive, the entropy $t \mapsto H(\rho(t))$ is a Lyapunov functional and we may obtain suitable estimates for w_i . In addition, the inverse transformation $w \mapsto \rho(w)$ guarantees that the densities $\rho_i = \rho_i(w)$ are positive and bounded, and it holds that $\sum_{i=1}^n \rho_i(w) = 1$; see Section 4.4 for details. This property is inherent of the transformation and it holds without the use of a maximum principle and independent of the functional setting. So if we can show the existence of a solution w for the system (1.12)-(1.13) in the new entropy variables, we immediately achieve a solution fulfilling our L^∞ bounds stated above. This technique has been used to prove existence of the system in [31, 93], but without electric force terms.

1.4.3 Mathematical Challenges and State of the Art

The main mathematical difficulties in the analysis of the quasilinear cross-diffusion system (1.12)-(1.13) are rooted in three challenges: the lack of a maximum principle, the handling of different molar masses and the coupling to the Poisson equation by an nonlinear drift term. In addition, our goal is to derive a structure preserving numerical scheme, which at the same time preserves the nonnegativity, the bound from above and the entropy inequality. In general, this is a challenge in itself, and not many results include the convergence of such schemes for a nonlinear system. We also remark that the recovery of the density ρ from the entropy variables in this case is not standard, since the inverse function is only known to exist, but no explicit formula is available; see Subsection 4.4.2. Before presenting our main results, we briefly review the state of the art of Maxwell–Stefan models.

Modeling:

The Maxwell–Stefan equations itself were already derived in the 19th century by Maxwell using kinetic gas theory [108] and Stefan using continuum mechanics [134]. A more mathematical derivation from the Boltzmann equation can be found in [18, 62], including a non-isothermal setting [79]. An advantage of the Maxwell–Stefan approach is that the definition of the driving forces can be adapted to the present physical situation, leading to very general and thermodynamically consistent models [16]. In order to also consider charged mixtures, like electrolytes, we need to include the electric force. In many applications, simulations for such mixtures are carried out using an instance of the Nernst–Planck model [113, 120] without any cross-diffusion effects. In the case of a ternary gas, Duncan and Toor [47] showed that cross-diffusion terms need to be taken into account. Dreyer et al. [46] outlined some deficiencies of Nernst–Planck models and propose thermodynamically consistent Maxwell–Stefan type models. A numerical comparison between Nernst–Planck and Maxwell–Stefan models can be found in [121], which also highlights that one needs to take cross-diffusion into account for an accurate description of a ternary electrolyte. These shortcomings of the classical Nernst–Planck approach are known, and several (non-linear) generalizations of the Poisson–Nernst–Planck system have been established in recent years, leading to cross-diffusion in most cases, e.g. [21, 45].

Analysis:

The first global-in-time existence result to the Maxwell–Stefan equations (1.7)-(1.8) without Poisson equation was proved by Giovangigli and Massot [63] for initial data around the constant equilibrium state. The local-in-time existence of classical solutions was shown by Bothe [15]. The entropy structure of the Maxwell–Stefan system was revealed in [93], and a general global existence theorem could be shown. Further global existence results can be found in [71, 107]. The Maxwell–Stefan system was coupled to the heat equation [80] and to the incompressible Navier–Stokes equations [31]. In [62, Theorem 9.7.4] and [71, Theorem 4.3], the large-time asymptotics for initial data close to equilibrium were analyzed. The convergence to equilibrium for any initial data was investigated in [31, 93] without production terms and in [39] with production terms for reversible reactions. Salvarani and Soares proved a relaxation limit of the Maxwell–Stefan system to a system of linear heat equations [126].

Numerics:

Surprisingly, there are not many papers concerned with numerical schemes which preserve the properties of the solution, like conservation of total mass, nonnegativity and entropy production. Many approximation schemes can be found in the engineering literature, for instance finite-difference [102, 105] or finite-element [25]

discretizations. In the mathematical literature, finite-volume [116] and mixed finite-element [109] schemes, as well as explicit finite-difference schemes with fast solvers [60] were proposed. The existence of discrete solutions was shown in [109], but only for ternary systems and under restrictions on the diffusion coefficients. The schemes of [17, 116] conserve the total mass, while those of [17, 43] also preserve the L^∞ bounds. The result of [43] is based on maximum principle arguments. Note that we are able to show the L^∞ bounds without the use of a maximum principle, as a result of the formulation in terms of entropy variables, and that we do not impose any restrictions on the diffusivities (except positivity).

All the cited results are concerned with the Maxwell–Stefan equations for neutral fluids, i.e. without electric effects.

1.5 Main Results and Outline

Chapter 2 is devoted to results for the parabolic-elliptic case of the Keller–Segel system, i.e. for the system (1.1) with $\Omega = \mathbb{R}^2$, $\varepsilon = 0$ and $\alpha = 1$. In short, we will derive an upper bound for the blow-up time for various time discretizations for the time-discretized system. This shows that the “continuous” methods carry over to the semi-discrete case. Let ρ_k be an approximation of $\rho(\cdot, k\tau)$, where $\tau > 0$ is the time step and $k \in \mathbb{N}$. We recall the definitions $M := \int_{\mathbb{R}^2} \rho_0 dx$ of the initial mass and $I_0 := \int_{\mathbb{R}^2} |x|^2 \rho_0 dx$ of the initial second moment.

- Existence of solutions to the implicit Euler scheme (Theorem 2.2): For a given $\rho_{k-1} \geq 0$ and sufficiently small time step τ , there exists a unique weak solution ρ_k to the semi-discrete equation. Moreover, the scheme preserves the positivity, conserves the mass and has finite second moment.
- Finite-time blow-up for the implicit Euler scheme (Theorem 2.3): Let $M > 8\pi$ and let I_0 be finite (if $\alpha = 0$) or I_0 and τ be sufficiently small (if $\alpha > 0$). Then, the semi-discrete solution exists only up to discrete times $k\tau \leq T^*$, where T^* is defined in (1.4).
- BDF schemes: For sufficiently small $\tau > 0$, there exists a unique weak solution to the BDF-2 and BDF-3 scheme, conserving the mass and having a finite second moment. Moreover, under the same assumptions as for the implicit Euler scheme, the solution blows up and $k\tau \leq T^*$ (Theorem 2.6 for BDF-2 and $\alpha \geq 0$, Theorem 2.8 for BDF-3 and $\alpha = 0$).
- Runge-Kutta schemes (Theorem 2.10): If $\alpha = 0$ and under the same assumptions as for the implicit Euler scheme, the solution blows up and $k\tau \leq T^*$. The same result holds for the implicit midpoint and trapezoidal rule if $\alpha > 0$.

- Numerical simulations are performed for several time-discretizations using an upwind-finite-element scheme in Section 2.4. A numerical study of the convergence rate in time confirms the formal order of convergence.

These results are based on the research together with A. Jüngel (TU Wien) published under the title *Blow-up of solutions to semi-discrete parabolic-elliptic Keller-Segel models* in the Journal *Discrete and Continuous Dynamical Systems-B* [86].

The second result, presented in **Chapter 3**, shows that the solutions of the model with additional cross-diffusion on a bounded domain, i.e. the system (1.2) with $\Omega \subset \mathbb{R}^d$ and $\beta = 1$, converge for δ going to zero to the solutions of the original Keller–Segel system (1.1).

- We prove the existence of nonnegative global-in-time solution for the regularized system (1.2) via the boundedness-by-entropy method in the case $\alpha < 2/d$, $\varepsilon = 0$, $\delta \geq 0$ and $d \leq 3$ in Section 3.2. In addition, the solution converges to a unique solution of the original Keller–Segel system (1.1), when δ goes to zero.
- There exists a unique smooth, nonnegative and local in time solution in the general case of (1.2) with $\varepsilon \geq 0$, $\alpha \geq 1$, see Section 3.3. According to Theorem 3.2, this solution converges, locally in time, for $\alpha = 1$ or $\alpha \geq 2$, as δ goes to zero, to the original solution of the Keller–Segel system (1.1).
- Numerical simulations for the different values of α are presented in Section 3.4. We treat the cases for α not covered by our analysis. Furthermore, we study an intermediate state of the solution for different values of δ and link the radius of this bump shaped state to the regularization parameter.

The results presented in this chapter are based on the research in cooperation with A. Jüngel (TU Wien) and S. Wang (Beijing University of Technology), submitted for publication under the title *Vanishing cross-diffusion limit in a Keller–Segel system with additional cross-diffusion* [88].

The aim of **Chapter 4** is to extend the global existence result of [31, 93] to Maxwell–Stefan systems with electric forces and to suggest a fully discrete and implicit Euler–Galerkin scheme that preserves the structure of the system, namely the nonnegativity of the particle densities, the L^∞ bound $\sum_{i=1}^n \rho_i = 1$, and a discrete analog of the entropy production inequality (1.14). The cross-diffusion terms cause some mathematical difficulties that are not present in Nernst–Planck models. The main results shown in this chapter are:

- In Section 4.3, the thermodynamic modeling of the system (1.7)-(1.9) is presented. Several identities for the fluxes J_i are derived and the inversion of the map $\rho \mapsto w$ is proved rigorously in Section 4.4.

- We prove the existence of a weak solution (ρ^k, Φ^k) , for every time-step k , to a fully discrete scheme, Galerkin in space and implicit Euler in time, for the system (1.12)-(1.13) with different molar masses in Section 4.5. The solution fulfills the L^∞ bounds with $\rho_i^k \in (0, 1)$, $i = 1, \dots, n$, the total conservation of mass and a discrete version of the entropy inequality (1.14).
- The solution converges to a weak solution of the system (1.12)-(1.13). In particular, we have global-in-time weak solutions for the Poisson–Maxwell–Stefan system with different molar masses; see Section 4.6.
- A implementation of the fully discrete scheme is discussed in Section 4.7, followed by numerical experiments to illustrate effects stemming from the coupling to the electric potential Φ . A numerical study of the convergence rate suggests a second order convergence in space.

These results are based on a collaboration with A. Jüngel (TU Wien) and are published under the title *Convergence of an implicit Euler Galerkin scheme for Poisson–Maxwell–Stefan systems* in *Advances in Computational Mathematics* [87].

1.6 Notation

1. We denote by $d \in \mathbb{N}$ the dimension of the spatial domain and with $n \in \mathbb{N}$ the number of components of a system of equations.
2. $\Omega \subseteq \mathbb{R}^d$ will always be an open bounded or unbounded set.
3. Given two matrices $A = (A_{ij})$, $B = (B_{ij}) \in \mathbb{R}^{m \times n}$, we define the Frobenius inner product by

$$A : B = \sum_{i=1}^m \sum_{j=1}^n A_{ij} B_{ij}.$$

4. Given two matrices $A = (A_{ij}) \in \mathbb{R}^{n \times n}$ and $D = (D_{ij}) \in \mathbb{R}^{n \times d}$ and a vector $\nu \in \mathbb{R}^d$, we define the two vectors $\operatorname{div}(AD)$, $(AD) \cdot \nu \in \mathbb{R}^n$ with the components

$$(\operatorname{div}(AD))_i = \sum_{j=1}^d \sum_{k=1}^n \frac{\partial}{\partial x_j} (A_{ik} D_{kj}), \quad ((AD) \cdot \nu)_i = \sum_{j=1}^d \sum_{k=1}^n A_{ik} D_{kj} \nu_j,$$

$$i = 1, \dots, n.$$

5. $\mathcal{D}(\Omega) = C_c^\infty(\Omega)$ denotes the space of test functions on a domain Ω .
6. $\langle \cdot, \cdot \rangle$ denotes the duality bracket between the elements of a Banach space X and its dual X' .



Die approbierte gedruckte Originalversion dieser Dissertation ist an der TU Wien Bibliothek verfügbar.
The approved original version of this doctoral thesis is available in print at TU Wien Bibliothek.

2 The Semi-Discrete Virial Argument for the Keller–Segel System

This chapter is concerned with the derivation of upper bounds for the blow-up time in the semi-discrete Keller–Segel system in \mathbb{R}^2 . As stated in the introduction, we will deal with the following parabolic-elliptic system:

$$\partial_t \rho = \operatorname{div}(\nabla \rho - \rho \nabla c), \quad -\Delta c + \beta c = \rho \quad \text{in } \mathbb{R}^2. \quad (2.1)$$

Denoting by B_β the Bessel potential if $\beta > 0$, and the Newton potential if $\beta = 0$ (see the Appendix A for the definitions), this system can be formulated more compactly as the single equation

$$\partial_t \rho = \operatorname{div}(\nabla \rho - \rho(\nabla B_\beta * \rho)) \quad \text{in } \mathbb{R}^2, \quad (2.2)$$

with the initial condition

$$\rho(\cdot, 0) = \rho_0 \quad \text{in } \mathbb{R}^2.$$

The chapter is organized as follows: We start with a brief revisit of the virial argument in the continuous setting in Section 2.1. Section 2.2 is concerned with the analysis of the implicit Euler scheme, while some higher-order schemes (BDF, Runge-Kutta) are investigated in Section 2.3. In Section 2.4 we provide some numerical examples to illustrate our theoretical statements.

2.1 Key Idea: The Virial Identity

In order to present the virial argument in a rigorous setting, we will follow the approach of [10] and define a special kind of weak solution for (2.1). We start by motivating this definition and assume the existence of a smooth solution $\rho \in C^1(0, T, C^2(\mathbb{R}^2)) \cap C(\mathbb{R}^2 \times [0, \infty))$, with compact support in space, for the system (2.1). As mentioned above, we can express the gradient of the concentration c via the Bessel or Newton potential, i.e.

$$\nabla c(x, t) = (\nabla B_\beta * \rho)(x, t),$$

for all $(x, t) \in \mathbb{R}^2 \times (0, \infty)$. Next, we observe that for $\beta \geq 0$,

$$\nabla B_\beta(z) = -\frac{1}{2\pi} \frac{z}{|z|^2} g_\beta(|z|), \quad z \in \mathbb{R}^2, \quad (2.3)$$

with

$$g_\beta(r) := \int_0^\infty e^{-s-\beta r^2/(4s)} ds \quad \text{for } r > 0, \quad (2.4)$$

using the substitution $s = |x|^2/(4t)$. In particular, we can use this identity and test the first equation of (2.1) with $\phi \in \mathcal{D}(\mathbb{R}^2)$. Integrating by parts leads to

$$\begin{aligned} \frac{d}{dt} \int_{\mathbb{R}^2} \phi(x) \rho(x, t) dx &= \int_{\mathbb{R}^2} \Delta \phi(x) \rho(x, t) dx \\ &\quad - \frac{1}{2\pi} \int_{\mathbb{R}^2 \times \mathbb{R}^2} \nabla \phi(x) \cdot \frac{x-y}{|x-y|^2} g_\beta(|x-y|) \rho(x, t) \rho(y, t) dy dx. \end{aligned}$$

Thus, we can observe a remarkable symmetry in the last term that allows us to rewrite it as

$$\begin{aligned} & - \frac{1}{2\pi} \int_{\mathbb{R}^2 \times \mathbb{R}^2} \nabla \phi(x) \cdot \frac{x-y}{|x-y|^2} g_\beta(|x-y|) \rho(x, t) \rho(y, t) dy dx \\ &= - \frac{1}{4\pi} \int_{\mathbb{R}^2 \times \mathbb{R}^2} [\nabla \phi(x) - \nabla \phi(y)] \cdot \frac{x-y}{|x-y|^2} g_\beta(|x-y|) \rho(x, t) \rho(y, t) dx dy. \end{aligned}$$

This reformulation improves the standard formulation in the distributional sense, since, using the fact that $[\nabla \phi(x) - \nabla \phi(y)] \cdot \frac{x-y}{|x-y|^2}$ is continuous and has compact support, it can also handle measure solutions.

Definition 2.1. *Let $\rho \in L_{loc}^\infty(\mathbb{R}^+; L^1(\mathbb{R}^2))$ be nonnegative. We say ρ is a very weak solution of (2.1), if ρ solves*

$$\begin{aligned} \frac{d}{dt} \int_{\mathbb{R}^2} \phi(x) \rho(x, t) dx - \int_{\mathbb{R}^2} \Delta \phi(x) \rho(x, t) dx &= \\ - \frac{1}{4\pi} \int_{\mathbb{R}^2 \times \mathbb{R}^2} [\nabla \phi(x) - \nabla \phi(y)] \cdot \frac{x-y}{|x-y|^2} g_\beta(|x-y|) \rho(x, t) \rho(y, t) dx dy \end{aligned}$$

for all $\phi \in \mathcal{D}(\mathbb{R}^2)$.

For the sake of simplicity, we set $\beta = 0$ and derive the virial identity; see [22] for $\beta > 0$. We start by the assumption that ρ is a very weak solution, in the sense of (2.1), on an interval $[0, T^*)$ and the second moment of the initial datum is bounded, i.e. $\int_{\mathbb{R}^2} |x|^2 \rho_0(x) dx < \infty$. This implies the conservation of mass

$$\|\rho\|_{L^1(\mathbb{R}^2)} = \|\rho_0\|_{L^1(\mathbb{R}^2)} := M,$$

if we use an appropriate approximation for $\phi(x) \equiv 1$ as a test function; see Theorem 2.2. Testing with $|x|^2$, modulo an approximation argument, see [10], leads to

$$\frac{d}{dt} \int_{\mathbb{R}^2} |x|^2 \rho(x, t) dx = \frac{M}{2\pi} (8\pi - M). \quad (2.5)$$

Now, the virial identity (2.5) implies a contradiction to the nonnegativity of ρ for $M > 8\pi$, and hence $T^* < \infty$. This argument builds on the following three crucial properties:

- conservation of mass
- nonnegativity of the solution
- and a symmetry in the drift term.

As mentioned above, we want to mimic this argument in the discrete setting. Hence, a numerical scheme should fulfill all of these three properties at the same time. Developing such a scheme is a highly nontrivial task and the rest of this chapter is dedicated to establishing the first results in this direction by handling the time discretization of (2.5) and the virial inequality in the case $\beta \geq 0$ mentioned above.

2.2 Implicit Euler Scheme

We start with the existence analysis for the implicit Euler case of the Keller–Segel system (2.2) and their finite-time blow-up, where

$$\frac{1}{\tau} (\rho_k - \rho_{k-1}) = \operatorname{div} (\nabla \rho_k - \rho_k \nabla B_\beta * \rho_k) \quad \text{in } \mathbb{R}^2. \quad (2.6)$$

Here, $\tau > 0$ is the time step and B_β is the Bessel potential if $\beta > 0$ and the Newton potential if $\beta = 0$ (see the Appendix A). First, we study the existence of solutions. For this, let $X := L^1(\mathbb{R}^2) \cap L^\infty(\mathbb{R}^2)$ with norm $\|u\|_X = \max\{\|u\|_{L^1(\mathbb{R}^2)}, \|u\|_{L^\infty(\mathbb{R}^2)}\}$ for $u \in X$.

Theorem 2.2 (Existence for the implicit Euler scheme). *Let $\rho_{k-1} \in X$ and*

$$\tau < \frac{1}{(\pi + 1/2)^2} \frac{1}{(\|\rho_{k-1}\|_X + 1)^4}.$$

Then there exists a unique weak solution $\rho_k \in X \cap H^1(\mathbb{R}^2)$ to (2.6) such that

- *nonnegativity: if $\rho_{k-1} \geq 0$ then $\rho_k \geq 0$ in \mathbb{R}^2 ,*
- *conservation of mass: $\int_{\mathbb{R}^2} \rho_k dx = \int_{\mathbb{R}^2} \rho_{k-1} dx$,*

- control of second moment: if $\int_{\mathbb{R}^2} \rho_{k-1} |x|^2 dx < \infty$ then $\int_{\mathbb{R}^2} \rho_k |x|^2 dx < \infty$.

Proof. The strategy is to prove first the existence of a unique very weak solution $\rho_k \in X$ to the truncated problem

$$\frac{1}{\tau} \int_{\mathbb{R}^2} (\rho_k - \rho_{k-1}) \phi dx = \int_{\mathbb{R}^2} \rho_k \Delta \phi dx + \int_{\mathbb{R}^2} \rho_k^+ (\nabla B_\beta * \rho_k) \cdot \nabla \phi dx \quad (2.7)$$

for all $\phi \in H^1(\mathbb{R}^2)$, where $\rho_k^+ = \max\{0, \rho_k\}$. The second step is to show that $\rho_k \in H^1(\mathbb{R}^2)$. Then we can use $\rho_k^- = \min\{0, \rho_k\}$ as a test function in the weak formulation and prove that $\rho_k \geq 0$.

Step 1: Solution to (2.7). To simplify the notation, we write $\rho := \rho_k$ and $\rho_0 := \rho_{k-1}$. We introduce the operator $\nabla c : X \rightarrow L^\infty(\mathbb{R}^2)^2$, $\nabla c[\rho] = \nabla B_\beta * \rho$. We claim that this operator is well-defined and continuous. Using (2.3) and the fact that $g_\beta \leq 1$, we conclude

$$\begin{aligned} |\nabla c[\rho](x)| &= \left| \frac{1}{2\pi} \int_{\mathbb{R}^2} \frac{x-y}{|x-y|^2} g_\beta(|x-y|) \rho(y) dy \right| \\ &\leq \frac{1}{2\pi} \int_{|x-y| \leq 1} \frac{|\rho(y)|}{|x-y|} dy + \frac{1}{2\pi} \int_{|x-y| > 1} \frac{|\rho(y)|}{|x-y|} dy \\ &\leq \|\rho\|_{L^\infty(\mathbb{R}^2)} + \frac{1}{2\pi} \|\rho\|_{L^1(\mathbb{R}^2)} \leq b \|\rho\|_X. \end{aligned} \quad (2.8)$$

where $b := 1 + 1/(2\pi)$. This shows the continuity of ∇c .

Next, for given $\tilde{\rho} \in X$, the linear problem

$$-\Delta \rho + \tau^{-1}(\rho - \rho_0) = -\operatorname{div}(\tilde{\rho}^+ \nabla c[\tilde{\rho}])$$

has a unique solution in $H^1(\mathbb{R}^2)$. Indeed, since we have $\tilde{\rho}^+ \in L^2(\mathbb{R}^2)$, $\nabla c[\tilde{\rho}] \in L^\infty(\mathbb{R}^2)^2$, and therefore $f := \tilde{\rho}^+ \nabla c[\tilde{\rho}] \in L^2(\mathbb{R}^2)^2$, we can apply Lemma A.3 in the Appendix yielding the unique solvability of the linear problem. The solution is given by

$$\rho = \frac{1}{\tau} B_{1/\tau} * \rho_0 - \nabla B_{1/\tau} * (\tilde{\rho}^+ \nabla c[\tilde{\rho}]). \quad (2.9)$$

Hence, we can define the fixed-point operator $T : X \rightarrow X$ by $T[\tilde{\rho}] := \rho$, and ρ is given by (2.9). Clearly, any fixed point of T is a solution to (2.7). We apply the Banach fixed-point theorem to T on the set $S := \{\rho \in X : \|\rho\|_X \leq \|\rho_0\|_X + 1\}$. For this, we need to show that $T : S \rightarrow S$ is a contraction.

For the proof of $T(S) \subset S$, we use Lemma A.1, the Young inequality with $p = q =$

$r = 1$ (see the Appendix A), and (2.8):

$$\begin{aligned} \|T[\rho]\|_{L^1(\mathbb{R}^2)} &\leq \frac{1}{\tau} \|B_{1/\tau} * \rho_0\|_{L^1(\mathbb{R}^2)} + \|\nabla B_{1/\tau} * (\rho^+ \nabla c[\rho])\|_{L^1(\mathbb{R}^2)} \\ &\leq \frac{1}{\tau} \|B_{1/\tau}\|_{L^1(\mathbb{R}^2)} \|\rho_0\|_{L^1(\mathbb{R}^2)} + \|\nabla B_{1/\tau}\|_{L^1(\mathbb{R}^2)} \|\nabla c[\rho]\|_{L^\infty(\mathbb{R}^2)} \|\rho\|_{L^1(\mathbb{R}^2)} \\ &\leq \|\rho_0\|_{L^1(\mathbb{R}^2)} + \frac{\pi}{2} \tau^{1/2} b \|\rho\|_X^2. \end{aligned}$$

Similarly, we obtain

$$\|T[\rho]\|_{L^\infty(\mathbb{R}^2)} \leq \|\rho_0\|_{L^\infty(\mathbb{R}^2)} + \frac{\pi}{2} \tau^{1/2} b \|\rho\|_X^2.$$

Combining the previous two estimates, we conclude that

$$\|T[\rho]\|_X \leq \|\rho_0\|_X + \frac{\pi}{2} \tau^{1/2} b \|\rho\|_X^2.$$

Then choosing $\tau < (\pi b)^{-2} (\|\rho_0\|_X + 1)^{-4}$, we see that $\|T[\rho]\|_X \leq \|\rho_0\|_X + 1/2$, which shows that $T[\rho] \in S$.

To show the contraction property, let $\rho, \bar{\rho} \in S$. Then, estimating as above,

$$\begin{aligned} \|T[\rho] - T[\bar{\rho}]\|_X &\leq \|\nabla B_{1/\tau} * (\rho^+ \nabla c[\rho] - \bar{\rho}^+ \nabla c[\bar{\rho}])\|_X \\ &\leq \|\nabla B_{1/\tau}\|_{L^1(\mathbb{R}^2)} \|(\rho^+ - \bar{\rho}^+) \nabla c[\rho] + \bar{\rho}^+ (\nabla c[\rho] - \nabla c[\bar{\rho}])\|_X \\ &\leq \frac{\pi}{2} \tau^{1/2} (\|\rho^+ - \bar{\rho}^+\|_X \|\nabla c[\rho]\|_{L^\infty(\mathbb{R}^2)} + \|\bar{\rho}\|_X \|\nabla c[\rho - \bar{\rho}]\|_{L^\infty(\mathbb{R}^2)}) \\ &\leq \pi \tau^{1/2} b (\|\rho_0\|_X + 1) \|\rho - \bar{\rho}\|_X. \end{aligned}$$

Since $\pi \tau^{1/2} b (\|\rho_0\|_X + 1) < 1$, T is a contraction. By the Banach fixed-point theorem, T has a fixed point $\rho_k \in X$, which is a solution to (2.7).

Step 2: Regularity of the solution to (2.7). We prove that for any $\beta \geq 0$, $\rho_k \in H^1(\mathbb{R}^2)$ solves

$$\frac{1}{\tau} \int_{\mathbb{R}^2} (\rho_k - \rho_{k-1}) \phi dx = - \int_{\mathbb{R}^2} \nabla \rho_k \cdot \nabla \phi dx + \int_{\mathbb{R}^2} \rho_k^+ (\nabla B_\beta * \rho_k) \cdot \nabla \phi dx \quad (2.10)$$

for all $\phi \in H^1(\mathbb{R}^2)$ and satisfies

$$\|\rho_k\|_{H^1(\mathbb{R}^2)} \leq C_0 \|\rho_{k-1}\|_{L^2(\mathbb{R}^2)}$$

for some positive constant C_0 which depends on τ and $\|\rho_{k-1}\|_X$.

Again, we set $\rho := \rho_k$ and $\rho_0 := \rho_{k-1}$. Since $\rho \in X \subset L^2(\mathbb{R}^2)$, we have $\rho^+ \nabla c[\rho] \in L^2(\mathbb{R}^2)^2$. Therefore, by Lemma A.3, $\rho \in H^1(\mathbb{R}^2)$ is the unique solution to (2.10). We

take ρ as a test function in that equation and use the Young inequality:

$$\begin{aligned} \frac{1}{2\tau} \int_{\mathbb{R}^2} (\rho^2 - \rho_0^2) dx &\leq \frac{1}{\tau} \int_{\mathbb{R}^2} (\rho - \rho_0) n dx = -\|\nabla \rho\|_{L^2(\mathbb{R}^2)}^2 + \int_{\mathbb{R}^2} \rho^+ \nabla c[\rho] \cdot \nabla \rho dx \\ &\leq -\frac{1}{2} \|\nabla \rho\|_{L^2(\mathbb{R}^2)}^2 + \frac{1}{2} \|\rho\|_{L^2(\mathbb{R}^2)}^2 \|\nabla c[\rho]\|_{L^\infty(\mathbb{R}^2)}^2. \end{aligned}$$

By (2.8) and $\|\rho\|_X \leq \|\rho_0\|_X + 1$, we find that

$$\frac{1}{\tau} \int_{\mathbb{R}^2} (\rho^2 - \rho_0^2) dx + \|\nabla \rho\|_{L^2(\mathbb{R}^2)}^2 \leq b^2 \|\rho\|_X^2 \|\rho\|_{L^2(\mathbb{R}^2)}^2 \leq b^2 (\|\rho_0\|_X + 1)^2 \|\rho\|_{L^2(\mathbb{R}^2)}^2.$$

Then, since $b_0 := 1 - b^2 (\|\rho_0\|_X + 1)^2 \tau > 0$, we infer that

$$\|\rho\|_{L^2(\mathbb{R}^2)}^2 \leq \frac{1}{b_0} \|\rho_0\|_{L^2(\mathbb{R}^2)}^2,$$

and the claim follows with $C_0 = 1/\sqrt{b_0}$.

Step 3: Nonnegativity of ρ_k . Let $\rho_{k-1} \geq 0$ in \mathbb{R}^2 . We use $\rho_k^- = \min\{0, \rho_k\} \in H^1(\mathbb{R}^2)$ as a test function in (2.10):

$$\begin{aligned} \frac{1}{\tau} \int_{\mathbb{R}^2} (\rho_k^-)^2 dx &\leq \frac{1}{\tau} \int_{\mathbb{R}^2} (\rho_k - \rho_{k-1}) \rho_k^- dx \\ &= - \int_{\mathbb{R}^2} |\nabla \rho_k^-|^2 dx + \int_{\mathbb{R}^2} \rho_k^+ \nabla c[\rho_k] \cdot \nabla \rho_k^- dx \leq 0, \end{aligned}$$

since $\rho_{k-1} \rho_k^- \leq 0$ and the last integral on the right-hand side vanishes. This shows that $\rho_k \geq 0$ in \mathbb{R}^2 , and $\rho_k^+ = \rho_k$ in (2.10).

Step 4: Mass conservation. The statement follows immediately if we could use $\phi(x) = 1$ as a test function in (2.7). Since this function is not integrable, we need to approximate. As in [98], we introduce the radially symmetric cut-off function $\phi_R(x) = \phi(|x|/R)$, where $R \geq 1$ and

$$\phi(r) = \begin{cases} 1 & \text{for } 0 \leq r \leq 1, \\ 1 - 2(r-1)^2 & \text{for } 1 < r \leq 3/2, \\ 2(2-r)^2 & \text{for } 3/2 < r \leq 2, \\ 0 & \text{for } r \geq 2. \end{cases} \quad (2.11)$$

The following properties hold:

$$\begin{aligned} \phi_R \in H^2(\mathbb{R}^2), \quad \lim_{R \rightarrow \infty} \phi_R(x) &= 1 && \text{for all } x \in \mathbb{R}^2, \\ |\nabla \phi_R(x) - \nabla \phi_R(y)| &\leq \frac{C_1}{R^2} |x - y|, \quad |\Delta \phi_R(x)| \leq \frac{C_2}{R^2} && \text{for all } x, y \in \mathbb{R}^2, \end{aligned} \quad (2.12)$$

for some constants $C_1, C_2 > 0$. Let $0 \leq \varphi^\varepsilon \in C_0^\infty(\mathbb{R}^2)$ be a standard mollifier and set $\phi_R^\varepsilon = \phi_R * \varphi^\varepsilon$. Then $\phi_R^\varepsilon \rightarrow \phi_R$ in $H^2(\mathbb{R}^2)$ as $\varepsilon \rightarrow 0$ [100, Lemma 1.8.2]. Consequently, up to a subsequence, which is not relabeled, $\phi_R^\varepsilon \rightarrow \phi_R$, $\nabla \phi_R^\varepsilon \rightarrow \nabla \phi_R$, and $\Delta \phi_R^\varepsilon \rightarrow \Delta \phi_R$ a.e. in \mathbb{R}^2 . We use ϕ_R^ε as a test function in (2.7) and insert (2.3):

$$\begin{aligned} \left| \frac{1}{\tau} \int_{\mathbb{R}^2} (\rho_k - \rho_{k-1}) \phi_R^\varepsilon dx \right| &= \left| \int_{\mathbb{R}^2} \rho_k \Delta \phi_R^\varepsilon dx + \int_{\mathbb{R}^2} \rho_k (\nabla B_\beta * \rho_k) \cdot \nabla \phi_R^\varepsilon dx \right| \\ &\leq \frac{C_2}{R^2} \|\rho_k\|_{L^1(\mathbb{R}^2)} + \frac{1}{2\pi} \left| \int_{\mathbb{R}^2} \int_{\mathbb{R}^2} \rho_k(x) \rho_k(y) g_\beta(|x-y|) \frac{x-y}{|x-y|^2} \cdot \nabla \phi_R^\varepsilon(x) dx dy \right|. \end{aligned}$$

By symmetry and (2.12), the second integral can be estimated as

$$\begin{aligned} \frac{1}{2\pi} \left| \int_{\mathbb{R}^2} \int_{\mathbb{R}^2} \rho_k(x) \rho_k(y) g_\beta(|x-y|) \frac{x-y}{|x-y|^2} \cdot \nabla \phi_R^\varepsilon(x) dx dy \right| \\ = \frac{1}{4\pi} \left| \int_{\mathbb{R}^2} \int_{\mathbb{R}^2} \rho_k(x) \rho_k(y) g_\beta(|x-y|) \frac{x-y}{|x-y|^2} \cdot (\nabla \phi_R^\varepsilon(x) - \nabla \phi_R^\varepsilon(y)) dy dx \right| \\ \leq \frac{C_1}{4\pi R^2} \int_{\mathbb{R}^2} \int_{\mathbb{R}^2} \rho_k(x) \rho_k(y) dy dx = \frac{C_1}{4\pi R^2} \|\rho_k\|_{L^1(\mathbb{R}^2)}^2. \end{aligned}$$

These estimates allow us to apply the dominated convergence theorem, which leads, in the limit $\varepsilon \rightarrow 0$, to

$$\frac{1}{\tau} \int_{\mathbb{R}^2} (\rho_k - \rho_{k-1}) \phi_R dx = \int_{\mathbb{R}^2} \rho_k \Delta \phi_R dx + \int_{\mathbb{R}^2} \rho_k (\nabla B_\beta * \rho_k) \cdot \nabla \phi_R dx.$$

The same estimates as before show that both integrals on the right-hand side can be estimated by a multiple of $1/R^2$ such that the limit $R \rightarrow \infty$ leads to

$$\frac{1}{\tau} \int_{\mathbb{R}^2} (\rho_k - \rho_{k-1}) dx = 0,$$

which gives mass conservation.

Step 5: Control of the second moment. Similarly as in step 4, we approximate $|x|^2$ by setting $\psi_R(x) = |x|^2 \phi_R(x)$, where ϕ_R is defined in (2.11). Then $\psi_R \in H^2(\mathbb{R}^2)$, $\nabla \psi_R$ is Lipschitz continuous on \mathbb{R}^2 , and $\Delta \psi_R$ is bounded. Taking a standard mollifier $\varphi^\varepsilon \geq 0$, we set $\psi_R^\varepsilon = \psi_R * \varphi^\varepsilon \in C_0^\infty(\mathbb{R}^2)$. Using ψ_R^ε as a test function in (2.7) and passing to the limit $\varepsilon \rightarrow 0$ and then $R \rightarrow \infty$, it follows that

$$\frac{1}{\tau} \int_{\mathbb{R}^2} (\rho_k - \rho_{k-1}) |x|^2 dx = 4 \int_{\mathbb{R}^2} \rho_k dx + 2 \int_{\mathbb{R}^2} \rho_k (\nabla B_\beta * \rho_k) \cdot x dx. \quad (2.13)$$

Young’s inequality and estimate (2.8) for $\nabla c[\rho_k] = \nabla B_\beta * \rho_k$ show that

$$\begin{aligned} 2 \left| \int_{\mathbb{R}^2} \rho_k (\nabla B_\beta * \rho_k) \cdot x dx \right| &\leq 2b \|\rho_k\|_X \int_{\mathbb{R}^2} \rho_k |x| dx \\ &\leq b \|\rho_k\|_X \int_{\mathbb{R}^2} \rho_k dx + b \|\rho_k\|_X \int_{\mathbb{R}^2} \rho_k |x|^2 dx. \end{aligned}$$

Therefore, with $\|\rho_k\|_X \leq \|\rho_{k-1}\|_X + 1$, (2.13) gives

$$(1 - \tau b (\|\rho_{k-1}\|_X + 1)) \int_{\mathbb{R}^2} \rho_k |x|^2 dx \leq \int_{\mathbb{R}^2} \rho_{k-1} |x|^2 dx + \tau (4 + b \|\rho_k\|_X) \int_{\mathbb{R}^2} \rho_0 dx.$$

Since $1 - \tau b (\|\rho_{k-1}\|_X + 1) > 0$, we infer that the second moment of ρ_k is bounded if the second moment of ρ_{k-1} does so. \square

Next, we turn to the finite-time blow up of semi-discrete solutions. Set, for $\beta > 0$,

$$I^* := \frac{(M - 8\pi)^2}{4\beta M}, \quad \tau^* := \frac{\pi(M - 8\pi)}{2\beta M^2}. \quad (2.14)$$

Theorem 2.3 (Blow-up for the implicit Euler scheme). *Assume that*

$$\rho_0 \geq 0, \quad I_0 := \int_{\mathbb{R}^2} \rho_0(x) |x|^2 dx < \infty, \quad M := \int_{\mathbb{R}^2} \rho_0 dx > 8\pi.$$

Let $(\rho_k) \subset L^1(\mathbb{R}^2) \cap H^1(\mathbb{R}^2)$ be a sequence of nonnegative weak solutions to (2.6). Then this sequence is finite with maximal index k_{\max} , where, if $\beta = 0$,

$$k_{\max} \leq \frac{2\pi I_0}{\tau M (M - 8\pi)}. \quad (2.15)$$

In case $\beta > 0$, if additionally $I_0 \leq I^*$ and $\tau < \tau^*$ then

$$k_{\max} \leq \frac{2\pi I_0}{\tau M (M - 8\pi - 2\sqrt{\beta M I_0})}. \quad (2.16)$$

Proof. Let first $\beta = 0$ and let ρ_k be a weak solution to (2.6) with $k > 2\pi I_0 / (\tau M (M - 8\pi))$, i.e., we assume that (2.15) does not hold. We set $I_k = \int_{\mathbb{R}^2} \rho_k |x|^2 dx$. Then, by (2.13), for any $j \leq k$,

$$\begin{aligned} I_j - I_{j-1} &= 4\tau \int_{\mathbb{R}^2} \rho_j dx + 2\tau \int_{\mathbb{R}^2} \rho_j (\nabla B_0 * \rho_j) \cdot x dx \\ &= 4\tau M - \frac{\tau}{\pi} \int_{\mathbb{R}^2} \int_{\mathbb{R}^2} \rho_j(x) \frac{x \cdot (x - y)}{|x - y|^2} \rho_j(y) dy dx, \end{aligned}$$

where we used the conservation of mass and the definition of $\nabla B_0 * \rho_k$. A symmetry argument leads to

$$\begin{aligned} I_j - I_{j-1} &= 4\tau M - \frac{\tau}{2\pi} \int_{\mathbb{R}^2} \int_{\mathbb{R}^2} \frac{(x-y) \cdot (x-y)}{|x-y|^2} \rho_j(x) \rho_j(y) dy dx \\ &= 4\tau M - \frac{\tau}{2\pi} M^2 = \frac{\tau M}{2\pi} (8\pi - M). \end{aligned}$$

Summing this identity over $j = 1, \dots, k$ and taking into account the choice of k gives

$$I_k = I_0 - \frac{k\tau M}{2\pi} (M - 8\pi) < 0,$$

which is a contradiction to $\rho_k \geq 0$.

Next, let $\beta > 0$. For the proof, we follow the lines of [22, Section 6] but the end of the proof is different. Let $\rho_k \geq 0$ be a weak solution to (2.6) such that (2.16) is not true. Similarly as above, we find that

$$\begin{aligned} I_k - I_{k-1} &= 4\tau \int_{\mathbb{R}^2} \rho_k dx + 2\tau \int_{\mathbb{R}^2} \rho_k (\nabla B_\beta * \rho_k) \cdot x dx \\ &= 4\tau M - \frac{\tau}{2\pi} \int_{\mathbb{R}^2} \int_{\mathbb{R}^2} g_\beta(|x-y|) \rho_k(x) \rho_k(y) dy dx \\ &= \frac{\tau M}{2\pi} (8\pi - M) + \frac{\tau}{2\pi} \int_{\mathbb{R}^2} \int_{\mathbb{R}^2} (1 - g_\beta(|x-y|)) \rho_k(x) \rho_k(y) dy dx, \quad (2.17) \end{aligned}$$

where we recall definition (2.4) of g_β .

We need to estimate $1 - g_\beta(r)$. For this, let $z \in \mathbb{R}^2$, $r = |z| \in (0, 1/\sqrt{\beta})$. We compute

$$\frac{d}{dr} (1 - g_\beta(r)) = \frac{\beta r}{2} \int_0^\infty \frac{1}{s} e^{-s - \beta r^2/(4s)} ds = 2\pi\beta |z| B_1(\sqrt{\beta}z) \leq \sqrt{\beta}K,$$

where $K = 2\pi \sup_{|x| < 1} |x| B_1(|x|)$. It is known that $B_1(x)$ behaves asymptotically as $-\log|x|$ as $|x| \rightarrow 0$, so K is finite. A numerical computation shows that we have $\sup_{|x| < 1} |x| B_1(|x|) \approx 0.0742$ and $K \approx 0.4662$. We conclude that

$$0 \leq 1 - g_\beta(|z|) \leq \sqrt{\beta}K|z| \quad \text{for } 0 < \sqrt{\beta}|z| < 1.$$

This bound, together with $1 - g_\beta(|z|) \leq 1$, shows that the last integral in (2.17) can

be estimated as follows:

$$\begin{aligned}
 & \frac{\tau}{2\pi} \int \int_{\{\sqrt{\beta}|x-y|<1\}} (1 - g_\beta(|x-y|)) \rho_k(x) \rho_k(y) dy dx \\
 & \quad + \frac{\tau}{2\pi} \int \int_{\{\sqrt{\beta}|x-y|\geq 1\}} (1 - g_\beta(|x-y|)) \rho_k(x) \rho_k(y) dy dx \\
 & \leq \tau \frac{\sqrt{\beta}}{2\pi} \max\{1, K\} \int_{\mathbb{R}^2} \int_{\mathbb{R}^2} |x-y| \rho_k(x) \rho_k(y) dy dx \\
 & \leq \tau \frac{\sqrt{\beta}}{\pi} M \int_{\mathbb{R}^2} |y| \rho_k(y) dy \leq \tau \frac{\sqrt{\beta}}{\pi} M^{3/2} I_k^{1/2}, \tag{2.18}
 \end{aligned}$$

where we have applied the Cauchy-Schwarz inequality in the last step. We infer from (2.17) that

$$I_k - I_{k-1} \leq \frac{\tau}{2\pi} M(8\pi - M) + \tau \frac{\sqrt{\beta}}{\pi} M^{3/2} I_k^{1/2}.$$

Now, the argument differs from that one used in [22]. Set $b_0 = \sqrt{\beta}M^{3/2}/\pi$ and $\gamma = M(M - 8\pi)/(2\pi)$. Then we need to solve the recursive inequality

$$I_k - I_{k-1} \leq \tau f(I_k) := \tau(b_0 I_k^{1/2} - \gamma). \tag{2.19}$$

By definition of I^* , we have $f(I^*) = 0$. Since f is increasing and $I_0 \leq I^*$, it holds that $f(I_0) \leq 0$. We proceed by induction. Let $f(I_{k-1}) \leq 0$. We suppose that $f(I_k) > 0$ and show that this leads to a contradiction. Inequality (2.19) is equivalent to

$$\frac{I_k^{1/2} - I_{k-1}^{1/2}}{I_k^{1/2} - \gamma/b_0} \frac{I_k^{1/2} + I_{k-1}^{1/2}}{b_0} \leq \tau,$$

Since $f(I_{k-1}) \leq 0$, the first factor is larger than or equal to one, and taking into account $f(I_k) > 0$ or $I_k^{1/2} > \gamma/b_0$, we deduce that

$$\frac{\gamma}{b_0^2} < \frac{I_k^{1/2}}{b_0} \leq \frac{I_k^{1/2} + I_{k-1}^{1/2}}{b_0} \leq \tau,$$

which contradicts the smallness condition $\tau < \tau^* = \gamma/b_0^2$. We infer that $f(I_k) \leq 0$.

Then, summing (2.19) from $k = 1, \dots, j$,

$$I_j \leq I_0 + \tau \sum_{k=1}^j f(I_k) \leq I_0 + \tau j f(I_0).$$

We deduce that I_j becomes negative for $j > -I_0/(\tau f(I_0))$ which contradicts $\rho_k \geq 0$. This completes the proof. \square

Remark 2.4 (Semi-discrete energy dissipation). *It is possible to design semi-discrete schemes that dissipate the discrete free energy*

$$E_k = \int_{\mathbb{R}^2} \left(\rho_k (\log \rho_k - 1) - \frac{1}{2} c_k \rho_k \right) dx$$

(and conserve the mass and preserve the positivity). An example, taken from [125], is the semi-implicit scheme

$$\tau^{-1}(\rho_k - \rho_{k-1}) = \operatorname{div}(\rho_k - \rho_k \nabla c_{k-1}), \quad -\Delta c_{k-1} + \beta c_{k-1} = \rho_{k-1} \quad \text{in } \mathbb{R}^2. \quad (2.20)$$

Indeed, by the convexity of $s \mapsto s \log s$, we obtain

$$\begin{aligned} & \int_{\mathbb{R}^2} (\rho_k (\log \rho_k - 1) - \rho_{k-1} (\log \rho_{k-1} - 1)) dx \\ & \leq \int_{\mathbb{R}^2} (\rho_k - \rho_{k-1}) \log \rho_k dx = \tau \int_{\mathbb{R}^2} \left(-\frac{|\nabla \rho_k|^2}{\rho_k} + \nabla c_{k-1} \cdot \nabla \rho_k \right) dx. \end{aligned}$$

Furthermore, translating the computation in [117, Section 5.2.1] to the semi-discrete case,

$$\begin{aligned} \frac{1}{2} \int_{\mathbb{R}^2} (\rho_k c_k - \rho_{k-1} c_{k-1}) dx &= \frac{1}{2} \int_{\mathbb{R}^2} ((\rho_k - \rho_{k-1}) c_k + \rho_{k-1} (c_k - c_{k-1})) dx \\ &= \frac{1}{2} \int_{\mathbb{R}^2} ((\rho_k - \rho_{k-1}) c_k + (-\Delta(c_k - c_{k-1}) + \beta(c_k - c_{k-1})) c_{k-1}) dx \\ &= \int_{\mathbb{R}^2} (\rho_k - \rho_{k-1}) c_{k-1} dx = -\tau \int_{\mathbb{R}^2} (\nabla \rho_k \cdot \nabla c_{k-1} + \rho_k |\nabla c_{k-1}|^2) dx. \end{aligned}$$

Subtracting the latter from the former expression, we conclude that

$$E_k - E_{k-1} \leq -\tau \int_{\mathbb{R}^2} \rho_k |\nabla(\log \rho_k - c_{k-1})|^2 dx \leq 0.$$

Unfortunately, scheme (2.20) does not allow us to apply the symmetrization argument used in the proof of Theorem 2.3, since the drift part depends on two different time steps. The question whether (2.20) admits solutions that blow up in finite time remains open. \square

2.3 Higher-Order Schemes

Next, we extend our analysis to higher order schemes. In particular, we will prove the virial inequality for BDF-2, the implicit midpoint rule and the trapezoidal rule in the case $\beta \geq 0$ and the case $\beta = 0$ for BDF-3 and general Runge-Kutta schemes.

2.3.1 BDF-2 Scheme

The scheme reads as

$$\frac{1}{\tau} \left(\frac{3}{2} \rho_k - 2\rho_{k-1} + \frac{1}{2} \rho_{k-2} \right) = \operatorname{div} (\nabla \rho_k - \rho_k (\nabla B_\beta * \rho_k)) \quad \text{in } \mathbb{R}^2 \quad (2.21)$$

for $k \geq 2$, where ρ_0 is given and ρ_1 is computed from ρ_0 using the implicit Euler scheme.

Lemma 2.5 (Existence for the BDF-2 scheme). *Let $\beta \geq 0$, $\rho_{k-2}, \rho_{k-1} \in L^1(\mathbb{R}^2) \cap L^\infty(\mathbb{R}^2)$, and*

$$\tau \leq \frac{3}{2} \frac{1}{(\pi + 1/2)^2} \frac{1}{(1 + \|2\rho_{k-1} - \frac{1}{2}\rho_{k-2}\|_X)^4}.$$

Then there exists a weak solution $\rho_k \in L^1(\mathbb{R}^2) \cap L^\infty(\mathbb{R}^2) \cap H^1(\mathbb{R}^2)$ to (2.21) with the following properties:

- *conservation of mass: $\int_{\mathbb{R}^2} \rho_k dx = \int_{\mathbb{R}^2} \rho_{k-1} dx$,*
- *control of second moment: if $\int_{\mathbb{R}^2} \rho_{k-1} |x|^2 dx < \infty$ then $\int_{\mathbb{R}^2} \rho_k |x|^2 dx < \infty$.*

Proof. The proof is exactly as for Theorem 2.2 since we can formulate scheme (2.21) as

$$-\Delta \rho_k + \frac{3}{2\tau} \rho_k = \frac{1}{\tau} \left(2\rho_{k-1} - \frac{1}{2}\rho_{k-2} \right) - \operatorname{div}(\rho_k \nabla B_\beta * \rho_k),$$

and the first term on the right-hand side plays the role of ρ_{k-1} in the implicit Euler scheme. The only difference to the proof of Theorem 2.2 is that we replace ρ_k^+ in (2.7) by ρ_k , since the truncation was only needed to show the nonnegativity of ρ_k , which we are not able to show for the BDF-2 scheme. \square

Theorem 2.6 (Blow-up for the BFD-2 scheme). *Assume that $\beta \geq 0$ and*

$$\rho_0 \geq 0, \quad I_0 := \int_{\mathbb{R}^2} \rho_0(x) |x|^2 dx < \infty, \quad M := \int_{\mathbb{R}^2} \rho_0 dx > 8\pi.$$

Let $(\rho_k) \subset L^1(\mathbb{R}^2) \cap H^1(\mathbb{R}^2)$ be a sequence of nonnegative weak solutions to (2.21). Then this sequence is finite with maximal index k_{\max} , where k_{\max} is bounded from above according to (2.15) (if $\beta = 0$) or (2.16) (if $\beta > 0$ and additionally $I_0 \leq I^$ and $\tau \leq \tau^*$, where I^* and τ^* are defined in (2.14)).*

Proof. The proof is similar to that one of Theorem 2.3 but the iteration argument is different. First, let $\beta = 0$. We know from the proof of Theorem 2.3 that

$$I_1 - I_0 = -\tau\gamma, \quad (2.22)$$

where we recall that $\gamma = M(M - 8\pi)/(2\pi)$. Using the same approximation of $|x|^2$ as in step 5 of the proof of Theorem 2.3, we can justify the weak formulation (see (2.13))

$$\begin{aligned} \int_{\mathbb{R}^2} (\rho_j - \rho_{j-1})|x|^2 dx &= \frac{1}{3} \int_{\mathbb{R}^2} (\rho_{j-1} - \rho_{j-2})|x|^2 dx + \frac{8}{3}\tau \int_{\mathbb{R}^2} \rho_j dx \\ &\quad + \frac{2}{3}\tau \int_{\mathbb{R}^2} \rho_k (\nabla B_\beta * \rho_k) \cdot x dx. \end{aligned}$$

The last integral can be calculated as in the proof of Theorem 2.3 and we end up with

$$I_k - I_{k-1} = \frac{1}{3}(I_{k-1} - I_{k-2}) + \frac{2}{3} \frac{\tau}{2\pi} M(8\pi - M).$$

We iterate this identity and insert (2.22):

$$I_k - I_{k-1} = \frac{1}{3^{k-1}}(I_1 - I_0) - \frac{2}{3}\tau\gamma \sum_{j=1}^{k-1} \frac{1}{3^j} = -\frac{\tau\gamma}{3^{k-1}} - \tau\gamma \left(1 - \frac{1}{3^{k-1}}\right) = -\tau\gamma.$$

As in the proof of Theorem 2.3, this leads to a contradiction for large values of k .

Next, let $\beta > 0$. As the first step is computed with the implicit Euler scheme, the proof of Theorem 2.3 gives the estimate

$$I_1 - I_0 \leq \tau f(I_1),$$

where $f(s) = b_0\sqrt{s} - \gamma$ and $b_0 = \sqrt{\beta}M^{3/2}/\pi$. Moreover, since $f(I_0) \leq 0$, we know that $I_1 \leq I_0$, and this gives $f(I_1) \leq 0$.

For the following time steps, we obtain

$$I_k - I_{k-1} \leq \frac{1}{3}(I_{k-1} - I_{k-2}) + \frac{2\tau}{3} f(I_k), \quad k \geq 2. \quad (2.23)$$

Let us assume, by induction, that $I_{k-1} \leq I_{k-2}$ and $f(I_{k-1}) \leq 0$ for $k \geq 2$. We will prove that $I_k \leq I_{k-1}$ and $f(I_k) \leq 0$. Assume by contradiction that $f(I_k) > 0$, which is equivalent to $I_k^{1/2} > \gamma/b_0$. Then, using $I_{k-1} - I_{k-2} \leq 0$, we reformulate (2.23) as

$$\frac{I_k^{1/2} - I_{k-1}^{1/2}}{I_k^{1/2} - \gamma/b_0} \frac{I_k^{1/2} + I_{k-1}^{1/2}}{b_0} \leq \frac{2\tau}{3}.$$

Since $f(I_{k-1}) \leq 0$, the first factor is larger than or equal to one, so

$$\frac{I_k^{1/2} + I_{k-1}^{1/2}}{b_0} \leq \frac{2\tau}{3},$$

and $\tau \leq \gamma/b_0^2$ leads to

$$\frac{I_k^{1/2}}{b_0} \leq \frac{I_k^{1/2} + I_{k-1}^{1/2}}{b_0} \leq \frac{2\tau}{3} \leq \frac{2}{3} \frac{\gamma}{b_0^2}$$

or $I_k^{1/2} < \gamma/b_0$, which contradicts $f(I_k) > 0$. We conclude that $f(I_k) \leq 0$ and therefore, by (2.23), $I_k \leq I_{k-1} \leq 0$, showing the claim.

We infer that $f(I_k) \leq f(I_{k-1}) \leq \dots \leq f(I_0)$, since f is nondecreasing. Hence, again from (2.23) and using $I_1 - I_0 \leq \tau f(I_0)$,

$$\begin{aligned} I_k - I_{k-1} &\leq \frac{1}{3}(I_{k-1} - I_{k-2}) + \frac{2\tau}{3}f(I_0) \leq \frac{1}{3^{k-1}}(I_1 - I_0) + 2\tau \sum_{j=1}^{k-1} \frac{1}{3^j}f(I_0) \\ &\leq \frac{\tau}{3^{k-1}}f(I_0) + \tau \left(1 - \frac{1}{3^{k-1}}\right)f(I_0) = \tau f(I_0). \end{aligned}$$

Thus, $I_k \leq I_0 + \tau \sum_{j=1}^k f(I_0) = I_0 + \tau k f(I_0)$, and this leads to the contradiction $I_k < 0$ for sufficiently large $k \in \mathbb{N}$, completing the proof. \square

2.3.2 BDF-3 Scheme

The finite-time blow-up can be also shown for solutions to higher-order BDF schemes, at least in the case $\beta = 0$. As an example, let us consider the BDF-3 scheme

$$\frac{1}{6\tau}(11\rho_k - 18\rho_{k-1} + 9\rho_{k-2} - 2\rho_{k-3}) = \operatorname{div}(\nabla\rho_k - \rho_k\nabla B_0 * \rho_k) \quad \text{in } \mathbb{R}^2, \quad (2.24)$$

where ρ_{k-1} , ρ_{k-2} , and ρ_{k-3} are given. The existence of solutions can be shown as in Lemma 2.5. First, we prove that the scheme preserves the mass.

Lemma 2.7 (Conservation of mass). *Let ρ_0 , ρ_1 , and ρ_2 be given and having the same mass M . Then the solution ρ_k has the same mass, $\int_{\mathbb{R}^2} \rho_k dx = M$, for $k \geq 3$.*

Proof. We proceed by induction. Employing the mollified version of the cut-off function (2.11) as a test function in (2.24) and passing to the limits $\varepsilon \rightarrow 0$ and $R \rightarrow \infty$, we arrive at

$$\frac{1}{6\tau} \int_{\mathbb{R}^2} (11\rho_k - 18\rho_{k-1} + 9\rho_{k-2} - 2\rho_{k-3}) dx = 0.$$

If $k = 3$, this is equivalent to

$$\int_{\mathbb{R}^2} \rho_3 dx = \int_{\mathbb{R}^2} \left(\frac{18}{11}\rho_2 - \frac{9}{11}\rho_1 + \frac{2}{11}\rho_0 \right) dx = M,$$

since ρ_2 , ρ_1 , and ρ_0 have the same mass M . For the induction step, if ρ_{k-1} , ρ_{k-2} ,

and ρ_{k-3} for $k > 4$ have the same mass, the same argument as above shows that $\int_{\mathbb{R}^2} \rho_k = M$. \square

We recall that $I_k = \int_{\mathbb{R}^2} \rho_k |x|^2 dx$ for $k \in \mathbb{N}_0$ and $\gamma = M(M - 8\pi)/(2\pi)$.

Theorem 2.8 (Blow-up for the BDF-3 scheme). *Assume that $\beta = 0$, $I_2 - I_1 = I_1 - I_0 = -\tau\gamma$, and*

$$\rho_0 \geq 0, \quad I_0 := \int_{\mathbb{R}^2} \rho_0(x) |x|^2 dx < \infty, \quad M := \int_{\mathbb{R}^2} \rho_0 dx > 8\pi.$$

Let $(\rho_k) \subset L^1(\mathbb{R}^2) \cap H^1(\mathbb{R}^2)$ be a sequence of nonnegative weak solutions to (2.24). Then this sequence is finite with maximal index k_{\max} , where k_{\max} is bounded from above according to (2.15) (if $\beta = 0$) or (2.16) (if $\beta > 0$ and additionally $I_0 \leq I^$ and $\tau \leq \tau^*$, where I^* and τ^* are defined in (2.14)).*

Proof. We claim that $I_k - I_{k-1} = -\tau\gamma$. To prove this, we proceed by induction. Let $k = 3$. We take an approximation of $|x|^2$ as a test function in (2.24). Then, arguing as in the previous sections, we find that

$$\begin{aligned} & \frac{11}{6}(I_3 - I_2) - \frac{7}{6}(I_2 - I_1) + \frac{1}{3}(I_1 - I_0) \\ &= \frac{1}{6}(11I_3 - 18I_2 + 9I_1 - 2I_0) = \frac{\tau}{2\pi}M(8\pi - M) = -\tau\gamma. \end{aligned}$$

Since $I_2 - I_1 = I_1 - I_0 = -\tau\gamma$, it follows that

$$\frac{11}{6}(I_3 - I_2) = -\frac{7}{6}\tau\gamma + \frac{1}{3}\tau\gamma - \tau\gamma = -\frac{11}{6}\tau\gamma.$$

For the induction step, we assume that $I_{k-1} - I_{k-2} = I_{k-2} - I_{k-3} = -\tau\gamma$ for $k > 3$. Then, as above,

$$\frac{11}{6}(I_k - I_{k-1}) - \frac{7}{6}(I_{k-1} - I_{k-2}) + \frac{1}{3}(I_{k-2} - I_{k-3}) = -\tau\gamma.$$

which shows that $I_k - I_{k-1} = -\tau\gamma$. As in the proof of Theorem 2.3, this leads to a contradiction for large values of k . \square

The previous proof can be generalized to all BDF- m methods

$$\frac{1}{\tau} \sum_{i=0}^m a_i \rho_{k-i} = \operatorname{div}(\nabla \rho_k - \nabla B_\beta * \rho_k),$$

where $a_i \in \mathbb{R}$ satisfy $\sum_{i=0}^m a_i = 1$. Note, however, that only the BDF- m schemes with $m \leq 6$ are $A(\alpha)$ -stable, while they are instable for $m > 6$.

2.3.3 Runge-Kutta Schemes

The Runge-Kutta scheme reads as follows:

$$\begin{aligned} \frac{1}{\tau}(\rho_k - \rho_{k-1}) &= \sum_{i=1}^s b_i K_i, \quad K_i = \operatorname{div}(\nabla m_i - m_i \nabla B_\beta * m_i), \\ m_i &= \rho_{k-1} + \tau \sum_{j=1}^s a_{ij} K_j, \quad i = 1, \dots, s, \end{aligned} \tag{2.25}$$

where $s \in \mathbb{N}$ is the number of stages, $b_i \geq 0$ are the weights, and a_{ij} are the Runge-Kutta coefficients. We assume that $\sum_{i=1}^s b_i = 1$. The existence of solutions is only shown for two particular Runge-Kutta schemes; see below.

First, we claim that the mass is conserved in the following sense.

Lemma 2.9 (Conservation of mass). *Let $\rho_k \in L^1(\mathbb{R}^2)$ be a solution to (2.25) such that $m_i \in L^1(\mathbb{R}^2)$ and*

$$\frac{1}{\tau} \int_{\mathbb{R}^2} (\rho_k - \rho_{k-1}) \phi dx = \sum_{i=1}^s \int_{\mathbb{R}^2} b_i (m_i \Delta \phi + m_i (\nabla B_\beta * m_i) \cdot \nabla \phi) dx$$

for all $\phi \in C_0^\infty(\mathbb{R}^2)$. Then

$$\int_{\mathbb{R}^2} m_i dx = \int_{\mathbb{R}^2} \rho_k dx = \int_{\mathbb{R}^2} \rho_{k-1} dx, \quad i = 1, \dots, s.$$

Note, however, that we do not know whether $m_i \geq 0$ in \mathbb{R}^2 . Although we expect physically that ρ_k is nonnegative, this cannot be generally expected for m_i .

Proof. Using the mollifier φ^ε and the cut-of function $\phi_R(x) = \phi(|x|/R)$, where ϕ is defined in (2.11), as a test function in the weak formulation of the equation for K_i and performing the limit $\varepsilon \rightarrow 0$, we find that

$$\int_{\mathbb{R}^2} K_i \phi_R dx = \int_{\mathbb{R}^2} m_i \Delta \phi_R dx + \int_{\mathbb{R}^2} m_i (\nabla B_\beta * m_i) \cdot \nabla \phi_R dx.$$

According to (2.12), the first term on the right-hand side can be estimated as

$$\left| \int_{\mathbb{R}^2} m_i \Delta \phi_R dx \right| \leq \frac{C_2}{R^2} \|m_i\|_{L^1(\mathbb{R}^2)}.$$

For the second term, we use formulation (2.3) of ∇B_β , the symmetry argument, and

the Lipschitz estimate (2.12) for $\nabla\phi_R$, which leads to

$$\begin{aligned} & \left| \int_{\mathbb{R}^2} m_i(\nabla B_\beta * m_i) \cdot \nabla\phi_R dx \right| \\ &= \frac{1}{2} \left| \int_{\mathbb{R}^2} m_i(x) \int_{\mathbb{R}^2} (\nabla\phi_R(x) - \nabla\phi_R(y)) \cdot \frac{x-y}{|x-y|} g_\beta(|x-y|) m_i(y) dy dx \right| \\ &\leq \frac{C_1}{2R^2} \int_{\mathbb{R}^2} |m_i(x)| \int_{\mathbb{R}^2} |m_i(y)| dy dx = \frac{C_1}{2R^2} \|m_i\|_{L^1(\mathbb{R}^2)}^2. \end{aligned}$$

We deduce that for $R \rightarrow \infty$, $\int_{\mathbb{R}^2} K_i dx = 0$. Hence,

$$\begin{aligned} \int_{\mathbb{R}^2} m_i dx &= \int_{\mathbb{R}^2} \rho_{k-1} dx + \tau \sum_{j=1}^s a_{ij} \int_{\mathbb{R}^2} K_j dx = \int_{\mathbb{R}^2} \rho_{k-1} dx, \\ \int_{\mathbb{R}^2} \rho_k dx &= \int_{\mathbb{R}^2} \rho_{k-1} + \tau \sum_{i=1}^s b_i \int_{\mathbb{R}^2} K_i dx = \int_{\mathbb{R}^2} \rho_{k-1} dx, \end{aligned}$$

which concludes the proof. \square

We are able to show finite-time blow-up for all Runge-Kutta schemes if $\beta = 0$.

Theorem 2.10 (Blow-up for Runge-Kutta schemes). *Let $\beta = 0$. Assume that*

$$\rho_0 \geq 0, \quad I_0 := \int_{\mathbb{R}^2} \rho_0(x) |x|^2 dx < \infty, \quad M := \int_{\mathbb{R}^2} \rho_0 dx > 8\pi.$$

Let $(\rho_k) \subset L^1(\mathbb{R}^2) \cap H^1(\mathbb{R}^2)$ be a sequence of nonnegative weak solutions to (2.25). Then this sequence is finite with maximal index k_{\max} defined in (2.15).

Proof. Using an approximation of $|x|^2$ as a test function in (2.25) and passing to the de-regularization limit (see step 5 of the proof of Theorem 2.3), we find that

$$I_k - I_{k-1} = \tau \sum_{i=1}^s b_i \left(4 \int_{\mathbb{R}^2} m_i dx - \frac{1}{\pi} \int_{\mathbb{R}^2} m_i(x) \int_{\mathbb{R}^2} \frac{x \cdot (x-y)}{|x-y|^2} m_i(y) dy dx \right).$$

By Lemma 2.9, the symmetry argument, and $\sum_{i=1}^s b_i = 1$,

$$\begin{aligned} I_k - I_{k-1} &= \tau \sum_{i=1}^s b_i \left(4M - \frac{1}{2\pi} \int_{\mathbb{R}^2} m_i(x) \int_{\mathbb{R}^2} m_i(y) dy dx \right) \\ &= \tau \sum_{i=1}^s b_i \left(4M - \frac{M^2}{2\pi} \right) = \frac{M}{2\pi} (8\pi - M). \end{aligned}$$

Now, we argue as in the proof of Theorem 2.3 to conclude. \square

The case $\beta > 0$ is more delicate since $m_i \geq 0$ is generally not guaranteed. Indeed, it follows that (see (2.17) and (2.18))

$$\begin{aligned} I_k - I_{k-1} &= \tau \sum_{i=1}^s b_i \left(\frac{M}{2\pi} (8\pi - M) + \frac{1}{2\pi} \int_{\mathbb{R}^2} \int_{\mathbb{R}^2} (1 - g_\beta(|x - y|)) m_i(x) m_i(y) dy dx \right) \\ &\leq \tau \sum_{i=1}^s b_i \left(-\gamma + \frac{\sqrt{\beta}}{2\pi} M \int_{\mathbb{R}^2} |y| |m_i(y)| dy \right), \end{aligned}$$

where we recall that $\gamma = M(M - 8\pi)/(2\pi)$. By the Cauchy-Schwarz inequality,

$$I_k - I_{k-1} \leq \tau \sum_{i=1}^s b_i \left\{ -\gamma + \frac{\sqrt{\beta}}{2\pi} M \left(\int_{\mathbb{R}^2} |m_i(y)| dy \right)^{1/2} \left(\int_{\mathbb{R}^2} |y|^2 |m_i(y)| dy \right)^{1/2} \right\},$$

and this cannot be estimated further as $m_i \geq 0$ may not hold. However, for the midpoint and trapezoidal rule, we are able to give a result. The reason is that these schemes can be reformulated in terms of ρ_k, ρ_{k-1} , etc. without the use of m_i . Clearly, we still need to assume that $\rho_k \geq 0$ but this is expected physically.

Implicit Midpoint Rule

The implicit midpoint rule is defined by $s = 1$, $a_{11} = 1/2$, and $b_1 = 1$. Then (2.25) becomes

$$\begin{aligned} \frac{1}{\tau}(\rho_k - \rho_{k-1}) &= \operatorname{div}(\nabla m_1 - m_1 \nabla B_\beta * m_1), \\ m_1 &= \rho_{k-1} + \frac{\tau}{2} \operatorname{div}(\nabla m_1 - m_1 \nabla B_\beta * m_1), \end{aligned}$$

and since $m_1 = \frac{1}{2}(\rho_k + \rho_{k-1})$, this can be rewritten as

$$\frac{1}{\tau}(\rho_k - \rho_{k-1}) = \operatorname{div} \left(\nabla \left(\frac{\rho_k + \rho_{k-1}}{2} \right) - \frac{\rho_k + \rho_{k-1}}{2} \nabla B_\beta * \frac{\rho_k + \rho_{k-1}}{2} \right). \quad (2.26)$$

Lemma 2.11 (Existence for the midpoint scheme). *Let $\beta \geq 0$, $\rho_{k-1} \in W^{1,1}(\mathbb{R}^2) \cap W^{1,\infty}(\mathbb{R}^2)$, and*

$$\tau \leq \frac{2}{(\pi + \frac{1}{2})^2} \frac{1}{(\|\rho_{k-1}\|_X + \frac{\pi b}{2} \|\rho_{k-1}\|_X^2 + \frac{\pi}{2} \|\nabla \rho_{k-1}\|_X + 1)^4}.$$

Then there exists a unique weak solution $\rho_k \in L^1(\mathbb{R}^2) \cap L^\infty(\mathbb{R}^2) \cap H^1(\mathbb{R}^2)$ to (2.26) with the following properties:

- *conservation of mass: $\int_{\mathbb{R}^2} \rho_k dx = \int_{\mathbb{R}^2} \rho_{k-1} dx$,*

- control of second moment: if $\int_{\mathbb{R}^2} \rho_{k-1} |x|^2 dx < \infty$ then $\int_{\mathbb{R}^2} \rho_k |x|^2 dx < \infty$.

Moreover, if $\beta > 0$ and $\rho_{k-1} \in Y := W^{1,1}(\mathbb{R}^2) \cap W^{1,\infty}(\mathbb{R}^2) \cap H^3(\mathbb{R}^2)$, then $\rho_k \in Y$.

Note that our technique of proof requires higher regularity for ρ_{k-1} compared to the implicit Euler scheme. For general Runge-Kutta schemes, the regularity requirement becomes even stronger, which is the reason why we show existence results only in special cases.

Proof. We set $\rho := \rho_k$ and $\rho_0 := \rho_{k-1}$. For given $\tilde{\rho} \in X$, we solve the linear problem

$$\left(-\Delta + \frac{2}{\tau}\right)\rho = \frac{2}{\tau}\rho_0 + \operatorname{div}\left(\nabla\rho_0 - \frac{1}{2}(\tilde{\rho} + \rho_0)\nabla B_\beta * (\tilde{\rho} + \rho_0)\right) \quad \text{in } \mathbb{R}^2.$$

By Lemma A.3, this problem has a unique solution $n \in H^1(\mathbb{R}^2)$, and it can be represented by

$$T[\tilde{\rho}] := \rho = \frac{2}{\tau}B_{2/\tau} * \rho_0 + \nabla B_{2/\tau} * \nabla\rho_0 - \frac{1}{2}\nabla B_{2/\tau} * ((\tilde{\rho} + \rho_0)\nabla c[\tilde{\rho} + \rho_0]), \quad (2.27)$$

writing $\nabla c[\rho] = \nabla B_\beta * \rho$ as in Section 2.2. This defines the fixed-point operator $T : S \rightarrow S$, where $S = \{\rho \in X : \|\rho\|_X \leq C_B\}$ and

$$C_B = \|\rho_0\|_X + \frac{\pi b}{2}\|\rho_0\|_X^2 + \frac{\pi}{2}\|\nabla\rho_0\|_X + 1.$$

It holds $T(S) \subset S$ since, using similar arguments as in the proof of Theorem 2.2 and the smallness condition on τ ,

$$\begin{aligned} \|T[\rho]\|_X &\leq \frac{2}{\tau}\|B_{2/\tau}\|_{L^1(\mathbb{R}^2)}\|\rho_0\|_X + \|\nabla B_{2/\tau}\|_{L^1(\mathbb{R}^2)}\|\nabla\rho_0\|_X \\ &\quad + \frac{1}{2}\|\nabla B_{2/\tau}\|_{L^1(\mathbb{R}^2)}\|\rho + \rho_0\|_X\|\nabla c[\rho + \rho_0]\|_X \\ &\leq \|\rho_0\|_X + \frac{\pi\sqrt{\tau}}{2\sqrt{2}}\|\nabla\rho_0\|_X + \frac{\pi b\sqrt{\tau}}{4\sqrt{2}}\|\rho + \rho_0\|_X^2 \\ &\leq C_B. \end{aligned}$$

We claim that $T : S \rightarrow S$ is a contraction. Indeed, let $\rho, \bar{\rho} \in S$. Then

$$\begin{aligned} \|T[\rho] - T[\bar{\rho}]\|_X &\leq \frac{1}{2} \left\| \nabla B_{2/\tau} * (\rho + \rho_0) \nabla B_\beta * (\rho + \rho_0) \right. \\ &\quad \left. - \nabla B_{2/\tau} * (\bar{\rho} + \rho_0) \nabla B_\beta * (\bar{\rho} + \rho_0) \right\|_X \\ &\leq \frac{\pi\sqrt{\tau}}{4\sqrt{2}} \left\| (\rho + \rho_0) \nabla B_\beta * (\rho + \rho_0) - (\bar{\rho} + \rho_0) \nabla B_\beta * (\bar{\rho} + \rho_0) \right\|_X \\ &\leq \frac{\pi\sqrt{\tau}}{4\sqrt{2}} \left(\|\rho \nabla B_\beta * \rho - \bar{\rho} \nabla B_\beta * \bar{\rho}\|_X \right. \\ &\quad \left. + \|\rho_0 \nabla B_\beta * (\rho - \bar{\rho})\|_X + \|(\rho - \bar{\rho}) \nabla B_\beta * \rho_0\|_X \right) \\ &\leq \frac{\pi b\sqrt{\tau}}{\sqrt{2}} (C_B + 1) \|\rho - \bar{\rho}\|_X, \end{aligned}$$

and we have $\pi b\sqrt{\tau}(C_B + 1)/2 < 1$. The Banach fixed-point theorem now implies that there exists a unique fixed point $\rho \in X$.

By the same arguments used in step 2 of the proof of Theorem 2.2, we infer that $\rho_k \in H^1(\mathbb{R}^2)$. Steps 4 and 5 show the conservation of mass and the finiteness of the second moment.

It remains to show that if $\rho_{k-1} \in Y$ then ρ_k has the same regularity. By Lemma A.1, $\rho_k \in H^1(\mathbb{R}^2)$ implies that $\nabla B_\beta * \rho_k \in H^2(\mathbb{R}^2)$. Therefore,

$$\left(-\Delta + \frac{2}{\tau} \right) \rho_k = \frac{2}{\tau} \rho_{k-1} + \Delta \rho_{k-1} - \operatorname{div}((\rho_k + \rho_{k-1}) \nabla c[\rho_k]) \in L^2(\mathbb{R}^2).$$

Elliptic regularity then gives $\rho_k \in H^2(\mathbb{R}^2)$. We bootstrap this argument to find that $\rho_k \in H^3(\mathbb{R}^2) \hookrightarrow W^{1,\infty}(\mathbb{R}^2)$. Taking the L^1 norm of the gradient of $\rho = \rho_k$ in (2.27) shows that $\|\nabla \rho_k\|_{L^1(\mathbb{R}^2)}$ can be estimated in terms of the H^3 norms of ρ_k, ρ_{k-1} , and $c[\rho_k]$. We conclude that $\rho_k \in W^{1,1}(\mathbb{R}^2)$, finishing the proof. \square

Lemma 2.12 (Blow-up for the midpoint scheme). *Let $\beta > 0$. Assume that*

$$\rho_0 \geq 0, \quad I_0 := \int_{\mathbb{R}^2} \rho_0(x) |x|^2 dx < \infty, \quad M := \int_{\mathbb{R}^2} \rho_0 dx > 8\pi.$$

Let $(\rho_k) \subset L^1(\mathbb{R}^2) \cap H^1(\mathbb{R}^2)$ be a sequence of nonnegative weak solutions to (2.26). Suppose that $I_0 \leq I^$ and $\tau \leq 2\tau^*$ (see (2.14)). Then this sequence is finite with maximal index k_{\max} defined in (2.16).*

Proof. Approximating $|x|^2$ as in step 5 of the proof of Theorem 2.3 and using the

nonnegativity of ρ_k and ρ_{k-1} , we can estimate as

$$\begin{aligned}
 I_k - I_{k-1} &= \int_{\mathbb{R}^2} (\rho_k - \rho_{k-1})|x|^2 dx \\
 &= 4\tau M - \frac{\tau}{2} \int_{\mathbb{R}^2} (\rho_k + \rho_{k-1}) \nabla B_\beta * (\rho_k + \rho_{k-1}) dx \\
 &= -\tau\gamma + \frac{\tau}{4\pi} \int_{\mathbb{R}^2} \int_{\mathbb{R}^2} (1 - g_\beta(|x-y|)) (\rho_k + \rho_{k-1})(x) (\rho_k + \rho_{k-1})(y) dy dx \\
 &\leq -\tau\gamma + \frac{\tau}{4\pi} \sqrt{\beta} \int_{\mathbb{R}^2} \int_{\mathbb{R}^2} |x-y| (\rho_k + \rho_{k-1})(x) (\rho_k + \rho_{k-1})(y) dy dx \\
 &\leq -\tau\gamma + \frac{\tau}{4\pi} \sqrt{\beta} (2M) M^{1/2} (I_k^{1/2} + I_{k-1}^{1/2}) = -\tau\gamma + \frac{b_0}{2} (I_k^{1/2} + I_{k-1}^{1/2}).
 \end{aligned}$$

Setting again $f(s) = b_0\sqrt{s} - \gamma$, it follows that

$$I_k - I_{k-1} \leq \frac{\tau}{2} (f(I_k) + f(I_{k-1})).$$

Again, since $f(I^*) = 0$ and f is increasing, we have $f(I_0) \leq 0$. Let $f(I_{k-1}) \leq 0$. Then

$$I_k - I_{k-1} \leq \frac{\tau}{2} f(I_k),$$

and we can proceed as in the proof of Theorem 2.3. \square

Trapezoidal Rule

The (implicit, two-stage) trapezoidal rule is defined by $s = 2$, $a_{11} = a_{12} = \frac{1}{2}$, $b_1 = b_2 = \frac{1}{2}$, which gives the scheme

$$\frac{1}{\tau} (\rho_k - \rho_{k-1}) = \frac{1}{2} \operatorname{div} (\nabla(\rho_k + \rho_{k-1}) + \rho_k \nabla B_\beta * \rho_k + \rho_{k-1} \nabla B_\beta * \rho_{k-1}). \quad (2.28)$$

The existence of weak solutions can be shown exactly as in the proof of Lemma 2.11, therefore we leave the details to the reader.

Proposition 2.13 (Finite-time blow-up for the trapezoidal rule). *Let $\beta > 0$. Assume that*

$$\rho_0 \geq 0, \quad I_0 := \int_{\mathbb{R}^2} \rho_0(x) |x|^2 dx < \infty, \quad M := \int_{\mathbb{R}^2} \rho_0 dx > 8\pi.$$

Let (ρ_k) be a sequence of nonnegative weak solutions to (2.28). Suppose that $I_0 \leq I^$ and $\tau \leq \tau^*$ (see (2.14)). Then this sequence is finite with maximal index k_{\max} defined in (2.16).*

Proof. Arguing as in the previous blow-up proofs, we obtain

$$\begin{aligned}
 I_k - I_{k-1} &= 4\tau M - \frac{\tau}{2} \int_{\mathbb{R}^2} \rho_k \nabla B_\beta * \rho_k dx - \frac{\tau}{2} \int_{\mathbb{R}^2} \rho_{k-1} \nabla B_\beta * \rho_{k-1} dx \\
 &\leq -\tau\gamma + \frac{\tau}{4\pi} \sqrt{\beta} \int_{\mathbb{R}^2} \int_{\mathbb{R}^2} |x - y| \rho_k(y) \rho_k(x) dy dx \\
 &\quad + \frac{\tau}{4\pi} \sqrt{\beta} \int_{\mathbb{R}^2} \int_{\mathbb{R}^2} |x - y| \rho_{k-1}(y) \rho_{k-1}(x) dy dx \\
 &\leq -\tau\gamma + \frac{\tau}{4\pi} \sqrt{\beta} M^{3/2} (I_k^{1/2} + I_{k-1}^{1/2}).
 \end{aligned}$$

Now, we proceed as in the proof of Proposition 2.12. □

Remark 2.14 (Explicit schemes). One may ask to what extent explicit schemes may be considered too. The implicit Euler schemes provides the nonnegativity of the cell density ρ_k , which generally cannot be proven for the explicit Euler scheme. Clearly, we assumed nonnegativity of ρ_k for higher-order implicit schemes, so, this argument does not apply to higher-order explicit schemes. In fact, the virial argument can be applied to explicit Runge-Kutta schemes as well, with the same blow-up conditions (for $\beta = 0$), since the analysis applies to *all* (explicit or implicit) Runge-Kutta schemes. On the other hand, BDF schemes are always implicit. Practically, implicit schemes help to handle the stiff part of the differential equation; recall, however, that there do not exist SSP *implicit* higher-order Runge-Kutta or multistep methods.

2.4 Numerical Examples

The numerical experiments are performed by using the finite-element method introduced by Saito in [122] and analyzed in [124]. In contrast to [122], we choose higher-order temporal approximations. The scheme uses a first-order upwind technique for the drift term, the lumped mass method, and a decoupling procedure. We take $\beta = 1$ in (2.1) and consider bounded domains only. Equations (2.1) are supplemented with no-flux boundary conditions. In the first example, the domain is large enough to avoid effects arising from boundary conditions. The second example, on the other hand, illustrates blow-up at the boundary.

2.4.1 Numerical Scheme

Let \mathcal{T}_h be a triangulation of the bounded set $\Omega \subset \mathbb{R}^2$, where $h = \max\{\text{diam}(K) : K \in \mathcal{T}_h\}$, and let D_i be the barycentric domain associated with the vertex P_i ; see [122, Section 2] for the definition. Let χ_i be the characteristic function on D_i and let Y_h be the span of all χ_i . Furthermore, let X_h be the space of linear finite elements. The

lumping operator $M_h : X_h \rightarrow Y_h$ is defined by $M_h v_h = \sum_i v_h(P_i) \chi_i$, where $v_h \in X_h$, and the mass-lumped inner product is given by

$$(v_v, w_h)_h = (M_h v_h, M_h w_h)_2, \quad v_h, w_h \in X_h,$$

where $(\cdot, \cdot)_2$ is the L^2 inner product.

For the discretization of the drift term, we define the discrete Green operator $G_h : X_h \rightarrow X_h$ as the unique solution $v_h = G_h f_h \in X_h$ to

$$(\nabla v_h, \nabla w_h)_2 + (v_h, w_h)_2 = (f_h, w_h)_2 \quad \text{for } w_h \in X_h.$$

(Recall that $\beta = 1$.) The drift term is approximated by the trilinear form $b_h : X_h^3 \rightarrow \mathbb{R}$,

$$b_h(u_h, v_h, w_h) = \sum_i w_h(P_i) \sum_{P_j \in \Lambda_i} (v_h(P_i) \beta_{ij}^+(u_h) - v_h(P_j) \beta_{ij}^-(u_h)),$$

where Λ_i is the set of vertices P_j that share an edge with P_i . For the definition of β_{ij}^\pm , we first introduce the set S_h^{ij} of all elements $K \in \mathcal{T}_h$ such that $P_i, P_j \in K$ and the exterior normal vector ν_{ij} to $\partial D_i \cap \partial D_j$ with respect to D_i . Then

$$\beta_{ij}^\pm(u_h) = \sum_{K \in S_h^{ij}} \text{meas}((\partial D_i \cap \partial D_j)|_K) [(\nabla G_h u_h)|_K \cdot \nu_{ij}|_K]_\pm,$$

where $[s]_\pm = \max\{0, \pm s\}$ for $s \in \mathbb{R}$. It is explained in [122] that the trilinear form approximates the integral $\int_\Omega v \nabla(Gu) \cdot \nabla w dx$, where Gu is the Green operator associated with $-\Delta + 1$ on L^2 .

Equation (2.2) is solved in a semi-implicit way. This means, for the BDF-2 scheme and for given u_h , that we solve the linear problem

$$\frac{1}{\tau} \left(\frac{3}{2} \rho_h^k - 2 \rho_h^{k-1} + \frac{1}{2} \rho_h^{k-2}, w_h \right)_h + (\nabla \rho_h^k, \nabla w_h)_2 + b_h(u_h, \rho_h^k, w_h) = 0 \quad (2.29)$$

for all $w_h \in X_h$. Here, ρ_h^k is an approximation of $\rho(\cdot, \tau k)$. This defines the solution operator $N(u_h) = \rho_h$ and the scheme is completed by choosing u_h . Saito has taken $u_h = \rho_h^{k-1}$, giving the usual semi-implicit scheme of first order. For higher-order schemes, we need to iterate. For this, we introduce the iteration $u_h^{(0)} := \rho_h^{k-1}$ and $u_h^{(m)} := N(u_h^{(m-1)})$ for $m \geq 1$. The iteration stops when $\|u_h^{(m)} - u_h^{(m-1)}\|_{L^\infty(\mathbb{R}^2)} < \varepsilon$ for some tolerance $\varepsilon > 0$ or if $m \geq m_{\max}$ for a maximal number m_{\max} of iterations. For later reference, we write scheme (2.29) as

$$\frac{1}{\tau} M_h (3 \rho_h^k - 4 \rho_h^{k-1} + \rho_h^{k-2}) = 2(A_h + B_h(\rho_h^k)) \rho_h^k, \quad (2.30)$$

where M_h is the lumped mass matrix, A_h the stiffness matrix, $B_h(\rho_h^k)$ the upwind

matrix, and ρ_h^k is the solution vector at time step k after the Picard iteration has terminated.

In a similar way, we define the scheme with the midpoint discretization:

$$\frac{1}{\tau}(\rho_h^k - \rho_h^{k-1}, w_h)_h + \frac{1}{2}(\nabla(\rho_h^k + \rho_h^{k-1}), \nabla w_h)_2 + \frac{1}{4}b_h(u_h + \rho_{k-1}, \rho_h^k + \rho_h^{k-1}, w_h) = 0$$

for all $w_h \in X_h$. The resulting linear systems are computed by using MATLAB. We choose the domain $\Omega = (0, 1)^2$, which is triangulated uniformly by $2a^2$ triangles with maximal size $h = \sqrt{2}/a$. The numerical parameters are $a = 64$, $\tau = 5 \cdot 10^{-5}$, $\varepsilon = 10^{-4}$, and $m_{\max} = 500$ if not stated otherwise. (In all presented simulations, the maximal number of iterations was $m = 17$, i.e., m_{\max} was never reached.)

2.4.2 Numerical Results

To illustrate the behavior of the solutions, we choose the initial data as a linear combination of the shifted Gaussians

$$W_{x_0, y_0}(x, y) = \frac{M}{2\pi\theta} \exp\left(-\frac{(x - x_0)^2 + (y - y_0)^2}{2\theta}\right),$$

where $(x_0, y_0) \in (0, 1)^2$, $M > 0$, and $\theta > 0$. Clearly, the mass of W_{x_0, y_0} equals M . For the first example, we choose $\theta = 1/500$, $M = 6\pi$, and

$$\rho_0 = W_{0.33, 0.33} + W_{0.33, 0.66} + W_{0.66, 0.33} + W_{0.66, 0.66}.$$

The initial mass is $24\pi > 8\pi$ and thus, we expect the solutions to blow up in finite time.

Figure 2.1 shows the cell density $\rho(x, t)$ at various time instances computed from the BDF-2 scheme. As expected, the solution blows up in finite time in the center of the domain. Note that the numerical solution is always nonnegative and conserve the total mass.

A nonsymmetric situation is given by the initial data

$$\rho_0 = \frac{1}{3}W_{0.33, 0.66} + \frac{1}{2}W_{0.33, 0.33} + W_{0.66, 0.66},$$

taking $\theta = 1/500$, $M = 6\pi$, and the same numerical parameters as above. The total mass of ρ_0 is 11π , so we expect again blow up of the solutions. This is illustrated in Figure 2.2. The solution aggregates, moves to the boundary and blows up. Again, the discrete solution stays nonnegative and conserves the mass.

We remark that boundary blow-up was analyzed in [129]; also see the presentation in [138, Theorem 5.1]. The proof uses a localized symmetrization argument, which possibly can be extended to a semi-discrete implicit Euler scheme.

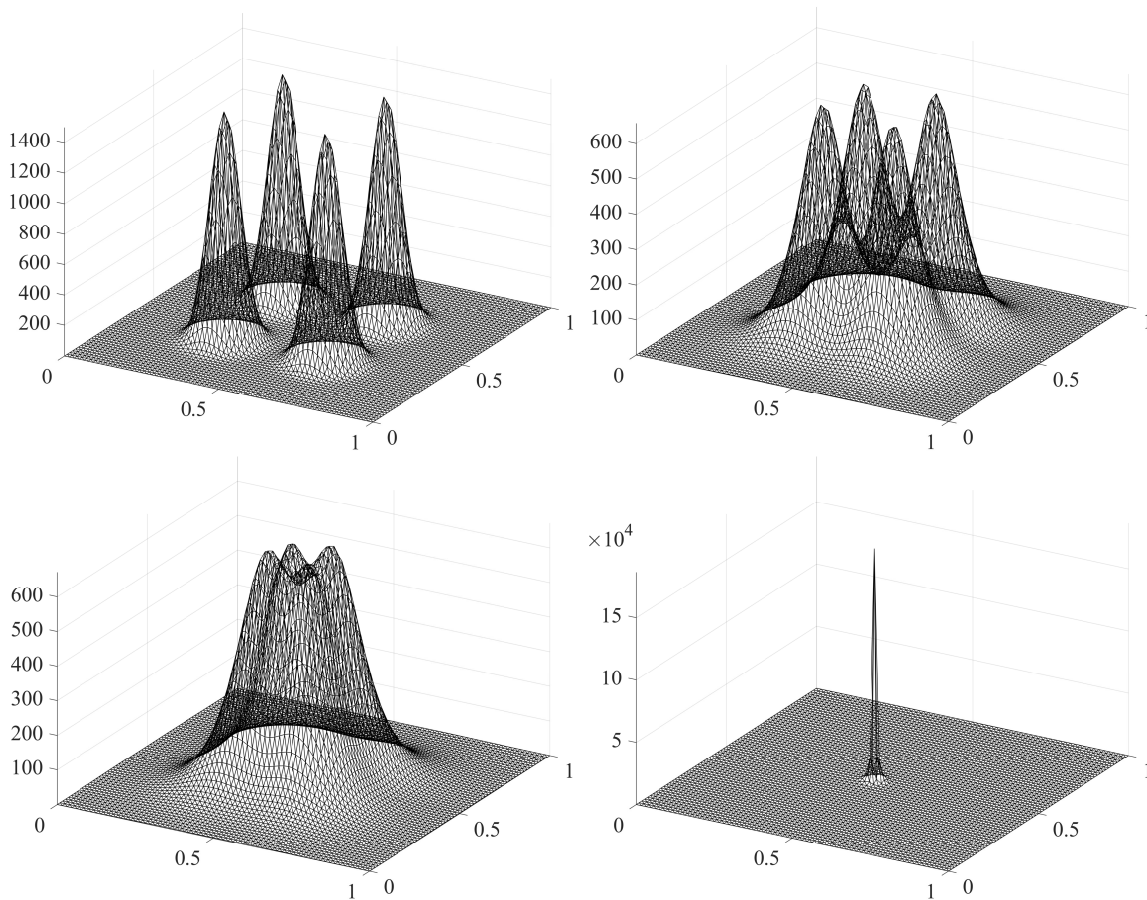


Figure 2.1: Cell density computed from the BDF-2 scheme at times $t = 0$ (top left), $t = 0.005$ (top right), $t = 0.007$ (bottom left), $t = 0.02$ (bottom right).

2.4.3 Convergence Rate

To calculate the temporal convergence rates and to show that the schemes are indeed of second order, we compute a reference solution ρ_{ref} with the very small time step $\tau = 10^{-6}$ and compare it in various L^p norms with the solutions ρ_τ using larger time step sizes τ . We choose the same initial datum as in the first example with $M = 24\pi$. Figure 2.3 shows the L^p error

$$e_p = \|\rho_\tau(\cdot, T) - \rho_{\text{ref}}(\cdot, T)\|_{L^p(\Omega)},$$

where the end time $T = 0.01$ is chosen such that the density already started to aggregate but blow up still did not happen. As expected, the L^p errors are approximately of second order.

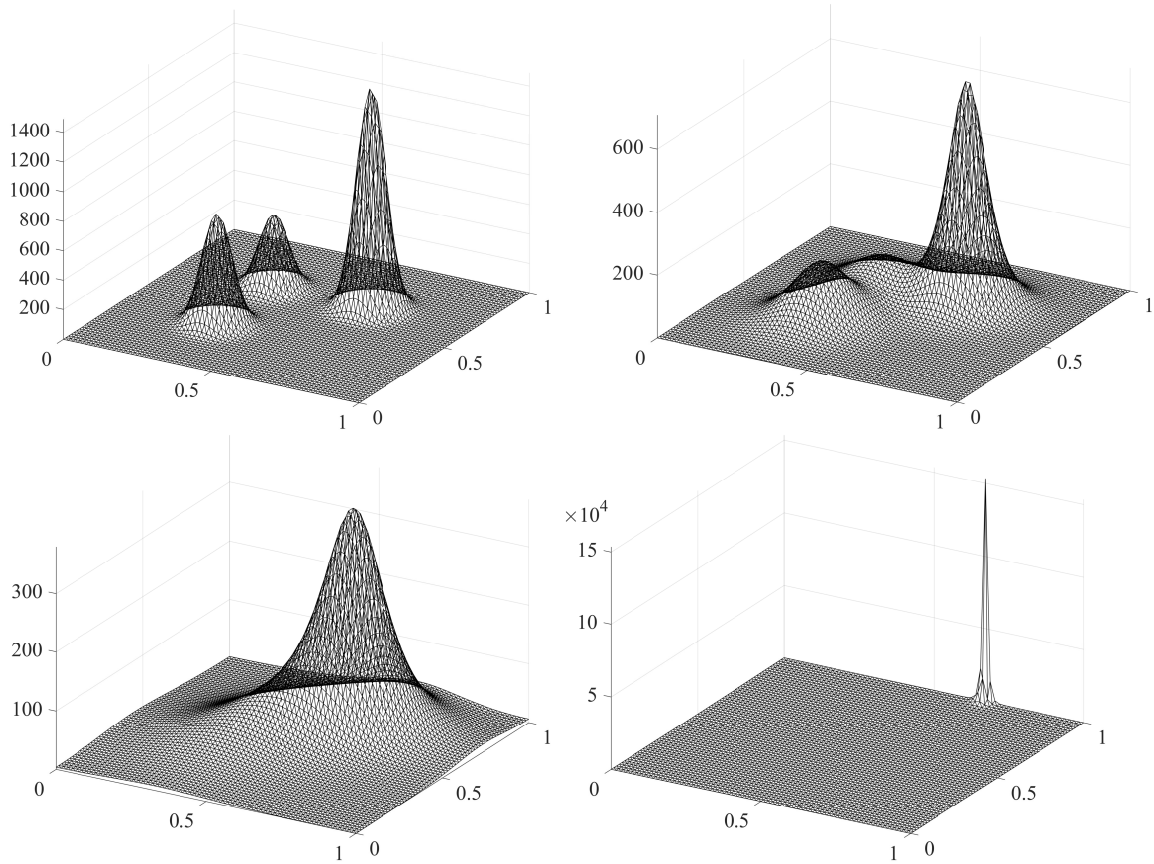


Figure 2.2: Cell density computed from the BDF-2 scheme at times $t = 0$ (top left), $t = 0.005$ (top right), $t = 0.02$ (bottom left), $t = 0.1001$ (bottom right).

2.4.4 Numerical Blow-up

We demonstrate that the bound for the blow-up time $T^* = \tau k_{\max}$ derived in the time-discrete situation can serve as a bound for the numerical blow up. It is well known that the computation of the numerical blow-up time is rather delicate. For instance, Chertock et al. [33] use the L^∞ norm of the density as a measure of the numerical blow-up time, since $\|\rho\|_{L^\infty(\Omega)}$ is proportional to h^2 (recall that h is the spatial grid size). Numerical blow-up may be reached, for instance, when the numerical solution becomes negative [32, 136] or when the second moment becomes negative [70]. However, since our scheme conserves the mass and the grid is finite, the numerical solution cannot blow up in the L^∞ norm. Instead, the solution converges to a state where the mass concentrates at certain points and no further growth is possible. Moreover, the second moment cannot become negative, provided nonnegativity is preserved (also see below). A lower bound for the blow-up time was derived in, for instance, [52, Theorem 2.2] in two space dimensions (but with a non explicit bound)

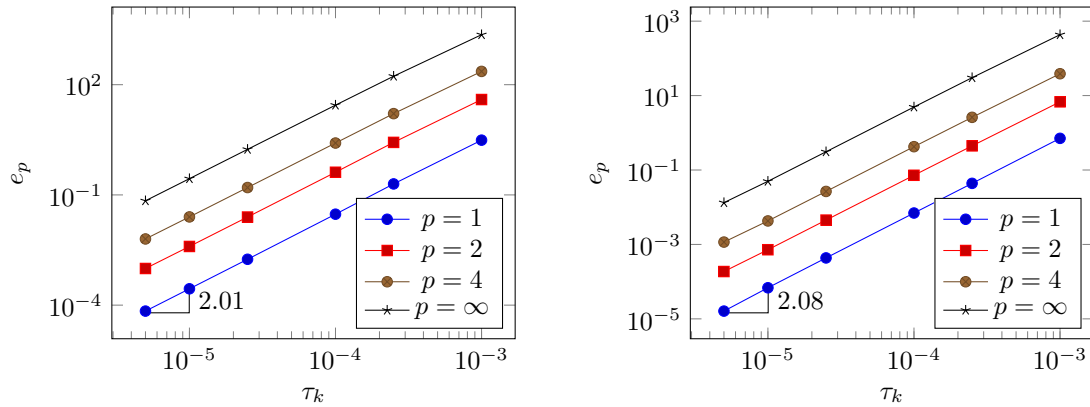


Figure 2.3: L^p error e_p for $p = 1, 2, 4, \infty$ at time $T = 0.01$ for various time step sizes $\tau_k = \tau$ (left: BDF-2 discretization; right: midpoint discretization).

and in [23, Prop. 3.1] in three space dimensions.

For the numerical test, we choose the initial datum $\rho_0 = W_{1,1}$ on the domain $\Omega = (0, 2)^2$ with parameters $\theta = 1/500$, $M = 30\pi$, and $\tau = 10^{-5}$. The grid sizes are $h = 0.02, 0.04, 0.08$. The initial density and the density at $k = 44$ are displayed in Figure 2.4. The density almost does not change for time steps $k > 44$.

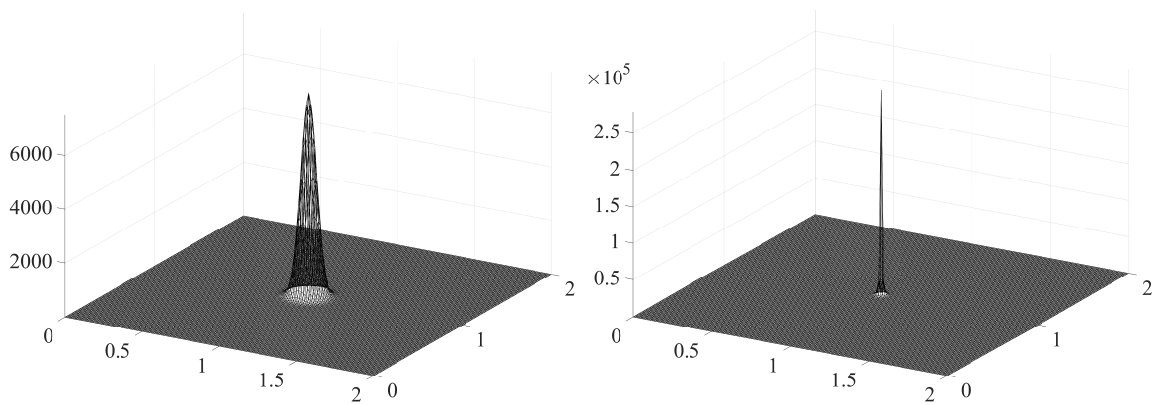


Figure 2.4: Cell density at time step $k = 0$ (left) and $k = k_{\max} = 44$. The mesh size is $h = 0.02$.

It seems that the solution to the fully discrete semi-implicit scheme exists numerically for all time. Saito observed in [123, p. 144] that his finite-element solution never blows up in finite time, and he argued that this is because of the preservation

of the L^1 norm. Note that he employed scheme (2.29) with $u_h = \rho_h^{k-1}$, while we used a Picard iteration in order to achieve second-order convergence. In fact, the solution in Figure 2.4 seems to be the steady state of the discrete nonlinear system (2.30). This is indicated by the behavior of the residuum $R_k = 2\|A_h \rho_h^k + B_h(\rho_h^k) \rho_h^k\|_{\ell^\infty}$, illustrated in Figure 2.5. The residuum tends to zero for increasing time steps k . This behavior is in contrast to the analytical results, where finite-time blow up occurs for *semi-discrete* solutions. Figure 2.6 illustrates the evolution of $\|\rho_k\|_{L^\infty(\Omega)}$ and I_k . The vertical line marks the bound k_{\max} from (2.16). We observe that the L^∞ norm and the second moment reach a limit close to k_{\max} .

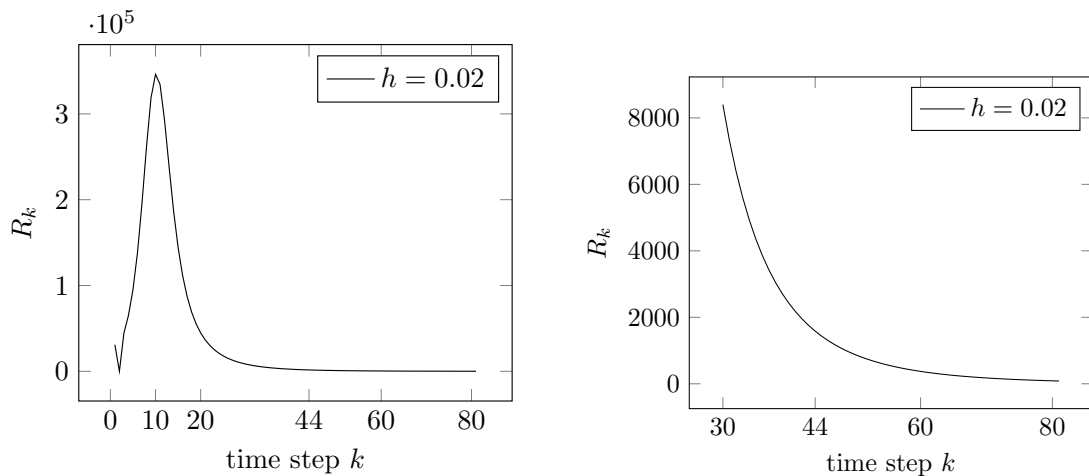


Figure 2.5: The residuum R_k for time steps 1 to 81 (left) and time steps 30 to 81 (right) versus time steps k .

For coarse meshes or large time steps, the numerical scheme may produce solutions with negative values. As an example, we take $\tau = 10^{-3}$ and $h = 0.02$ and choose an initial datum with steep gradients,

$$\rho_0(x, y) = \begin{cases} 250\pi & \text{for } \frac{1}{3} < x, y < \frac{2}{3}, \\ 0 & \text{else;} \end{cases}$$

see Figure 2.7 (top left). For small times, the solution becomes negative around the steep gradient, but the regions with negative values disappear for larger times. This is confirmed in the plot L^1 norm over time, where the L^1 norm is larger than the total mass in a certain time interval due to the negative values (note that $\|\rho\|_{L^1(\Omega)} \neq \int_{\Omega} \rho dx$ for functions $\rho : \Omega \rightarrow \mathbb{R}$). The total mass stays constant over time. It seems to be natural to obtain negative values, since higher-order in time schemes usually require

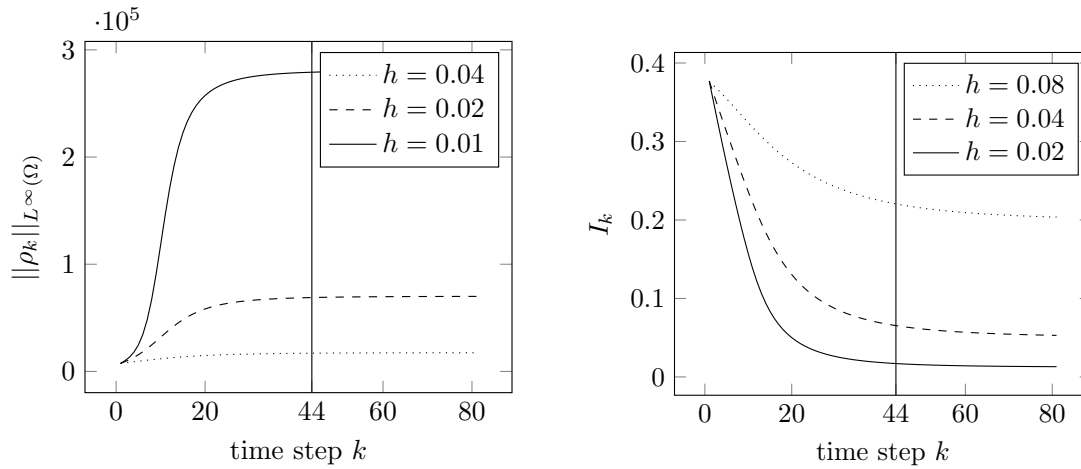


Figure 2.6: L^∞ norm $\|\rho_k\|_{L^\infty(\Omega)}$ (left) and second moment I_k (right) versus time. The vertical line marks the upper bound k_{\max} defined in (2.16).

a CFL-type condition to remain nonnegative [13]. However, after some time, the L^1 norm stabilizes and equals the total mass again.

2.5 Discussion and Outlook

Discussion

The main focus in this chapter lies on the extension of the fundamental blow-up argument for the Keller–Segel system, the virial inequality, to the semi-discrete case in time. We cluster the discussion of the results in this chapter into the semi-discrete and the fully discrete part.

Semi-Discrete Results:

The existence of discrete-in-time solutions was proven for implicit Euler, BDF and implicit Runge-Kutta schemes via a fixed point argument. Observe that the existence results do not require the condition $M < 8\pi$, since they are local. In addition, the smallness condition on τ is natural, and the time step needs to be chosen smaller and smaller when the blow-up time is approached. Furthermore, we have shown the conservation of mass and the virial inequality for these methods. Unfortunately, only the implicit Euler method guarantees nonnegativity of the solution if the previous time step was in L^∞ . Nevertheless, we have proven an upper bound for the maximal number of time steps, i.e a maximum time of existence for nonnegative solutions of

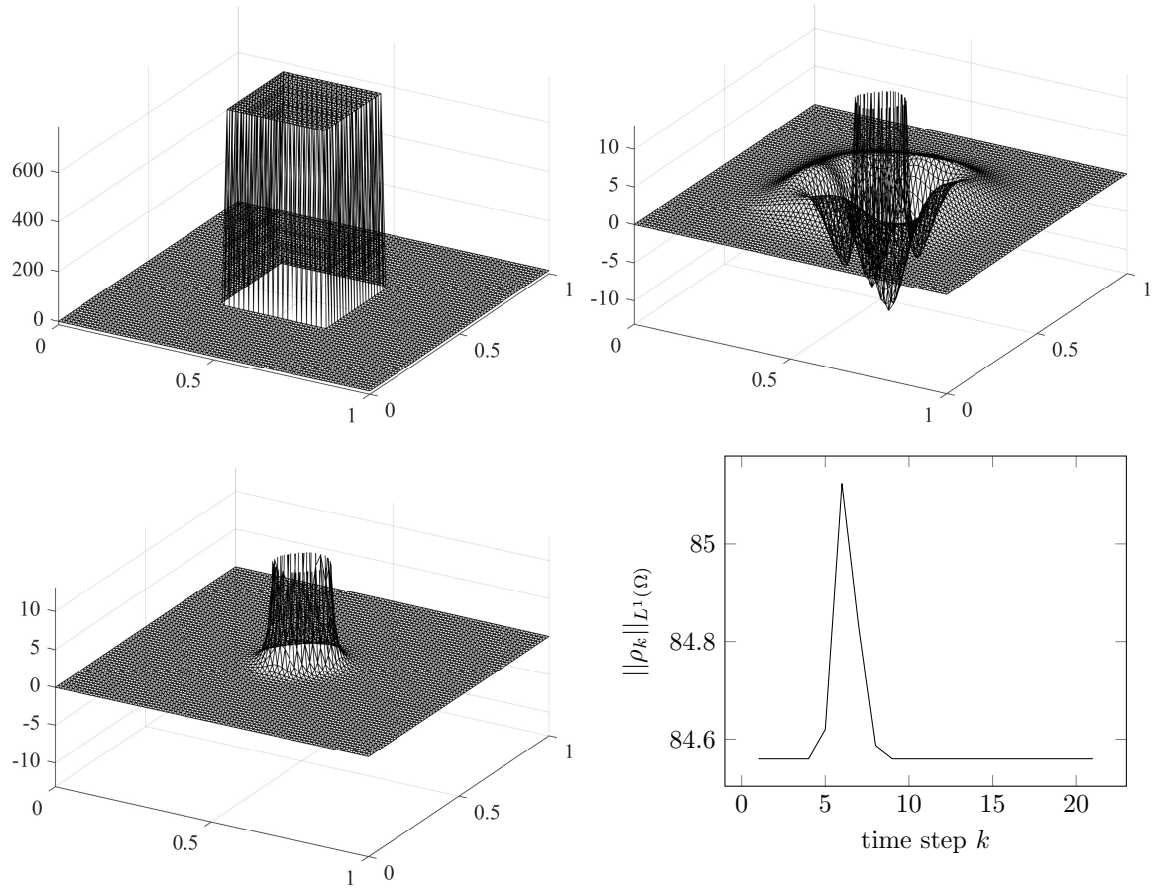


Figure 2.7: Cell density computed from the BDF-2 scheme with a coarse mesh at times $t = 0$ (top left), $t = 0.006$ (top right), $t = 0.021$ (bottom left) and the L^1 norm of ρ_k (bottom right).

the semi-discrete problem, in the supercritical case $M > 8\pi$. An interesting fact is that the upper bound T^* is the same for both the continuous and semi-discrete equations. Although one could expect that the strategy of the implicit Euler case carries over to other methods, more than minor revisions are needed to adapt to other discretizations. This struggle surfaces in the case of BDF-3 and $\beta > 0$, where we are not able to prove the virial inequality at this point in time.

Fully Discrete Results:

We have studied a second order in time discretization on the fully discrete level with a finite element upwind scheme in space. The second order convergence rate in time is established, at least numerically, for the nonlinear discrete case. This is possible by the application of a Picard iteration method to resolve the nonlinear term. The

original linearized scheme proposed by Saito is numerically only first order in time, also for a formally higher order in time discretization. The scheme preserves the total mass and converges to a discrete steady state before reaching the predicted upper bound for the blow-up time via the semi-discrete virial argument. The nonnegativity of the solution is numerically preserved if the mesh and time steps are fine enough. For coarser meshes or larger time steps, the scheme stays stable but can produce, temporally, negative values in regions with steep gradients. These numerical results are the first of their kind, since most numerical studies do not focus on higher order time discretizations or only use explicit methods.

Outlook

In order to derive a numerical scheme that resolves the blow-up time more accurately, we want to translate the virial argument to the fully discrete case. Therefore, the path ahead can be described as follows:

Fully Discrete Virial Argument

A next logical step is to discretize only in space and try to mimic the argument. Major difficulties arise in the discretization of the drift term. This has to be done in a way that allows us to perform a discrete version of integration by parts twice in the diffusion term and still preserve the symmetry properties of the Bessel/Newton potential. In addition, one has to incorporate the conservation of mass into the scheme in order to prove the virial argument on a discrete level in space. Each of these features is not difficult to obtain alone, but to combine them is challenging and poses many open questions for a future work. Since we are not interested in boundary aggregation at this point in time, a possible direction is to start with the radial-symmetric case and to develop a purpose-built finite difference scheme.

Numerics

The numerical scheme presented above shows promising results. The conservation of mass and nonnegativity lead to a rather stable scheme with second order in time convergence rate. A more detailed numerical analysis should be performed for this scheme, built on the already existing analysis for the linearized implicit Euler case [122]. In addition, the L^∞ norm of the cell density seems to be strongly related to the mesh size in space; see Figure 2.6. Hence, in order to increase the number of elements near the blow-up point, an adaptive mesh refinement strategy similar to [19, 27, 104] should be implemented.



Die approbierte gedruckte Originalversion dieser Dissertation ist an der TU Wien Bibliothek verfügbar.
The approved original version of this doctoral thesis is available in print at TU Wien Bibliothek.

3 Vanishing Cross-Diffusion Regularization in a Keller–Segel System

This chapter is concerned with the regularized system (1.2) and its limit to the Keller–Segel system (1.1) on a bounded domain $\Omega \subset \mathbb{R}^d$. Thus, we will deal with the following system

$$\partial_t \rho_\delta = \operatorname{div}(\nabla \rho_\delta - \rho_\delta \nabla c_\delta), \quad \varepsilon \partial_t c_\delta = \Delta c_\delta + \delta \Delta \rho_\delta - c_\delta + \rho_\delta^\alpha \quad \text{in } \Omega, \quad t > 0, \quad (3.1)$$

already introduced above, subject to the no-flux boundary conditions and initial conditions

$$\nabla \rho_\delta \cdot \nu = \nabla c_\delta \cdot \nu = 0 \quad \text{on } \partial\Omega, \quad t > 0, \quad \rho_\delta(0) = \rho^0, \quad \varepsilon c_\delta(0) = \varepsilon c^0 \quad \text{in } \Omega, \quad (3.2)$$

where $\Omega \subset \mathbb{R}^d$ ($d = 2, 3$) is a bounded domain, ν is the exterior unit normal vector of $\partial\Omega$, $\delta > 0$ describes the strength of the additional cross-diffusion, and the term ρ_δ^α with $\alpha > 0$ is the nonlinear signal production. In particular, we are interested in the limit $\delta \rightarrow 0$ in (3.1) leading to the Keller–Segel equations

$$\partial_t \rho = \operatorname{div}(\nabla \rho - \rho \nabla c), \quad \varepsilon \partial_t c = \Delta c - c + \rho^\alpha \quad \text{in } \Omega, \quad t > 0, \quad (3.3)$$

with the initial and boundary conditions (3.2).

We will prove two results in this chapter. The first one is the convergence of the solutions of the parabolic-elliptic model (3.1) with $\varepsilon = 0$ to a solution of the parabolic-elliptic Keller–Segel system (3.3) with $\varepsilon = 0$. Since this result holds globally in time without restriction on the initial mass, we need the restriction $\alpha < 1$. The second result is concerned with the derivation of a convergence rate both in the parabolic-parabolic, i.e. $\varepsilon > 0$, and parabolic-elliptic case, $\varepsilon = 0$. For $\alpha \geq 1$, we cannot generally expect global solutions and it is therefore natural to consider local solutions in this case.

The chapter is organized as follows: we will start with a discussion of the key ideas behind the analysis of the two cases in Section 3.1. The parabolic-elliptic case, for $\alpha < 1$, is investigated in Section 3.2, while the general case is presented in Section 3.3. Numerical simulations for the model (3.1) are performed in Section 3.4. We

also mention here, that some technical tools for this chapter, including a nonlinear Gronwall inequality, are recalled in Appendix B.

3.1 Key Idea: Entropy and Gronwall Inequalities

In order to justify the artificial entropy structure introduced in [28, 75] and the regularizing effect, we want to prove that the solutions of the regularized system can approximate the solution of the original system in a satisfying way. On the one hand, this allows us to study the Keller–Segel system from a different perspective and we can observe what happens when the artificial entropy structure vanishes. On the other hand, we will see that the regularized system features an intriguing aggregation behavior without blow-up. We will investigate this behavior in numerical simulations later on. In particular, we will link the radius of an aggregated bump solution, in its intermediate state, to the parameter δ . As mentioned above, we will attack the parabolic-elliptic case with sublinear signal production and the general case with two different strategies.

The Case $\alpha < 1$:

We know that the regularized system features global-in-time weak solutions for $\alpha = 1$, while the classical Keller–Segel system can experience a blow-up if the initial mass is too big. The prove for the global-in-time existence of the regularized system builds on the entropy inequality (1.6) depending on δ and the application of the boundedness-by-entropy method. Thus, we cannot expect to find a uniform estimate in δ , which would allow us to pass to the limit. Nevertheless, we can show a global-in-time existence result for the parabolic-elliptic case in the case $\alpha < 1$ and $\delta \geq 0$. The idea of the proof is to reformulate (3.1) via introducing the new variable $v_\delta := c_\delta + \delta\rho_\delta$ as the system

$$\partial_t \rho_\delta = \operatorname{div}((1 + \delta\rho_\delta)\nabla\rho_\delta - \rho_\delta\nabla v_\delta), \quad -\Delta v_\delta + v_\delta = \delta\rho_\delta + \rho_\delta^\alpha \quad \text{in } \Omega, \quad t > 0, \quad (3.4)$$

together with the initial and boundary conditions

$$\nabla\rho_\delta \cdot \nu = \nabla v_\delta \cdot \nu = 0 \quad \text{in } \partial\Omega, \quad \rho_\delta(0) = \rho^0 \quad \text{in } \Omega. \quad (3.5)$$

This reformulation was already used in [75] to prove the existence of weak solutions in the two-dimensional case with $\alpha = 1$. It transforms the asymptotically singular expression $\delta\Delta\rho_\delta$ to a quasilinear parabolic equation, thus simplifying considerably the asymptotic limit problem. Still, we need estimates uniform in δ to apply compactness

arguments. For this, we use the entropy functional $H_1(\rho_\delta) = \int_\Omega \rho_\delta (\log \rho_\delta - 1) dx$:

$$\frac{dH_1}{dt} + 4 \int_\Omega |\nabla \rho_\delta^{1/2}|^2 dx + \delta \int_\Omega |\nabla \rho_\delta|^2 dx \leq \int_\Omega (\delta \rho_\delta^2 + \rho_\delta^{\alpha+1}) dx. \quad (3.6)$$

By the Gagliardo–Nirenberg inequality, the right-hand side can be estimated as

$$\delta \int_\Omega \rho_\delta^2 dx \leq \frac{\delta}{2} \|\nabla \rho_\delta\|_{L^2(\Omega)}^2 + C \|\rho_\delta\|_{L^1(\Omega)}^2,$$

see Section 3.2 for the proof. The first term on the right-hand side is absorbed by the left-hand side of (3.6) and the second term is bounded since the total mass is conserved. In order to pass the limit, we can use the estimate from above combined with another “entropy” functional $H_p(\rho) = \int_\Omega \rho^p dx$. For $p = 2$ or $p = 3$, this leads to

$$\frac{dH_p}{dt} + \int_\Omega |\nabla \rho_\delta^{p/2}|^2 dx + \delta \int_\Omega |\nabla \rho_\delta^{(p+1)/2}|^2 dx \leq C \|\rho_\delta\|_{L^{(p+1)/2}(\Omega)}^{(p+1)/2} + C \|\rho_\delta^{p/2}\|_{L^1(\Omega)}^{\beta(p)}, \quad (3.7)$$

where $\beta(p) \geq 2$ is some function depending on p . If $p = 2$, the last term is the total mass, which is bounded uniformly in time. Moreover, the estimate for $\rho_\delta^{1/2}$ in $H^1(\Omega)$ from (3.6) implies that ρ_δ is bounded in $W^{1,1}(\Omega) \hookrightarrow L^{3/2}(\Omega)$ such that the first term on the right-hand side of (3.7) is uniformly bounded as well. Higher-order $L^p(\Omega)$ bounds are then obtained for $p \geq 3$.

Clearly, these arguments are formal. In particular, the estimate for H_1 requires the test function $\log \rho_\delta$ in (3.1), which may not be defined if $\rho_\delta = 0$. Therefore, we consider an implicit Euler discretization in time with parameter $\tau > 0$ and an elliptic regularization in space with parameter $\eta > 0$ to prove first the existence of approximate weak solutions with strictly positive ρ_δ . This is done by using the entropy method of [75]. The approximate solutions also satisfy the δ -uniform bounds, and they hold true when passing to the limit $(\eta, \tau) \rightarrow 0$. Then the limit $\delta \rightarrow 0$ can be performed by applying the Aubin–Lions lemma and weak compactness arguments.

The Case $\alpha \geq 1$:

In the general case, we have to change our viewpoint and derive higher order estimates to pass to the limit for classical solutions. We will use a generalized Gronwall inequality as in [77] by deriving carefully $H^s(\Omega)$ estimates for the difference $(\rho_R, c_R) := (\rho_\delta - \rho, c_\delta - c)$. The index $s \in \mathbb{N}$ is chosen such that we obtain $L^\infty(\Omega)$ estimates in order to handle the nonlinearities. If $\varepsilon = 1$, we introduce the functions

$$\Gamma(t) = \|(\rho_R, c_R)(t)\|_{H^2(\Omega)}^2, \quad G(t) = \|(\rho_R, c_R)(t)\|_{H^2(\Omega)}^2 + \|\nabla \Delta(\rho_R, c_R)(t)\|_{L^2(\Omega)}^2.$$

The aim is to prove the inequality

$$\Gamma(t) + C \int_0^t G(s) ds \leq C \int_0^t (\Gamma(s) + \Gamma(s)^{\max\{2, \alpha\}}) ds + C \int_0^t \Gamma(s) G(s) ds + C \delta^2,$$

where $C > 0$ is a constant independent of δ . This inequality allows us to apply a variant of Gronwall's lemma (see Lemma B.2 in the Appendix), implying an almost quadratic convergence rate. In the parabolic-elliptic case $\varepsilon = 0$, the functions $\Gamma(t)$ and $G(t)$ are defined without c_R , and the final inequality contains the additional integral $\int_0^t \Gamma(s)^{\alpha+1} G(s) ds$, which is still covered by Lemma B.2.

3.2 The Parabolic-Elliptic Case

In this section we will deal with the system (3.4)-(3.5) in the case $\alpha < 2/d$. We set $Q_T = \Omega \times (0, T)$ and state an existence result for $\delta > 0$ and the corresponding convergence result in one theorem:

Theorem 3.1 (Convergence for the parabolic-elliptic model). *Let $\Omega \subset \mathbb{R}^d$ ($d = 2, 3$) be bounded with $\partial\Omega \in C^{1,1}$, $T > 0$, $\delta > 0$, $\varepsilon = 0$, and $0 \leq \rho^0 \in L^\infty(\Omega)$. If $\alpha < 2/d$, there exists a weak solution $(\rho_\delta, c_\delta) \in L^2(0, T; H^1(\Omega))^2$ to (3.1)-(3.2) satisfying*

$$\partial_t \rho_\delta \in L^2(0, T; H^1(\Omega)'), \quad \rho_\delta \in L^\infty(0, T; L^3(\Omega)), \quad c_\delta + \delta \rho_\delta \in L^\infty(0, T; W^{1,p}(\Omega)),$$

for any $p < \infty$. Furthermore, as $\delta \rightarrow 0$,

$$\begin{aligned} \rho_\delta &\rightarrow \rho && \text{strongly in } L^2(Q_T), \\ \nabla \rho_\delta &\rightharpoonup \nabla \rho && \text{weakly in } L^2(Q_T), \\ c_\delta + \delta \rho_\delta &\rightharpoonup^* c && \text{weakly}^* \text{ in } L^\infty(0, T; W^{1,p}(\Omega)), \quad p < \infty, \end{aligned}$$

where $(\rho, c) \in (L^\infty(0, T; L^\infty(\Omega)))^2$ is the unique solution to (3.2)-(3.3).

Proof. We start by an approximation procedure and by deriving the uniform bounds from discrete versions of the entropy inequalities (3.6) and (3.7). This will allow us to use the strategy discussed in Section 3.1 in a rigorous way.

Step 1: Solution of a regularized system and entropy estimates. We show the existence of solutions to a discretized and regularized version of (3.4). For this, let $N \in \mathbb{N}$ and $\tau = T/N$, and set $\rho(w) = \exp(w/\delta)$. This means that we transform $w = \delta \log \rho$. Let $w^{k-1} \in H^2(\Omega)$ and $v^{k-1} \in H^1(\Omega)$ be given and set $\rho^j = \rho(w^j)$ for

$j = k, k - 1$. Consider for given $\tau > 0$ and $\eta > 0$ the regularized system

$$\begin{aligned} & \frac{1}{\tau} \int_{\Omega} (\rho^k - \rho^{k-1}) \phi dx + \int_{\Omega} ((1 + \delta \rho^k) \nabla \rho^k - \rho^k \nabla v^k) \cdot \nabla \phi dx \\ & = -\eta \int_{\Omega} (\Delta w^k \Delta \phi + \delta^{-2} |\nabla w^k|^2 \nabla w^k \cdot \nabla \phi + w^k \rho^k \phi) dx, \end{aligned} \quad (3.8)$$

$$\int_{\Omega} (\nabla v^k \cdot \nabla \theta + v^k \theta) dx = \int_{\Omega} (\delta \rho^k + (\rho^k)^\alpha) \theta dx \quad (3.9)$$

for $\phi \in H^2(\Omega)$ and $\theta \in H^1(\Omega)$. The time discretization is needed to handle issues due to low time regularity, while the elliptic regularization guarantees $H^2(\Omega)$ solutions which, by Sobolev embedding (recall that $d \leq 3$), are bounded. The higher-order gradient term $|\nabla w^k|^2 \nabla w^k \cdot \nabla \phi$ is necessary to derive $L^p(\Omega)$ estimates. The existence of a solution $w^k \in H^2(\Omega)$, $0 \leq v^k \in H^1(\Omega)$ follows from the techniques used in the proof of Proposition 3.1 in [75] employing the Leray–Schauder fixed-point theorem. Since these techniques are rather standard now, we omit the proof and refer to [75, 83, 84] for similar arguments.

Inequality $w^k \rho^k = w^k e^{w^k/\delta} \geq e^{w^k/\delta} - 1 = \rho^k - 1$ allows us to show as in [75, page 1004] that the total mass $\|\rho^k\|_{L^1(\Omega)}$ is bounded uniformly in δ .

Entropy estimates are derived from (3.8)–(3.9) by choosing the test functions $\phi = w^k/\delta = \log \rho^k$ and $\theta = \rho^k$, respectively, and adding both equations. Then the terms involving ∇v^k cancel and after some elementary computations, we end up with

$$\begin{aligned} & \frac{1}{\tau} \int_{\Omega} (h(\rho^k) - h(\rho^{k-1})) dx + 4 \int_{\Omega} |\nabla(\rho^k)^{1/2}|^2 dx + \delta \int_{\Omega} |\nabla \rho^k|^2 dx \\ & + \frac{\eta}{\delta} \int_{\Omega} ((\Delta w^k)^2 + \delta^{-2} |\nabla w^k|^4 + (w^k)^2 \rho^k) dx \\ & \leq \int_{\Omega} (-v^k \rho^k + \delta(\rho^k)^2 + (\rho^k)^{\alpha+1}) dx \leq \int_{\Omega} (\delta(\rho^k)^2 + (\rho^k)^{\alpha+1}) dx, \end{aligned} \quad (3.10)$$

where $h(s) = s(\log s - 1)$ for $s \geq 0$. Using the Gagliardo–Nirenberg inequality with $\sigma = d/(d+2)$, the Poincaré–Wirtinger inequality, and then the Young inequality with $p = 1/\sigma$, $p' = 1/(1-\sigma)$, it holds for any $u \in H^1(\Omega)$ and $\mu > 0$ that

$$\begin{aligned} \|u\|_{L^2(\Omega)}^2 & \leq C \|u\|_{H^1(\Omega)}^{2\sigma} \|u\|_{L^1(\Omega)}^{2(1-\sigma)} = C (\|\nabla u\|_{L^2(\Omega)}^2 + \|u\|_{L^1(\Omega)}^2)^\sigma \|u\|_{L^1(\Omega)}^{2(1-\sigma)} \\ & \leq \mu (\|\nabla u\|_{L^2(\Omega)}^2 + \|u\|_{L^1(\Omega)}^2) + C(\mu) \|u\|_{L^1(\Omega)}^2 = \mu \|\nabla u\|_{L^2(\Omega)}^2 + C(\mu) \|u\|_{L^1(\Omega)}^2. \end{aligned} \quad (3.11)$$

We deduce from this inequality that the first term on the right-hand side of (3.10) can be estimated as

$$\delta \int_{\Omega} (\rho^k)^2 dx \leq \frac{\delta}{4} \|\nabla \rho^k\|_{L^2(\Omega)}^2 + C \|\rho^k\|_{L^1(\Omega)}^2,$$

where here and in the following, $C > 0$ denotes a constant independent of η , τ , and δ , with values varying from line to line. The first term on the right-hand side can be absorbed by the left-hand side of (3.10), while the second term is bounded. Using $s^{\alpha+1} \leq s^2 + 1$ for $s \geq 0$ (since $\alpha < 1$) and (3.11), the second term on the right-hand side of (3.10) becomes

$$\int_{\Omega} (\rho^k)^{\alpha+1} dx \leq \int_{\Omega} ((\rho^k)^2 + 1) dx \leq \frac{\delta}{4} \|\nabla \rho^k\|_{L^2(\Omega)}^2 + C \|\rho^k\|_{L^1(\Omega)}^2 + C(\Omega).$$

Inserting these estimations into (3.10), we conclude that

$$\begin{aligned} & \frac{1}{\tau} \int_{\Omega} (h(\rho^k) - h(\rho^{k-1})) dx + 4 \int_{\Omega} |\nabla(\rho^k)^{1/2}|^2 dx + \frac{\delta}{2} \int_{\Omega} |\nabla \rho^k|^2 dx \\ & + \frac{\eta}{\delta} \int_{\Omega} ((\Delta w^k)^2 + \delta^{-2} |\nabla w^k|^4 + (w^k)^2 \rho^k) dx \leq C(\Omega). \end{aligned} \quad (3.12)$$

Step 2: Further uniform estimates. The estimates from (3.12) are not sufficient for the limit $\delta \rightarrow 0$, therefore, we derive further uniform bounds. Let $p = 2$ or $p = 3$. We choose the admissible test functions $p(\rho^k)^{p-1}$ and $(p-1)(\rho^k)^p$ in (3.8)–(3.9), respectively, and add both equations. The convexity of $s \mapsto s^p$ implies that $s^p - t^p \leq p(s-t)s^{p-1}$. Then, observing that the terms involving ∇v^k cancel, we find that

$$\begin{aligned} & \frac{1}{\tau} \int_{\Omega} ((\rho^k)^p - (\rho^{k-1})^p) dx + \frac{4}{p}(p-1) \int_{\Omega} |\nabla(\rho^k)^{p/2}|^2 dx + \delta \frac{4p(p-1)}{(p+1)^2} \int_{\Omega} |\nabla(\rho^k)^{(p+1)/2}|^2 dx \\ & + \eta p \int_{\Omega} (\Delta w^k \Delta(\rho^k)^{p-1} + \delta^{-2} |\nabla w^k|^2 \nabla w^k \cdot \nabla(\rho^k)^{p-1} + w^k (\rho^k)^p) dx \\ & \leq (p-1) \int_{\Omega} (\delta(\rho^k)^{p+1} + (\rho^k)^{p+\alpha}) dx. \end{aligned}$$

By (3.11), we find that

$$\delta \int_{\Omega} (\rho^k)^{p+1} dx = \delta \|(\rho^k)^{(p+1)/2}\|_{L^2(\Omega)}^2 \leq \frac{\delta}{2} \|\nabla(\rho^k)^{(p+1)/2}\|_{L^2(\Omega)}^2 + C \|(\rho^k)^{(p+1)/2}\|_{L^1(\Omega)}^2.$$

The estimate for $(\rho^k)^{\alpha+p}$ requires that $\alpha < 2/d$. Indeed, we deduce from the Gagliardo–Nirenberg inequality with $\sigma = d(2\alpha + p)/((d+2)(\alpha + p))$ and similar

arguments as in (3.11) that

$$\begin{aligned} \int_{\Omega} (\rho^k)^{\alpha+p} dx &= \|(\rho^k)^{p/2}\|_{L^{2(\alpha+p)/p}(\Omega)}^{2(\alpha+p)/p} \leq C \|(\rho^k)^{p/2}\|_{H^1(\Omega)}^{2(\alpha+p)\sigma/p} \|(\rho^k)^{p/2}\|_{L^1(\Omega)}^{2(\alpha+p)(1-\sigma)/p} \\ &= C (\|\nabla(\rho^k)^{p/2}\|_{L^2(\Omega)}^2 + \|(\rho^k)^{p/2}\|_{L^1(\Omega)}^2)^{(\alpha+p)\sigma/p} \|(\rho^k)^{p/2}\|_{L^1(\Omega)}^{2(\alpha+p)(1-\sigma)/p} \\ &\leq \frac{1}{2} (\|\nabla(\rho^k)^{p/2}\|_{L^2(\Omega)}^2 + \|(\rho^k)^{p/2}\|_{L^1(\Omega)}^2) + C \|(\rho^k)^{p/2}\|_{L^1(\Omega)}^{\beta(p)}, \end{aligned}$$

where $\beta(p) := 2(\alpha + p)(1 - \sigma)/((\alpha + p)(1 - \sigma) - \alpha) \geq 2$ (the exact value of $\beta(p)$ is not important in the following). For the last step, we used the crucial inequality $(\alpha + p)\sigma/p < 1$ (which is equivalent to $\alpha < p/d$).

Because of $\rho^k = \exp(w^k/\delta)$, a computation shows that the integral with factor η can be written as

$$\begin{aligned} &\eta p \int_{\Omega} (\Delta w^k \Delta(\rho^k)^{p-1} + \delta^{-2} |\nabla w^k|^2 \nabla w^k \cdot \nabla(\rho^k)^{p-1} + w^k (\rho^k)^p) dx \\ &= \frac{\eta}{\delta} p(p-1) \int_{\Omega} (\rho^k)^{p-1} \left[\left(\Delta w^k + \frac{p-1}{2\delta} |\nabla w^k|^2 \right)^2 + \frac{1}{4\delta^2} (4 - (p-1)^2) |\nabla w^k|^4 \right] dx \\ &\quad + \eta p \int_{\Omega} w^k e^{pw^k/\delta} dx. \end{aligned}$$

The last integral is bounded from below, independently of δ . Since $p = 2$ or $p = 3$, the first integral on the right-hand side is nonnegative. (At this point, we need the term $|\nabla w^k|^2 \nabla w^k \cdot \nabla \phi$.) Summarizing these estimates, we infer that

$$\begin{aligned} &\frac{1}{\tau} \int_{\Omega} ((\rho^k)^p - (\rho^{k-1})^p) dx + \int_{\Omega} |\nabla(\rho^k)^{p/2}|^2 dx + \frac{\delta}{4} \int_{\Omega} |\nabla(\rho^k)^{(p+1)/2}|^2 dx \\ &\leq C \|(\rho^k)^{(p+1)/2}\|_{L^1(\Omega)}^2 + C \|(\rho^k)^{p/2}\|_{L^1(\Omega)}^{\beta(p)}. \end{aligned} \quad (3.13)$$

Step 3: Limit $(\eta, \tau) \rightarrow 0$. Let $w_{\tau}(x, t) = w^k(x)$, $\rho_{\tau}(x, t) = \rho(w^k(x))$, $v_{\tau}(x, t) = v^k(x)$ for $x \in \Omega$ and $t \in ((k-1)\tau, k\tau]$, $k = 1, \dots, N$, be piecewise constant functions in time. At time $t = 0$, we set $w_{\tau}(x, 0) = \log \rho^0(x)$ and $\rho_{\tau}(x, 0) = \rho^0(x)$ for $x \in \Omega$. (Here, we need $\rho^0 \geq C > 0$ in Ω and another approximation procedure which we omit; see, e.g., [84, Proof of Theorem 4.1].) Furthermore, we introduce the shift operator $\pi_{\tau} \rho_{\tau}(x, t) = \rho_{\tau}(x, t - \tau)$ for $x \in \Omega$, $t \geq \tau$. Then the weak formulation

(3.8)–(3.9) can be written as

$$\begin{aligned} & \frac{1}{\tau} \int_0^T \int_{\Omega} (\rho_{\tau} - \pi_{\tau} \rho_{\tau}) \phi dxdt + \int_0^T \int_{\Omega} ((1 + \delta \rho_{\tau}) \nabla \rho_{\tau} - \rho_{\tau} \nabla v_{\tau}) \cdot \nabla \phi dxdt \\ & = -\eta \int_0^T \int_{\Omega} (\Delta w_{\tau} \Delta \phi + \delta^{-2} |\nabla w_{\tau}|^2 \nabla w_{\tau} \cdot \nabla \phi + w_{\tau} \rho_{\tau} \phi) dxdt, \end{aligned} \quad (3.14)$$

$$\int_0^T \int_{\Omega} (\nabla v_{\tau} \cdot \nabla \theta + v_{\tau} \theta) dxdt = \int_0^T \int_{\Omega} (\delta \rho_{\tau} + \rho_{\tau}^{\alpha}) \theta dxdt, \quad (3.15)$$

where $\phi : (0, T) \rightarrow H^2(\Omega)$ and $\theta : (0, T) \rightarrow H^1(\Omega)$ are piecewise constant functions.

Multiplying (3.12) by τ , summing over $k = 1, \dots, N$, and applying the discrete Gronwall inequality [84, Lemma A.2] provides the following uniform estimates:

$$\|\rho_{\tau}\|_{L^{\infty}(0, T; L^1(\Omega))} + \|\rho_{\tau}^{1/2}\|_{L^2(0, T; H^1(\Omega))} + \delta^{1/2} \|\rho_{\tau}\|_{L^2(0, T; H^1(\Omega))} \leq C, \quad (3.16)$$

$$\eta^{1/2} \|\Delta w_{\tau}\|_{L^2(Q_T)} + \eta^{1/4} \delta^{-1/2} \|\nabla w_{\tau}\|_{L^4(Q_T)} + \eta^{1/2} \|w_{\tau} \rho_{\tau}^{1/2}\|_{L^2(Q_T)} \leq C. \quad (3.17)$$

The (simultaneous) limit $(\eta, \tau) \rightarrow 0$ does not require estimates uniform in δ . Therefore, we can exploit the bound for ρ_{τ} in $L^2(0, T; H^1(\Omega))$. Together with the uniform $L^{\infty}(0, T; L^1(\Omega))$ bound, we obtain from the Gagliardo–Nirenberg inequality as in [84, page 95] that (ρ_{τ}) is bounded in $L^{2+2/d}(Q_T)$, recalling that $Q_T = \Omega \times (0, T)$. Since $-\Delta v_{\tau} + v_{\tau} = \delta \rho_{\tau} + \rho_{\tau}^{\alpha}$ is bounded in $L^{2+2/d}(Q_T)$, we deduce from elliptic regularity a uniform bound for v_{τ} in $L^{2+2/d}(0, T; W^{2, 2+2/d}(\Omega))$. Therefore, $\rho_{\tau} \nabla v_{\tau}$ is uniformly bounded in $L^{1+1/d}(Q_T)$ and $\rho_{\tau} \nabla \rho_{\tau}$ is uniformly bounded in $L^{(2d+2)/(2d+1)}(Q_T)$. Consequently, $(\rho_{\tau} - \pi_{\tau} \rho_{\tau})/\tau = \operatorname{div}((1 + \delta \rho_{\tau}) \nabla \rho_{\tau} - \rho_{\tau} \nabla v_{\tau})$ is uniformly bounded in $L^{(2d+2)/(2d+1)}(0, T; W^{-1, (2d+2)/(2d+1)}(\Omega))$.

The Aubin–Lions lemma in the version of [44] shows that there exists a subsequence, which is not relabeled, such that, as $(\eta, \tau) \rightarrow 0$,

$$\rho_{\tau} \rightarrow \rho \quad \text{strongly in } L^2(0, T; L^p(\Omega))$$

for any $p < 6$ and in $L^q(Q_T)$ for any $q < 2 + 2/d$. Moreover, because of the bounds (3.16), again for a subsequence, as $(\eta, \tau) \rightarrow 0$,

$$\begin{aligned} \nabla \rho_{\tau} & \rightharpoonup \nabla \rho \quad \text{weakly in } L^2(Q_T), \\ \tau^{-1}(\rho_{\tau} - \pi_{\tau} \rho_{\tau}) & \rightharpoonup \partial_t \rho \quad \text{weakly in } L^{(2d+2)/(2d+1)}(0, T; W^{-1, (2d+2)/(2d+1)}(\Omega)), \\ v_{\tau} & \rightharpoonup v \quad \text{weakly in } L^{2+2/d}(0, T; W^{2, 2+2/d}(\Omega)). \end{aligned}$$

We deduce that $\rho_{\tau} \nabla \rho_{\tau} \rightharpoonup \rho \nabla \rho$ and $\rho_{\tau} \nabla v_{\tau} \rightharpoonup \rho \nabla v$ weakly in $L^1(Q_T)$ as well as $\rho_{\tau}^{\alpha} \rightarrow \rho^{\alpha}$ strongly in $L^2(Q_T)$.

The limit in the term involving η is performed as in [75]: Estimates (3.17) imply

that, for any $\phi \in L^4(0, T; H^2(\Omega))$,

$$\begin{aligned} & \left| \eta \int_0^T \int_{\Omega} (\Delta w_{\tau} \Delta \phi + \delta^{-2} |\nabla w_{\tau}|^2 \nabla w_{\tau} \cdot \nabla \phi + w_{\tau} \rho_{\tau} \phi) dx dt \right| \\ & \leq \eta \|\Delta w_{\tau}\|_{L^2(Q_T)} \|\Delta \phi\|_{L^2(Q_T)} + \eta \delta^{-2} \|\nabla w_{\tau}\|_{L^4(Q_T)}^3 \|\nabla \phi\|_{L^4(Q_T)} \\ & \quad + \eta \|w_{\tau} \rho_{\tau}^{1/2}\|_{L^2(Q_T)} \|\rho_{\tau}^{1/2}\|_{L^4(Q_T)} \|\phi\|_{L^4(Q_T)} \\ & \leq C(\delta) (\eta^{1/2} + \eta^{1/4}) \|\phi\|_{L^4(0, T; H^2(\Omega))} \rightarrow 0 \quad \text{as } \eta \rightarrow 0. \end{aligned}$$

Thus, performing the limit $(\eta, \tau) \rightarrow 0$ in (3.14)–(3.15), it follows that (ρ, c) solve

$$\int_0^T \langle \partial_t \rho, \phi \rangle dt + \int_0^T \int_{\Omega} ((1 + \delta \rho) \nabla \rho - \rho \nabla v) \cdot \nabla \phi dx dt = 0, \quad (3.18)$$

$$\int_0^T \int_{\Omega} (\nabla v \cdot \nabla \theta + v \theta) dx dt = \int_0^T \int_{\Omega} (\delta \rho + \rho^{\alpha}) \theta dx dt, \quad (3.19)$$

where, by density, we can choose test functions $\phi \in L^{\infty}(0, T; H^1(\Omega))$ and $\theta \in L^2(0, T; H^1(\Omega))$. The initial datum $\rho(0) = \rho^0$ is satisfied in the sense of $H^1(\Omega)'$; see, e.g., [83, pp. 1980f.] for a proof.

Step 4: Limit $\delta \rightarrow 0$. For this limit, we need further uniform estimates. Let (ρ_{τ}, v_{τ}) be a solution to (3.14)–(3.15). We formulate (3.13) as

$$\begin{aligned} & \int_{\Omega} (\rho_{\tau}^p - (\pi_{\tau} \rho_{\tau})^p) dx + \int_0^T \int_{\Omega} |\nabla \rho_{\tau}^{p/2}|^2 dx dt + \frac{\delta}{4} \int_0^T \int_{\Omega} |\nabla \rho_{\tau}^{(p+1)/2}|^2 dx dt \\ & \leq C \int_0^T \|\rho_{\tau}^{(p+1)/2}\|_{L^1(\Omega)}^2 dt + C \int_0^T \|\rho_{\tau}^{p/2}\|_{L^1(\Omega)}^{\beta(p)} dt, \end{aligned} \quad (3.20)$$

where we recall that $C > 0$ is independent of (η, τ, δ) . The $L^{\infty}(0, T; L^2(\Omega))$ and $L^2(0, T; H^1(\Omega))$ bounds for $(\rho_{\tau}^{1/2})$ show that

$$\begin{aligned} \int_0^T \|\nabla \rho_{\tau}\|_{L^1(\Omega)}^2 dt &= 4 \int_0^T \|\rho_{\tau}^{1/2} \nabla \rho_{\tau}^{1/2}\|_{L^1(\Omega)}^2 dt \leq 4 \int_0^T \|\rho_{\tau}^{1/2}\|_{L^2(\Omega)}^2 \|\nabla \rho_{\tau}^{1/2}\|_{L^2(\Omega)}^2 dt \\ &\leq 4 \|\rho_{\tau}\|_{L^{\infty}(0, T; L^1(\Omega))} \int_0^T \|\nabla \rho_{\tau}^{1/2}\|_{L^2(\Omega)}^2 dt \leq C. \end{aligned}$$

Thus, (ρ_{τ}) is bounded in $L^2(0, T; W^{1,1}(\Omega)) \hookrightarrow L^2(0, T; L^{3/2}(\Omega))$, as $d \leq 3$.

Let $p = 2$ in (3.20). As the right-hand side of (3.20) is uniformly bounded, we infer the bounds

$$\|\rho_{\tau}\|_{L^{\infty}(0, T; L^2(\Omega))} + \|\rho_{\tau}\|_{L^2(0, T; H^1(\Omega))} + \delta^{1/2} \|\rho_{\tau}^{3/2}\|_{L^2(0, T; H^1(\Omega))} \leq C.$$

Choosing $p = 3$ in (3.20), the right-hand side is again bounded, yielding the estimates

$$\|\rho_\tau\|_{L^\infty(0,T;L^3(\Omega))} + \delta^{1/2}\|\rho_\tau^2\|_{L^2(0,T;H^1(\Omega))} \leq C.$$

By elliptic regularity, since $-\Delta v_\tau + v_\tau = \delta\rho_\tau + \rho_\tau^\alpha \in L^\infty(0, T; L^3(\Omega))$, the family (v_τ) is bounded in $L^\infty(0, T; W^{2,3}(\Omega)) \hookrightarrow L^\infty(0, T; W^{1,p}(\Omega))$ for all $p < \infty$.

We know from Step 3 that (ρ_τ, v_τ) converges in some norms to $(\rho_\delta, v_\delta) := (\rho, v)$ solving (3.18)–(3.19). By the weakly lower semicontinuity of the norm and the a.e. convergence $\rho_\tau^2 \rightarrow \rho^2$ in Q_T , it follows that, after performing the limit $(\eta, \tau) \rightarrow 0$,

$$\|\rho_\delta\|_{L^\infty(0,T;L^3(\Omega))} + \|\rho_\delta\|_{L^2(0,T;H^1(\Omega))} + \delta^{1/2}\|\rho_\delta^2\|_{L^2(0,T;H^1(\Omega))} + \|v_\delta\|_{L^\infty(0,T;W^{1,p}(\Omega))} \leq C. \quad (3.21)$$

We wish to derive a uniform estimate for the time derivative $\partial_t \rho_\delta$. Let $\phi \in L^2(0, T; H^1(\Omega))$. Then

$$\begin{aligned} \left| \int_0^T \langle \partial_t \rho_\delta, \phi \rangle dt \right| &\leq \left(\|\nabla \rho_\delta\|_{L^2(Q_T)} + \frac{\delta}{2} \|\nabla(\rho_\delta^2)\|_{L^2(Q_T)} \right) \|\nabla \phi\|_{L^2(Q_T)} \\ &\quad + \|\rho_\delta\|_{L^2(0,T;L^4(\Omega))} \|\nabla v_\delta\|_{L^\infty(0,T;L^4(\Omega))} \|\nabla \phi\|_{L^2(Q_T)} \leq C. \end{aligned}$$

This shows that $(\partial_t \rho_\delta)$ is bounded in $L^2(0, T; H^1(\Omega)')$. By the Aubin–Lions lemma in the version of [130], there exists a subsequence, which is not relabeled, such that, as $\delta \rightarrow 0$,

$$\rho_\delta \rightarrow \rho \quad \text{strongly in } L^2(0, T; L^p(\Omega)), \quad p < 6.$$

Furthermore, we deduce from the bounds (3.21), again for a subsequence, that

$$\begin{aligned} \nabla \rho_\delta &\rightharpoonup \nabla \rho \quad \text{weakly in } L^2(Q_T), \\ \delta \nabla(\rho_\delta^2) &\rightarrow 0 \quad \text{strongly in } L^2(Q_T), \\ \partial_t \rho_\delta &\rightharpoonup \partial_t \rho \quad \text{weakly in } L^2(0, T; H^1(\Omega)'), \\ v_\delta &\rightharpoonup^* v \quad \text{weakly* in } L^\infty(0, T; W^{1,p}(\Omega)), \quad p < \infty. \end{aligned}$$

In particular, $\rho_\delta \nabla v_\delta \rightharpoonup \rho \nabla v$ weakly in $L^2(Q_T)$. Thus, we can perform the limit $\delta \rightarrow 0$ in (3.18)–(3.19), which gives

$$\begin{aligned} \int_0^T \langle \partial_t \rho, \phi \rangle dt + \int_0^T \int_\Omega (\nabla \rho - \rho \nabla v) \cdot \nabla \phi dx dt &= 0, \\ \int_0^T \int_\Omega (\nabla v \cdot \nabla \theta + v \theta) dx dt &= \int_0^T \int_\Omega \rho^\alpha \theta dx \end{aligned}$$

for all $\phi, \theta \in L^2(0, T; H^1(\Omega))$. Furthermore, we show as in [83, pp. 1980f.] that $\rho(0) = \rho^0$ in the sense of $H^1(\Omega)'$.

Step 5: Convergence of the whole sequence. The whole sequence (ρ_δ, v_δ) converges if the limit problem has a unique solution. Uniqueness follows by standard estimates if $\rho, \nabla c \in L^\infty(0, T; L^\infty(\Omega))$. Since $-\Delta c + c = \rho^\alpha \in L^\infty(0, T; L^{3/\alpha}(\Omega))$ and $3/\alpha > 3 \geq d$, elliptic regularity shows that $c \in L^\infty(0, T; W^{2,3/\alpha}(\Omega)) \hookrightarrow L^\infty(0, T; W^{1,\infty}(\Omega))$. Then [74, Lemma 1] shows that $\rho \in L^\infty(0, T; L^\infty(\Omega))$, finishing the proof. \square

3.3 The Parabolic-Parabolic Case

It is shown in [75] that (3.1)–(3.2) with $\alpha = 1$ has a global weak solution in two space dimensions. Since the solutions to the limiting Keller–Segel system may blow up after finite time, we cannot generally expect estimates that are uniform in δ globally in time. In order to follow the local-in-time approach presented above, we need higher-order estimates not provided by the results of [75]. Therefore, we first show the local existence of smooth solutions and then the corresponding uniform $H^s(\Omega)$ bounds. These bounds will be sufficient to use a nonlinear Gronwall argument and to prove the following theorem:

Theorem 3.2 (Convergence rates). *Let $\Omega \subset \mathbb{R}^d$ ($d \leq 3$) be a bounded domain with smooth boundary and let $(\rho^0, c^0) \in (W^{1,p}(\Omega))^2$ for $p > d$ if $\varepsilon = 1$ and $\rho^0 \in C^{2+\gamma}(\bar{\Omega})$ for some $\gamma \in (0, 1)$ if $\varepsilon = 0$. Furthermore, let $\alpha = 1$ or $\alpha \geq 2$ and let (ρ_δ, c_δ) and (ρ, c) be (weak) solutions to (3.1) and (3.3), (3.2), respectively, with the same initial data. Then these solutions are smooth locally in time and there exist constants $C > 0$ and $\delta_0 > 0$ such that for all $0 < \delta < \delta_0$ and $\lambda > 0$,*

$$\|(\rho_\delta - \rho, c_\delta - c)\|_{L^\infty(0,T;H^2(\Omega))} \leq C\delta^{1-\lambda}.$$

Proof. Step 1: Local existence of smooth solutions. Let $\varepsilon = 1$. The eigenvalues of the diffusion matrix associated to (3.1),

$$A(\rho, c) = \begin{pmatrix} 1 & -\rho \\ \delta & 1 \end{pmatrix},$$

equal $\lambda = 1 \pm i\sqrt{\delta\rho}$, and they have a positive real part for all $\rho > 0$, i.e., $A(\rho, c)$ is normally elliptic. Therefore, according to [2, Theorem 14.1] (also see [85, Theorem 3.1]), there exists a unique maximal solution to (3.1)–(3.2) satisfying $(\rho, c) \in C^\infty(\bar{\Omega} \times (0, T^*); \mathbb{R}^2)$, where $0 < T^* \leq \infty$.

Next, let $\varepsilon = 0$. We use the Schauder fixed-point theorem to prove the regularity of the solutions to (3.4)–(3.5). We only sketch the proof, since the arguments are rather standard. We introduce the set

$$S = \{\tilde{\rho} \in C^0(\bar{\Omega} \times [0, T]) : 0 \leq \tilde{\rho} \leq R, \|\tilde{\rho}\|_{C^{\gamma,\gamma/2}(\bar{\Omega} \times [0, T])} \leq K\}$$

for some $R > 0$ and $M > 0$. Let $\tilde{\rho} \in S$. By elliptic regularity (combining Theorems

2.4.2.7 and 2.5.1.1 in [66]), the unique solution to

$$-\Delta v + v = \delta \tilde{\rho} + \tilde{\rho}^\alpha \quad \text{in } \Omega, \quad \nabla \tilde{\rho} \cdot \nu = 0 \quad \text{on } \partial\Omega,$$

satisfies $v \in C^0([0, T]; W^{2,p}(\Omega))$ for all $p < \infty$. Hence, by Sobolev embedding, $h := \tilde{\rho} \nabla v \in C^0(\bar{\Omega} \times [0, T])$. Thus, using [101, Lemma 2.1 iv], the unique solution to

$$\partial_t \rho = \operatorname{div}((1 + \delta \tilde{\rho}) \nabla \rho - h) \quad \text{in } \Omega, \quad t > 0, \quad \nabla \rho \cdot \nu = 0 \quad \text{on } \partial\Omega,$$

satisfies $\rho \in C^{\gamma, \gamma/2}(\bar{\Omega} \times [0, T])$. By elliptic regularity again, $v \in C^{2, \gamma/2}(\bar{\Omega} \times [0, T])$. Consequently, $h \in C^{\gamma, \gamma/2}(\bar{\Omega} \times [0, T])$ and applying [101, Lemma 2.1iv] again, we infer that $\rho \in C^{2,1}(\bar{\Omega} \times [0, T])$. It is possible to show that $\rho \in S$ for suitable $R > 0$ and $M > 0$. Hence, the existence of a solution to (3.4)–(3.5) follows from the Schauder fixed-point theorem.

Elliptic regularity implies that $v \in C^{4,1}(\bar{\Omega} \times [0, T])$. Then $f := \operatorname{div}(\rho \nabla v) \in C^{1,1}(\bar{\Omega} \times [0, T])$ and the solution $u = \rho$ to the linear parabolic equation $\partial_t u - \Delta u - \operatorname{div}(\rho \nabla u) = f$ in Ω , $t > 0$, with no-flux boundary conditions satisfies $u \in C^{2+\gamma, 1+\gamma/2}(\bar{\Omega} \times [0, T])$ [106, Corollary 5.1.22] (here we need $\rho^0 \in C^{2+\gamma}(\bar{\Omega})$). Thus, the regularity of f improves to $f \in C^{1+\gamma, 1+\gamma/2}(\bar{\Omega} \times [0, T])$. By parabolic regularity [54, Theorem 9.2, p. 137], we infer that $u \in C^{2+\gamma, 2}(\bar{\Omega} \times [0, T])$. Bootstrapping this argument and using [54, Theorems 10.1–10.2, pp. 139f.], we find that $\rho = u \in C^\infty(\bar{\Omega} \times (0, T])$ and consequently $v \in C^\infty(\bar{\Omega} \times (0, T])$.

Step 2: Preparations. Let $\varepsilon = 1$, let (ρ_δ, c_δ) be a local smooth solution to (3.1)–(3.2) with $0 < \delta < 1$, and let (ρ, c) be a local smooth solution to (3.2)–(3.3). Then $\rho_R := \rho_\delta - \rho$ and $c_R := c_\delta - c$ solve

$$\partial_t \rho_R = \operatorname{div}(\nabla \rho_R - \rho_R \nabla(c + c_R) - \rho \nabla c_R), \quad (3.22)$$

$$\partial_t c_R = \Delta c_R - c_R + \delta \Delta(\rho + \rho_R) + (\rho + \rho_R)^\alpha - \rho^\alpha \quad \text{in } \Omega, \quad t > 0, \quad (3.23)$$

(ρ_R, c_R) satisfies homogeneous Neumann boundary conditions and vanishing initial conditions:

$$\nabla \rho_R \cdot \nu = \nabla c_R \cdot \nu = 0 \quad \text{on } \partial\Omega, \quad t > 0, \quad \rho_R(0) = c_R(0) = 0 \quad \text{in } \Omega.$$

The aim is to prove a differential inequality for

$$\Gamma(t) = \|(\rho_R, c_R)(t)\|_{H^2(\Omega)}^2, \quad G(t) = \|(\rho_R, c_R)(t)\|_{H^2(\Omega)}^2 + \|\nabla \Delta(\rho_R, c_R)(t)\|_{L^2(\Omega)}^2,$$

where $\|(\rho_R, c_R)\|_X^2 = \|\rho_R\|_X^2 + \|c_R\|_X^2$ for suitable norms $\|\cdot\|_X$.

Step 3: $H^1(\Omega)$ estimates. We use ρ_R as a test function in (3.22):

$$\begin{aligned} \frac{1}{2} \frac{d}{dt} \|\rho_R\|_{L^2(\Omega)}^2 + \|\nabla \rho_R\|_{L^2(\Omega)}^2 &= \int_{\Omega} \rho_R \nabla(c + c_R) \cdot \nabla \rho_R dx + \int_{\Omega} \rho \nabla c_R \cdot \nabla \rho_R dx \\ &=: I_1 + I_2. \end{aligned}$$

By Young's inequality, for any $\eta > 0$, we have

$$I_2 \leq \frac{\eta}{2} \|\nabla \rho_R\|_{L^2(\Omega)}^2 + \frac{1}{2\eta} \|\rho\|_{L^\infty(\Omega)}^2 \|\nabla c_R\|_{L^2(\Omega)}^2 \leq \frac{\eta}{2} \|\nabla \rho_R\|_{L^2(\Omega)}^2 + C(\eta) \|\nabla c_R\|_{L^2(\Omega)}^2,$$

where here and in the following, $C > 0$ and $C(\eta) > 0$ denote generic constants independent of δ but depending on suitable norms of (ρ, c) . The embedding $H^2(\Omega) \hookrightarrow L^\infty(\Omega)$ (for $d \leq 3$) gives

$$\begin{aligned} I_1 &\leq \eta \|\nabla \rho_R\|_{L^2(\Omega)}^2 + \frac{1}{2\eta} \|\nabla c\|_{L^\infty(\Omega)}^2 \|\rho_R\|_{L^2(\Omega)}^2 + \frac{1}{2\eta} \|\rho_R\|_{L^\infty(\Omega)}^2 \|\nabla c_R\|_{L^2(\Omega)}^2 \\ &\leq \eta \|\nabla \rho_R\|_{L^2(\Omega)}^2 + C(\eta) \|\rho_R\|_{L^2(\Omega)}^2 + C(\eta) \|\rho_R\|_{H^2(\Omega)}^2 \|\nabla c_R\|_{L^2(\Omega)}^2. \end{aligned}$$

Combining the estimates for I_1 and I_2 and choosing $\eta > 0$ sufficiently small, we find that

$$\frac{d}{dt} \|\rho_R\|_{L^2(\Omega)}^2 + C \|\nabla \rho_R\|_{L^2(\Omega)}^2 \leq C(1 + \|\rho_R\|_{H^2(\Omega)}^2) \|\nabla c_R\|_{L^2(\Omega)}^2 + C \|\rho_R\|_{L^2(\Omega)}^2. \quad (3.24)$$

Next, we use the test function c_R in (3.23):

$$\begin{aligned} \frac{1}{2} \frac{d}{dt} \|c_R\|_{L^2(\Omega)}^2 + \|c_R\|_{H^1(\Omega)}^2 &= -\delta \int_{\Omega} \nabla(\rho + \rho_R) \cdot \nabla c_R dx + \int_{\Omega} ((\rho + \rho_R)^\alpha - \rho^\alpha) c_R dx \\ &= I_3 + I_4. \end{aligned}$$

Thus, for any $\eta > 0$,

$$\begin{aligned} I_3 &\leq \frac{\eta}{2} \|\nabla c_R\|_{L^2(\Omega)}^2 + \frac{\delta^2}{2\eta} (\|\nabla \rho\|_{L^2(\Omega)}^2 + \|\nabla \rho_R\|_{L^2(\Omega)}^2) \\ &\leq \frac{\eta}{2} \|\nabla c_R\|_{L^2(\Omega)}^2 + C(\eta) \|\nabla \rho_R\|_{L^2(\Omega)}^2 + C(\eta) \delta^2. \end{aligned}$$

For the estimate of I_4 , we apply the mean-value theorem to the function $s \mapsto s^\alpha$ (recalling that $\alpha \geq 1$):

$$|(\rho + \rho_R)^\alpha - \rho^\alpha| \leq C(1 + \|\rho_R\|_{L^\infty(\Omega)})^{\alpha-1} |\rho_R| \leq C(1 + \|\rho_R\|_{L^\infty(\Omega)}^{\alpha-1}) |\rho_R|.$$

Hence, together with the embedding $H^2(\Omega) \hookrightarrow L^\infty(\Omega)$,

$$I_4 \leq \eta \|c_R\|_{L^2(\Omega)}^2 + C(\eta)(1 + \|\rho_R\|_{H^2(\Omega)}^{2(\alpha-1)}) \|\rho_R\|_{L^2(\Omega)}^2.$$

Collecting these estimates and choosing $\eta > 0$ sufficiently small, it follows that

$$\frac{1}{2} \frac{d}{dt} \|c_R\|_{L^2(\Omega)}^2 + C \|c_R\|_{H^1(\Omega)}^2 \leq C \|\nabla \rho_R\|_{L^2(\Omega)}^2 + C(1 + \|\rho_R\|_{H^2(\Omega)}^{2(\alpha-1)}) \|\rho_R\|_{L^2(\Omega)}^2 + C\delta^2. \quad (3.25)$$

Thus, summing (3.24) and (3.25),

$$\frac{d}{dt} \|(\rho_R, c_R)\|_{L^2(\Omega)}^2 + C \|(\rho_R, c_R)\|_{H^1(\Omega)}^2 \leq C(\Gamma(t) + \Gamma(t)^2 + \Gamma(t)^\alpha) + C\delta^2. \quad (3.26)$$

Step 4: $H^2(\Omega)$ estimates. We multiply (3.22) by $-\Delta \rho_R$ and integrate by parts in the expression with the time derivative:

$$\begin{aligned} \frac{1}{2} \frac{d}{dt} \|\nabla \rho_R\|_{L^2(\Omega)}^2 + \|\Delta \rho_R\|_{L^2(\Omega)}^2 &= \int_{\Omega} \operatorname{div}(\rho_R \nabla(c + c_R)) \Delta \rho_R dx + \int_{\Omega} \operatorname{div}(\rho \nabla c_R) \Delta \rho_R dx \\ &= \int_{\Omega} (\nabla \rho_R \cdot \nabla(c + c_R) + \rho_R \Delta(c + c_R)) \Delta \rho_R dx \\ &\quad + \int_{\Omega} (\nabla \rho \cdot \nabla c_R + \rho \Delta c_R) \Delta \rho_R dx =: I_5 + I_6. \end{aligned}$$

Then, taking into account inequality (B.1) in the Appendix,

$$\begin{aligned} I_5 &\leq \eta \|\Delta \rho_R\|_{L^2(\Omega)}^2 + C(\eta) \|\nabla \rho_R\|_{L^2(\Omega)}^2 + C(\eta) \|\nabla \rho_R\|_{H^1(\Omega)}^2 \|\nabla c_R\|_{H^1(\Omega)}^2 \\ &\quad + C(\eta) \|\rho_R\|_{L^2(\Omega)}^2 + C(\eta) \|\rho_R\|_{H^1(\Omega)}^2 \|\Delta c_R\|_{H^1(\Omega)}^2, \\ I_6 &\leq \eta \|\Delta \rho_R\|_{L^2(\Omega)}^2 + C(\eta) \|\nabla c_R\|_{L^2(\Omega)}^2 + C(\eta) \|\Delta c_R\|_{L^2(\Omega)}^2, \end{aligned}$$

and choosing $\eta > 0$ sufficiently small, we end up with

$$\begin{aligned} \frac{1}{2} \frac{d}{dt} \|\nabla \rho_R\|_{L^2(\Omega)}^2 + C \|\Delta \rho_R\|_{L^2(\Omega)}^2 &\leq C \|\rho_R\|_{H^1(\Omega)}^2 + C(1 + \|\nabla \rho_R\|_{H^1(\Omega)}^2) \|c_R\|_{H^2(\Omega)}^2 \\ &\quad + C \|\rho_R\|_{H^1(\Omega)}^2 \|\Delta c_R\|_{H^1(\Omega)}^2. \end{aligned} \quad (3.27)$$

We multiply (3.23) by $-\Delta c_R$ and estimate similarly as in Step 3:

$$\begin{aligned} \frac{1}{2} \frac{d}{dt} \|\nabla c_R\|_{L^2(\Omega)}^2 + \|\Delta c_R\|_{L^2(\Omega)}^2 + \|\nabla c_R\|_{L^2(\Omega)}^2 \\ &= \delta \int_{\Omega} \Delta(\rho + \rho_R) \Delta c_R dx + \int_{\Omega} ((\rho + \rho_R)^\alpha - \rho^\alpha) \Delta c_R dx \\ &\leq \eta \|\Delta c_R\|_{L^2(\Omega)}^2 + C(1 + \|\rho_R\|_{H^2(\Omega)}^{2(\alpha-1)}) \|\rho_R\|_{L^2(\Omega)}^2 + C\delta^2 \|\Delta \rho_R\|_{L^2(\Omega)}^2 + C\delta^2. \end{aligned}$$

Hence, for sufficiently small $\eta > 0$,

$$\begin{aligned} & \frac{1}{2} \frac{d}{dt} \|\nabla c_R\|_{L^2(\Omega)}^2 + \|\Delta c_R\|_{L^2(\Omega)}^2 + \|\nabla c_R\|_{L^2(\Omega)}^2 \\ & \leq C(1 + \|\rho_R\|_{H^2(\Omega)}^{2(\alpha-1)}) \|\rho_R\|_{L^2(\Omega)}^2 + C\delta^2 \|\Delta \rho_R\|_{L^2(\Omega)}^2 + C\delta^2. \end{aligned} \quad (3.28)$$

Adding this inequality and (3.27), adding $\|c_R\|_{L^2(\Omega)}^2$ on both sides, using (B.2) in the Appendix, and choosing $\delta > 0$ sufficiently small to absorb the term $C\delta^2 \|\Delta \rho_R\|_{L^2(\Omega)}^2$, we infer that

$$\begin{aligned} & \frac{d}{dt} \|\nabla(\rho_R, c_R)\|_{L^2(\Omega)}^2 + C\|(\rho_R, c_R)\|_{H^2(\Omega)}^2 \leq C\|(\rho_R, c_R)\|_{H^2(\Omega)}^2 + C\|\nabla \rho_R\|_{H^1(\Omega)}^2 \|\nabla c_R\|_{H^1(\Omega)}^2 \\ & \quad + C\|\rho_R\|_{H^1(\Omega)}^2 \|\Delta c_R\|_{H^1(\Omega)}^2 + C\|\rho_R\|_{H^2(\Omega)}^{2(\alpha-1)} \|\rho_R\|_{L^2(\Omega)}^2 + C\delta^2 \\ & \leq C(\Gamma(t) + \Gamma(t)^2 + \Gamma(t)^\alpha + \Gamma(t)G(t)) + C\delta^2. \end{aligned} \quad (3.29)$$

Step 5: $H^3(\Omega)$ estimates. We apply the Laplacian to (3.22) and (3.23) and multiply both equations by $\Delta \rho_R$, Δc_R , respectively:

$$\begin{aligned} & \frac{1}{2} \frac{d}{dt} \|\Delta \rho_R\|_{L^2(\Omega)}^2 + \|\nabla \Delta \rho_R\|_{L^2(\Omega)}^2 = \int_{\Omega} \nabla \operatorname{div}(\rho_R \nabla(c + c_R)) \cdot \nabla \Delta \rho_R dx \\ & \quad + \int_{\Omega} \nabla \operatorname{div}(\rho \nabla c_R) \cdot \nabla \Delta \rho_R dx = I_7 + I_8, \\ & \frac{1}{2} \frac{d}{dt} \|\Delta c_R\|_{L^2(\Omega)}^2 + \|\nabla \Delta c_R\|_{L^2(\Omega)}^2 + \|\Delta c_R\|_{L^2(\Omega)}^2 = \delta \int_{\Omega} \nabla \Delta(\rho + \rho_R) \cdot \nabla \Delta c_R dx \\ & \quad + \int_{\Omega} \nabla((\rho + \rho_R)^\alpha - \rho^\alpha) \cdot \nabla \Delta c_R dx = I_9 + I_{10}. \end{aligned}$$

We estimate

$$\begin{aligned} I_8 & \leq \eta \|\nabla \Delta \rho_R\|_{L^2(\Omega)}^2 + C(\eta) \|\nabla \operatorname{div}(\rho \nabla c_R)\|_{L^2(\Omega)}^2 + C(\eta) \|\rho_R\|_{H^2(\Omega)}^2 \\ & \leq \eta \|\nabla \Delta \rho_R\|_{L^2(\Omega)}^2 + C(\eta) \|c_R\|_{H^2(\Omega)}^2 + C(\eta) \|\nabla \Delta c_R\|_{L^2(\Omega)}^2 + C(\eta) \|\rho_R\|_{H^2(\Omega)}^2. \end{aligned}$$

Taking into account

$$\begin{aligned} \nabla \operatorname{div}(\rho_R \nabla c_R) & = \nabla(\nabla \rho_R \cdot \nabla c_R + \rho_R \Delta c_R) \\ & = (\nabla c_R \cdot \nabla) \nabla \rho_R + (\nabla \rho_R \cdot \nabla) \nabla c_R + \nabla \rho_R \Delta c_R + \rho_R \nabla \Delta c_R, \end{aligned}$$

and inequalities (B.1) and (B.3) in the Appendix as well as the embedding $H^2(\Omega) \hookrightarrow$

$L^\infty(\Omega)$, we obtain

$$\begin{aligned} \|\nabla \operatorname{div}(\rho_R \nabla c_R)\|_{L^2(\Omega)}^2 &\leq \|\nabla c_R\|_{L^\infty(\Omega)}^2 \|\nabla^2 \rho_R\|_{L^2(\Omega)}^2 + \|\nabla \rho_R\|_{H^1(\Omega)}^2 \|\nabla^2 c_R\|_{H^1(\Omega)}^2 \\ &\quad + \|\nabla \rho_R\|_{H^1(\Omega)}^2 \|\Delta c_R\|_{H^1(\Omega)}^2 + \|\rho_R\|_{L^\infty(\Omega)}^2 \|\nabla \Delta c_R\|_{L^2(\Omega)}^2 \\ &\leq C \|\rho_R\|_{H^2(\Omega)}^2 (\|\nabla \Delta c_R\|_{L^2(\Omega)}^2 + \|c_R\|_{H^2(\Omega)}^2), \end{aligned}$$

which gives

$$I_7 \leq \eta \|\nabla \Delta c_R\|_{L^2(\Omega)}^2 + C(\eta) \|\rho_R\|_{H^2(\Omega)}^2 + C(\eta) \|\rho_R\|_{H^2(\Omega)}^2 (\|\nabla \Delta c_R\|_{L^2(\Omega)}^2 + \|c_R\|_{H^2(\Omega)}^2).$$

This gives, again for sufficiently small $\eta > 0$,

$$\begin{aligned} \frac{1}{2} \frac{d}{dt} \|\Delta \rho_R\|_{L^2(\Omega)}^2 + C \|\nabla \Delta \rho_R\|_{L^2(\Omega)}^2 &\leq C \|(\rho_R, c_R)\|_{H^2(\Omega)}^2 + C \|\rho_R\|_{H^2(\Omega)}^2 \|c_R\|_{H^2(\Omega)}^2 \\ &\quad + C(1 + \|\rho_R\|_{H^2(\Omega)}^2) \|\nabla \Delta c_R\|_{L^2(\Omega)}^2. \end{aligned} \quad (3.30)$$

Next, we estimate I_9 and I_{10} :

$$\begin{aligned} I_9 &\leq \eta \|\nabla \Delta c_R\|_{L^2(\Omega)}^2 + C(\eta) \delta^2 \|\nabla \Delta \rho_R\|_{L^2(\Omega)}^2 + C\delta^2, \\ I_{10} &= \alpha \int_{\Omega} ((\rho + \rho_R)^{\alpha-1} - \rho^{\alpha-1}) \nabla \rho \cdot \nabla \Delta c_R dx \\ &\quad + \alpha \int_{\Omega} (\rho + \rho_R)^{\alpha-1} \nabla \rho_R \cdot \nabla \Delta c_R dx = J_1 + J_2. \end{aligned}$$

We find that

$$J_2 \leq \eta \|\nabla \Delta c_R\|_{L^2(\Omega)}^2 + C(\eta) (1 + \|\rho_R\|_{H^2(\Omega)}^{2(\alpha-1)}) \|\nabla \rho_R\|_{L^2(\Omega)}^2.$$

By the Hölder continuity of $s \mapsto s^{\alpha-1}$, it follows that

$$\begin{aligned} J_2 &\leq C \int_{\Omega} |\rho_R|^{\alpha-1} |\nabla \Delta c_R| dx \leq \eta \|\nabla \Delta c_R\|_{L^2(\Omega)}^2 + C(\eta) \|\rho_R\|_{L^{2(\alpha-1)}(\Omega)}^{2(\alpha-1)} \\ &\leq \eta \|\nabla \Delta c_R\|_{L^2(\Omega)}^2 + C(\eta) \|\rho_R\|_{H^2(\Omega)}^{2(\alpha-1)}. \end{aligned}$$

Consequently, for sufficiently small $\eta > 0$,

$$\begin{aligned} \frac{1}{2} \frac{d}{dt} \|\Delta c_R\|_{L^2(\Omega)}^2 + C \|\nabla \Delta c_R\|_{L^2(\Omega)}^2 + \|\Delta c_R\|_{L^2(\Omega)}^2 \\ \leq C \|\rho_R\|_{H^2(\Omega)}^{2(\alpha-1)} + C(1 + \|\rho_R\|_{H^2(\Omega)}^{2(\alpha-1)}) \|\nabla \rho_R\|_{L^2(\Omega)}^2 + C\delta^2 \|\nabla \Delta \rho_R\|_{L^2(\Omega)}^2 + C\delta^2. \end{aligned} \quad (3.31)$$

Adding the previous inequality and (3.30) and taking $\delta > 0$ sufficiently small

such that the term $C\delta^2\|\nabla\Delta\rho_R\|_{L^2(\Omega)}^2$ is absorbed by the corresponding term on the left-hand side of (3.30), we infer that

$$\begin{aligned} & \frac{d}{dt}\|(\rho_R, c_R)\|_{L^2(\Omega)}^2 + C\|\nabla\Delta(\rho_R, c_R)\|_{L^2(\Omega)}^2 + C\|\Delta c_R\|_{L^2(\Omega)}^2 \\ & \leq C\|(\rho_R, c_R)\|_{H^2(\Omega)}^2 + C(1 + \|\rho_R\|_{H^2(\Omega)}^2)\|\nabla\Delta c_R\|_{L^2(\Omega)}^2 + C\|\rho_R\|_{H^2(\Omega)}^2\|c_R\|_{H^2(\Omega)}^2 \\ & \quad + C\|\rho_R\|_{H^2(\Omega)}^{2(\alpha-1)} + C(1 + \|\rho_R\|_{H^2(\Omega)}^{2(\alpha-1)})\|\nabla\rho_R\|_{L^2(\Omega)}^2 + C\delta^2 \\ & \leq C(\Gamma(t) + \Gamma(t)^{\alpha-1} + \Gamma(t)^2 + \Gamma(t)^\alpha + \Gamma(t)G(t)) + C\delta^2. \end{aligned} \quad (3.32)$$

Step 6: End of the proof for $\varepsilon = 1$. We sum inequalities (3.26), (3.29), and (3.32):

$$\begin{aligned} & \frac{d}{dt}(\|(\rho_R, c_R)\|_{H^1(\Omega)}^2 + \|\Delta(\rho_R, c_R)\|_{L^2(\Omega)}^2) \\ & \quad + C(\|(\rho_R, c_R)\|_{H^2(\Omega)}^2 + \|\nabla\Delta(\rho_R, c_R)\|_{L^2(\Omega)}^2) \\ & \leq C(\Gamma(t) + \Gamma(t)^{\alpha-1} + \Gamma(t)^2 + \Gamma(t)^\alpha + \Gamma(t)G(t)) + C\delta^2. \end{aligned} \quad (3.33)$$

To get rid of the term $\Gamma(t)^{\alpha-1}$, we need the condition $\alpha \geq 2$. Indeed, under this condition,

$$\Gamma(t)^{\alpha-1} \leq \Gamma(t) + \Gamma(t)^\alpha.$$

We also remove the term $\Gamma(t)^2$ by defining $\kappa := \max\{\alpha, 2\}$ and estimating

$$\Gamma(t)^2 \leq \Gamma(t) + \Gamma(t)^\kappa.$$

We deduce from elliptic regularity that

$$\Gamma(t) \leq C\|\Delta(\rho_R, c_R)\|_{L^2(\Omega)}^2 + C\|(\rho_R, c_R)\|_{H^1(\Omega)}^2.$$

Therefore, integrating (3.33) over $(0, t)$ and observing that $(\rho_R, c_R)(0) = 0$, (3.33) becomes

$$\Gamma(t) + C \int_0^t G(s)ds \leq C \int_0^t (\Gamma(s) + \Gamma(s)^\kappa)ds + C \int_0^t \Gamma(s)G(s)ds + C\delta^2.$$

Lemma B.2 proves the result for $\varepsilon = 1$.

Step 7: Parabolic-elliptic case $\varepsilon = 0$. Since there is no time derivative of c_R anymore, we need to change the definition of the functionals $\Gamma(t)$ and $G(t)$:

$$\Gamma_0(t) = \|\rho_R\|_{H^2(\Omega)}^2, \quad G_0(t) = \|\rho_R\|_{H^2(\Omega)}^2 + \|\nabla\Delta\rho_R\|_{L^2(\Omega)}^2.$$

The estimates are very similar to the parabolic-parabolic case with two exceptions: In (3.32), we have estimated the terms $\|\rho_R\|_{H^2(\Omega)}^2\|\nabla\Delta c_R\|_{L^2(\Omega)}^2$ and $\|\rho_R\|_{H^2(\Omega)}^2\|c_R\|_{H^2(\Omega)}^2$ from above by $\Gamma(t)G(t)$. In the present case, we cannot estimate $\|\nabla\Delta c_R\|_{L^2(\Omega)}^2$ by

$G_0(t)$ and we need to proceed in a different way.

Estimates (3.28) and (3.31), adapted to the case $\varepsilon = 0$, become

$$\begin{aligned} \|\Delta c_R\|_{L^2(\Omega)}^2 + \|\nabla c_R\|_{L^2(\Omega)}^2 &\leq C(1 + \|\rho_R\|_{H^2(\Omega)}^{2(\alpha-1)})\|\rho_R\|_{L^2(\Omega)}^2 + C\delta^2\|\Delta\rho_R\|_{L^2(\Omega)}^2 + C\delta^2 \\ &\leq C(\Gamma_0(t) + \Gamma_0(t)^\alpha) + C\delta^2, \\ \|\nabla\Delta c_R\|_{L^2(\Omega)}^2 + \|\Delta c_R\|_{L^2(\Omega)}^2 &\leq C\|\rho_R\|_{H^2(\Omega)}^{2(\alpha-1)} + C(1 + \|\rho_R\|_{H^2(\Omega)}^{2(\alpha-1)})\|\nabla\rho_R\|_{L^2(\Omega)}^2 \\ &\quad + C\delta^2\|\nabla\Delta\rho_R\|_{L^2(\Omega)}^2 + C\delta^2. \end{aligned}$$

The term $\delta^2\|\nabla\Delta\rho_R\|_{L^2(\Omega)}^2$ can be absorbed by the corresponding term on the left-hand side of (3.30). The critical term $\|\rho_R\|_{H^2(\Omega)}^{2(\alpha-1)}\|\nabla\rho_R\|_{L^2(\Omega)}^2$ is bounded from above by $\Gamma(t)^\alpha$. Thus, $\|\nabla\Delta c_R\|_{L^2(\Omega)}^2$ is estimated by $\Gamma_0(t)^\alpha$ and lower-order terms, and consequently, $\|\rho_R\|_{H^2(\Omega)}^2 \times \|\nabla\Delta c_R\|_{L^2(\Omega)}^2$ in (3.30) is estimated by $\Gamma_0(t)^\alpha G_0(t)$, together with lower-order terms. Furthermore, $\|\rho_R\|_{H^2(\Omega)}^2\|c_R\|_{H^2(\Omega)}^2$ is bounded by $\Gamma_0(t)^{\alpha+1}$, up to lower-order terms. More precisely, a computation shows that

$$\begin{aligned} \frac{d}{dt}(\|\rho_R\|_{H^1(\Omega)}^2 + \|\Delta\rho_R\|_{L^2(\Omega)}^2) &+ C(\|\rho_R\|_{H^2(\Omega)}^2 + \|\nabla\Delta\rho_R\|_{L^2(\Omega)}^2) + CG_0(t) \\ &\leq C(\Gamma_0(t) + \Gamma_0(t)^2 + \Gamma_0(t)^{\alpha-1} + \Gamma_0(t)^\alpha + \Gamma_0(t)^{\alpha+1} + \Gamma_0(t)G_0(t) \\ &\quad + \Gamma_0(t)^\alpha G_0(t) + \delta^2 G_0(t)) + C\delta^2. \end{aligned}$$

Observing that $\Gamma_0(t) \leq C(\|\rho_R\|_{H^1(\Omega)}^2 + \|\Delta\rho_R\|_{L^2(\Omega)}^2)$ and $\Gamma_0(t)^{\alpha-1} + \Gamma_0(t)^\alpha \leq \Gamma_0(t) + \Gamma_0(t)^{\alpha+1}$, choosing $\delta > 0$ sufficiently small, integrating in time, and observing that $\Gamma_0(0) = 0$, we arrive at

$$\begin{aligned} \Gamma_0(t) + C \int_0^t G_0(s)ds &\leq C \int_0^t (\Gamma_0(s) + \Gamma_0(s)^{\alpha+1})ds \\ &\quad + C \int_0^t (\Gamma_0(s) + \Gamma_0(s)^{\alpha+1})G_0(s)ds + C\delta^2. \end{aligned}$$

An application of Lemma B.2 finishes the proof. \square

3.4 Numerical Simulations

We present some numerical examples for system (3.1)–(3.2) in two space dimensions and for various choices of the parameters α and δ . Equations (3.1) are discretized by the implicit Euler method in time and by cubic finite elements in space. The scheme is implemented by using the finite-element library NGSolve/Netgen (<http://ngsolve.org>); see also [127, 128]. The mesh is refined in regions where large gradients are expected. The number of vertices is between 2805 and 12,448, and the

number of elements is between 5500 and 24,030. The time step is chosen between 10^{-3} and 10^{-4} when no blow up is expected and is decreased down to 10^{-13} close to expected blow-up times. The resulting nonlinear discrete systems are solved by the standard Newton method. The Jacobi matrix is computed by the NGSolve routine `AssembleLinearization`. The surface plots are generated by the Python package Matplotlib [78]. We do not use any kind of additional regularizations, smoothing tools, or slope-limiters. All simulations are performed for the parabolic-parabolic equations with $\delta > 0$.

We choose the same domain and initial conditions as in [28], i.e. $\Omega = \{x \in \mathbb{R}^2 : |x| < 1\}$ and

$$\rho^0(x, y) = 80(x^2 + y^2 - 1)^2(x - 0.1)^2 + 5, \quad c^0(x, y) = 0, \quad (x, y) \in \Omega. \quad (3.34)$$

A computation shows that the total mass $M = \int_{\Omega} \rho^0 dx = 25\pi/3 > 8\pi$ is supercritical, i.e., the solution to the classical Keller–Segel system can blow up in the interior of the domain. A sufficient condition is that the initial density is sufficiently concentrated in the sense that $\int_{\Omega} |x - x_0|^2 \rho^0 dx$ is sufficiently small for some $x_0 \in \Omega$. Blow up at the boundary can occur if $x_0 \in \partial\Omega$ and $M > 4\pi$.

Experiment 1: $\alpha = 1$. We choose the initial datum (3.34) and the values $\alpha = 1$, $\delta = 10^{-3}$. In this nonsymmetric setting, the solution exists for all time and the density is expected to concentrate at the boundary [75]. Figure 3.1 shows the surface plots for the cell density at various times. Since the total mass is initially concentrated near the boundary, we observe a boundary peak. Observe that there is no L^∞ blow-up. The steady state is reached at approximately $T = 2.5$. By Theorem 3.2, the peak approximates the blow-up solution to the classical Keller–Segel system, as illustrated in Figure 3.2. We see that the L^∞ norm of the density becomes larger with decreasing values of δ .

Experiment 2: $\alpha > 1$. First, we choose the value $\alpha = 1.5$. The initial datum is still given by (3.34). Since $\alpha > 1$, we cannot exclude finite-time blow-up, which is confirmed by the numerical simulations in Figure 3.3. Numerically, the solution seems to exist until time $T^* \approx 0.079$. The numerical scheme breaks down at slightly smaller times when δ becomes smaller. This may indicate that the numerical breakdown is an upper bound for the blow-up time for the classical Keller–Segel model. The break-down time becomes smaller for larger values of α . Indeed, Figure 3.4 shows a stronger and faster concentration behavior when we take $\alpha = 2.5$.

Experiment 3: Multi-bump initial datum. We take $\alpha = 1$ and $\delta = 5 \cdot 10^{-3}$. As initial datum, we choose a linear combination of the bump function

$$W_{x_0, y_0, M}(x, y) = \frac{M}{2\pi\theta} \exp\left(-\frac{(x - x_0)^2 + (y - y_0)^2}{2\theta}\right), \quad (x, y) \in \Omega,$$

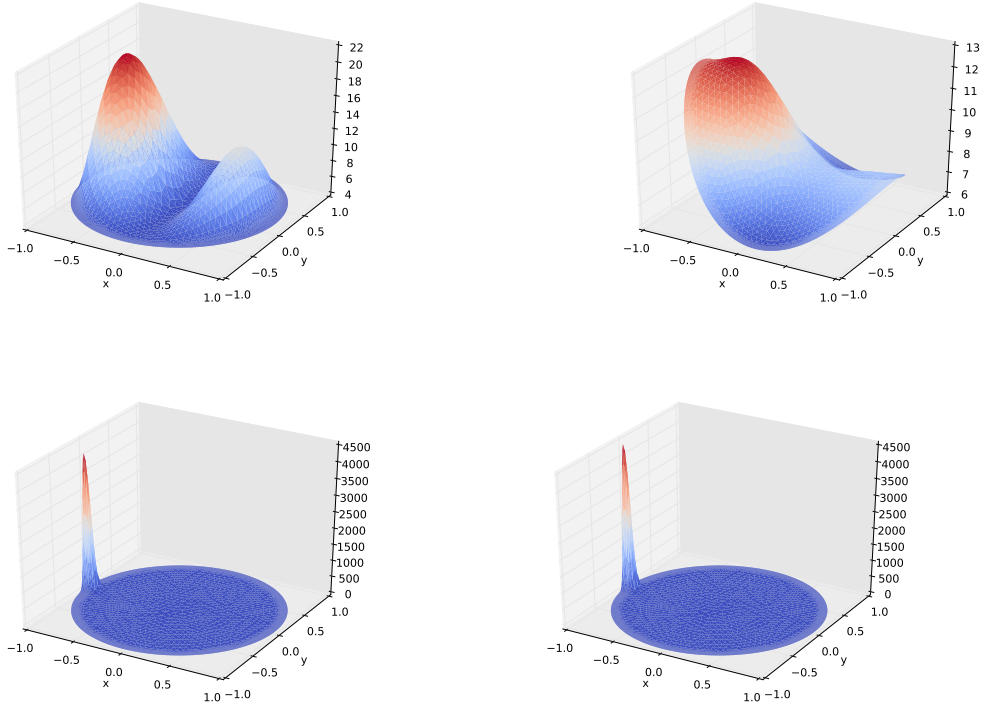


Figure 3.1: Cell density with $\alpha = 1$ and $\delta = 10^{-3}$ at times $t = 0$ (top left), $t = 0.1$ (top right), $t = 2.0$ (bottom left), $t = 5.0$ (bottom right).

where $(x_0, y_0) \in \Omega$, $M > 0$, and $\theta > 0$. Setting $\theta = 10^{-2}$, we define $c^0 = 0$ and

$$\begin{aligned} \rho^0 = & W_{0.25,0,10\pi} + W_{-0.25,0,4\pi} + W_{0,-0.25,4\pi} + W_{0,0.25,4\pi} \\ & + W_{0,0.5,4\pi} + W_{0,0.35,4\pi} + W_{0.5,0,4\pi} + W_{0.5,0.25,4\pi}. \end{aligned}$$

The evolution of the density is presented in Figure 3.5. The density concentrates in the interior of the domain and the peak travels to the boundary. At time $t = 1$, the peak is close to the boundary which is reached later at $t = 2.5$ (not shown). A similar behavior was already mentioned in [5] for the parabolic-elliptic model using a single-bump initial datum.

Experiment 4: Shape of peaks. The previous experiments show that the shape of the peaks depends on the value of δ . In this experiment, we explore this dependence in more detail. We claim that the diameter and the height of the bump can be controlled by δ . We choose $\alpha = 1$ and the initial datum $\rho^0 = W_{0,0,20\pi}$ with $\theta = 1/400$ and $c^0 = 0$. Furthermore, we prescribe homogeneous Dirichlet boundary conditions for c to avoid that the aggregated bump of cells moves to the boundary. Figure 3.6 (top row) shows the stationary cell densities for two values of δ . As expected,

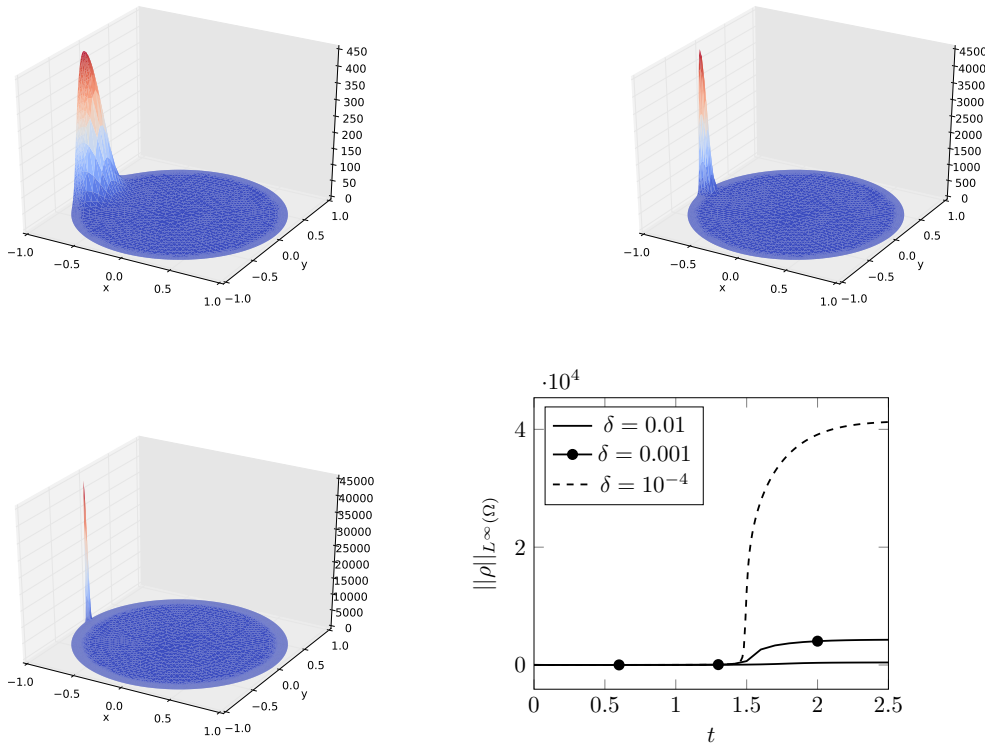


Figure 3.2: Cell density at time $T = 2.5$ with $\alpha = 1$ and $\delta = 10^{-2}$ (top left), $\delta = 10^{-3}$ (top right), $\delta = 10^{-4}$ (bottom left). The L^∞ norm of the density is shown in the bottom right panel.

the maximal diameter of the peak (defined at height 10^{-2}) becomes smaller and the maximum of the peak becomes larger for decreasing values of δ . The level sets show that the solutions are almost radially symmetric and the level set for $\rho = 10^{-2}$ is approximately a circle. This behavior is quantified in Figure 3.6 (bottom row). We observe that the radius depends on δ approximately as $r \sim \delta^{0.43}$ and the height approximately as $\rho_{\max} \sim \delta^{-1.00}$.

We remark that under no-flux boundary conditions for the chemical concentration, the same behavior of the bumps can be observed for intermediate times. However, the bump will eventually move to the boundary (as in Figure 3.5), since the chemical substance is not absorbed by the boundary as in the Dirichlet case.

Experiment 5: Two peaks and their journey. In this experiment we consider the rectangle $\Omega = [0, 1] \times [0, 0.4]$ with the same parameters as in the last experiments and $\delta = 0.0003$. This time, we consider two bumps as initial conditions, i.e. $\rho^0 = W_{0.2,0.2,13\pi} + W_{0.2,0.6,13\pi}$ and $c^0 = 0$ with $\theta = 1/500$, and follow their path to a stationary state. The results can be observed in Figure 3.7 for the density ρ . In

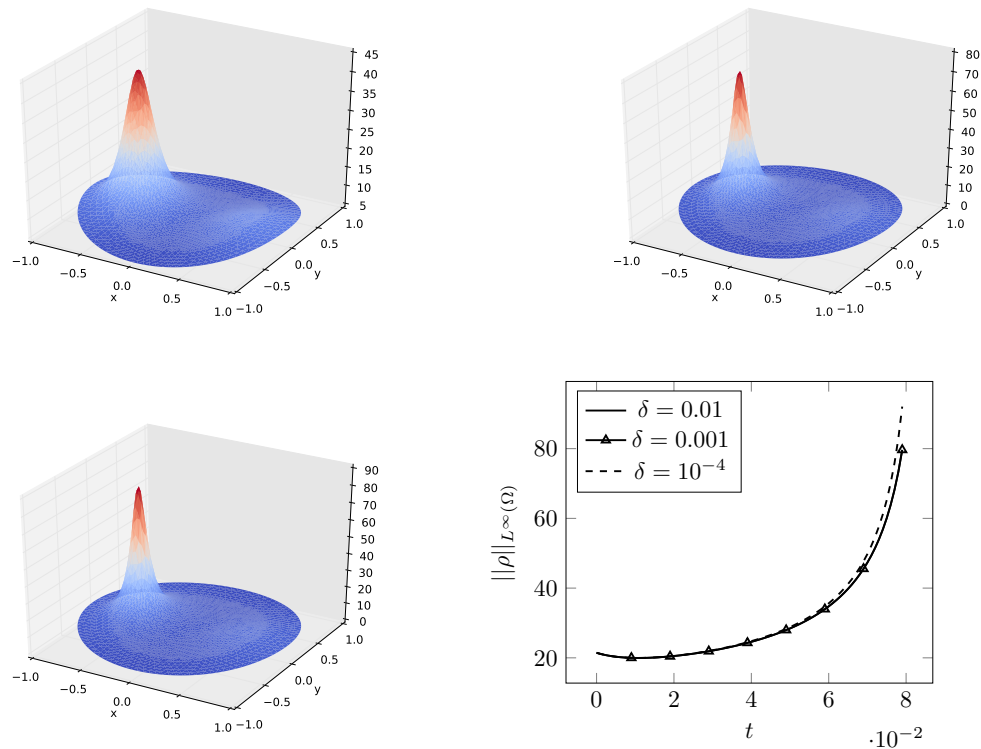


Figure 3.3: Cell density at time $T^* = 0.079$ with $\alpha = 1.5$ and $\delta = 10^{-2}$ (top left), $\delta = 10^{-3}$ (top right), $\delta = 10^{-4}$ (bottom left). The L^∞ norm of the density is shown in the bottom right panel.

addition, we added a contour plot for the density ρ in Figure 3.8 and for concentration c in Figure 3.9. After a short time of diffusing, since no chemoattractant is initially present, we see an aggregation of the density ρ at two different points. When the aggregation has concluded, we can observe that the bumps are traveling and fusing into one bump. Finally, this bump moves to the boundary and a stationary state is reached numerically. We remark that the domain is symmetric in the y direction and the concentration c should therefore be distributed in both corners evenly. This creates a checkmate situation for the density ρ . Nevertheless, this stationary state is a rather unstable. If the mesh size is not fine enough, the bump will leave this state and travel to one of the two nearby corners.

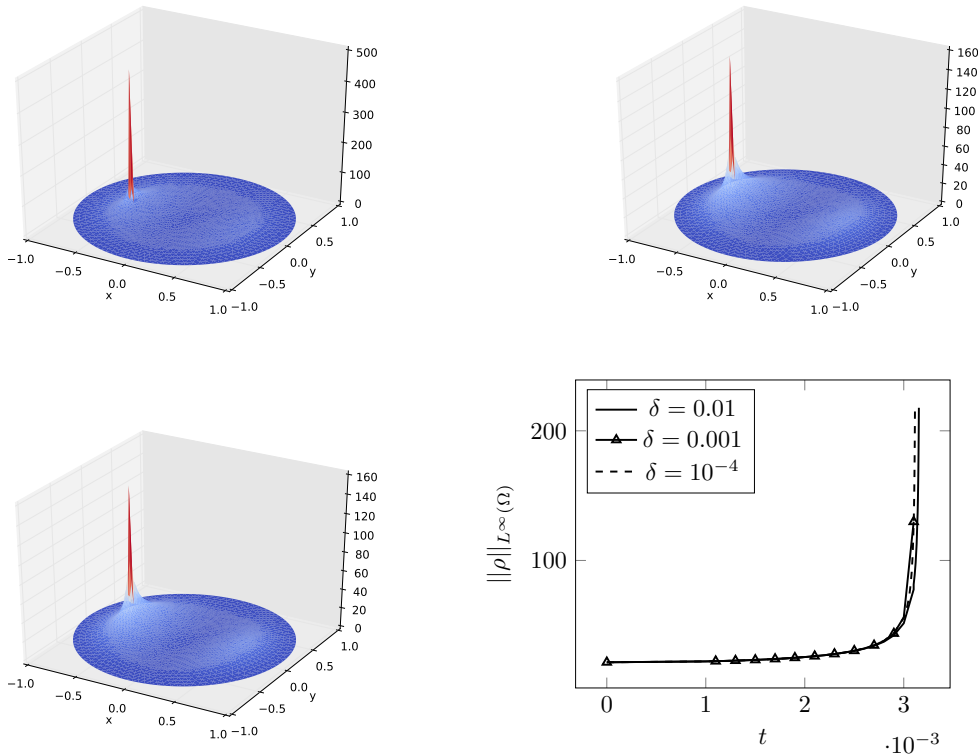


Figure 3.4: Cell density at time $T^* = 3.35 \cdot 10^{-3}$ with $\alpha = 2.5$ and $\delta = 10^{-2}$ (top left), $\delta = 10^{-3}$ (top right), $\delta = 10^{-4}$ (bottom left). The L^∞ norm of the density is shown in the bottom right panel.

3.5 Discussion and Outlook

Discussion

The topic of this chapter was a cross-diffusion regularization of the Keller–Segel system on bounded domains and its rigorous limit to the classical Keller–Segel system. We will structure the discussion of the results in two parts: a review of the analytical part and the conclusions that we can draw from the numerical simulations.

Analytical Results:

We have used two different strategies to pass to the limit in the regularized equations. In the parabolic-elliptic case with sublinear production rate, we could apply the boundedness-by-entropy method to establish the existence of a solution to an approximating system. In particular, we have discretized in time and added a higher

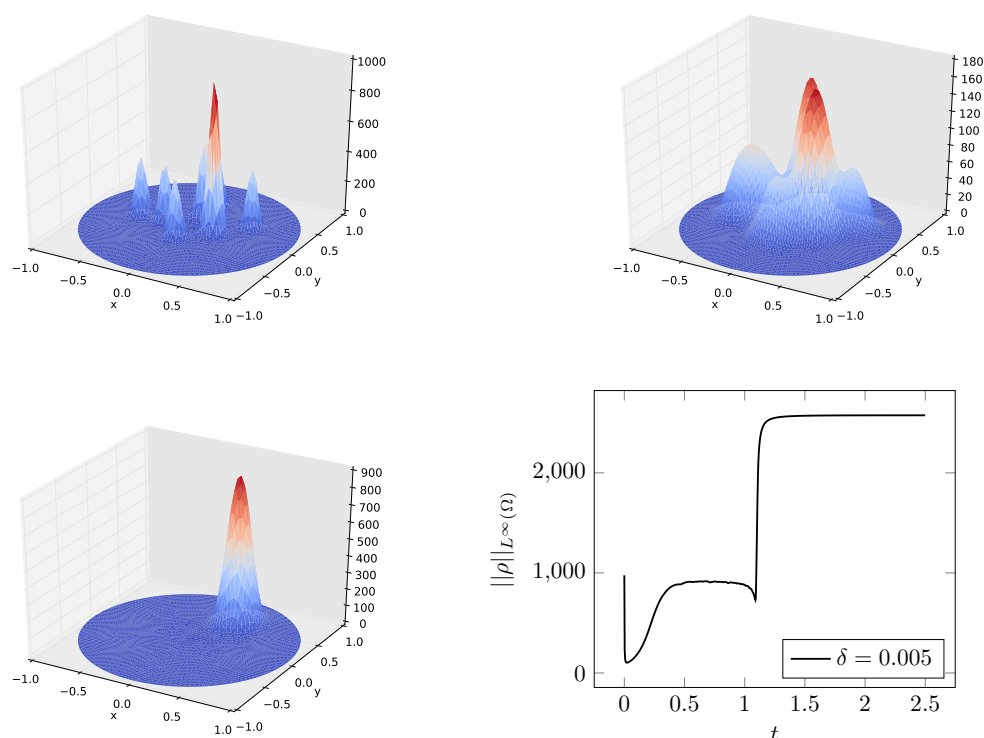


Figure 3.5: Cell density with $\alpha = 1$ and $\delta = 5 \cdot 10^{-3}$ at times $t = 0$ (top left), $t = 5 \cdot 10^{-3}$ (top right), $t = 1$ (bottom left). The L^∞ norm of the density is shown in the bottom right panel.

order regularization in space. The combination of two entropy functionals allowed us to derive H^1 and higher order L^p bounds uniform in all three regularization parameters. A discrete and continuous version of the Aubin-Lions lemma was then used to pass to the limit in a subsequence. We have simultaneously performed the limit in the time and space approximation, proving the existence of solutions to the cross-diffusion regularized problem for sublinear signal production. The gathered estimates are then used to pass to the limit in the cross-diffusion regularization. In particular, we have shown the existence of bounded solutions to the Keller–Segel model in the sublinear signal production case. Furthermore, the boundedness implies the uniqueness of the solution by a standard argument. This allows us to conclude that, in fact, the whole sequence is converging.

The general case with linear or at least quadratic signal production was attacked by a different approach. Since the solutions to the limit equations are known to blow up, there is no hope for uniform estimates of weak solutions. A compactness argument as in the previous case seems therefore futile. Thus, we chose a different

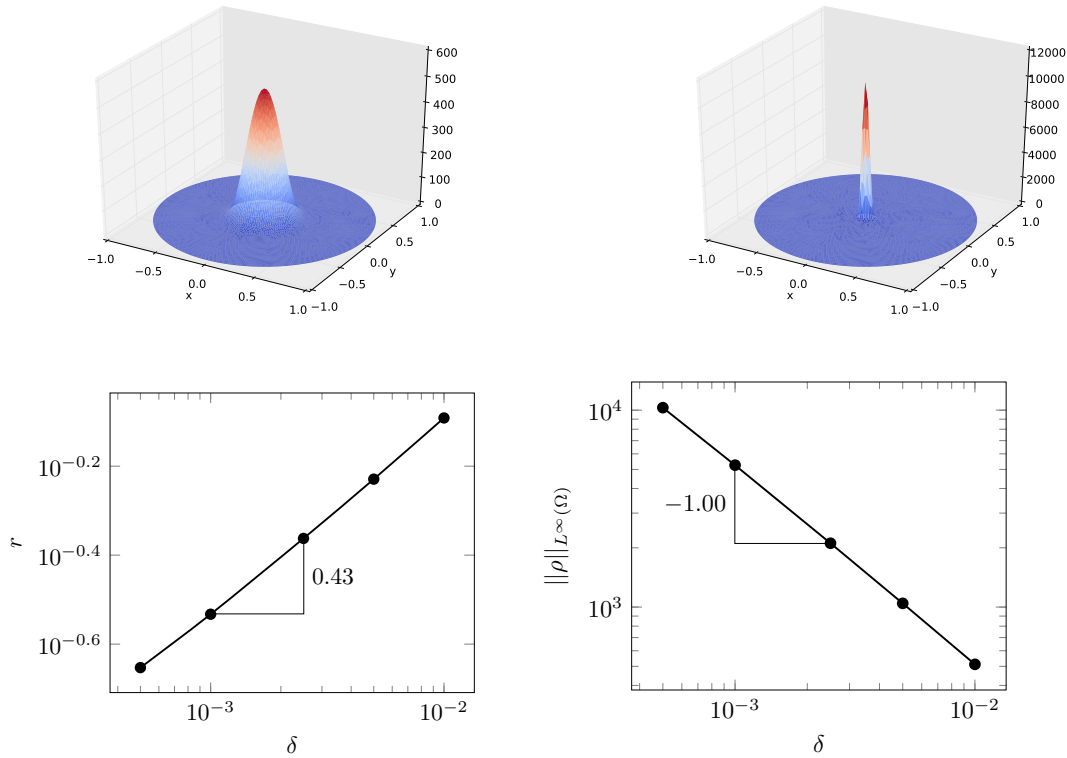


Figure 3.6: Cell density at time $t = 5$ (stationary case) with $\alpha = 1$ and $\delta = 10^{-2}$ (top left), $\delta = 5 \cdot 10^{-4}$ (top right). Log-log plots of the radius of the density level set $\rho = 10^{-2}$ versus δ (bottom left) and of the maximum of ρ versus δ (bottom right).

path and discussed the problem for smooth solutions. The proof for the existence of local-in-time smooth solutions to the regularized parabolic-parabolic and parabolic-elliptic system for at least linear signal production is standard, but the result is original. After establishing a series of tedious higher order estimates, we were able to use a nonlinear Gronwall lemma to derive an almost linear convergence rate. The optimal convergence rate is expected to be linear in this case. The reason for the non-optimality comes from the variant of the nonlinear Gronwall lemma proved in Lemma B.2. We conjecture that an optimal rate holds (changing the constants in Lemma B.2), but since this issue is of less interest, we did not explore it further. The condition of linear or at least quadratic signal production comes from the fact that the derivative of the mapping $s \mapsto s^\alpha$ is Hölder continuous exactly for these values.

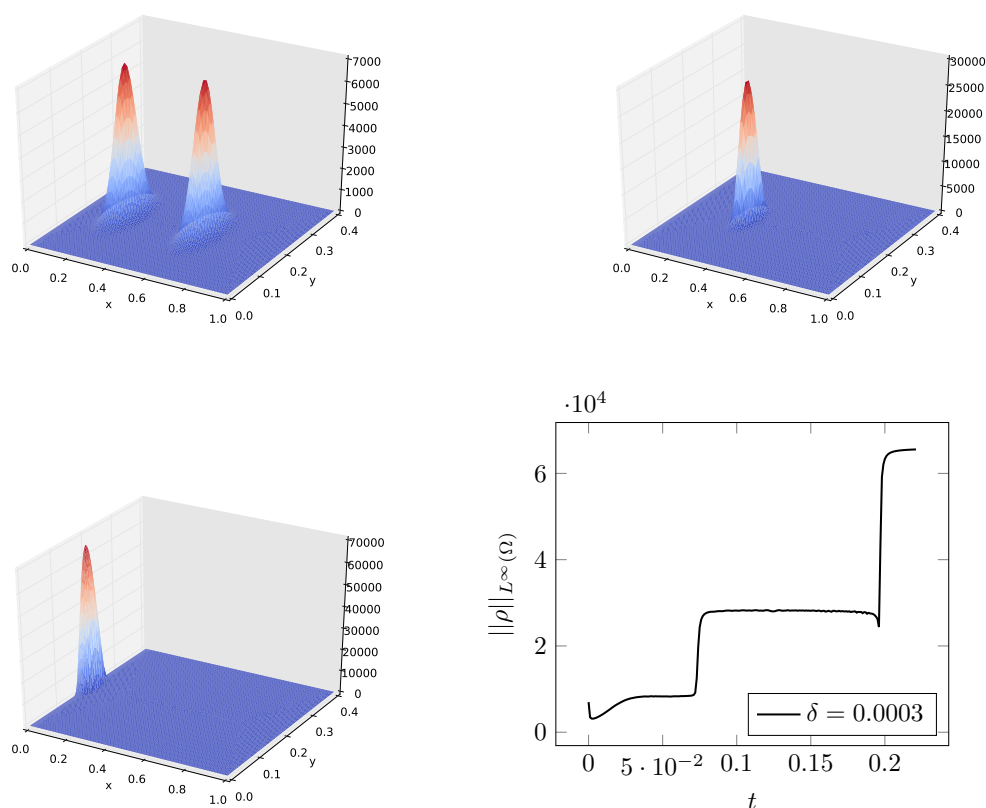


Figure 3.7: Cell density with $\alpha = 1$ and $\delta = 0.0003$ at times $t = 0$ (top left), $t = 0.08$ (top right), $t = 0.22$ (bottom left). The L^∞ norm of the density is shown in the bottom right panel.

Numerical Results:

The theoretical results are illustrated by numerical simulations, using the software tool NGSolve/Netgen. We used higher order finite elements in space and an implicit Euler discretization in time. The implicit scheme guarantees, at least numerically, the conservation of mass. In particular, the numerical results in Section 3.4 indicate that the convergence result may still hold for $\alpha \in (1, 2)$. For positive values of δ , the (globally existing) cell density forms bumps at places where the solution of the classical Keller–Segel system develops an $L^\infty(\Omega)$ blow up. Compared to the numerical results in [5, 68, 75], we investigate the dependence of the shape of the bumps on δ . In a radially symmetric situation, it turns out that the radius of the bump (more precisely the diameter of a level set $\rho_\delta \approx 0$) behaves like δ^a with $a \approx 0.43$, and the maximum of the bump behaves like δ^{-b} with $b \approx 1.00$. In addition, we observed the merging of two aggregated bumps into one subjected to no-flux boundary conditions

for both quantities. This bump is then traveling to a (heuristically correct) point at the boundary. The surface-, heat- and L^∞ -plots indicate the existence of these two different intermediate states and one final stationary state. The distribution of chemoattractant in both corners keeps the bump then in a rather unstable stationary state. We remark, that in this case, the same stationary state is reached with homogeneous Dirichlet boundary conditions for the chemoattractant.

Outlook

The results presented are limited to a certain parameter setting. Several extensions can be considered in a future work. First, the limitation of linear and quadratic signal production seems quite technical and should be treatable with a different approach. Second, one could extend the solution concept to measures, as in the previous chapter. This would allow to derive uniform estimates, independent of the signal production rate. Such a uniform bound seems hard to establish, but a possible compactness argument in this case would round off the analysis performed in this chapter. In general, it seems to be an obvious next step to approach the analysis of the classical Keller–Segel blow-up through the cross-diffusion regularization. A more detailed study of the relation between the aggregation radius and the regularization parameter should therefore be performed. Furthermore, this simple control over the aggregation radius could be used to capture the aggregation of cells in a more physically meaningful way. More modeling in this direction, using additional terms and parameter fitting, could be performed to establish tailored extensions of the Keller–Segel model in order to describe biological and physical phenomena. Last but not least, we mention here, that this cross-diffusion regularization also introduces an artificial entropy for this system. In particular, this allows one to use a structure preserving discrete entropy variable scheme for systems without entropy structure. Using a similar strategy as in the next chapter, we have performed numerical simulations with such a scheme; not presented in this thesis. This could lead the way for a new general method to design structure preserving schemes via the use of artificial entropy variables.

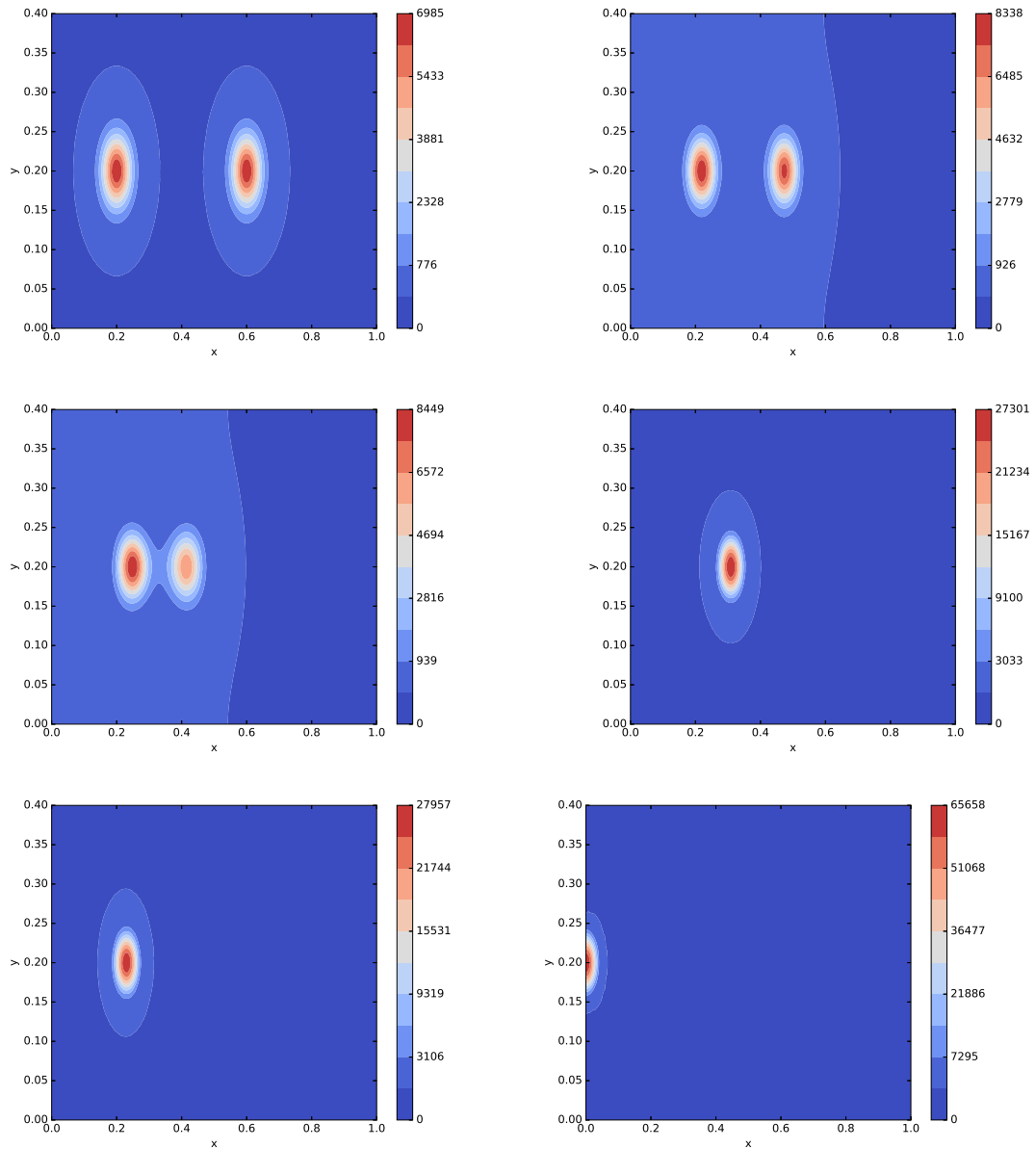


Figure 3.8: Filled contour plot of the cell density with $\alpha = 1$ and $\delta = 0.0003$ at times $t = 0, 0.62, 0.07, 0.08, 0.15$ and 0.22 (top left - bottom right).

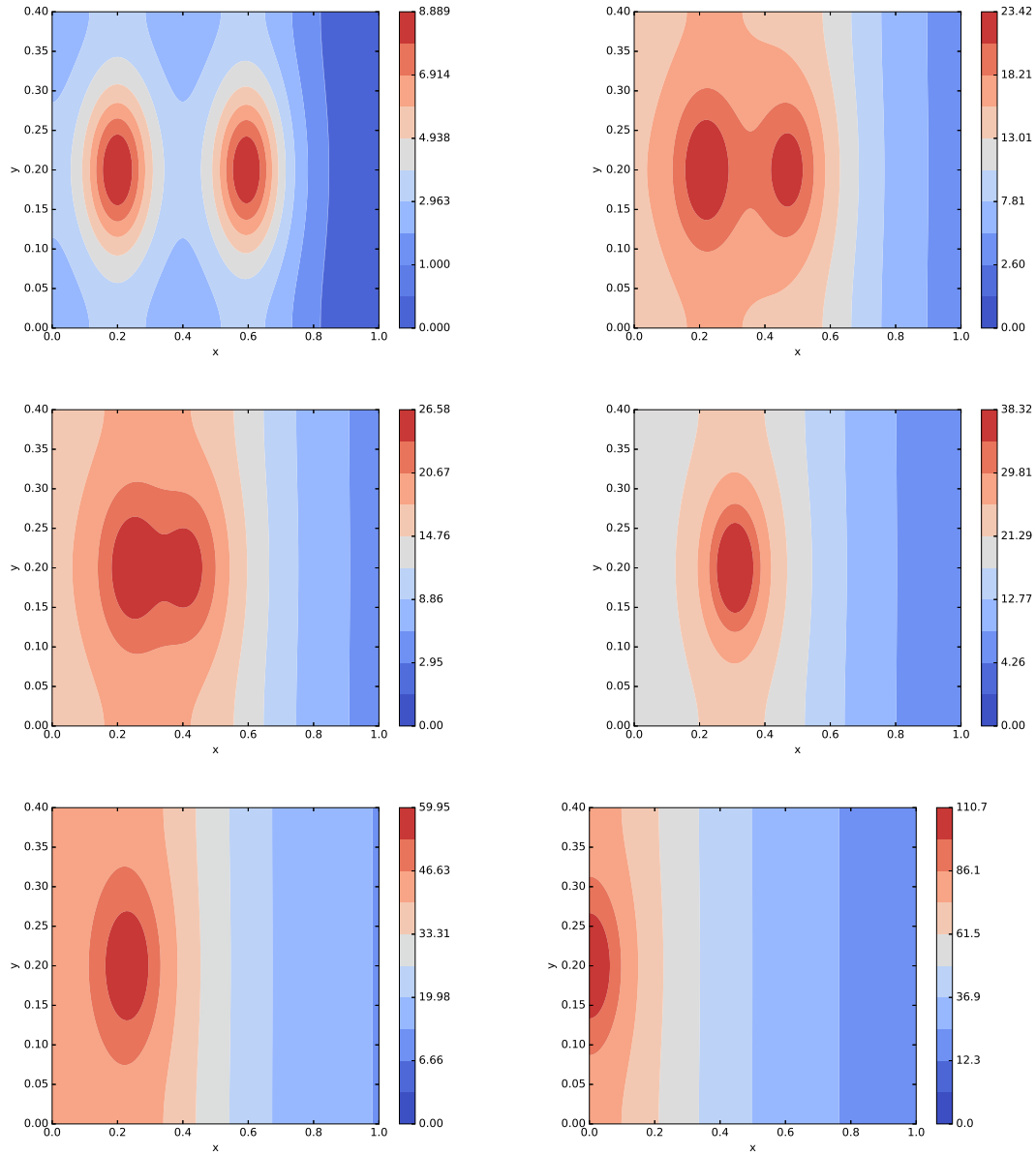


Figure 3.9: Filled contour plot of the concentration c with $\alpha = 1$ and $\delta = 0.0003$ at times $t = 0.015, 0.62, 0.07, 0.08, 0.15$ and 0.22 (top left - bottom right).



Die approbierte gedruckte Originalversion dieser Dissertation ist an der TU Wien Bibliothek verfügbar.
The approved original version of this doctoral thesis is available in print at TU Wien Bibliothek.

4 A Structure Preserving Scheme for a Poisson–Maxwell–Stefan System

In this chapter, we mathematically analyze Poisson–Maxwell–Stefan systems for the first time and show a discrete entropy production inequality. In particular, we extend the existence result of [93] for neutral mixtures to the case of charged mixtures and handle at the same time different molar masses as in [31]. This leads to a coupling of the Maxwell–Stefan system with a Poisson equation and the additional cross-diffusion terms cause some mathematical difficulties that are not present in a Nernst–Planck model, nor in the model for uncharged mixtures. As already stated in the introduction, we will deal with the system

$$\begin{aligned}
 \partial_t \rho' &= \operatorname{div}(A_0^{-1}(\rho) D'(\rho, \Phi)) + r'(x), & \rho_n &= 1 - \sum_{i=1}^{n-1} \rho_i, \\
 D_i &= \nabla x_i + (z_i x_i - (z \cdot x) \rho_i) \nabla \Phi, & i &= 1, \dots, n-1, \\
 -\lambda \Delta \Phi &= \sum_{i=1}^n z_i c_i + f(y), & & \text{in } \Omega,
 \end{aligned} \tag{4.1}$$

where $\rho' = (\rho_1, \dots, \rho_{n-1})$, $D' = (D_1, \dots, D_{n-1})$ and A_0^{-1} is neither positive definite nor symmetric. In addition, we impose the mixed boundary conditions

$$\begin{aligned}
 A_0^{-1} D' \cdot \nu &= 0 & \text{on } \partial\Omega, & i = 1, \dots, n-1, \\
 \Phi &= \Phi_D & \text{on } \Gamma_D, & \nabla \Phi \cdot \nu = 0 & \text{on } \Gamma_N,
 \end{aligned} \tag{4.2}$$

with $A_0^{-1} D' \cdot \nu$ and $\operatorname{div}(A_0^{-1} D')$ defined in the Section 1.6. Under the assumptions stated in Section 4.2, this is an equivalent formulation of the Poisson–Maxwell–Stefan system (1.7)-(1.11). The aim for this chapter is to translate the boundedness-by-entropy method for such a system into the fully discrete setting. In particular, this will provide us with the corresponding L^∞ bounds of the discrete solution, and a discrete version of the entropy production inequality. Furthermore, we will show that this scheme converges to a solution of the continuous model (4.1)-(4.2).

The chapter is structured as follows: we begin by presenting the key idea of this chapter in Section 4.1 and the main results in Section 4.2. In Section 4.3, we detail the thermodynamic modeling of system (1.7)-(1.9). Some auxiliary results on the formulation of the fluxes J_i and the inversion of the map $\rho \mapsto w$ are presented in

Section 4.4. Sections 4.5 and 4.6 are devoted to the proof of the main theorems. Finally, some numerical simulations are shown in Section 4.7.

4.1 Key Idea: A Discrete Boundedness-by-Entropy Method

We start by introducing the entropy variables

$$w_i = \frac{\log x_i}{M_i} - \frac{\log x_n}{M_n} + \left(\frac{z_i}{M_i} - \frac{z_n}{M_n} \right) \Phi, \quad i = 1, \dots, n-1, \quad (4.3)$$

where M_i is the molar mass and z_i is the charge of the i th component, and formulate the first equation of (4.1) as

$$\partial_t \rho'(w, \Phi) - \operatorname{div}(B(w, \Phi) \nabla w) = r'(x(w, \Phi)), \quad (4.4)$$

where $B = (B_{ij}) \in \mathbb{R}^{(n-1) \times (n-1)}$ is symmetric and positive definite; see Section 4.4.1 for details. The Poisson equation reads as

$$-\lambda \Delta \Phi = \sum_{i=1}^n z_i c_i(w, \Phi) + f(y). \quad (4.5)$$

We observe that now ρ' , c and x are functions of w and Φ . In particular, the system is now fully nonlinear, with a nonlinear function acting on the time derivative and a nonlinear diffusion term in (4.4), and a nonlinear source term in (4.5). The first advantage of this formulation is the positive definiteness of the matrix B . It allows us to derive an inequality for the already introduced entropy functional

$$H(\rho) = \int_{\Omega} h(\rho) dy, \quad h(\rho) = c_{\text{tot}} \sum_{i=1}^n x_i \log x_i + \frac{\lambda}{2} |\nabla(\Phi - \Phi_D)|^2,$$

since a formal computation shows that

$$\frac{dH}{dt} + \int_{\Omega} \nabla w : B \nabla w dy = \int_{\Omega} \sum_{i=1}^n r_i(x) \frac{\partial h}{\partial \rho_i} dy, \quad (4.6)$$

if Φ_D is constant and $\nabla w : B \nabla w = \sum_{i,j=1}^{n-1} B_{ij} \nabla w_i \cdot \nabla w_j$. As already stated in the introduction, this inequality and the positive definiteness of B reveals the Lyapunov functional property of the entropy H . In addition, we will show that the inversion of $\rho \mapsto w$ is well defined, nonnegative, bounded from above by one, and it holds that $\sum_{i=1}^n \rho_i(w) = 1$; see Subsection 4.4.2. In many cases, such a structure paves the

way for the usage of the boundedness-by-entropy method to show the existence of a solution; see e.g. [83]. These are the properties we want to carry over to the discrete realm. Simplified, the approach consists of the following steps:

1. Transform the system into entropy variables and show the existence of an inverse transformation.
2. Discretize in time and regularize in space.
3. Use the entropy inequality in a fixed-point argument to show the existence of a weak solution in the new variables.
4. Pass to the limit in the regularization and the time discretization.

We will now propose a fully discrete version of this argument and a numerical implementation that will preserve the structural properties discussed above.

An Implicit Euler Galerkin Scheme

First, as the method already builds on the discretization in time of a weak formulation, we choose a Galerkin discretization in space. Set $H_D^1(\Omega) = \{u \in H^1(\Omega) : u = 0 \text{ on } \Gamma_D\}$ and let $(\theta^{(k)})$ be a basis of $H_D^1(\Omega)$ and $(v^{(k)})$ be a basis of $H^1(\Omega; \mathbb{R}^{n-1})$ such that $v^{(k)} \in L^\infty(\Omega; \mathbb{R}^{n-1})$. For example, we can choose the eigenvectors of a compact symmetric operator like the Laplacian with the corresponding boundary conditions, see Appendix Lemma A.4 for a regularity result. We introduce the Galerkin spaces

$$P_N = \text{span}\{\theta^{(1)}, \dots, \theta^{(N)}\}, \quad V_N = \text{span}\{v^{(1)}, \dots, v^{(N)}\}.$$

Furthermore, let $T > 0$ and $N \in \mathbb{N}$ and set $\tau = T/N > 0$. These definitions allow us to consider the implicit Euler Galerkin scheme

$$\begin{aligned} \frac{1}{\tau} \int_{\Omega} (\rho'(u^k + w_D, \Phi^k) - \rho'(u^{k-1} + w_D, \Phi^{k-1})) \cdot \phi dy + \varepsilon \int_{\Omega} u^k \cdot \phi dy \\ + \int_{\Omega} \nabla \phi : B(u^k + w_D, \Phi^k) \nabla (u^k + w_D) dy = \int_{\Omega} r'(x(u^k + w_D, \Phi^k)) \cdot \phi dy, \end{aligned} \quad (4.7)$$

$$\lambda \int_{\Omega} \nabla \Phi^k \cdot \nabla \theta dy = \int_{\Omega} \left(\sum_{i=1}^n z_i c_i(u^k + w_D, \Phi^k) + f(y) \right) \theta dy \quad (4.8)$$

for $\phi \in V_N$, $\theta \in P_N$, $\varepsilon > 0$, and we have defined

$$w_D = (w_{D,1}, \dots, w_{D,n-1}), \quad w_{D,i} = \left(\frac{z_i}{M_i} - \frac{z_n}{M_n} \right) \Phi_D.$$

The discrete entropy variables are given by $w^k = u^k + w_D$, and we used the notation $c_i(w^k, \Phi^k) = \rho_i(w^k, \Phi^k)/M_i$, $x_i(w^k, \Phi^k) = c_i(w^k, \Phi^k)/c_{\text{tot}}^k$ for $i = 1, \dots, n$, and $c_{\text{tot}}^k = \sum_{i=1}^n \rho_i(w^k, \Phi^k)/M_i$.

Furthermore, let $\Phi^0 \in H^1(\Omega) \cap L^\infty(\Omega)$ be the unique solution to

$$-\lambda \Delta \Phi^0 = \sum_{i=1}^n z_i \frac{\rho_i^0}{M_i} + f(y) \text{ in } \Omega, \quad \nabla \Phi^0 \cdot \nu = 0 \text{ on } \Gamma_N, \quad \Phi^0 = \Phi_D \text{ on } \Gamma_D.$$

This defines (ρ^0, Φ^0) . We will show in Theorem 4.1 and Theorem 4.3, that this discrete formulation has a solution, that the inverse of the entropy transformation exists and that this scheme converges to a weak solution of the continuous problem. In order to implement this scheme, we have to take care of the nonlinear terms. We will accomplish this by combining a semi-implicit approach with a classical Newton iteration. In addition, we only know that the inverse of the entropy transformation exists, but no explicit formula is available. Hence, we have to use a fixed point argument in order to regain the original variables. This discretization and iteration procedure is carried out in Section 4.7.

4.2 Main Results

Before we continue with the rigorous arguments, we will state the main results of this chapter in detail. Therefore, we impose the following assumptions:

- (A1) Domain: $\Omega \subset \mathbb{R}^d$ is a bounded domain with Lipschitz boundary $\partial\Omega = \Gamma_D \cup \Gamma_N$, where $\Gamma_D \cap \Gamma_N = \emptyset$, Γ_N is open in $\partial\Omega$, and $\text{meas}(\Gamma_D) > 0$.
- (A2) Given functions: The initial datum $\rho^0 = (\rho_1^0, \dots, \rho_n^0)$ is nonnegative and measurable, satisfying $\rho_n^0 = 1 - \sum_{i=1}^{n-1} \rho_i^0 \geq 0$. The boundary data $\Phi_D \in H^1(\Omega) \cap L^\infty(\Omega)$ solves $-\lambda \Delta \Phi_D = f$ in Ω and $\nabla \Phi_D \cdot \nu = 0$ on Γ_N . Furthermore, let $f \in L^\infty(\Omega)$.
- (A3) Diffusion matrix: For any given $\rho \in [0, \infty)^n$ satisfying $\sum_{i=1}^n \rho_i = 1$, the transpose of the matrix $A = (A_{ij}) \in \mathbb{R}^{n \times n}$, defined by

$$A_{ij} = \begin{cases} \sum_{\ell=1, \ell \neq i}^n k_{i\ell} \rho_\ell & \text{for } i = j, \\ -k_{ij} \rho_i & \text{for } i \neq j, \end{cases}$$

has the kernel $\ker(A^\top) = \text{span}\{\mathbf{1}\}$, where $\mathbf{1} = (1, \dots, 1) \in \mathbb{R}^n$.

- (A4) Production rates: The functions $r_i \in C^0([0, 1]^n; \mathbb{R})$ satisfy $\sum_{i=1}^n r_i(x) \log x_i / M_i \leq C_r$ for some constant $C_r > 0$ and all $x \in (0, 1]^n$, $i = 1, \dots, n$.

Assumptions (A1) and (A2) are rather natural. By definition of A , it holds that $\ker(A^\top) \subset \text{span}\{\mathbf{1}\}$. If $k_{ij} > 0$ (and $\rho_j > 0$), a computation shows that $\text{span}\{\mathbf{1}\} = \ker(A^\top)$. For the general case $k_{ij} \geq 0$, this property cannot be guaranteed and needs to be assumed. This explains Assumption (A3). Assumption (A4) is needed to derive the entropy production inequality (4.6). It is satisfied for reversible reactions, see [39, Lemma 6] or [41]. It also holds in the context of a tumor-growth model, see [92].

Theorem 4.1 (Existence for the Galerkin scheme). *Let Assumptions (A1)-(A4) hold. Then there exists a weak solution $(w^k, \Phi^k) \in V_N \times P_N$ to (4.7)-(4.8) with $w^k = u^k + w_D$, satisfying*

- *preservation of L^∞ bounds: $0 < \rho_i^k < 1$ for $i = 1, \dots, n$;*
- *conservation of total mass: $\sum_{i=1}^n \rho_i^k = 1$ in Ω ;*
- *discrete entropy production inequality:*

$$\begin{aligned} H(\rho^k) + \tau \int_{\Omega} \nabla(w^k - w_D) : B(w^k, \Phi^k) \nabla w^k dy + \varepsilon \tau \int_{\Omega} |w^k - w_D|^2 dy \\ \leq \tau C_r |\Omega| + \tau \int_{\Omega} \sum_{i=1}^n \frac{z_i}{M_i} r_i(x^k) (\Phi^k - \Phi_D) dy + H(\rho^{k-1}), \end{aligned} \quad (4.9)$$

where $\rho^k = \rho(w^k, \Phi^k)$.

Theorem 4.1 is proved by using a fixed-point argument in the entropy variables. Using $w^k - w_D$ as a test function in the fully discrete version of (4.4), we show in Section 4.5 that

$$H(\rho^k) + \tau K \int_{\Omega} \sum_{i=1}^n |\nabla(x_i^k)^{1/2}|^2 dy + \varepsilon \tau \int_{\Omega} |w^k - w_D|^2 dy \leq \tau k K + H(\rho^{k-1}),$$

where $K > 0$ only depends on the given data. This is an estimated version of (4.6). The term involving ε is needed to conclude a uniform L^2 estimate for w^k , which is sufficient to apply the Leray-Schauder fixed-point theorem in the finite-dimensional Galerkin space. The ε -independent gradient estimate for x_i^k cannot be used since it does not give an estimate for w_i^k (see (4.3)). It is possible to analyze system (4.7)-(4.8) for $\varepsilon = 0$ – see Step 2 of the proof of Theorem 4.3 –, but we lose the information about w^k and obtain a solution in terms of ρ^k . The term involving ε is technical and not essential for the numerical simulations (or the structure preservation). However, we are not able to prove an existence result in terms of the entropy variable without such a regularization.

Remark 4.2 (Conservation of partial mass). *When $r_i = 0$, we have from (1.7) conservation of the partial mass $\|\rho_i\|_{L^1(\Omega)}$. This conservation property does not hold*

exactly on the discrete level because of the ε -regularization. It holds that for any $\delta > 0$, there exists $\varepsilon_0 > 0$ such that for any $0 < \varepsilon < \varepsilon_0$ (ε is the value in (4.7)),

$$\begin{aligned} \left| \|\rho_i^k\|_{L^1(\Omega)} - \|\rho_i^0\|_{L^1(\Omega)} \right| &\leq \delta \|\rho_i^0\|_{L^1(\Omega)}, \quad i = 1, \dots, n-1, \\ \left| \|\rho_n^k\|_{L^1(\Omega)} - \|\rho_n^0\|_{L^1(\Omega)} \right| &\leq \delta \sum_{i=1}^{n-1} \|\rho_i^0\|_{L^1(\Omega)}. \end{aligned}$$

The proof is the same as in [93, Theorem 4.1]. As $\delta > 0$ can be chosen arbitrarily small, this shows that the numerical scheme preserves the partial mass approximately.

Theorem 4.3 (Convergence of the Galerkin solution). *Let Assumptions (A1)-(A4) hold. Let (ρ^k, Φ^k) be a solution to (4.7)-(4.8) and set*

$$\rho_i^\tau(y, t) = \rho_i^k(y), \quad x_i^\tau(y, t) = x_i^k(y), \quad c_i^\tau(y, t) = c_i^k(y), \quad \Phi^\tau(y, t) = \Phi^k(y)$$

for $y \in \Omega$, $t \in ((k-1)\tau, k\tau]$, $i = 1, \dots, n$ and introduce the shift operator $(\sigma_\tau \rho_i^\tau)(y, t) = \rho_i^{k-1}(y)$ for $y \in \Omega$ and $t \in ((k-1)\tau, k\tau]$. Then there exist subsequences (not relabeled) such that, in the subsequent limits $\varepsilon \rightarrow 0$, then $N \rightarrow \infty$, and finally $\tau \rightarrow 0$,

$$\begin{aligned} \rho_i^\tau &\rightarrow \rho_i \quad \text{strongly in } L^p(0, T; L^p(\Omega)) \text{ for any } p < \infty, \\ x_i^\tau &\rightarrow x_i, \quad \Phi^\tau \rightarrow \Phi \quad \text{weakly in } L^2(0, T; H^1(\Omega)), \\ \tau^{-1}(\rho_i^\tau - \sigma_\tau \rho_i^\tau) &\rightarrow \partial_t \rho \quad \text{weakly in } L^2(0, T; H^1(\Omega)'), \quad i = 1, \dots, n, \end{aligned}$$

and the limit (ρ, Φ) satisfies for all $\phi \in L^2(0, T; H^1(\Omega; \mathbb{R}^{n-1}))$ and $\theta \in H_D^1(\Omega)$,

$$\int_0^T \langle \partial_t \rho', \phi \rangle dt + \int_0^T \int_\Omega \nabla \phi : A_0^{-1}(\rho) D' dy dt = \int_0^T \int_\Omega r'(x) \cdot \phi dy dt, \quad (4.10)$$

$$\lambda \int_\Omega \nabla \Phi \cdot \nabla \theta dy = \int_\Omega \left(\sum_{i=1}^n z_i \frac{\rho_i}{M_i} + f(y) \right) \theta dy, \quad (4.11)$$

where $D_i = \nabla x_i + (z_i x_i - (z \cdot x) \rho_i) \nabla \Phi$, $\rho_i = c_{\text{tot}} M_i x_i$, and $c_{\text{tot}} = \sum_{i=1}^n \rho_i / M_i$. Moreover, $\rho_n = 1 - \sum_{i=1}^{n-1} \rho_i$.

In Theorem 4.3, $\langle \cdot, \cdot \rangle$ denotes the duality bracket between the $H^1(\Omega; \mathbb{R}^{n-1})'$ and $H^1(\Omega; \mathbb{R}^{n-1})$. The difficult part of the proof is the estimate of the diffusion term because of the contribution of the electric field. We show in Lemma 4.8 that

$$\int_\Omega \nabla w^k : B \nabla w^k dy \geq K \int_\Omega \sum_{i=1}^n M_i^{1/2} \frac{|D_i^k|^2}{x_i^k} dy \geq K_1 \int_\Omega \sum_{i=1}^n |\nabla(x_i^k)^{1/2}|^2 dy - K_2$$

holds for some constants $K, K_1, K_2 > 0$, which are independent of ε, N , and τ . Then the uniform L^∞ bound for x_i^k gives a uniform $H^1(\Omega)$ bound for x_i^k and consequently

for ρ_i^k . Weak compactness allows us to pass to the limits $\varepsilon \rightarrow 0$ and $N \rightarrow \infty$, and the limit $\tau \rightarrow 0$ is performed by means of the Aubin-Lions lemma.

4.3 Modeling

We consider an isothermal electrolytic mixture of n fluid components in the bounded domain $\Omega \subset \mathbb{R}^d$ ($d \geq 1$) with boundary $\partial\Omega$. We assume that the mixture is not moving, so the barycentric velocity vanishes. The thermodynamic state of the mixture is described by the partial mass densities ρ_1, \dots, ρ_n and the electric field E . The partial mass density represents the mass of the substance per unit volume. In thermodynamics, one introduces also the molar concentrations c_i , signifying the amount of substance per unit volume. These quantities are related by $\rho_i = M_i c_i$, where M_i is the molar mass, the mass of the substance, divided by its amount. The total concentration is defined by $c_{\text{tot}} = \sum_{i=1}^n c_i$. Furthermore, $x_i = c_i/c_{\text{tot}} = \rho_i/(c_{\text{tot}} M_i)$ denotes the molar fraction, being the amount of the substance, divided by the total amount of all constituents of the mixture. We suppose the quasi-static approximation $E = -\nabla\Phi$, where Φ is the electric potential.

The evolution of the mass densities ρ_i is governed by the partial mass balances [45, (4)]

$$\partial_t \rho_i + \operatorname{div} J_i = r_i(x) \quad \text{in } \Omega, \quad t > 0, \quad i = 1, \dots, n,$$

where $x = (x_1, \dots, x_n)$ is the vector of molar fractions, J_i the diffusion flux, and $r_i(x)$ the mass production rate of the i th species. We assume that the total flux and the total production vanishes,

$$\sum_{i=1}^n J_i = 0, \quad \sum_{i=1}^n r_i(x) = 0,$$

which are necessary constraints to achieve total mass conservation, $\partial_t \sum_{i=1}^n \rho_i = 0$. We suppose that the total initial mass is constant in space, $\sum_{i=1}^n \rho_i^0 = \rho_{\text{tot}} > 0$, which implies that the total mass is constant in space and time, $\sum_{i=1}^n \rho_i(t) = \rho_{\text{tot}}$ for $t > 0$.

The electric potential Φ is given by the Poisson equation [46, (3) and (25)]

$$-\varepsilon_0(1 + \chi)\Delta\Phi = F \sum_{i=1}^n z_i c_i + f(y) \quad \text{in } \Omega,$$

where ε_0 is the dielectric constant, χ the dielectric susceptibility, F the Faraday constant, z_i the charge number of the i th species, and $f(y)$ with $y \in \Omega$ models the charge of fixed background ions.

The basic assumption of the Maxwell–Stefan theory is that the difference in speed and molar fractions leads to a diffusion flux. They are implicitly given by the driving

forces d_i according to [16, (200)]

$$-\sum_{j=1}^n \frac{x_j(J_i/M_i) - x_i(J_j/M_j)}{c_{\text{tot}}D_{ij}} = d_i, \quad i = 1, \dots, n,$$

where the numbers $D_{ij} = D_{ji}$ are the Maxwell–Stefan diffusivities. Inserting the definition $x_i = \rho_i/(c_{\text{tot}}M_i)$, we find that

$$-\sum_{j=1}^n \frac{\rho_j J_i - \rho_i J_j}{c_{\text{tot}}^2 M_i M_j D_{ij}} = d_i. \quad (4.12)$$

In the present situation, the driving force is given by two components, the variation of the chemical potential μ_i and the contribution of the body forces b_i [16, (211)]:

$$d_i = \frac{c_i M_i}{RT} \nabla \mu_i - \frac{\rho_i}{RT} (b_i - b_{\text{tot}}), \quad i = 1, \dots, n,$$

where R is the gas constant and T the (constant) temperature. Since (D_{ij}) is symmetric, summing (4.12) from $i = 1, \dots, n$ leads to $\sum_{i=1}^n d_i = 0$. Furthermore, $\sum_{i=1}^n \nabla \mu_i$ vanishes too; see below. This shows that $b_{\text{tot}} = \rho_{\text{tot}}^{-1} \sum_{i=1}^n \rho_i b_i$. We assume that the only force is due to the electric field (i.e., we neglect effects of gravity), $b_i = -(z_i/M_i)F\nabla\Phi$ [121, (3)].

It remains to determine the chemical potential. We define it by $\mu_i = \partial h_{\text{mix}}/\partial \rho_i$, where $h_{\text{mix}}(\rho) = c_{\text{tot}}RT(\sum_{i=1}^n x_i \log x_i + 1)$ is the mixing free energy density [45, (23)]. Then

$$\mu_i = \frac{1}{c_{\text{tot}}M_i} \frac{\partial h_{\text{mix}}}{\partial x_i} = \frac{RT}{M_i} (\log x_i + 1),$$

and the driving force becomes

$$\begin{aligned} d_i &= c_i \nabla \log x_i + \frac{\rho_i F}{RT} \left(\frac{z_i}{M_i} - \frac{1}{\rho_{\text{tot}}} \sum_{j=1}^n \frac{z_j \rho_j}{M_j} \right) \nabla \Phi \\ &= c_{\text{tot}} \left(\nabla x_i + \frac{F}{RT} \left(z_i x_i - (z \cdot x) \frac{\rho_i}{\rho_{\text{tot}}} \right) \nabla \Phi \right), \end{aligned} \quad (4.13)$$

where $z = (z_1, \dots, z_n)$ and $x = (x_1, \dots, x_n)$. The Gibbs–Duhem equation

$$\sum_{i=1}^n \rho_i \frac{\partial h_{\text{mix}}}{\partial \rho_i} - h_{\text{mix}}(\rho) = RT \sum_{i=1}^n \rho_i \frac{\log x_i + 1}{M_i} - c_{\text{tot}} RT \left(\sum_{i=1}^n x_i \log x_i + 1 \right) = 0$$

shows that the pressure vanishes, which is consistent with our choice of the driving force (see [16, (211)]). The driving force in [121, (7)] contains a non-vanishing pressure that is related to our expression for the total body force. The resulting driving force

(4.13), however, is the same.

We summarize the model equations:

$$\partial_t \rho_i + \operatorname{div} J_i = r_i(x), \quad i = 1, \dots, n, \quad (4.14)$$

$$-\varepsilon_0(1 + \chi)\Delta\Phi = F \sum_{i=1}^n z_i c_i + f(y), \quad (4.15)$$

$$-\sum_{j=1}^n \frac{\rho_j J_i - \rho_i J_j}{c_{\text{tot}}^3 M_i M_j D_{ij}} = \frac{d_i}{c_{\text{tot}}} = \nabla x_i + \frac{F}{RT} \left(z_i x_i - (z \cdot x) \frac{\rho_i}{\rho_{\text{tot}}} \right) \nabla \Phi, \quad (4.16)$$

and the relations

$$c_i = \frac{\rho_i}{M_i}, \quad x_i = \frac{\rho_i}{c_{\text{tot}} M_i}, \quad c_{\text{tot}} = \sum_{i=1}^n c_i.$$

The original system (1.7)-(1.9) is obtained from (4.14)-(4.16) after setting $\lambda = \varepsilon_0(1 + \chi)/F$, $k_{ij} = 1/(c_{\text{tot}}^3 M_i M_j D_{ij})$, and $D_i = d_i/c_{\text{tot}}$ and after nondimensionalization. In particular, we scale the particle densities by ρ_{tot} (then the scaled quantities satisfy $\sum_{i=1}^n \rho_i = 1$) and the electric potential by $F/(RT)$.

4.4 Auxiliary Results

We collect some auxiliary results needed for the existence analysis. The starting point is relation (1.8) between the fluxes J_i and the gradients ∇x_i . Observe that the coefficients k_{ij} depend on ρ_i via $c_{\text{tot}} = \sum_{i=1}^n \rho_i/M_i$. This dependency does not complicate the analysis since the results in this section hold pointwise for any given ρ_i and c_{tot} is uniformly bounded by

$$\frac{1}{\max_{i=1, \dots, n} M_i} \leq c_{\text{tot}} = \sum_{i=1}^n \frac{\rho_i}{M_i} \leq \frac{1}{\min_{i=1, \dots, n} M_i}.$$

4.4.1 Expressions for the Diffusion Fluxes

We review three different expressions for the diffusion fluxes following [31, 93] and extend the formulas to electro-chemical potentials. We reformulate (1.8):

$$D_i = - \sum_{j \neq i} k_{ij} (\rho_j J_i - \rho_i J_j) = - \sum_{j \neq i} k_{ij} \rho_i \rho_j \left(\frac{J_i}{\rho_i} - \frac{J_j}{\rho_j} \right). \quad (4.17)$$

The symmetry of (k_{ij}) implies that $\sum_{i=1}^n D_i = 0$. Compactly, we may write $D = -AJ$, where $D = (D_1, \dots, D_n)^\top$, $J = (J_1, \dots, J_n)^\top$, and $A = (A_{ij})$ with

$$A_{ij} = \begin{cases} \sum_{\ell=1, \ell \neq i}^n k_{i\ell} \rho_\ell & \text{for } i = j, \\ -k_{ij} \rho_i & \text{for } i \neq j. \end{cases}$$

By Assumption (A3), it holds that $\text{im}(A) = \ker(A^\top)^\perp = \text{span}\{\mathbf{1}\}^\perp$, where $\mathbf{1} = (1, \dots, 1)^\top \in \mathbb{R}^n$. We conclude from [93, Lemma 2.2] that all eigenvalues of $\tilde{A} := A|_{\text{im}(A)}$ are positive uniformly in $\rho \in [0, 1]^n$ and that \tilde{A} is invertible. Since $\sum_{i=1}^n J_i = 0$, each row of $J = (J_1, \dots, J_n)$ is an element of $\text{im}(A)$, so the linear system $D = -\tilde{A}J$ can be inverted, yielding $J = -\tilde{A}^{-1}D$.

We obtain another formulation by inverting the system in the first $n - 1$ variables. Setting $D' = (D_1, \dots, D_{n-1})$ and $J' = (J_1, \dots, J_{n-1})$, we can write $D' = -A_0 J'$, where the matrix $A_0 = (A_{ij}^0) \in \mathbb{R}^{(n-1) \times (n-1)}$ is defined by

$$A_{ij}^0 = \begin{cases} \sum_{\ell=1, \ell \neq i}^{n-1} (k_{i\ell} - k_{in}) \rho_\ell + k_{in} & \text{if } i = j, \\ -(k_{ij} - k_{in}) \rho_i & \text{if } i \neq j. \end{cases}$$

It is shown in [31, Lemma 4] that A_0 is invertible and A_0^{-1} is bounded uniformly in $\rho \in [0, 1]^n$. Thus, $J' = -A_0^{-1}D'$.

Finally, we invert the relations (4.17). Using $J_n = -\sum_{i=1}^{n-1} J_i$, these relations (or the equivalent form $D_i = -\sum_{j=1}^n A_{ij} J_j$) can be written as

$$\frac{D_i}{\rho_i} - \frac{D_n}{\rho_n} = -\sum_{j=1}^{n-1} C_{ij} J_j, \quad (4.18)$$

where

$$C_{ij} = \frac{A_{ij}}{\rho_i} - \frac{A_{in}}{\rho_i} - \frac{A_{nj}}{\rho_n} + \frac{A_{nn}}{\rho_n} = \frac{Y_{ij}}{\rho_i \rho_j} - \frac{Y_{in}}{\rho_i \rho_n} - \frac{Y_{nj}}{\rho_n \rho_j} + \frac{Y_{nn}}{\rho_n^2},$$

$$Y_{ij} = \begin{cases} \sum_{\ell=1, \ell \neq i}^n k_{i\ell} \rho_i \rho_\ell & \text{for } i = j, \\ -k_{ij} \rho_i \rho_j & \text{for } i \neq j. \end{cases}$$

The matrix $-Y = (-Y_{ij}) \in \mathbb{R}^{n \times n}$ is symmetric (since (k_{ij}) is symmetric), quasi-positive, irreducible, and it has the strictly positive eigenvector $\mathbf{1}$ with eigenvalue zero. Hence, by the Perron-Frobenius theorem, the spectral bound of $(-Y_{ij})$ is a simple eigenvalue (with value zero) and the spectrum of (Y_{ij}) consists of numbers with positive real part and zero. Thus, Y is positive semidefinite.

We claim that the matrix $C = (C_{ij}) \in \mathbb{R}^{(n-1) \times (n-1)}$ is positive definite on $\text{span}\{\mathbf{1}\}^\perp$. Indeed, let $y \in \text{span}\{\rho\}^\perp$. Then $y \cdot \rho = 0$. Since $\mathbf{1} \cdot \rho = 1$, we have $y \notin \text{span}\{\mathbf{1}\} = \ker(Y)$ and consequently, $\text{span}\{\rho\}^\perp \subset \ker(Y)^c$. This means that $-Y$ is negative

definite on $\text{span}\{\rho\}^\perp$. A computation shows that for any vector $w = (w_1, \dots, w_{n-1}) \in \mathbb{R}^{n-1}$, it holds that

$$\sum_{i,j=1}^{n-1} C_{ij} w_i w_j = \sum_{i,j=1}^n \frac{Y_{ij}}{\rho_i \rho_j} \tilde{w}_i \tilde{w}_j$$

where $\tilde{w}_i = w_i$ for $i = 1, \dots, n-1$ and $\tilde{w}_n = -\sum_{i=1}^{n-1} w_i$. Then $\tilde{w} = (\tilde{w}_1, \dots, \tilde{w}_n) \in \text{span}\{\mathbf{1}\}^\perp$. Since $-Y$ is negative definite on $\text{span}\{\rho\}^\perp$, we infer that $(-Y_{ij}/(\rho_i \rho_j))$ is negative definite on $\text{span}\{\mathbf{1}\}^\perp$. Therefore, C is positive definite on $\text{span}\{\mathbf{1}\}^\perp$. Its inverse $B := c_{\text{tot}} C^{-1}$ with $B = (B_{ij})$ exists, only depends on the mass density vector ρ , and is positive definite uniformly for all $\rho \in [0, 1]^n$ satisfying $\sum_{i=1}^n \rho_i = 1$ [31, Lemma 10]. We deduce from (4.18) and (1.8) that

$$\begin{aligned} J_i &= -\sum_{j=1}^{n-1} B_{ij} \left(\frac{D_j}{\rho_j} - \frac{D_n}{\rho_n} \right) \\ &= -\sum_{j=1}^{n-1} B_{ij} \left(\frac{\nabla \log x_j}{M_j} - \frac{\nabla \log x_n}{M_n} + \left(\frac{z_j}{M_j} - \frac{z_n}{M_n} \right) \nabla \Phi \right) \\ &= -\sum_{j=1}^{n-1} B_{ij} \nabla w_j \end{aligned}$$

for $i = 1, \dots, n-1$ and $J_n = -\sum_{i=1}^{n-1} J_i$, recalling definition (4.3) of w_i . We summarize:

Lemma 4.4 (Formulations of J_i). *Equations (4.17) can be written equivalently as*

$$J = -\tilde{A}^{-1} D, \quad J' = -A_0^{-1} D', \quad J' = -B \nabla w.$$

The last expression for J_i shows that the partial mass balances (1.7) can be formulated as

$$\partial_t \rho' - \text{div}(B \nabla w) = r'(\rho),$$

where $\rho = \rho(w)$ and $B = B(\rho(w))$. By Definition (4.3), w is a function of ρ (and Φ). The inverse relation $\rho(w)$ is discussed in the following subsection.

4.4.2 Inversion of $\rho \mapsto w$

Definition (4.3) defines, for given $\Phi \in \mathbb{R}$, a mapping $x \mapsto w$. We claim that this mapping can be inverted. If the molar masses are all the same, $M := M_i$, this can be done explicitly:

$$\rho_i(w) = \frac{\exp(M w_i - (z_i - z_n) \Phi)}{1 + \sum_{j=1}^{n-1} \exp(M w_j - (z_j - z_n) \Phi)}, \quad i = 1, \dots, n-1,$$

and $\rho_n = 1 - \sum_{i=1}^{n-1} \rho_i$. Unfortunately, when the molar masses are different, we cannot derive an explicit formula. Instead we adapt Lemma 6 in [31].

Lemma 4.5 (Inversion of w and x). *Let $\Phi \in \mathbb{R}$ and define the function*

$$W_\Phi : \left\{ x = (x_1, \dots, x_n) \in (0, 1)^n : \sum_{i=1}^n x_i = 1 \right\} \rightarrow \mathbb{R}^{n-1}$$

by $W_\Phi(x) = (w_1(x), \dots, w_{n-1}(x))$, where

$$w_i(x) = \frac{\log x_i}{M_i} - \frac{\log x_n}{M_n} + \left(\frac{z_i}{M_i} - \frac{z_n}{M_n} \right) \Phi, \quad i = 1, \dots, n-1.$$

Then W_Φ is invertible and we can define $x(w, \Phi) = (x'(w, \Phi), x_n(w, \Phi)) := W_\Phi^{-1}(w)$, where $x'(w, \Phi) = (x_1, \dots, x_{n-1})$ and $x_n(w, \Phi) := 1 - \sum_{i=1}^{n-1} x_i$.

Proof. The proof is similar to that one of [31, Lemma 6]. Let $w = (w_1, \dots, w_{n-1}) \in \mathbb{R}^{n-1}$ and $\Phi \in \mathbb{R}$ be given. Define the function $f : [0, 1] \rightarrow [0, \infty)$ by

$$f(s) = \sum_{i=1}^{n-1} (1-s)^{M_i/M_n} \exp \left[M_i w_i - M_i \left(\frac{z_i}{M_i} - \frac{z_n}{M_n} \right) \Phi \right], \quad s \in [0, 1].$$

Then f is continuous, strictly decreasing, and $0 = f(1) < f(s) < f(0)$ for $s \in (0, 1)$. Hence, there exists a unique fixed point $s_0 \in (0, 1)$ such that $f(s_0) = s_0$. We define

$$x_i = (1-s_0)^{M_i/M_n} \exp \left[M_i w_i - M_i \left(\frac{z_i}{M_i} - \frac{z_n}{M_n} \right) \Phi \right] > 0, \quad i = 1, \dots, n-1. \quad (4.19)$$

By definition, we have $\sum_{i=1}^{n-1} x_i = f(s_0) = s_0 < 1$. We set $x_n = 1 - s_0 > 0$ such that $\sum_{i=1}^n x_i = 1$. Moreover, (4.19) can be written equivalently as

$$\frac{\log x_i}{M_i} + \frac{\log(1-s_0)}{M_n} + \left(\frac{z_i}{M_i} - \frac{z_n}{M_n} \right) \Phi = w_i,$$

and since $1 - s_0 = x_n$, this shows that $W_\Phi^{-1}(w) = (x', x_n)$ is the inverse mapping. \square

Given $\rho \in [0, 1]^n$, we know that $x_i = \rho_i / (c_{\text{tot}} M_i)$ for $i = 1, \dots, n$ and $\sum_{i=1}^n x_i = 1$. This relation can be inverted too. We recall [31, Lemma 7]:

Lemma 4.6 (Inversion of ρ and x). *Let $x' \in (0, 1)^{n-1}$ and $x_n = 1 - \sum_{i=1}^{n-1} x_i > 0$ be given and define for $i = 1, \dots, n$,*

$$\rho_i(x') = \rho_i := c_{\text{tot}} M_i x_i, \quad \text{where } c_{\text{tot}} = \left(\sum_{j=1}^n M_j x_j \right)^{-1}.$$

Then $\rho = (\rho_1, \dots, \rho_n)$ is the unique vector satisfying $\rho_n = 1 - \sum_{i=1}^{n-1} \rho_i > 0$, $x_i = \rho_i / (c_{\text{tot}} M_i)$ for $i = 1, \dots, n$, and $c_{\text{tot}} = \sum_{i=1}^n \rho_i / M_i$.

Combining Lemmas 4.5 and 4.6, we conclude as in [31] that the mapping $\rho \mapsto w$ can be inverted. In fact, we just have to define $\rho' = \rho'(x'(w, \Phi))$.

Corollary 4.7 (Inversion of ρ and w). *Let $w = (w_1, \dots, w_{n-1}) \in \mathbb{R}^{n-1}$ and $\Phi \in \mathbb{R}$ be given. Then there exists a unique vector $\rho = (\rho_1, \dots, \rho_n) \in (0, 1)^n$ satisfying $\sum_{i=1}^n \rho_i = 1$ such that (4.3) holds for $\rho_n = 1 - \sum_{i=1}^{n-1} \rho_i$ and $x_i = \rho_i / (c_{\text{tot}} M_i)$ with $c_{\text{tot}} = \sum_{i=1}^n \rho_i / M_i$. The mapping $\rho' : \mathbb{R}^n \rightarrow (0, 1)^{n-1}$, $\rho'(w, \Phi) = (\rho_1, \dots, \rho_{n-1})$, is bounded, i.e. $|\rho'(w, \Phi)| \leq 1$ for all $(w, \Phi) \in \mathbb{R}^n$.*

4.5 Existence of a Discrete Solution

Proof of Theorem 4.1

Step 1: existence of solutions. The idea is to apply the Leray-Schauder fixed-point theorem. We need to define the fixed-point operator. For this, let $\chi \in L^\infty(\Omega; \mathbb{R}^{n-1})$ and $\sigma \in [0, 1]$. Since $(y, \Phi) \mapsto \rho_i(\omega(y), \Phi)$ is a bounded function with values in $(0, 1)$, we can use Schauder's fixed-point theorem and standard arguments to show the existence of a solution $\Phi^k - \Phi_D \in P_N$ of the nonlinear finite-dimensional problem

$$\lambda \int_{\Omega} \nabla \Phi^k \cdot \nabla \theta dy = \int_{\Omega} \left(\sum_{i=1}^n z_i c_i (\chi + w_D, \Phi^k) + f(y) \right) \theta dy$$

for all $\theta \in P_N$. In particular, the solution is unique and we have $\Phi^k \in L^\infty(\Omega)$, for $\Phi \mapsto \rho_i(\omega, \Phi)$ is Lipschitz continuous and $\Phi_D \in L^\infty(\Omega)$.

Next, we wish to solve the linear finite-dimensional problem

$$a(u, \phi) = \sigma F(\phi) \quad \text{for all } \phi \in V_N, \quad (4.20)$$

where

$$\begin{aligned} a(u, \phi) &= \int_{\Omega} \nabla \phi : B(\chi + w_D, \Phi^k) \nabla u dy + \varepsilon \int_{\Omega} u \cdot \phi dy, \\ F(\phi) &= -\frac{1}{\tau} \int_{\Omega} (\rho'(\chi + w_D, \Phi^k) - \rho'(u^{k-1} + w_D, \Phi^{k-1})) \cdot \phi dy \\ &\quad + \int_{\Omega} r'(x(\chi + w_D, \Phi^k)) \cdot \phi dy - \int_{\Omega} \nabla \phi : B(\chi + w_D, \Phi^k) \nabla w_D dy \end{aligned}$$

for $u, \phi \in V_N$, where we set in case $k = 1$, $\rho'(u^0 + w_D) := (\rho^0)'$. Since $\chi + w_D \in L^\infty(\Omega; \mathbb{R}^{n-1})$ and $\Phi^k \in L^\infty(\Omega)$, Corollary 4.7 shows that $\rho(\chi + w_D, \Phi^k)$ is bounded. We know from Section 4.4.1 that the matrix $B = B(\chi + w_D, \Phi^k)$ is positive definite

and its elements are bounded. We deduce that the forms a and F are continuous on V_N . Exploiting the equivalence of the norms in the finite-dimensional space V_N , we find that

$$a(u, u) \geq \varepsilon \|u\|_{L^2(\Omega)}^2 \geq \varepsilon K_N \|u\|_{H^1(\Omega)}^2$$

for some constant $K_N > 0$, which implies that a is coercive on V_N . By the Lax–Milgram lemma, there exists a unique solution $u \in V_N \subset L^\infty(\Omega; \mathbb{R}^{n-1})$ to (4.20) satisfying

$$\varepsilon K_N \|u\|_{H^1(\Omega)}^2 \leq a(u, u) = \sigma F(u) \leq K_F \|u\|_{H^1(\Omega)}, \quad (4.21)$$

for some constant K_F , which is independent of τ and σ . Using again the bounds for ρ' and r' , we find that the constant K_F is independent of Φ^k . Since all norms are equivalent in the finite-dimensional setting, this provides a uniform $L^\infty(\Omega)$ bound for u .

This defines the fixed-point operator $S : L^\infty(\Omega; \mathbb{R}^{n-1}) \times [0, 1] \rightarrow L^\infty(\Omega; \mathbb{R}^{n-1})$, $S(\chi, \sigma) = u$. Standard arguments, see for example [83], show that S is continuous. Since V_N is finite-dimensional, S is also compact. Furthermore, $S(\chi, 0) = 0$. Estimate (4.21) provides a uniform bound for all fixed points of $S(\cdot, \sigma)$. Thus, by the Leray–Schauder fixed-point theorem, there exists $u^k \in V_N$ such that $S(u^k, 1) = u^k$, and $w^k := u^k + w_D$, Φ^k solve (4.7)–(4.8).

Step 2: proof of the discrete entropy production inequality (4.9). We use the test function $\tau(w^k - w_D) \in V_N$ in (4.7) and set $\rho^k := \rho'(w^k, \Phi^k)$:

$$\begin{aligned} & \int_{\Omega} (\rho^k - \rho^{k-1}) \cdot (w^k - w_D) dy + \tau \int_{\Omega} \nabla(w^k - w_D) : B(w^k, \Phi^k) \nabla w^k dy \\ & + \varepsilon \tau \int_{\Omega} |w^k - w_D|^2 dy \leq \tau \int_{\Omega} r'(x^k) \cdot (w^k - w_D) dy. \end{aligned}$$

We claim that the first term on the left-hand side is greater than the difference of the entropies at time steps k and $k - 1$. To show this, we split the entropy density into two parts, $h(\rho^k) = h_1(\rho^k) + h_2(\rho^k)$, where

$$h_1(\rho^k) = c_{\text{tot}}^k \sum_{i=1}^n x_i^k \log x_i^k, \quad h_2(\rho^k) = \frac{\lambda}{2} |\nabla(\Phi^k - \Phi_D)|^2,$$

where we recall that $x_i^k = \rho_i^k / (c_{\text{tot}}^k M_i)$ and $c_{\text{tot}}^k = \sum_{i=1}^n \rho_i^k / M_i$. By the convexity of h_1 , we have

$$h_1(\rho^k) - h_1(\rho^{k-1}) \leq \frac{\partial h_1}{\partial \rho'}(\rho^k) \cdot (\rho^k - \rho^{k-1}) = \sum_{i=1}^n (\rho_i^k - \rho_i^{k-1}) \frac{\log x_i^k}{M_i}.$$

Therefore, using $\rho_n^k - \rho_n^{k-1} = -\sum_{i=1}^{n-1}(\rho_i^k - \rho_i^{k-1})$,

$$\begin{aligned} \int_{\Omega} (h_1(\rho^k) - h_1(\rho^{k-1})) dx &\leq \int_{\Omega} \left(\sum_{i=1}^{n-1} (\rho_i^k - \rho_i^{k-1}) \frac{\log x_i^k}{M_i} + (\rho_n^k - \rho_n^{k-1}) \frac{\log x_n^k}{M_n} \right) dy \\ &= \int_{\Omega} \sum_{i=1}^{n-1} (\rho_i^k - \rho_i^{k-1}) \left(\frac{\log x_i^k}{M_i} - \frac{\log x_n^k}{M_n} \right) dy. \end{aligned} \quad (4.22)$$

For the estimate of h_2 , we first observe that

$$\begin{aligned} \sum_{i=1}^{n-1} (\rho_i^k - \rho_i^{k-1}) \left(\frac{z_i}{M_i} - \frac{z_n}{M_n} \right) &= \sum_{i=1}^{n-1} (\rho_i^k - \rho_i^{k-1}) \frac{z_i}{M_i} + (\rho_n^k - \rho_n^{k-1}) \frac{z_n}{M_n} \\ &= \sum_{n=1}^n (\rho_i^k - \rho_i^{k-1}) \frac{z_i}{M_i}. \end{aligned}$$

We infer from the Poisson equation (4.8) and Young's inequality that

$$\begin{aligned} &\int_{\Omega} \sum_{i=1}^{n-1} (\rho_i^k - \rho_i^{k-1}) \left(\frac{z_i}{M_i} - \frac{z_n}{M_n} \right) (\Phi^k - \Phi_D) dy \\ &= \int_{\Omega} \sum_{i=1}^n (\rho_i^k - \rho_i^{k-1}) \frac{z_i}{M_i} (\Phi^k - \Phi_D) dy = \int_{\Omega} \sum_{i=1}^n z_i (c_i^k - c_i^{k-1}) (\Phi^k - \Phi_D) dy \\ &= \lambda \int_{\Omega} \nabla((\Phi^k - \Phi_D) - (\Phi^{k-1} - \Phi_D)) \cdot \nabla(\Phi^k - \Phi_D) dy \\ &\geq \frac{\lambda}{2} \int_{\Omega} |\nabla(\Phi^k - \Phi_D)|^2 dy - \frac{\lambda}{2} \int_{\Omega} |\nabla(\Phi^{k-1} - \Phi_D)|^2 dy \\ &= \int_{\Omega} (h_2(\Phi^k) - h_2(\Phi^{k-1})) dy. \end{aligned}$$

Taking into account the property $r_n(\rho^k) = -\sum_{i=1}^{n-1} r_i(\rho^k)$, definition (4.3) of w_i^k , and

Assumption (A4), we compute

$$\begin{aligned}
 \int_{\Omega} r'(x^k) \cdot (w^k - w_D) dy &= \int_{\Omega} \sum_{i=1}^{n-1} r_i(x^k) \left(\frac{\log x_i^k}{M_i} - \frac{\log x_n^k}{M_n} \right) dy \\
 &\quad + \int_{\Omega} \sum_{i=1}^{n-1} r_i(x^k) \left(\frac{z_i}{M_i} - \frac{z_n}{M_n} \right) (\Phi^k - \Phi_D) dy \\
 &= \int_{\Omega} \sum_{i=1}^n r_i(x^k) \frac{\log x_i^k}{M_i} dy + \int_{\Omega} \sum_{i=1}^n r_i(x^k) \frac{z_i}{M_i} (\Phi^k - \Phi_D) dy \\
 &\leq C_r |\Omega| + \int_{\Omega} \sum_{i=1}^n r_i(x^k) \frac{z_i}{M_i} (\Phi^k - \Phi_D) dy,
 \end{aligned} \tag{4.23}$$

Combining (4.22)-(4.23) gives the conclusion.

4.6 Convergence of the Scheme

Proof of Theorem 4.3

Let (w^k, Φ^k) be a weak solution to scheme (4.7)-(4.8) and define $\rho^k = \rho(w^k, \Phi^k)$.

Step 1: uniform estimates. We derive estimates for ρ^k and Φ^k independent of ε , τ , and N . The starting point is the discrete entropy production inequality (4.9), and the main task is to estimate the diffusion part.

Lemma 4.8 (Estimate of the diffusion part). *There exist constants $K_1 > 0$ and $K_2 > 0$, both independent of ε , τ , and N , such that*

$$\int_{\Omega} \nabla(w^k - w_D) : B \nabla w^k dy \geq K_1 \sum_{i=1}^n \|\nabla(x_i^k)^{1/2}\|_{L^2(\Omega)}^2 - K_2.$$

Proof. We drop the superindex k in the proof to simplify the notation. Recall that $\tilde{A} = A|_{\text{im}(A)}$, where $\text{im}(A) = \text{span}\{\mathbf{1}\}^\perp$. We introduce as in the proof of Lemma 12 in [31] the symmetrization $\tilde{A}_S = P^{-1/2} \tilde{A} P^{1/2}$, where $P^{1/2} = M^{1/2} X^{1/2}$ and $M^{1/2} := \text{diag}(M_1^{1/2}, \dots, M_n^{1/2})$, $X^{1/2} := \text{diag}(x_1^{1/2}, \dots, x_n^{1/2})$. Then $\tilde{A}_S^{-1} = P^{-1/2} \tilde{A}^{-1} P^{1/2}$ is a self-adjoint endomorphism whose smallest eigenvalue is bounded from below by some positive constant which depends only on (k_{ij}) .

Since $0 = \sum_{i=1}^n J_i = \sum_{i=1}^n (B \nabla w)_i$, we can express the last component in terms of the other components, $(B \nabla w)_n = -\sum_{i=1}^{n-1} (B \nabla w)_i$, where $(B \nabla w)_i = \sum_{j=1}^{n-1} B_{ij} \nabla w_j$

for $i = 1, \dots, n-1$. Then

$$\begin{aligned} \nabla w : B\nabla w &= \sum_{i=1}^{n-1} \left\{ \frac{\nabla \log x_i}{M_i} - \frac{\nabla \log x_n}{M_n} + \left(\frac{z_i}{M_i} - \frac{z_n}{M_n} \right) \nabla \Phi \right\} \cdot (B\nabla w)_i \\ &= \sum_{i=1}^{n-1} \frac{1}{M_i} \nabla(\log x_i + z_i \Phi) \cdot (B\nabla w)_i - \frac{1}{M_n} \nabla(\log x_n + z_n \Phi) \sum_{i=1}^{n-1} (B\nabla w)_i \\ &= \sum_{i=1}^n \frac{1}{M_i} \nabla(\log x_i + z_i \Phi) \cdot (B\nabla w)_i. \end{aligned}$$

To simplify the notation, we set $\Psi_i = \nabla(\log x_i + z_i \Phi)/M_i$, and $\Psi = (\Psi_1, \dots, \Psi_n)$. By Lemma 4.4, $B\nabla w = \tilde{A}^{-1}D = P^{1/2}\tilde{A}_S^{-1}P^{-1/2}D$. Hence,

$$\begin{aligned} \nabla w : B\nabla w &= \Psi : B\nabla w = \Psi : M^{1/2}X^{1/2}\tilde{A}_S^{-1}X^{-1/2}M^{-1/2}D \\ &= \sum_{i,j=1}^n \Psi_i M_i^{1/2} x_i^{1/2} (\tilde{A}_S^{-1})_{ij} x_j^{-1/2} M_j^{-1/2} D_i \\ &= \sum_{i,j=1}^n (2\nabla x_i^{1/2} + z_i x_i^{1/2} \nabla \Phi) M_i^{-1/2} (\tilde{A}_S^{-1})_{ij} M_j^{-1/2} \\ &\quad \times (2\nabla x_j^{1/2} + (z_j x_j^{1/2} - (x \cdot z) \rho_j x_j^{-1/2}) \nabla \Phi). \end{aligned} \quad (4.24)$$

In view of $\sum_{i=1}^n (B\nabla w)_i = 0$, it follows that

$$\begin{aligned} &\sum_{i,j=1}^n (M_i^{-1/2} x_i^{-1/2} (z \cdot x) \rho_i \nabla \Phi) (\tilde{A}_S^{-1})_{ij}^{-1} M_j^{-1/2} (2\nabla x_j^{1/2} + (z_j x_j^{1/2} - (x \cdot z) \rho_j x_j^{-1/2}) \nabla \Phi) \\ &= \sum_{i,j=1}^n (c(z \cdot x) \nabla \Phi) \tilde{A}_{ij}^{-1} (\nabla x_j + (z_j x_j - (x \cdot z) \rho_j) \nabla \Phi) \\ &= (c(z \cdot x) \nabla \Phi) \cdot \sum_{i=1}^n (B\nabla w)_i = 0. \end{aligned}$$

Adding this expression to (4.24), we find that

$$\begin{aligned} \nabla w : B\nabla w &= \sum_{i,j=1}^n M_i^{-1/2} (2\nabla x_i^{1/2} + (z_i x_i^{1/2} - (z \cdot x) \rho_i x_i^{-1/2}) \nabla \Phi) (\tilde{A}_S^{-1})_{ij}^{-1} M_j^{-1/2} \\ &\quad \times (2\nabla x_j^{1/2} + (z_j x_j^{1/2} - (z \cdot x) \rho_j x_j^{-1/2}) \nabla \Phi). \end{aligned}$$

The matrix \tilde{A}_S^{-1} is positive definite on $\text{im}(\tilde{A}_S) = \text{span}\{\rho^{1/2}\}^\perp$. A simple computation shows that the vector $M^{-1/2}(2\nabla x_i^{1/2} + (z_i x_i^{1/2} - (x \cdot z) \rho_i x_i^{-1/2}) \nabla \Phi)_{i=1}^n$ lies in

$\text{span}\{\rho^{1/2}\}^\perp$. We obtain

$$\begin{aligned} \nabla w : B\nabla w &\geq K_B \sum_{i=1}^n M_i^{-1} |2\nabla x_i^{1/2} + (z_i x_i^{1/2} - (x \cdot z) \rho_i x_i^{-1/2}) \nabla \Phi|^2 \\ &\geq K_1 \sum_{i=1}^n |\nabla x_i^{1/2}|^2 - K_2 \sum_{i=1}^n |(z_i x_i^{1/2} - (x \cdot z) \rho_i x_i^{-1/2}) \nabla \Phi|^2, \end{aligned}$$

where $K_1 > 0$ and $K_2 > 0$ depend on M_1, \dots, M_n . Since x_i and $\rho_i x_i^{-1/2} = (\rho_i c_{\text{tot}} M_i)^{1/2}$ are bounded, the previous inequality becomes

$$\nabla w : B\nabla w \geq K_1 \sum_{i=1}^n |\nabla x_i^{1/2}|^2 - K_3 |\nabla \Phi|^2, \quad (4.25)$$

where K_3 depends on K_2 and z_i .

In the following, let $K > 0$ be a generic constant independent of ε , n , and τ . We estimate the expression involving the boundary term

$$\begin{aligned} \nabla w_D : B\nabla w &= \nabla w_D : A_0^{-1} D' \\ &= \sum_{i,j=1}^{n-1} (A_0^{-1})_{ij} \left(\frac{z_i}{M_i} - \frac{z_n}{M_n} \right) \nabla \Phi_D \cdot (\nabla x_i + (z_i x_i - (z \cdot x) \rho_i) \nabla \Phi) \\ &\leq \frac{K}{\delta} + \delta \sum_{i=1}^{n-1} |\nabla x_i + (z_i x_i - (z \cdot x) \rho_i) \nabla \Phi|^2, \end{aligned}$$

where $K > 0$ depends on $\nabla \Phi_D$, z_i , M_i , and A_0^{-1} . Since $0 \leq x_i \leq 1$, we have $|\nabla x_i|^2 = 4x_i |\nabla x_i^{1/2}|^2 \leq 4 |\nabla x_i^{1/2}|^2$ and therefore,

$$\nabla w_D : B\nabla w \leq \frac{K}{\delta} + 4\delta |\nabla x_i^{1/2}|^2 + \delta K |\nabla \Phi|^2. \quad (4.26)$$

We infer from (4.25) and (4.26) that

$$\int_{\Omega} \nabla(w - w_D) : B\nabla w dy \geq (K_1 - 4\delta) \sum_{i=1}^n \|\nabla x_i^{1/2}\|_{L^2(\Omega)}^2 - K_3 \|\nabla \Phi\|_{L^2(\Omega)}^2 - \frac{K}{\delta}.$$

By the boundedness of c_i , the elliptic estimate for the Poisson equation gives

$$\|\Phi\|_{H^1(\Omega)} \leq K(1 + \|c_i\|_{L^2(\Omega)}) \leq K. \quad (4.27)$$

This proves the lemma. \square

Combining the discrete entropy inequality (4.9) and the estimate of Lemma 4.8

and summation over k leads to the following result.

Corollary 4.9. *There exist constants $K_1 > 0$ and $K_2 > 0$, both independent of ε , n , and τ , such that*

$$H(\rho^k) + \tau K_1 \sum_{j=1}^k \sum_{i=1}^n \|\nabla(x_i^k)^{1/2}\|_{L^2(\Omega)}^2 + \varepsilon \tau \sum_{j=1}^k \|w^j - w_D\|_{L^2(\Omega)}^2 \leq \tau k K_2 + H(\rho^0). \quad (4.28)$$

Step 2: limit $\varepsilon \rightarrow 0$. For a fixed time step k , let $(w^\varepsilon, \Phi^\varepsilon)$ be a solution to (4.7)-(4.8) with $\rho^\varepsilon = \rho(w^\varepsilon, \Phi^\varepsilon)$ and $x_i^\varepsilon = \rho_i^\varepsilon / (c_{\text{tot}}^\varepsilon M_i)$. Estimates (4.27) and (4.28) yield the following uniform bounds:

$$\|\rho_i^\varepsilon\|_{L^\infty(\Omega)} + \|x_i^\varepsilon\|_{L^\infty(\Omega)} \leq 2, \quad i = 1, \dots, n, \quad (4.29)$$

$$\|x_i^\varepsilon\|_{H^1(\Omega)} + \|\Phi^\varepsilon\|_{H^1(\Omega)} + \varepsilon^{1/2} \|w_i^\varepsilon\|_{L^2(\Omega)} \leq K, \quad (4.30)$$

where $K > 0$ is independent of ε and N . The bound for x_i^ε in $H^1(\Omega)$ is a consequence of the bound for $(x_i^\varepsilon)^{1/2}$ in $H^1(\Omega)$ from (4.28) and the uniform L^∞ bound for x_i^ε from (4.29). We claim that (ρ_i^ε) is bounded in $H^1(\Omega)$. Indeed, according to Lemma 4.6, it holds that $c_{\text{tot}}^\varepsilon = (\sum_{j=1}^n M_j x_j^\varepsilon)^{-1}$, and this expression has the uniform lower bound $(\max_i M_i)^{-1}$ and the uniform upper bound $(\min_i M_i)^{-1}$. Then, since (x_i^ε) is bounded in $H^1(\Omega)$, also $(c_{\text{tot}}^\varepsilon)$ is bounded in $H^1(\Omega)$. This implies that $\rho_i^\varepsilon = c_{\text{tot}}^\varepsilon M_i x_i^\varepsilon$ is uniformly bounded in $H^1(\Omega)$, proving the claim. Observing that the embedding $H^1(\Omega) \hookrightarrow L^2(\Omega)$ is compact, there exist subsequences, which are not relabeled, such that as $\varepsilon \rightarrow 0$,

$$\begin{aligned} x_i^\varepsilon &\rightharpoonup x_i, & \rho_i^\varepsilon &\rightharpoonup \rho_i, & \Phi^\varepsilon &\rightarrow \Phi & \text{strongly in } L^2(\Omega), \\ x_i^\varepsilon &\rightharpoonup x_i, & \rho_i^\varepsilon &\rightharpoonup \rho_i, & \Phi^\varepsilon &\rightharpoonup \Phi & \text{weakly in } H^1(\Omega), \\ \varepsilon w_i^\varepsilon &\rightarrow 0 & & & & & \text{strongly in } L^2(\Omega). \end{aligned}$$

In view of the L^∞ bounds for (x_i^ε) and (ρ_i^ε) , the strong convergences for these (sub-)sequences hold in $L^p(\Omega)$ for any $p < \infty$. Consequently, $c_{\text{tot}}^\varepsilon \rightarrow c_{\text{tot}} := \sum_{i=1}^n \rho_i / M_i$ strongly in $L^2(\Omega)$, and we can identify $\rho_i = c_{\text{tot}} M_i x_i$ for $i = 1, \dots, n$. Furthermore,

$$c_i^\varepsilon = \rho_i^\varepsilon / M_i \rightarrow c_i := \rho_i / M_i \quad \text{strongly in } L^2(\Omega), \quad i = 1, \dots, n.$$

Recalling definition (1.8) of D_i , we have

$$D_i^\varepsilon = \nabla x_i^\varepsilon + (z_i x_i^\varepsilon - (z \cdot x^\varepsilon) \rho_i^\varepsilon) \nabla \Phi^\varepsilon \rightharpoonup D_i := \nabla x_i + (z_i x_i - (z \cdot x) \rho_i) \nabla \Phi \quad (4.31)$$

weakly in $L^q(\Omega)$ for any $q < 2$ and $i = 1, \dots, n$. Since (D_i^ε) is bounded in $L^2(\Omega)$, there exists a subsequence which converges to some function \tilde{D}_i weakly in $L^2(\Omega)$. By the uniqueness of the weak limits, we can identify $\tilde{D}_i = D_i$. This shows that

the convergence (4.31) holds in $L^2(\Omega)$. We deduce from the strong convergence of (x_i^ε) , the boundedness of (x_i^ε) in $L^\infty(\Omega)$, and the continuity of r_i that $r_i(x^\varepsilon) \rightarrow r_i(x)$ strongly in $L^2(\Omega)$.

We know from Lemma 4.4 that $B(w^\varepsilon)\nabla w^\varepsilon = A_0^{-1}(\rho^\varepsilon)(D^\varepsilon)'$. As $A_0^{-1}(\rho)$ is uniformly bounded for $\rho \in [0, 1]^n$ and (ρ^ε) converges strongly to ρ , we infer that $A_0^{-1}(\rho^\varepsilon) \rightarrow A_0^{-1}(\rho)$ strongly in $L^2(\Omega)$; the convergence holds even in every $L^p(\Omega)$ for $p < \infty$. Then, because of (4.31) and using the continuity of $\rho \mapsto A_0^{-1}(\rho)$,

$$A_0^{-1}(\rho^\varepsilon)(D^\varepsilon)' \rightharpoonup A_0^{-1}(\rho)D' \quad \text{weakly in } L^q(\Omega) \text{ for all } q < 2.$$

In fact, since $A_0^{-1}(\rho^\varepsilon)(D^\varepsilon)'$ is bounded in $L^2(\Omega)$ and thus (up to a subsequence) weakly converging in $L^2(\Omega)$, the convergence holds in $L^2(\Omega)$.

These convergences are sufficient to perform the limit $\varepsilon \rightarrow 0$ in (4.7)-(4.8). We conclude that $(\rho^k, \Phi^k) := (\rho, \Phi)$ solves

$$\frac{1}{\tau} \int_{\Omega} ((\rho^k)' - (\rho^{k-1})') \cdot \phi dy + \int_{\Omega} \nabla \phi : A_0^{-1}(\rho^k) \nabla \rho^k dy = \int_{\Omega} r'(x^k) \cdot \phi dy, \quad (4.32)$$

$$\lambda \int_{\Omega} \nabla \Phi^k \cdot \nabla \theta dy = \int_{\Omega} \left(\sum_{i=1}^n z_i c_i^k + f(y) \right) \theta dy \quad (4.33)$$

for all $\phi \in V_N$, $\theta \in P_N$.

Step 3: limit $N \rightarrow \infty$. Let (ρ^N, Φ^N) be a solution to (4.32)-(4.33). Estimates (4.29)-(4.30) are independent of N . Thus, we can exactly argue as in step 2 and obtain limit functions (x, ρ, Φ) and $c_i = c_{\text{tot}} M_i x_i$ for $i = 1, \dots, n$ as $N \rightarrow \infty$. These functions satisfy (4.32)-(4.33) for all $\phi \in V_N$ and $\theta \in P_N$ and for all $N \in \mathbb{N}$. The union of all V_N is dense in $H^1(\Omega; \mathbb{R}^{n-1})$ and the union of all P_N is dense in $H_D^1(\Omega)$. Thus, by a density argument, system (4.32)-(4.33) holds for all test functions $\phi \in H^1(\Omega; \mathbb{R}^{n-1})$ and $\theta \in H_D^1(\Omega)$.

Step 4: limit $\tau \rightarrow 0$. Let (ρ^k, Φ^k) be a solution to (4.32)-(4.33) with test functions $\phi \in H^1(\Omega; \mathbb{R}^{n-1})$ and $\theta \in H_D^1(\Omega)$. Then $\rho_i^k = c_{\text{tot}}^k M_i x_i^k$ and $c_i^k = \rho_i^k / M_i$ for $i = 1, \dots, n$. We set

$$\rho_i^\tau(y, t) = \rho_i^k(y), \quad x_i^\tau(y, t) = x_i^k(y), \quad c_i^\tau(y, t) = c_i^k(y), \quad \Phi^\tau(y, t) = \Phi^k(y)$$

for $y \in \Omega$, $t \in ((k-1)\tau, k\tau]$, $i = 1, \dots, n$ and introduce the shift operator $(\sigma_\tau \rho^\tau)(y, t) = \rho^{k-1}(y)$ for $y \in \Omega$ and $t \in ((k-1)\tau, k\tau]$. Finally, we set $D_i^\tau = \nabla x_i^\tau + (z_i x_i^\tau - (z \cdot x^\tau) \rho_i^\tau) \nabla \Phi^\tau$ and $T = m\tau$ for some fixed $m \in \mathbb{N}$. Then we can write system (4.32)-

(4.33) as

$$\begin{aligned} & \frac{1}{\tau} \int_0^T \int_{\Omega} ((\rho^\tau)' - \sigma_\tau(\rho^\tau)') \cdot \phi dy dt + \int_0^T \int_{\Omega} \nabla \phi : A_0^{-1}(\rho^\tau)(D^\tau)' dy dt \\ & = \int_0^t \int_{\Omega} r'(x^\tau) \cdot \phi dy dt, \end{aligned} \quad (4.34)$$

$$\lambda \int_{\Omega} \nabla \Phi^\tau \cdot \nabla \theta dy = \int_{\Omega} \left(\sum_{i=1}^n z_i c_i^\tau + f(y) \right) \theta dy \quad (4.35)$$

for all piecewise constant functions $\phi : (0, T) \rightarrow H^1(\Omega; \mathbb{R}^{n-1})$ and $\theta : (0, T) \rightarrow H_D^1(\Omega)$. The entropy inequality (4.28), formulated in terms of (ρ^τ, Φ^τ) , provides us with further uniform bounds since the right-hand side of (4.28) does not depend on τ :

$$\|\rho_i^\tau\|_{L^\infty(\Omega_T)} + \|x_i^\tau\|_{L^\infty(\Omega_T)} \leq K, \quad (4.36)$$

$$\|\rho_i^\tau\|_{L^2(0,T;H^1(\Omega))} + \|x_i^\tau\|_{L^2(0,T;H^1(\Omega))} + \|\Phi^\tau\|_{L^2(0,T;H^1(\Omega))} \leq K, \quad (4.37)$$

where we have set $\Omega_T = \Omega \times (0, T)$. As a consequence, (D_i^τ) is bounded in the space $L^2(0, T; H^1(\Omega))$.

It remains to derive a uniform estimate for the discrete time derivative of ρ^τ . Taking into account the uniform bound for $A_0^{-1}(\rho^\tau)$, it follows that

$$\begin{aligned} \frac{1}{\tau} \left| \int_0^T \int_{\Omega} ((\rho^\tau)' - \sigma_\tau(\rho^\tau)') \cdot \phi dy dt \right| & \leq \int_0^T \|\nabla \phi\|_{L^2(\Omega)} \|A_0^{-1}(\rho^\tau)\|_{L^\infty(\Omega)} \|(D^\tau)'\|_{L^2(\Omega)} dt \\ & + \int_0^T \|r'(x^\tau)\|_{L^2(\Omega)} \|\phi\|_{L^2(\Omega)} dt \leq C \|\phi\|_{L^2(0,T;H^1(\Omega))}. \end{aligned}$$

As the piecewise constant functions $\phi : (0, T) \rightarrow H^1(\Omega; \mathbb{R}^{n-1})$ are dense in the space $L^2(0, T; H^1(\Omega; \mathbb{R}^{n-1}))$, this estimate also holds for all $\phi \in L^2(0, T; H^1(\Omega; \mathbb{R}^{n-1}))$, and we conclude that

$$\tau^{-1} \|(\rho^\tau)' - \sigma_\tau(\rho^\tau)'\|_{L^2(0,T;H^1(\Omega)')} \leq K, \quad i = 1, \dots, n-1.$$

This estimate also holds for $i = n$ since $\rho_n^\tau = 1 - \sum_{i=1}^{n-1} \rho_i^\tau$.

By the Aubin-Lions lemma in the version of [44], there exists a subsequence of (ρ^τ) which is not relabeled such that, as $\tau \rightarrow 0$,

$$\rho_i^\tau \rightarrow \rho_i \quad \text{strongly in } L^2(\Omega_T), \quad i = 1, \dots, n.$$

In view of the L^∞ bound (4.36) for ρ^τ , this convergence also holds in $L^p(\Omega_T)$ for any

$p < \infty$. Furthermore, by (4.37), we have up to subsequences,

$$\begin{aligned} x_i^\tau &\rightharpoonup x_i, & \Phi^\tau &\rightharpoonup \Phi & \text{weakly in } L^2(0, T; H^1(\Omega)), \\ \tau^{-1}(\rho_i^\tau - \sigma_\tau(\rho_i^\tau)) &\rightharpoonup \partial_t \rho_i & \text{weakly in } L^2(0, T; H^1(\Omega)'). \end{aligned}$$

In particular, $D_i^\tau \rightharpoonup D_i$ weakly in $L^2(\Omega_T)$, and we can identify $D_i = \nabla x_i + (z_i x_i - (z \cdot x) \rho_i) \nabla \Phi$. The strong convergence of (ρ^τ) and the weak convergence of (D_i^τ) imply that

$$A_0^{-1}(\rho^\tau)(D^\tau)' \rightharpoonup A_0^{-1}(\rho)D' \quad \text{weakly in } L^q(\Omega_T), \quad q < 2.$$

Again, since $(A_0^{-1}(\rho^\tau)(D^\tau)')$ is bounded in $L^2(\Omega_T)$, this convergence holds in $L^2(\Omega_T)$. Furthermore, $r'(x^\tau) \rightarrow r'(x)$ strongly in $L^2(\Omega_T)$. Therefore, we can pass to the limit $\tau \rightarrow 0$ in (4.34)-(4.35) yielding (4.10)-(4.11).

4.7 Numerical Simulations

In this section, some numerical experiments based on scheme (4.7)-(4.8) in one space dimension are presented. We stress the fact that the experiments just serve as a feasibility study and more effort is necessary to perform two- or three-dimensional simulations showing, for instance, the effects coming from the mixed boundary conditions. In the context of semiconductor simulations, we refer to [56]. The one-dimensional setting presented here models liquid electrolytes, which can be used as a simplified version of a model for dye-sensitized solar cells [121].

4.7.1 Discretization and Iteration Procedure

Let $\Omega = (0, 1)$ be divided into $n_p \in \mathbb{N}$ uniform subintervals of length $h = 1/n_p$. We use uniform time steps with time step size $\tau > 0$ and piecewise linear finite elements with the usual conforming P1 finite-element space on the uniform partition, i.e.

$$\begin{aligned} P_N &:= \{p \in C(\bar{\Omega}) : p|_I \text{ is affine on each subinterval } I\}, \\ V_N &:= \{v \in C(\bar{\Omega}; \mathbb{R}^{n-1}) : v|_I \text{ is affine on each subinterval } I\}. \end{aligned}$$

We impose Dirichlet boundary condition for the electric potential Φ : $\Phi(0) = 0$ and $\Phi(1) = U$, where U is the applied voltage. Given the variables (w, Φ) , the molar fractions x_i are computed from the fixed-point problem (see the proof of Lemma 4.5)

$$f(s) = \sum_{i=1}^{n-1} (1-s)^{M_i/M_n} \exp \left[M_i w_i - M_i \left(\frac{z_i}{M_i} - \frac{z_n}{M_n} \right) \Phi_0 \right], \quad s \in [0, 1], \quad (4.38)$$

with unique solution $s_0 \in (0, 1)$. This nonlinear set of equations is solved by the

MATLAB routine `fzero`. The molar fractions are recovered from (4.19),

$$x_i = (1 - s_0)^{M_i/M_n} \exp \left[M_i w_i - M_i \left(\frac{z_i}{M_i} - \frac{z_n}{M_n} \right) \Phi \right], \quad i = 1, \dots, n-1,$$

and $x_n = 1 - s_0$. Then we set (see Lemma 4.6) $c_{\text{tot}} = (\sum_{i=1}^n M_i x_i)^{-1}$ and $\rho_i = c_{\text{tot}} M_i x_i$ for $i = 1, \dots, n$. Note that we can compute the diffusion matrix $B(\rho(w, \Phi))$, given w and Φ , explicitly from the formula $B(\rho(w, \Phi)) = c_{\text{tot}} C^{-1}(\rho(w, \Phi))$, where the matrix $C(\rho)$ is defined in Section 4.4.1.

Instead of solving the nonlinear discrete system (4.7)-(4.8) by a full Newton method, we employ a linearized semi-implicit approach, i.e., we linearize $\rho(w, \Phi)$ and use the previous time step in the diffusion matrix $B(w)$. More precisely, let $\bar{w} \in V_N$ and $\bar{\Phi} \in P_N$ be given. We linearize $\rho(w, \Phi)$ by

$$\rho(\bar{w}, \bar{\Phi}) + \nabla_{(w, \Phi)} \rho'(\bar{w}, \bar{\Phi}) \cdot (w - \bar{w}, \Phi - \bar{\Phi}).$$

This leads to the problem in the variable $\zeta = (w - \bar{w}, \Phi - \bar{\Phi})$:

$$L(\zeta, \phi) = F(\phi), \quad K(\zeta_n, \theta) = G(\theta) \quad \text{for all } \phi \in V_N, \theta \in P_N, \quad (4.39)$$

where

$$\begin{aligned} L(\zeta, \phi) &= \int_{\Omega} \nabla_{(w, \Phi)} \rho'(\bar{w}, \bar{\Phi}) \cdot (\zeta, \phi) dy + \tau \int_{\Omega} \partial_x \phi \cdot B(\bar{w}, \bar{\Phi}) \partial_x \zeta dy \\ &\quad + \varepsilon \tau \int_{\Omega} (\zeta - w_D) \cdot \phi dy, \\ F(\phi) &= - \int_{\Omega} (\rho'(\bar{w}, \bar{\Phi}) - \rho'(w^{k-1}, \Phi^{k-1})) \cdot \phi dy - \tau \int_{\Omega} \partial_x \phi \cdot B(\bar{w}, \bar{\Phi}) \partial_x \bar{w} dy, \\ K(\zeta_n, \theta) &= \lambda \int_{\Omega} \partial_x \zeta_n \partial_x \phi dy - \int_{\Omega} \sum_{i=1}^n \frac{z_i}{M_i} \nabla_{(w, \Phi)} \rho_i(\bar{w}, \bar{\Phi}) \cdot \zeta \theta dy, \\ G(\theta) &= -\lambda \int_{\Omega} \partial_x \bar{\Phi} \partial_x \theta dy + \int_{\Omega} \left(\sum_{i=1}^n z_i \frac{\rho_i(\bar{w}, \bar{\Phi})}{M_i} + f(y) \right) \theta dy. \end{aligned}$$

The iteration with starting point $(w_h^{(0)}, \Phi_h^{(0)}) := (w^{k-1}, \Phi^{k-1})$ is then defined by $(w_h^{(m+1)}, \Phi_h^{(m+1)}) := (\bar{w}, \bar{\Phi}) + \zeta$ for $m \geq 0$. The iteration stops when $\|\zeta\|_{\ell^\infty} < \varepsilon_{\text{tol}}$ for some tolerance $\varepsilon_{\text{tol}} > 0$ or if $m \geq m_{\text{max}}$ for a maximal number of iterations. We summarize the scheme in Algorithm 1.

All integrals appearing in the scheme are computed by a three-point Gaussian quadrature rule. The matrix $B = c_{\text{tot}} C^{-1}$ is evaluated explicitly, where C is the matrix from Section 4.4.1. The linear system (4.39) and the fixed-point problem (4.38) are solved using MATLAB. We choose the numerical parameters $h = 10^{-2}$,

Algorithm 1 (Pseudo-code for the finite-element scheme in entropy variables.)

- 1: **procedure** MAXWELL-STEFAN SYSTEM IN ENTROPY VARIABLES
 - 2: Set $(\bar{w}_h^{(0)}, \bar{\Phi}_h^{(0)}) = (w^{k-1}, \Phi^{k-1})$, $\rho_h^{(0)} = \rho'(\bar{w}_h^{(0)}, \bar{\Phi}_h^{(0)})$, $x_h^{(0)} = \rho_h^{(0)} / (M_i c_h^{(0)})$, $c_h^{(0)} = \sum_{i=1}^n (\rho_h^{(0)})_i / M_i$, $m = 0$, $\varepsilon_{\text{tol}} > 0$, and m_{max} .
 - 3: **while** $err > \varepsilon_{\text{tol}}$ and $m \leq m_{\text{max}}$ **do**
 - 4: Solve linear system (4.39) with solution ζ .
 - 5: Set $(\bar{w}_h^{(m+1)}, \bar{\Phi}_h^{(m+1)}) := (\bar{w}_h^{(m)}, \bar{\Phi}_h^{(m)}) + \zeta$.
 - 6: Solve the fixed-point problem (4.38) with solution s_0 .
 - 7: Compute $x_h^{(m+1)}$ and $\rho_h^{(m+1)}$.
 - 8: Set $err := \|(\bar{w}_h^{(m+1)}, \bar{\Phi}_h^{(m+1)}) - (\bar{w}_h^{(m)}, \bar{\Phi}_h^{(m)})\|_{\ell^\infty}$.
 - 9: $(m + 1) \leftarrow (m)$.
 - 10: **end while**
 - 11: **end procedure**
-

$\tau = 10^{-3}$, $\varepsilon_{\text{tol}} = 10^{-12}$, and $\varepsilon = 2^{-52} \approx 2.2204 \cdot 10^{-16}$ (the scheme works also for $\varepsilon = 0$). We have compared our results with the solutions from a finite-element scheme derived from the original system in the variables ρ_i and a Picard iteration procedure for the nonlinear discrete system. It turned out that the results are basically the same, i.e. $\|\rho_i - \rho_i(w, \Phi)\|_{L^\infty(\Omega)} \leq 10^{-10}$.

4.7.2 Numerical Examples

In all numerical examples, we neglect reaction terms, set $m_{\text{max}} = 200$, and choose the diffusivities according to [17, 58]: $D_{12} = 0.833$, $D_{13} = 0.680$, and $D_{23} = 0.168$ for $n = 3$. The charges are given by $z_1 = z_2 = 1$ and $z_3 = 0$ and the initial data is defined as in [17]:

$$\rho_1^0(y) = \begin{cases} 0.7 & \text{for } y < 0.25, \\ -2(0.7 - \eta)y - 2(0.25\eta - (0.7 \cdot 0.75)) & \text{for } 0.25 \leq y < 0.75, \\ \eta & \text{for } 0.75 \leq y \leq 1 \end{cases}$$

for $\eta = 2^{-52}$, $\rho_2^0(y) = 0.2$, and $\rho_3^0(y) = (1 - \rho_1^0 - \rho_2^0)(y)$ for $y \in \Omega = (0, 1)$. The parameter $\eta > 0$ is needed to transform the initial conditions to the entropy variables. It can be avoided by changing the first step of the iteration procedure but since η equals the machine precision, there is practically no difference in the results.

For the first example, we suppose that all three molar masses are equal to one and that the boundary conditions for the electric potential are in equilibrium, i.e. $M_1 = M_2 = M_3 = 1$ and $\Phi(y) = 0$ for $y \in \{0, 1\}$. The dynamics of the particle densities and the electric potential are shown in Figure 4.1. The solution at time $t = 17$ is essentially stationary and, in fact, in equilibrium. Because of the choice of

the parameters, the stationary solution is symmetric around $x = \frac{1}{2}$.

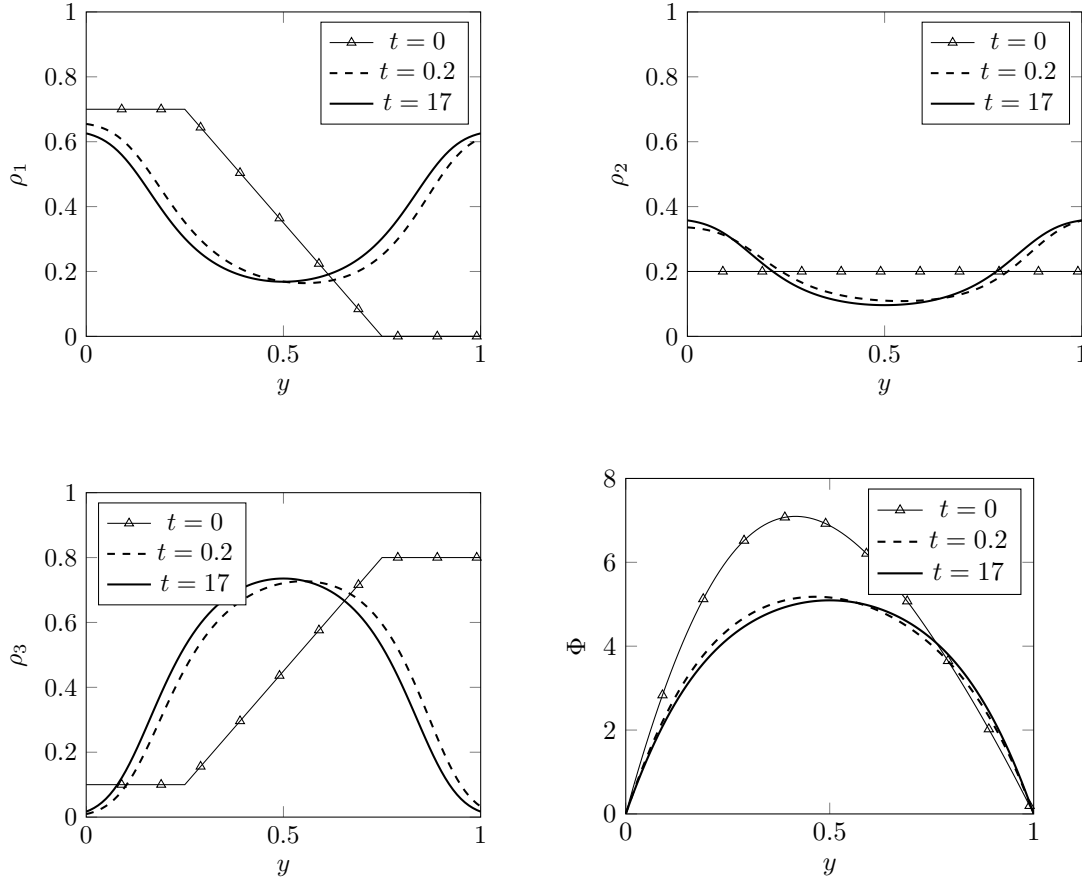


Figure 4.1: Example 1: Particle densities ρ_i and electric potential for molar masses $M_1 = M_2 = M_3 = 1$ versus position at various times. The boundary conditions for the electric potential are in equilibrium.

In order to study the convergence of our iterative linearization procedure, we plot the evolution of the iteration parameter m over time in Figure 4.2. It turns out that the number of iterations is decreasing as time progresses. Initially, the algorithm needs $m = 48$ iterations and for $t \geq 0.2$ only $m = 9$ iterations. The maximum number $m_{\max} = 200$ was never reached in all examples and the maximum number of iteration was always beyond $m = 50$.

The situation changes drastically when the molar masses are different (example 2). Figure 4.3 shows the stationary solutions with the same parameters as in the

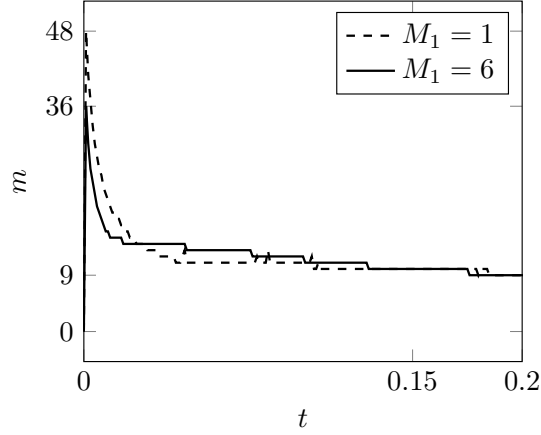


Figure 4.2: Example 1 and 2: Plot of the iteration parameter m versus time t . After $t \geq 0.2$, iterations stop at $m = 9$ in both examples.

previous example except $M_1 = 6$. Here, the discrete relative entropy is defined by

$$H^*(\rho_h^k) = \int_0^1 \left(c_{\text{tot},h}^k \sum_{i=1}^n (x_h^k)_i \log \frac{(x_h^k)_i}{(x_h^\infty)_i} + \frac{\lambda}{2} |\nabla(\Phi_h^k - \Phi_h^\infty)|^2 \right) dy,$$

where (ρ_h^k, Φ_h^k) is the finite-element solution at time $k\tau$ and $(x_h^\infty, \Phi_h^\infty)$ is the stationary solution. The integral and gradients are computed by the trapezoidal and gradient routines of MATLAB. The semi-logarithmic plot of the relative entropy shows that the entropy converges to zero exponentially fast.

For example 3, we choose the same initial conditions and parameters as before, but we take non-equilibrium boundary data $\Phi(0) = 10$, $\Phi(1) = 0$. The solutions at time $t = 8$ for various molar masses M_1 are displayed in Figure 4.4. Since ρ_1 and ρ_2 have both positive charge and the potential on the left boundary is positive, both species avoid the left boundary and move to the right.

In example 4, we interchange the roles of M_1 and M_2 , i.e., we choose $M_1 = 1$ and $M_2 \in \{2, 4, 6\}$. We observe in Figure 4.5 that the first species is more concentrated at the right boundary while in the previous example, this holds true for the second species.

The previous examples show that the convergence rate to equilibrium strongly depends on the ratio of the molar masses. It turns out that this effect is triggered by the drift term, and without electric field, the convergence rates are similar for different molar masses. This behavior can be observed in Figure 4.6 (example 5), where we have taken the same parameters as in the previous example but neglect the electric field. In this situation, the steady state is constant in space and explicitly

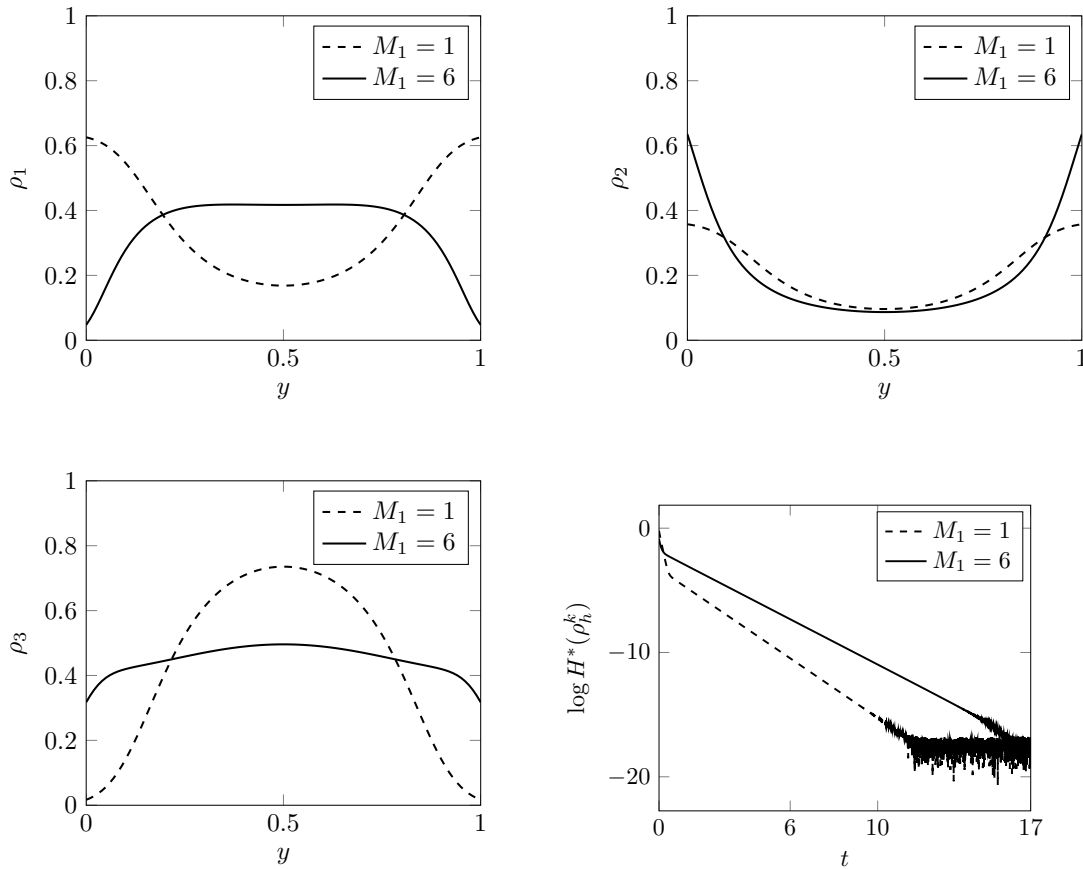


Figure 4.3: Example 2: Particle densities ρ_i at time $t = 4$ versus position and relative entropy (bottom right) for molar masses $M_1 = 6$ and $M_2 = M_3 = 1$. The boundary conditions for the electric potential are in equilibrium.

computable; indeed, we have $\rho_i^\infty = \text{mean}(\Omega)^{-1} \|\rho_i^0\|_{L^1(\Omega)}$. Note that the steady state in the previous examples is not constant.

Finally, we compute the numerical convergence rate when the grid size tends to zero for the situation of example 3 (non-equilibrium boundary conditions for the potential). We choose the time $t = 0.01$ and the time step size $\tau = 10^{-4}$. The solutions are computed on nested meshes with grid sizes $h \in \{0.01, 0.005, 0.0025, 0.0006, 0.0001\}$ and compared to the reference solution, computed on a very fine mesh with 25601 elements ($h \approx 4 \cdot 10^{-5}$). As expected, we observe a second-order convergence in space; see Figure 4.7.

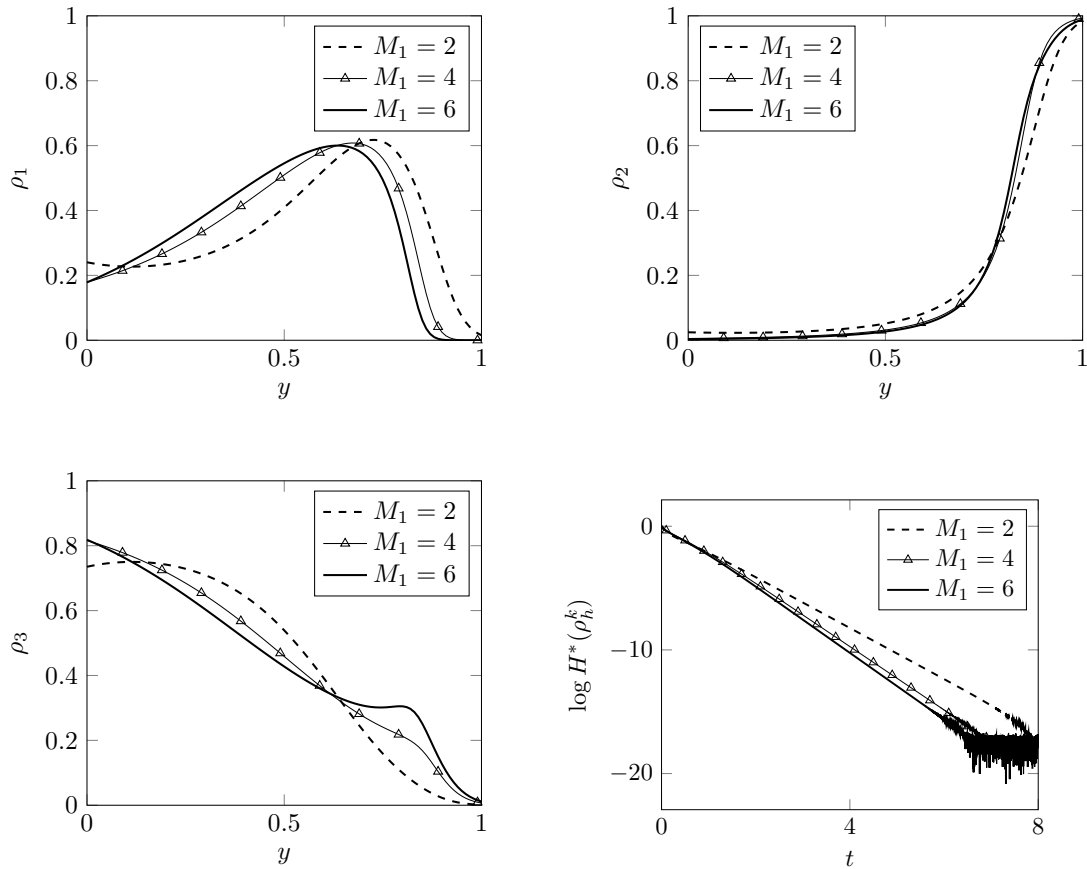


Figure 4.4: Example 3: Particle densities ρ_i at time $t = 8$ versus position and relative entropy (bottom right) for various molar masses M_1 . The boundary conditions for the electric potential are not in equilibrium.

4.8 Discussion and Outlook

Discussion

The results presented in this chapter regarding the rigorous mathematical treatment of the PMS system are first of their kind. We will discuss them from an analytical and numerical perspective.

Analytic Point of View:

In this chapter, we have derived the Poisson–Maxwell–Stefan system for an ionized fluid mixture in the isothermal and diffusive regime. In particular, we stated the physically correct driving force and revealed the Lyapunov property of the corre-

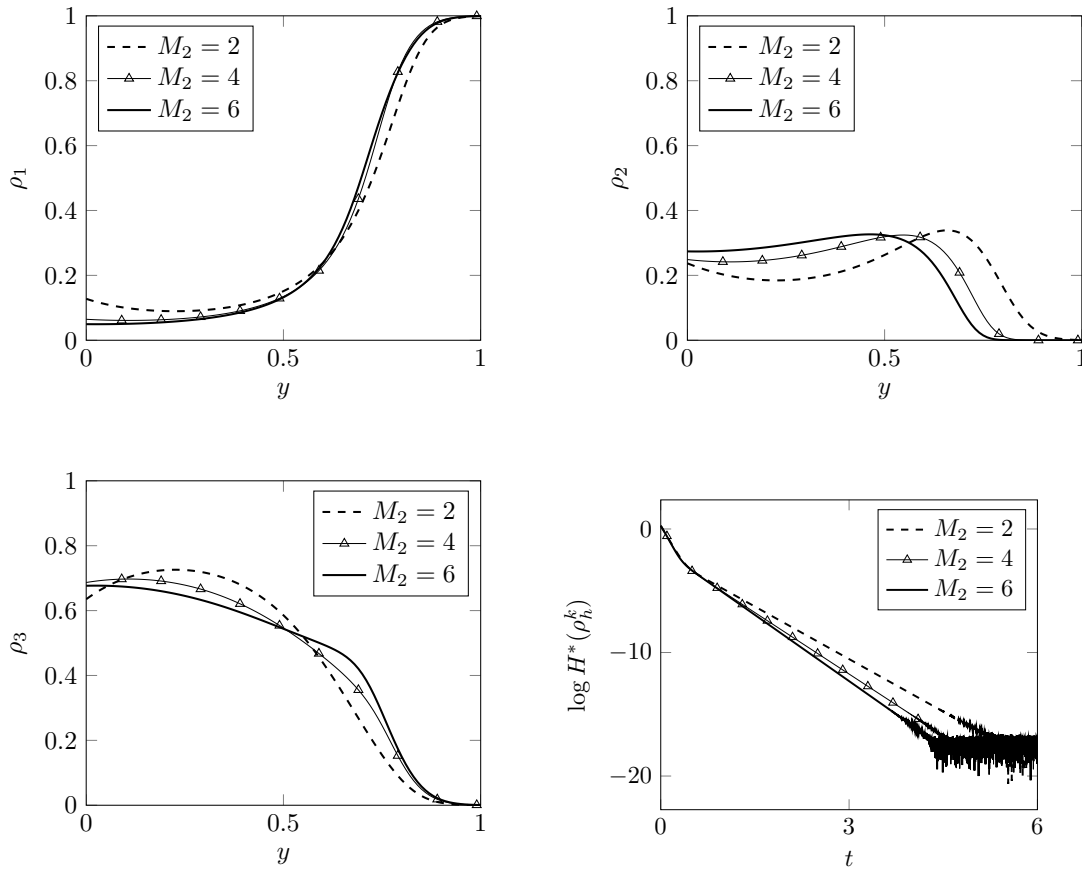


Figure 4.5: Example 4: Particle densities ρ_i at time $t = 8$ versus position and relative entropy (bottom right) for various molar masses M_2 . The boundary conditions for the electric potential are not in equilibrium.

sponding entropy functional. This was achieved by using the entropy variables and the corresponding reformulation of the diffusion flux. Although the thermodynamical background of the modeling implies the existence of an entropy structure by assumption, one finds that the derivation of the thermodynamical consistent driving force, that includes the electric potential, is still a challenging task. Furthermore, we have shown the first global-in-time existence result for this system. In addition, the solution fulfills the expected L^∞ bounds. The main extension with respect to previous results and difficulty from a theoretical point of view is the derivation of gradient estimates and the handling of the electric potential in the drift term.

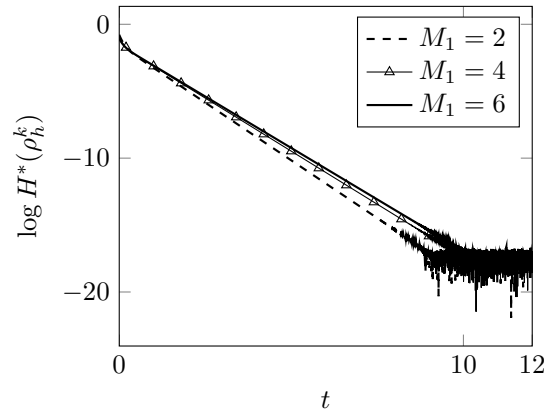


Figure 4.6: Example 5: Semi-logarithmic plot of the relative entropy $H^*(\rho_h^k)$ versus time, without electric potential and for different molar masses.

Numerical Point of View:

We have shown the existence of solutions for a fully-discrete implicit Euler Galerkin scheme. The idea and strategy for this scheme is the translation of the boundedness-by-entropy method into the discrete setting. Hence, the scheme is based on the reformulation of the problem via the entropy variables. The existence on the discrete level is proved via the Leray–Schauder fixed point theorem. The scheme preserves the upper and lower bounds of the continuous solution. In particular, the solutions are nonnegative and hence, the scheme is positivity-preserving. Furthermore, the scheme conserves the total mass and fulfills the corresponding discrete entropy inequality with an arbitrarily small regularization term. The regularization leads to a failure of partial mass conservation, but the error can be made arbitrarily small; see Remark 4.2. In addition, a subsequence of the solutions to the discrete scheme converges to a solution of the continuous problem. The convergence is shown with the help of the discrete entropy inequality. In the last part of the chapter, we also propose an implementation of this scheme in one dimension. The main issue here is to recover the original variables, since no explicit inverse transformation is available. We remark that this problem only appears in the case with different molar masses. Fortunately, we can bypass this problem via a fixed point iteration. The implementation uses a linear finite element discretization and a semi-implicit approach to resolve the nonlinearities. This approach circumvents the computation of the gradient of the diffusion matrix B with respect to the entropy variables. In particular, the coefficients of B are only known with respect to the original variables. Thus, an additional fixed point iteration would be required to compute the gradient of B . The convergence rate is numerically of second order in space. In addition, several simulations that show the dependence of the nonconstant steady and of the equilibration rate on

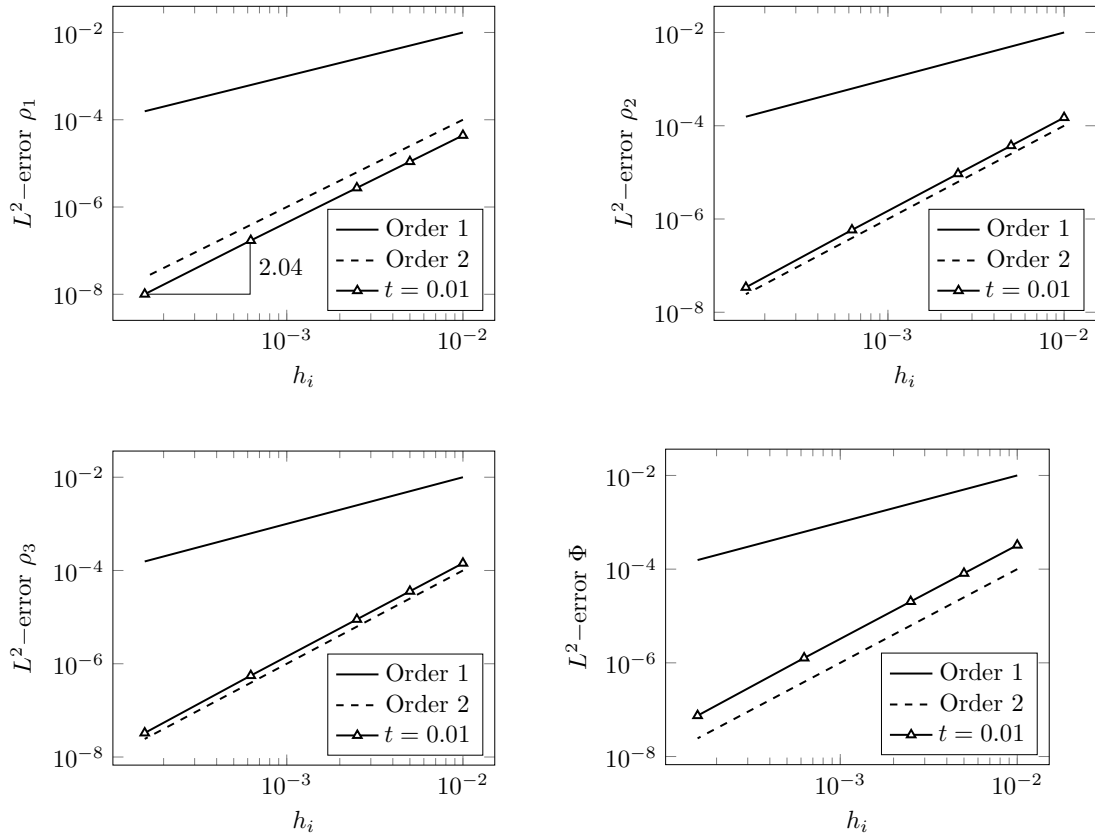


Figure 4.7: Discrete L^2 -error relative to the reference solution for the densities and the potential (bottom right) at time $t = 0.01$.

the molar masses were performed.

Outlook

This is the first mathematically rigorous treatment of the Poisson–Maxwell–Stefan system and hence it paves the path to several open questions connected to this system.

Analysis of the Longtime Behavior:

The numerical simulations indicate that solutions converge exponentially fast to a nonconstant steady state. Usually, one can exploit the entropy functional to derive a relative entropy. Combined with Sobolev embeddings, this has led to an analytical result for the decay rate in the case without electric potential [93]. Such an approach is not straightforward in our case, since the electric potential leads to a nonconstant steady state. In particular, we have to solve two problems in a future work: first,

one has to show the existence of a stationary solution of the equation, and second, we have to find a way to extend the usual relative entropy argument with respect to a drift term. While the first obstacle should be a simple adaption of our proof for the nonstationary system, it seems unclear how to deal with the drift term at this point in time.

Convergence of the Full Scheme:

The linearization procedure in the implementation is not captured by our analysis, since this would be beyond the scope of this thesis and is postponed to a future work. A possible approach in this direction could be a combination of the scalar results in [30] to ensure stability of the linearized system and [24] to show the convergence of the linearization procedure. Furthermore, we would like to achieve some kind of uniqueness result, under additional conditions, for the continuous equation. This is challenging for cross-diffusion systems, but it would be an important ingredient to prove the convergence of the whole scheme instead of a subsequence. A rather limited result for uniqueness could be the consequence of the Gajewski entropy approach [57]. The strategy was used to show uniqueness for a similar model, but with the very strong assumption that all charges are equal, i.e. $z_i = z$, $i = 1, \dots, n$, and that all diffusion coefficients are equal to one [61].

Numerics:

Our implementation is carried out in one dimension and the only obstacle for higher dimensions is the recovery of the original variables. Thus, one has to implement a fixed point iteration in two or three dimensions. In addition, the scheme should be tested with real world parameters and the performance compared to other available options.

Long Term Goal: A Discrete Boundedness-by-Entropy Method

The bigger picture for these results is an analytical and numerical framework that translates the abstract boundedness-by-entropy method into a fully discrete scheme. A first step in this direction was done in [48], but without any kind of convergence result or numerical implementation. In particular, also other kinds of space discretizations should be considered, e.g. [14]. The advantage of such an approach is quite obvious: one could use this framework to derive a positivity-preserving scheme that respects also upper bounds and preserves the entropy structure. In addition, one could use this structure to show the convergence of the scheme, a very rare result for numerical schemes that deal with nonlinear systems.

A Appendix: Some Auxiliary Results

We recall that the function

$$B_\beta(x) = \begin{cases} -\frac{1}{2\pi} \log |x| & \text{for } \beta = 0, \\ \frac{1}{(4\pi)^{n/2}} \int_0^\infty t^{-n/2} e^{-\beta t - |x|^2/(4t)} dt & \text{for } \beta > 0, \end{cases}$$

defined for $x \in \mathbb{R}^n$, is called the Newton potential if $\beta = 0$ and the Bessel potential if $\beta \neq 0$. We need the following properties of the Bessel potential.

Lemma A.1 (Bessel potential). *Let $\beta > 0$ and $k \in \mathbb{N}_0$. Then B_β is a fundamental solution of the operator $-\Delta + \beta$. For given $f \in H^k(\mathbb{R}^n)$, the function $u = B_\beta * f \in H^{k+2}(\mathbb{R}^n)$ solves*

$$-\Delta u + \beta u = f \quad \text{in } \mathbb{R}^n.$$

Furthermore, it holds that $D^\gamma(B_\beta * f) = B_\beta * D^\gamma f$ for all multi-indices $\gamma \in \mathbb{N}^n$, $|\gamma| \leq k$ and

$$B_\beta \geq 0, \quad \|B_\beta\|_{L^1(\mathbb{R}^n)} = \frac{1}{\beta}, \tag{A.1}$$

$$\|\nabla B_\beta\|_{L^1(\mathbb{R}^n)} = \frac{C(n)}{\pi^{(n-1)/2} \beta^{1/2}}, \quad \|\nabla B_\beta\|_{L^1(\mathbb{R}^2)} = \frac{\pi}{2\beta^{1/2}}, \tag{A.2}$$

where the constant $C(n) > 0$ only depends on n .

Proof. We only prove (A.2), since the other properties are standard; see, e.g., Theorem 1.7.1, Corollary 1.7.2, and Examples 12.5.8 in [100]. By Fubini's theorem and the substitution $u = x/\sqrt{4t}$, we find that

$$\begin{aligned} \|\nabla B_\beta\|_{L^1(\mathbb{R}^n)} &= \frac{1}{2(4t)^{n/2}} \int_0^\infty t^{n/2+1} e^{-\beta t} \int_{\mathbb{R}^n} e^{-|x|^2/(4t)} |x| dx dt \\ &= \frac{1}{\pi^{n/2}} \int_0^\infty t^{-1/2} e^{-\beta t} dt \int_{\mathbb{R}^n} e^{-|u|^2} |u| du = \frac{1}{\pi^{(n-1)/2}} \beta^{-1/2} C(n), \end{aligned}$$

where $C(n) = \int_{\mathbb{R}^n} e^{-|u|^2} |u| du$. In particular, when $n = 2$, we obtain

$$C(2) = \int_0^\infty \int_0^{2\pi} e^{-r^2} r^2 d\phi dr = \frac{\pi^{3/2}}{2},$$

ending the proof. □

Lemma A.2 (Young's inequality). *Let $g \in L^q(\mathbb{R}^n)$, $h \in L^r(\mathbb{R}^n)$ for $1 \leq q, r \leq \infty$, and $1/q + 1/r = 1/p + 1$. Then $g * h \in L^p(\mathbb{R}^n)$ and*

$$\|g * h\|_{L^p(\mathbb{R}^n)} \leq \|g\|_{L^q(\mathbb{R}^n)} \|h\|_{L^r(\mathbb{R}^n)}.$$

Lemma A.3 (Elliptic problem). *Let $\tau > 0$, $f \in L^2(\mathbb{R}^2)^2$, and $g \in L^2(\mathbb{R}^2)$. Then there exists a unique weak solution $\rho \in H^1(\mathbb{R}^2)$ to*

$$-\Delta\rho + \tau^{-1}(\rho - g) = -\operatorname{div} f \quad \text{in } \mathbb{R}^2, \quad (\text{A.3})$$

and this solution can be represented as

$$\rho = \frac{1}{\tau} B_{1/\tau} * g - \nabla B_{1/\tau} * f \quad \text{in } \mathbb{R}^2. \quad (\text{A.4})$$

Equation (A.3) corresponds to the implicit Euler discretization of a parabolic problem with ρ being the solution at the actual time step and g being the solution at the previous time step. Although the result is standard, we give proof for the sake of completeness.

Proof. Let $f_k \in C_0^\infty(\mathbb{R}^2)^2$ be such that $f_k \rightarrow f$ in $L^2(\mathbb{R}^2)^2$ as $k \rightarrow \infty$. By Lemma A.1, there exists a unique solution $\rho_k \in H^1(\mathbb{R}^2)$ to

$$-\Delta\rho_k + \tau^{-1}\rho_k = \tau^{-1}g - \operatorname{div} f_k, \quad (\text{A.5})$$

and, by the variation-of-constants formula and integration by parts,

$$\rho_k(x) = \frac{1}{\tau} (B_{1/\tau} * g)(x) - \int_{\mathbb{R}^2} (\nabla B_{1/\tau})(x - y) \cdot f_k(y) dy. \quad (\text{A.6})$$

Taking the test function $\rho_k - \rho_\ell$ in the difference of the weak formulations for ρ_k, ρ_ℓ corresponding to f_k, f_ℓ , respectively, it follows that

$$\begin{aligned} \|\nabla(\rho_k - \rho_\ell)\|_{L^2(\mathbb{R}^2)}^2 + \frac{1}{\tau} \|\rho_k - \rho_\ell\|_{L^2(\mathbb{R}^2)}^2 &= \int_{\mathbb{R}^2} (f_k - f_\ell) \cdot \nabla(\rho_k - \rho_\ell) dx \\ &\leq \frac{1}{2} \|f_k - f_\ell\|_{L^2(\mathbb{R}^2)}^2 + \frac{1}{2} \|\nabla(\rho_k - \rho_\ell)\|_{L^2(\mathbb{R}^2)}^2. \end{aligned}$$

Since (f_k) is a Cauchy sequence, (ρ_k) is a Cauchy sequence in $H^1(\mathbb{R}^2)$ and hence there exists a $\tilde{\rho} \in H^1(\mathbb{R}^2)$, such that $\rho_k \rightarrow \tilde{\rho}$ strongly in $H^1(\mathbb{R}^2)$ as $k \rightarrow \infty$. Therefore, we can perform the limit $k \rightarrow \infty$ in the weak formulation of (A.5) leading to (A.3).

It remains to show (A.4). Let $\rho = (1/\tau)B_{1/\tau} * g - \nabla B_{1/\tau} * f$.

Then, by Lemma A.2 and (A.6),

$$\begin{aligned}\|\tilde{\rho} - \rho\|_{L^2(\mathbb{R}^2)} &\leq \|\tilde{\rho} - \rho_k\|_{L^2(\mathbb{R}^2)} + \|\rho_k - \rho\|_{L^2(\mathbb{R}^2)} \\ &\leq \|\tilde{\rho} - \rho_k\|_{L^2(\mathbb{R}^2)} + \|\nabla B_{1/\tau}\|_{L^2(\mathbb{R}^2)} \|f_k - f\|_{L^2(\mathbb{R}^2)}.\end{aligned}$$

The right-hand side can be made arbitrarily small by choosing k sufficiently large. This shows that $\tilde{\rho} = \rho$ in \mathbb{R}^2 . \square

Lemma A.4. *Let $\Omega \subset \mathbb{R}^d$ be a open and bounded set with $\partial\Omega \in C^{0,1}$. Then there exists an orthonormal basis $(v_n)_{n \geq 1}$ of $L^2(\Omega)$ with $v_n \in H^1(\Omega) \cap C^\infty(\Omega)$.*

Proof. Let $f \in L^2(\Omega)$ and define the solution operator $K : L^2(\Omega) \rightarrow L^2(\Omega)$ by $Kf = u$, with $u \in H^1(\Omega)$ the unique solution to the elliptic problem

$$\int_{\Omega} \nabla u \cdot \nabla \varphi dx + \int_{\Omega} u \varphi dx = \int_{\Omega} f \varphi dx \quad \text{for all } \varphi \in H^1(\Omega).$$

We claim that K is a compact, positive and self-adjoint operator. The first property follows by Rellich-Kondrachov, i.e. by the compact embedding $H^1(\Omega) \hookrightarrow L^2(\Omega)$. Positivity of K is straight forward, since for $f \in L^2(\Omega)$ and $Kf = u$, we have

$$(Kf, f)_{L^2(\Omega)} = (u, f)_{L^2(\Omega)} = \|\nabla u\|_{L^2(\Omega)}^2 + \|u\|_{L^2(\Omega)}^2 \geq 0.$$

Furthermore, we have for $Kf = u_1$ and $Kg = u_2$, $f, g \in L^2(\Omega)$,

$$\int_{\Omega} \nabla u_1 \nabla u_2 dx + \int_{\Omega} u_1 u_2 dx = \int_{\Omega} f u_2 dx = \int_{\Omega} g u_1 dx.$$

Thus, K is self-adjoint and the spectral theorem for compact symmetric operators, see e.g. [37][Chapter 2, Section 5], implies the existence of a Hilbert basis $(v_n)_{n \geq 1}$ of $L^2(\Omega)$ consisting of eigenfunctions of K . Since K is positive and injective, we conclude that the corresponding sequence of eigenvalues $(\mu_n)_{n \geq 1}$ are strictly positive. Let $v_n \in H^1(\Omega)$ be an eigenvector for the eigenvalue μ_n , then we have

$$\int_{\Omega} \nabla v_n \cdot \nabla \varphi dx + \int_{\Omega} v_n \varphi dx = \int_{\Omega} \frac{1}{\mu_n} v_n \varphi dx \quad \text{for all } \varphi \in H^1(\Omega).$$

Hence, by interior elliptic regularity, see [51][Subsection 6.3.1] and bootstrapping we have $v_n \in H_{\text{loc}}^m(\Omega)$ for every $m \geq 1$ and the standard Sobolev embedding implies $v_n \in C^\infty(\Omega)$. \square



Die approbierte gedruckte Originalversion dieser Dissertation ist an der TU Wien Bibliothek verfügbar.
The approved original version of this doctoral thesis is available in print at TU Wien Bibliothek.

B Appendix: A Nonlinear Gronwall Inequality

Lemma B.1 (Inequalities). *Let $d \leq 3$, $\Omega \subset \mathbb{R}^d$ be a bounded domain, and $\partial\Omega \in C^{2,1}$. There exists a constant $C > 0$ such that for all $u, v \in H^1(\Omega)$,*

$$\|uv\|_{L^2(\Omega)} \leq C\|u\|_{H^1(\Omega)}\|v\|_{H^1(\Omega)}, \quad (\text{B.1})$$

for all $u \in H^2(\Omega)$ with $\nabla u \cdot \nu = 0$ on $\partial\Omega$,

$$\|u\|_{H^2(\Omega)}^2 \leq C(\|\Delta u\|_{L^2(\Omega)}^2 + \|u\|_{L^2(\Omega)}^2), \quad (\text{B.2})$$

and for all $u \in H^3(\Omega)$ with $\nabla u \cdot \nu = 0$ on $\partial\Omega$,

$$\|u\|_{H^3(\Omega)}^2 \leq C(\|\nabla \Delta u\|_{L^2(\Omega)}^2 + \|u\|_{H^2(\Omega)}^2). \quad (\text{B.3})$$

Inequality (B.1) follows after applying the Cauchy–Schwarz inequality and then the continuous embedding $H^1(\Omega) \hookrightarrow L^4(\Omega)$; (B.2) is proved in [66, Theorem 2.3.3.6], while (B.3) is a consequence of [140, Theorem 2.24].

Lemma B.2 (Nonlinear Gronwall inequality). *Let $\delta > 0$ and $\Gamma, G \in C^0([0, T])$ be nonnegative functions, possibly depending on δ , satisfying*

$$\begin{aligned} \Gamma(t) + C_0 \int_0^t G(s) ds &\leq C_1 \Gamma(0) + C_2 \int_0^t (\Gamma(s) + \Gamma(s)^\alpha) ds \\ &\quad + C_3 \delta^\beta \int_0^t (\Gamma(s) + \Gamma(s)^\gamma) G(s) ds + C_4 \delta^\nu, \end{aligned}$$

where $\alpha > 1$, $\beta \geq 0$, $\gamma > 0$, $\nu > 0$, and $C_0, \dots, C_4 > 0$ are constants independent of δ . Furthermore, let $\Gamma(0) \leq C_5 \delta^\nu$ for some $C_5 > 0$. Then there exists $\delta_0 > 0$ such that for all $0 < \delta < \delta_0$, $0 \leq t \leq T$, and $0 < \varepsilon < \nu$,

$$\Gamma(t) \leq C_5 \delta^{\nu-\varepsilon}.$$

Proof. A slightly simpler variant of the lemma was proved in [77, Lemma 10]. Assume, by contradiction, that for all $\delta_0 \in (0, 1)$, there exist $\delta \in (0, \delta_0)$, $t_0 \in [0, T]$, and $\varepsilon \in (0, \nu)$ such that $\Gamma(t_0) > C_5 \delta^{\nu-\varepsilon}$. Since $\Gamma(0) \leq C_5 \delta^\nu$ by assumption and Γ is

B Appendix: A Nonlinear Gronwall Inequality

continuous, there exists $t_1 \in [0, t_0]$ such that $\Gamma(t_1) = C_5\delta^{\nu-\varepsilon}$ and $\Gamma(t) \leq C_5\delta^{\nu-\varepsilon}$ for all $t \in [0, t_1]$. This leads for $t \in [0, t_1]$ to

$$\begin{aligned} \Gamma(t) + C_0 \int_0^t G(s)ds &\leq C_1C_5\delta^\nu + C_2(1 + (C_5\delta^{\nu-\varepsilon})^{\alpha-1}) \int_0^t \Gamma(s)ds \\ &\quad + C_3\delta^\beta (C_5\delta^{\nu-\varepsilon} + (C_5\delta^{\nu-\varepsilon})^\gamma) \int_0^t G(s)ds + C_4\delta^\nu. \end{aligned}$$

Since $\nu - \varepsilon > 0$, the integral over $G(s)$ on the right-hand side can be absorbed for sufficiently small $\delta > 0$ by the corresponding term on the left-hand side. This implies that

$$\Gamma(t) \leq (C_1C_5 + C_4)\delta^\nu + 2C_2 \int_0^t \Gamma(s)ds, \quad 0 \leq t \leq t_1.$$

Then Gronwall's lemma gives, for sufficiently small $\delta_0 > 0$ and $0 < \delta < \delta_0$,

$$\Gamma(t) \leq (C_1C_5 + C_4)\delta^\nu e^{2C_2T} \leq \frac{C_5}{2}\delta^{\nu-\varepsilon} < C_5\delta^{\nu-\varepsilon}, \quad 0 \leq t \leq t_1.$$

which contradicts $\Gamma(t_1) = C_5\delta^{\nu-\varepsilon}$. □

Bibliography

- [1] M. Akhmouch and M. Amine. A time semi-exponentially fitted scheme for chemotaxis-growth models. *Calcolo* 54 (2017), 609–641.
- [2] H. Amann. Nonhomogeneous linear and quasilinear elliptic and parabolic boundary value problems. In: H. J. Schmeisser and H. Triebel (eds), *Function Spaces, Differential Operators and Nonlinear Analysis*, pp. 9–126. Teubner, Stuttgart, 1993.
- [3] D. Bartolucci and D. Castorina. A global existence result for a Keller–Segel type system with supercritical initial data. *J. Ellipt. Parabol. Eqs.* 1 (2015), 243–262.
- [4] N. Bellomo, A. Bellouquid, Y. Tao, and M. Winkler. Toward a mathematical theory of Keller–Segel models of pattern formation in biological tissues. *Math. Models Meth. Appl. Sci.* 25 (2015), 1663–1763.
- [5] M. Bessemoulin-Chatard and A. Jüngel. A finite volume scheme for a Keller–Segel model with additional cross-diffusion. *IMA J. Numer. Anal.* 34 (2014), 96–122.
- [6] A. Blanchet. On the parabolic-elliptic Patlak–Keller–Segel system in dimension 2 and higher. *Séminaire L. Schwartz – EDP Appl.* 8 (2011–2012), 26 pages.
- [7] A. Blanchet. A gradient flow approach to the Keller–Segel systems. *RIMS Kokyuroku’s lecture note* vol. 1837 (2013), 52–73.
- [8] A. Blanchet, V. Calvez, and J. A. Carrillo. Convergence of the mass-transport steepest descent scheme for the subcritical Patlak–Keller–Segel model. *SIAM J. Numer. Anal.* 46 (2008), 691–721.
- [9] A. Blanchet, J. A. Carrillo, and N. Masmoudi. Infinite time aggregation for the critical Patlak–Keller–Segel model in \mathbb{R}^2 . *Commun. Pure Appl. Math.* 61 (2008), 1449–1481.
- [10] A. Blanchet, J. Dolbeault, and B. Perthame. Two-dimensional Keller–Segel model: Optimal critical mass and qualitative properties of the solutions. *Electr. J. Diff. Eqs.* 2006 (2006), article 44, 32 pages.

- [11] C. Bolley and M. Crouzeix. Conservation de la positivité lors de la discrétisation des problèmes d'évolution paraboliques. *RAIRO Anal. Numér.* 12 (1979), 237–245.
- [12] A. Bonami, D. Hilhorst, E. Logak, and M. Mimura. A free boundary problem arising in a chemotaxis model. In: *Free Boundary Problems, Theory and Applications (Zakopane, 1995)*. *Pitman Res. Notes Math. Ser.* 363, pp. 363–373. Longman, Harlow, 1996.
- [13] L. Bonaventura and A. Della Rocca. Unconditionally strong stability preserving extensions of the TR-BDF2 method. *J. Sci. Comput.* 70 (2017), 859–895.
- [14] F. Bonizzoni, M. Braukhoff, A. Jüngel, and I. Perugia. A structure-preserving discontinuous Galerkin scheme for the Fisher-KPP equation. Submitted for publication, 2019.
- [15] D. Bothe. On the Maxwell-Stefan equations to multicomponent diffusion. In: J. Escher et al. (eds). *Parabolic Problems. Progress in Nonlinear Differential Equations and their Applications*, pp. 81–93. Springer, Basel, 2011.
- [16] D. Bothe and W. Dreyer. Continuum thermodynamics of chemically reacting fluid mixtures. *Acta Mech.* 226 (2015), 1757–1805.
- [17] L. Boudin, B. Grec, and F. Salvarani. A mathematical and numerical analysis of the Maxwell–Stefan diffusion equations. *Discrete Cont. Dyn. Sys. B* 17 (2012), 1427–1440.
- [18] L. Boudin, B. Grec, M. Pavić, and F. Salvarani. Diffusion asymptotics of a kinetic model for gaseous mixtures. *Kinetic Related Models* 6 (2013), 137–157.
- [19] C. Budd, R. Carretero-González, and R. Russell. Precise computations of chemotactic collapse using moving mesh methods. *J. Comput. Phys.* 202 (2005), 463–487.
- [20] M. Burger, M. Di Francesco, and Y. Dolak-Struss. The Keller-Segel model for chemotaxis with prevention of overcrowding: linear vs. nonlinear diffusion. *SIAM J. Math. Anal.* 38 (2006), 1288–1315.
- [21] M. Burger, B. Schlake, and M.-T. Wolfram. Nonlinear Poisson-Nernst-Planck equations for ion flux through confined geometries. *Nonlinearity* 25 (2012), 961–990.
- [22] V. Calvez and L. Corrias. The parabolic-parabolic Keller–Segel model in \mathbb{R}^2 . *Commun. Math. Sci.* 6 (1008), 417–447.

- [23] V. Calvez, L. Corrias, and M. A. Ebde. Blow-up, concentration phenomena and global existence for the Keller-Segel model in high dimensions. *Commun. Partial Diff. Eqs.* 37 (2012), 561–584.
- [24] C. Cancès, F. Nabet, and M. Vohralik. Convergence and a posteriori error analysis for energy-stable finite element approximations of degenerate parabolic equations. Preprint, 2018. hal-01894884.
- [25] B. Carnes and G. Carey. Local boundary value problems for the error in FE approximation of non-linear diffusion systems. *Intern. J. Numer. Meth. Engrg.* 73 (2008), 665–684.
- [26] J. A. Carrillo, H. Ranetbauer, and M.-T. Wolfram. Numerical simulation of continuity equations by evolving diffeomorphisms. *J. Comput. Phys.* 327 (2016), 186–202.
- [27] J. A. Carrillo, N. Kolbe and M. Lukáčová-Medvidová. A hybrid mass transport finite element method for Keller-Segel type systems. *arXiv preprint arXiv:1709.07394* (2017).
- [28] J. A. Carrillo, S. Hittmeir, and A. Jüngel. Cross diffusion and nonlinear diffusion preventing blow up in the Keller–Segel model. *Math. Models Meth. Appl. Sci.* 22 (2012), 1250041, 35 pages.
- [29] M. Chapwanya, J. Lubuma, and R. Mickens. Positivity-preserving nonstandard finite difference schemes for cross-diffusion equations in biosciences. *Comput. Math. Appl.* 68 (2014), 1071–1082.
- [30] P. Chatzipantelidis, Z. Horváth, and V. Thomée. On preservation of positivity in some finite element methods for the heat equation. *Comput. Meth. Appl. Math.* 15 (2015), 417–437.
- [31] X. Chen and A. Jüngel. Analysis of an incompressible Navier–Stokes–Maxwell–Stefan system. *Commun. Math. Phys.* 340 (2015), 471–497.
- [32] A. Chertock and A. Kurganov. A second-order positivity preserving central-upwind scheme for chemotaxis and haptotaxis models. *Numer. Math.* 111 (2008), 169–205.
- [33] A. Chertock, Y. Epshteyn, H. Hu, and A. Kurganov. High-order positivity-preserving hybrid finite-volume finite-difference methods for chemotaxis systems. *Adv. Comput. Math.*, (2017), online first. DOI: <https://doi.org/10.1007/s10444-017-9545-9>.
- [34] Y. Choi and Z. Wang. Prevention of blow-up by fast diffusion in chemotaxis. *Journal of Mathematical Analysis and Applications* 362, no. 2, (2010), 553–564.

- [35] S. Christiansen, H. Munthe-Kaas and B. Owren. Topics in structure-preserving discretization. *Acta Numerica* 20 (2011), 1–119.
- [36] T. Cieřlak, Tomasz, and C. Stinner. Finite-time blowup and global-in-time unbounded solutions to a parabolic–parabolic quasilinear Keller–Segel system in higher dimensions. *Journal of Differential Equations* 252, no. 10, (2012), 5832–5851.
- [37] J. B. Conway. A course in functional analysis, Graduate Texts in Mathematics 96, Springer, 1990.
- [38] L. Corrias, B. Perthame, and H. Zaag. Global solutions of some chemotaxis and angiogenesis systems in high space dimensions. *Milan J. Math.* 72 (2004), 1–28.
- [39] E. Daus, A. Jünger, and B.-Q. Tang. Exponential time decay of solutions to reaction-cross-diffusion systems of Maxwell–Stefan type. Submitted for publication, 2018. arXiv:1802.10274.
- [40] S. Dejak, D. Egli, P. Lushnikov, and I. Sigal. On blowup dynamics in the Keller–Segel model of chemotaxis. *Algebra i Analiz* 25 (2013), 47–84; translation in *St. Petersburg Math. J.* 25 (2014), 547–574.
- [41] L. Desvillettes, K. Fellner, M. Pierre, and J. Vovelle. Global existence for quadratic systems of reaction-diffusion. *Adv. Nonlin. Stud.* 7 (2007), 491–511.
- [42] M. Di Francesco and J. Rosado. Fully parabolic Keller–Segel model for chemotaxis with prevention of overcrowding. *Nonlinearity* 21 (2008), 2715–2730.
- [43] K. Dieter-Kisling, H. Marschall, and D. Bothe. Numerical method for coupled interfacial surfactant transport on dynamic surface meshes of general topology. *Computers & Fluids* 109 (2015), 168–184.
- [44] M. Dreher and A. Jünger. Compact families of piecewise constant functions in $L^p(0, T; B)$. *Nonlin. Anal.* 75 (2012), 3072–3077.
- [45] W. Dreyer, P.-E. Druet, P. Gajewski, and C. Gohlke. Analysis of improved Nernst–Planck–Poisson models of compressible isothermal electrolytes. Part I: Derivation of the model and survey of the results. WIAS Berlin, Germany, preprint no. 2395, 2017.
- [46] W. Dreyer, C. Gohlke, and R. Müller. Overcoming the shortcomings of the Nernst–Planck–Poisson model. *Phys. Chem. Chem. Phys.* 15 (2013), 7075–7086.
- [47] J. Duncan and H. Toor. An experimental study of three component gas diffusion. *AIChE J.* 8 (1962), 38–41.

- [48] H. Egger. Structure preserving approximation of dissipative evolution problems. *arXiv preprint arXiv:1804.08648* (2018).
- [49] T. W. Engelmann. Neue Methode zur Untersuchung der Sauerstoffausscheidung pflanzlicher und thierischer Organismen. *Pfl. Arch. Ges. Physiol. Mens. Tiere* 25 (1881), 285–292.
- [50] Y. Epshtyn. Discontinuous Galerkin methods for the chemotaxis and haptotaxis models. *J. Comput. Appl. Math.* 224 (2009), 168–181.
- [51] L. C. Evans. *Partial Differential Equations*. Graduate studies in mathematics Volume 19, American Mathematical Society, 1998.
- [52] M. A. Farina, M. Marras, and G. Vigliani. On explicit lower bounds and blow-up times in a model of chemotaxis. *Dyn. Sys., Diff. Eqs. and Appl., AIMS Proceedings* (2015), 409–417.
- [53] F. Filbet. A finite volume scheme for the Patlak-Keller-Segel chemotaxis model. *Numer. Math.* 104 (2006), 457–488.
- [54] A. Friedman. *Partial Differential Equations*. Dover, Mineola, 2008.
- [55] D. Furihata and T. Matsuo. *Discrete variational derivative method: a structure-preserving numerical method for partial differential equations*. Chapman and Hall/CRC, 2010.
- [56] S. Gadau and A. Jüngel. A three-dimensional mixed finite-element approximation of the semiconductor energy-transport equations. *SIAM J. Sci. Comput.* 31 (2008), 1120–1140.
- [57] H. Gajewski. On a variant of monotonicity and its application to differential equations. *Nonlinear Analysis: Theory, Methods and Applications* 22, no. 1, (1994): 73–80.
- [58] V. Galkin and N. Makashev. Modification of the first approximation of the Chapman-Enskog method for a gas mixture. *Fluid Dynam.* 27 (1993), 590–596. Translated from *em Izv. Ross. Akad. Nauk Mekh. Zhidk. Gaza* 4 (1992), 178–185 (Russian).
- [59] P. Gaudet et al. An Anatomy Ontology to Represent Biological Knowledge in Dictyostelium Discoideum. *BMC Genomics* 9 (2008), 130.
- [60] J. Geiser. Iterative solvers for the Maxwell-Stefan diffusion equations: Methods and applications in plasma and particle transport. *Cogent Math.* 2 (2015), 1092913, 16 pages.

- [61] A. Gerstenmayer and A. Jüngel. Analysis of a degenerate parabolic cross-diffusion system for ion transport. *J. Math. Anal. Appl.* 461 (2018), 523–543.
- [62] V. Giovangigli. *Multicomponent Flow Modeling*. Birkhäuser, Basel, 1999.
- [63] V. Giovangigli and M. Massot. The local Cauchy problem for multicomponent flows in full vibrational non-equilibrium. *Math. Meth. Appl. Sci.* 21 (1998), 1415–1439.
- [64] S. Gottlieb, C.-W. Shu, and E. Tadmor. Strong stability-preserving high-order time discretization methods. *SIAM Review* 43 (2001), 89–112.
- [65] E. E. Graham and J. S. Dranoff. Application of the Stefan-Maxwell equations to diffusion in ion exchangers. 1. Theory. *Industrial and Engineering Chemistry Fundamentals* 21 (4) (1982), 360–365.
- [66] P. Grisvard. *Elliptic Problems in Nonsmooth Domains*. Pitman, Boston, 1985.
- [67] L. Guo, X. H. Li and Y. Yang. Energy Dissipative Local Discontinuous Galerkin Methods for Keller–Segel Chemotaxis Model. *Journal of Scientific Computing* 78(3) (2019), 1387–1404.
- [68] A. Gurusamy and K. Balachandran. Finite element method for solving Keller–Segel chemotaxis system with cross-diffusion. *International Journal of Dynamics and Control* 6(2) (2019), 539–549.
- [69] E. Hairer, C. Lubich and G. Wanner. *Geometric Numerical Integration*. Springer-Verlag, Heidelberg, 2002.
- [70] J. Haskovec and C. Schmeiser. Stochastic particle approximation for measure valued solutions of the 2D Keller-Segel system. *J. Stat. Phys.* 135 (2009), 133–151.
- [71] M. Herberg, M. Meyries, J. Prüss, and M. Wilke. Reaction-diffusion systems of Maxwell–Stefan type with reversible mass-action kinetics. *Nonlin. Anal.* 159 (2017), 264–284.
- [72] M. A. Herrero and J. J. L. Velázquez. Singularity patterns in a chemotaxis model. *Math. Ann.* 306 (1996), 583–623.
- [73] T. Hillen and K. Painter. A user’s guide to PDE models for chemotaxis. *Journal of mathematical biology* 58, no. 1-2 (2009), 183.
- [74] T. Hillen, K. Painter, and C. Schmeiser. Global existence for chemotaxis with finite sampling radius. *Discrete Contin. Dyn. Sys.* 7 (2007), 125–144.

- [75] S. Hittmeir and A. Jüngel. Cross diffusion preventing blow up in the two-dimensional Keller–Segel model. *SIAM J. Math. Anal.* 43 (2011), 997–1022.
- [76] D. Horstmann. From 1970 until present: the Keller–Segel model in chemotaxis and its consequences I. *Jahresberichte der DMW* 105 (2003), 103–165.
- [77] L. Hsiao and S. Wang. Quasineutral limit of a time-dependent drift-diffusion–Poisson model for p-n junction semiconductor devices. *J. Diff. Eqs.* 225 (2006), 411–439.
- [78] J. Hunter. Matplotlib: A 2D graphics environment. *Comput. Sci. Engin.* 9 (2007), 90–95.
- [79] H. Hutridurga and F. Salvarani. Maxwell–Stefan diffusion asymptotics for gas mixtures in non-isothermal setting. *Nonlin. Anal.* 159 (2017), 285–297.
- [80] H. Hutridurga and F. Salvarani. Existence and uniqueness analysis of a non-isothermal cross-diffusion system of Maxwell–Stefan type. *Appl. Math. Lett.* 75 (2018), 108–113.
- [81] S. Ishida and T. Yokota. Global existence of weak solutions to quasilinear degenerate Keller–Segel systems of parabolic–parabolic type. *Journal of Differential Equations* 252, no. 2, (2012), 1421–1440.
- [82] W. Jäger and S. Luckhaus. On explosions of solutions to a system of partial differential equations modelling chemotaxis. *Transactions of the american mathematical society* 329(2) (1992), 819–824.
- [83] A. Jüngel. The boundedness-by-entropy method for cross-diffusion systems. *Nonlinearity* 28 (2015), 1963–2001.
- [84] A. Jüngel. *Entropy Methods for Diffusive Partial Differential Equations*. SpringerBriefs in Mathematics, Springer, 2016.
- [85] A. Jüngel. Cross-diffusion systems with entropy structure. In: K. Mikula, D. Ševčovič, and J. Urbán (eds.), *Proceedings of Equadiff 2017 Conference*, pp. 181–190. Spektrum Stu Publishing, Bratislava, 2017.
- [86] A. Jüngel and O. Leingang. Blow-up of solutions to semi-discrete parabolic-elliptic Keller–Segel models. *Discrete and Continuous Dynamical Systems - B* 24(9) (2019), 4755–4782.
- [87] A. Jüngel and O. Leingang. Convergence of an implicit Euler Galerkin scheme for Poisson–Maxwell–Stefan systems. *Advances in Computational Mathematics*, (2019), 1469–1498.

- [88] A. Jüngel, O. Leingang and S. Wang. Vanishing cross-diffusion limit in a Keller–Segel system with additional cross-diffusion. Submitted for publication, 2019. arXiv:1907.11387.
- [89] A. Jüngel and J.-P. Milišić. Entropy dissipative one-leg multistep time approximations of nonlinear diffusive equations. *Numer. Meth. Partial Diff. Eqs.* 31 (2015), 1119–1149.
- [90] A. Jüngel and S. Schuchnigg. A discrete Bakry-Emery method and its application to the porous-medium equation. *Discrete Cont. Dyn. Sys.* 37 (2017), 5541–5560.
- [91] A. Jüngel and S. Schuchnigg. Entropy-dissipating semi-discrete Runge-Kutta schemes for nonlinear diffusion equations. *Commun. Math. Sci.* 15 (2017), 27–53.
- [92] A. Jüngel and I. Stelzer. Entropy structure of a cross-diffusion tumor-growth model. *Math. Models Meth. Appl. Sci.* 22 (2012), 1250009, 26 pages.
- [93] A. Jüngel and I. Stelzer. Existence analysis of Maxwell-Stefan systems for multicomponent mixtures. *SIAM J. Math. Anal.* 45 (2013), 2421–2440.
- [94] N. I. Kavallaris and T. Suzuki. Non-local partial differential equations for engineering and biology. *Mathematical modeling and analysis* 31, Springer, 2018.
- [95] E. Keller and L. Segel. Initiation of slime mold aggregation viewed as an instability. *J. Theor. Biol.* 26 (1970), 399–415.
- [96] D. Ketcheson. Step sizes for strong stability preservation with downwind-biased operators. *SIAM J. Numer. Anal.* 49 (2011), 1649–1660.
- [97] R. Kowalczyk. Preventing blow-up in a chemotaxis model. *Journal of Mathematical Analysis and Applications* 305.2 (2005), 566–588.
- [98] H. Kozono and Y. Sugiyama. Local existence and finite time blow-up in the 2-D Keller-Segel system. *J. Evol. Eqs.* 8 (2008), 353–378.
- [99] R. Krishna. Diffusing uphill with James Clerk Maxwell and Josef Stefan. *Chemical Engineering Science Volume* 195 (2019), 851–880.
- [100] N. Krylov. *Lectures on Elliptic and Parabolic Equations in Sobolev Spaces.* Amer. Math. Soc., Providence, Rhode Island, USA, 2008.
- [101] J. Lankeit. Locally bounded global solutions to a chemotaxis consumption model with singular sensitivity and nonlinear diffusion. *J. Diff. Eqs.* 262 (2017), 4052–4084.

- [102] E. Leonardia and C. Angeli. On the Maxwell–Stefan approach to diffusion: a general resolution in the transient regime for one-dimensional systems. *J. Phys. Chem. B* 114 (2010), 151–164.
- [103] D.M. Liu and Y.S. Tao. Boundedness in a chemotaxis system with nonlinear signal production. *Applied Mathematics-A Journal of Chinese Universities* 31.4 (2016), 379–388.
- [104] J. G. Liu, L. Wang and Z. Zhou. Positivity-preserving and asymptotic preserving method for 2D Keller-Segal equations. *Mathematics of Computation* 87(311) (2018), 1165–1189.
- [105] J.-P. Loos, P. Verheijen, and J. Moulin. Numerical simulation of the generalized Maxwell–Stefan model for multicomponent diffusion in microporous sorbents. *Collect. Czech. Chem. Commun.* 57 (1992), 687–697.
- [106] A. Lunardi. *Analytic Semigroups and Optimal Regularity in Parabolic Problems*. Springer, Basel, 1995.
- [107] M. Marion and R. Temam. Global existence for fully nonlinear reaction-diffusion systems describing multicomponent reactive flows. *J. Math. Pures Appl.* 104 (2015), 102–138.
- [108] C. Maxwell. On the dynamical theory of gases. *Phil. Trans. Roy. Soc. London* 157 (1866), 49–88.
- [109] M. McLeod and Y. Bourgault. Mixed finite element methods for addressing multi-species diffusion using the Maxwell-Stefan equations. *Comput. Meth. Appl. Mech. Engrg.* 279 (2014), 515–535.
- [110] J. D. Murray. *Mathematical Biology I: An Introduction*, volume I. Springer, 2003.
- [111] T. Nagai. Blowup of nonradial solutions to parabolic-elliptic systems modeling chemotaxis in two-dimensional domains. *Journal of Inequalities and Applications* no. 1, (2001), 970292.
- [112] E. Nakaguchi and A. Yagi. Fully discrete approximation by Galerkin Runge-Kutta methods for quasilinear parabolic systems. *Hokkaido Math. J.* 31 (2002), 385–429.
- [113] W. Nernst. Die elektromotorische Wirksamkeit der Ionen. *Z. Physikalische Chemie* 4 (1889), 129–181.

- [114] K. J. Painter. Mathematical models for chemotaxis and their applications in self-organisation phenomena. *Journal of Theoretical Biology* (2018), <https://doi.org/10.1016/j.jtbi.2018.06.019>
- [115] C. Patlak. Random walk with persistence and external bias. *Bull. Math. Biophys.* 15 (1953), 311–338.
- [116] K. Peerenboom, J. van Dijk, J. Boonkkamp, L. Liu, W. Goedheer, and J. van der Mullen. Mass conservative finite volume discretization of the continuity equations in multi-component mixtures. *J. Comput. Phys.* 230 (2011), 3525–3537.
- [117] B. Perthame. *Transport Equations in Biology*. Birkhäuser, Basel, 2007.
- [118] B. Perthame, N. Vauchelet and Z. Wang. The flux limited Keller–Segel system; properties and derivation from kinetic equations. arXiv preprint arXiv:1801.07062 (2018).
- [119] W. F. Pfeffer. Locomotorische Richtungsbewegungen durch chemische Reize. *Unters. Bot. Inst. Tübingen* 1 (1884), 363–482.
- [120] M. Planck. Über die Potentialdifferenz zwischen zwei verdünnten Lösungen binärer Electrolyte. *Annalen der Physik* 276 (1890), 561–576.
- [121] S. Psaltis and T. Farrell. Comparing charge transport predictions for a ternary electrolyte using the Maxwell–Stefan and Nernst–Planck equations. *J. Electrochem. Soc.* 158 (2011), A33–A42.
- [122] N. Saito. Conservative upwind finite-element method for a simplified Keller–Segel system modelling chemotaxis. *IMA J. Numer. Anal.* 27 (2007), 332–365.
- [123] N. Saito. Conservative numerical schemes for the Keller–Segel system and numerical results. *RIMS Kôkyûroku Bessatsu* B15 (2009), 125–146.
- [124] N. Saito. Error analysis of a conservative finite-element approximation for the Keller–Segel system of chemotaxis. *Commun. Pure Appl. Anal.* 11 (2012), 339–364.
- [125] N. Saito and T. Suzuki. Notes on finite difference schemes to a parabolic-elliptic system modelling chemotaxis. *Appl. Math. Comput.* 171 (2005), 72–90.
- [126] F. Salvarani and J. Soares. On the relaxation of the Maxwell–Stefan system to linear diffusion. Submitted for publication, 2018. hal-01791067.
- [127] J. Schöberl. NETGEN – An advancing front 2D/3D-mesh generator based on abstract rules. *Comput. Visual. Sci.* 1 (1997), 41–52.

- [128] J. Schöberl. C++11 Implementation of Finite Elements in NGSolve. Preprint, 2014. Available at <https://www.asc.tuwien.ac.at/~schoeberl/wiki/publications/ngs-cpp11.pdf>
- [129] T. Senba and T. Suzuki. Parabolic system of chemotaxis: blowup in a finite and the infinite time. *Meth. Appl. Anal.* 8 (2001), 349–368.
- [130] J. Simon. Compact sets in the space $L^p(0, T; B)$. *Ann. Math. Pura. Appl.* 146 (1987), 65–96.
- [131] M. Smiley. A monotone conservative Eulerian-Lagrangian scheme for reaction-diffusion-convection equations modeling chemotaxis. *Numer. Meth. Partial Diff. Eqs.* 23 (2007), 553–586.
- [132] M. N. Spijker. Contractivity in the numerical solution of initial value problems. *Numer. Math.* 42 (1983), 271–290.
- [133] M. Sulman and T. Nguyen. A Positivity Preserving Moving Mesh Finite Element Method for the Keller–Segel Chemotaxis Model. *Journal of Scientific Computing* 80(1) (2019), 649–666.
- [134] J. Stefan. Über das Gleichgewicht und Bewegung, insbesondere die Diffusion von Gasgemengen. *Sitzungsberichte Kaiserl. Akad. Wiss. Wien* 63 (1871), 63–124.
- [135] A. Stevens. The derivation of chemotaxis equations as limit dynamics of moderately interacting stochastic many-particle systems. *SIAM Journal on Applied Mathematics* 61, no. 1, (2000), 183–212.
- [136] R. Strehl, A. Sokolov, D. Kuzmin, and S. Turek. A flux-corrected finite element method for chemotaxis problems. *Comput. Meth. Appl. Math.* 10 (2010), 219–232.
- [137] R. Strehl, A. Sokolov, D. Kuzmin, D. Horstmann, and S. Turek. A positivity-preserving finite element method for chemotaxis problems in 3D. *J. Comput. Appl. Math.* 239 (2013), 290–303.
- [138] T. Suzuki. *Free Energy and Self-Interacting Particles*. Birkhäuser, Boston, 2005.
- [139] T. Tao. Nonlinear dispersive equations: local and global analysis. American Mathematical Soc. No. 106, 2006.
- [140] G. M. Troianiello. *Elliptic Differential Equations and Obstacle Problems*. Plenum Press, New York, 1987.

- [141] J. Valenciano and M. Chaplain. Computing highly accurate solutions of a tumour angiogenesis model. *Math. Models Meth. Appl. Sci.* 13 (2003), 747–766.
- [142] V. .K. Vanag and I. R. Epstein. Cross-diffusion and pattern formation in reaction–diffusion systems. *Physical Chemistry Chemical Physics* 11, no. 6, (2009), 897–912.
- [143] J. J. L. Velázquez. Stability of some mechanisms of chemotactic aggregation. *SIAM J. Appl. Math.* 62 (2002), 1581–1633.
- [144] M. Winkler Chemotaxis with logistic source: Very weak solutions and their boundedness properties. *J. Math. Anal. Appl.* 348, (2008), 708–729.
- [145] M. Winkler. Aggregation vs. global diffusive behavior in the higher-dimensional Keller–Segel model. *Journal of Differential Equations* 248, no. 12 (2010), 2889–2905.
- [146] M. Winkler. Finite-time blow-up in the higher-dimensional parabolic–parabolic Keller–Segel system. *Journal de Mathématiques Pures et Appliquées* 100, no. 5, (2013), 748–767.
- [147] M. Winkler. Chemotactic cross-diffusion in complex frameworks. *Mathematical Models and Methods in Applied Sciences* Vol. 26, No. 11, (2016), 2035–2040.
- [148] M. Winkler. A critical blow-up exponent in a chemotaxis system with nonlinear signal production. *Nonlinearity* 31.5 (2018), 2031.
- [149] C. Xue. Bacterial chemotaxis: a classic example of multiscale modeling in biology. In *Cell Movement*, pp. 143–167. Birkhäuser, Cham, 2018.
- [150] R. Zhang, J. Zhu, A. Loula, and X. Yu. Operator splitting combined with positivity-preserving discontinuous Galerkin method for the chemotaxis model. *J. Comput. Appl. Math.* 302 (2016), 312–326.
- [151] P. Zheng, M. Chunlai and H. Xuegang. Boundedness and blow-up for a chemotaxis system with generalized volume-filling effect and logistic source. *Discrete and Continuous Dynamical Systems-A* 35, no. 5, (2015), 2299–2323.
- [152] G. Zhou and N. Saito. Finite volume methods for a Keller–Segel system: discrete energy, error estimates and numerical blow-up analysis. *Numer. Math.* 135 (2017), 265–311.

Curriculum Vitae

Personal Data

Name	Oliver Leingang
Citizenship	Austria
E-Mail	oliver.leingang@tuwien.ac.at

Educational Background

09/2015–current	PhD in Technical Mathematics, TU Wien. Supervisor: Prof. Ansgar Jüngel.
10/2011–04/2015	MSc in Mathematics, University of Vienna. Supervisor: Prof. Christian Schmeiser.
10/2007–09/2011	BSc in Mathematics, University of Vienna. Supervisor: Prof. Gerald Teschl.
2006–2007	Alternative service (ambulance man), Red Cross, Steyr.
2006	Austrian High school Degree (Matura), Business Academy, Steyr.

Professional Experience

2015–current	University assistant, Institute for Analysis and Scientific Computing, TU Wien.
04/2012–09/2013	Advisor for the office of education politics at the Austrian National Union of Students.
03/2010–06/2014	Tutor at the University of Vienna and the TU Wien.
08/2009–09/2013	Student counselor and office worker for the Students representatives of Mathematics, University of Vienna.
08/2008, 07/2009, 08/2010	Vacation replacement, ambulance man/driver and instructor, Red Cross Steyr.

Publications and Preprints

- 2019 A. Jüngel, O. Leingang and S. Wang. Vanishing cross-diffusion limit in a Keller–Segel system with additional cross-diffusion. Submitted for publication, 2019.
- 2018 A. Jüngel and O. Leingang. Convergence of an implicit Euler Galerkin scheme for Poisson–Maxwell–Stefan systems. *Advances in Computational Mathematics*, (2019), 1469–1498.
- 2017 A. Jüngel and O. Leingang. Blow-up of solutions to semi-discrete parabolic-elliptic Keller–Segel models. *Discrete and Continuous Dynamical Systems - B* 24(9) (2019), 4755–4782.
-

Scientific Talks and Posters

- 10/2018 Poster at workshop “Applied Mathematics and Simulation for Semiconductors”, Berlin, Germany.
- 08/2018 Contributed talk at the workshop “Analysis and Advanced Numerical Methods for Partial Differential Equations”, Särkisaari, Finland.
- 08/2017 Contributed talk at Equadiff conference, Bratislava, Slovakia.
-

Teaching Experience

Exercise classes for the following subjects:

03/2019–06/2019	Calculus of variations, TU Wien.
10/2018–01/2019	Mathematics 3 for Electrical Engineering, TU Wien.
03/2018–06/2018	Differential equations 1, TU Wien.
10/2017–01/2018	Partial differential equations, TU Wien.
03/2017–06/2017	Differential equations 1, TU Wien.
10/2016–01/2017	Analysis 3, TU Wien.
03/2016–06/2016	Analysis 2, TU Wien.
10/2015–01/2016	Analysis 1, TU Wien.
03/2014–06/2014	Mathematics for Molecular Biologists, University of Vienna.
10/2011–06/2013	Mathematics for Mechanical Engineering 1 and 2, TU Wien.
03/2010–06/2013	Introduction to Computer Infrastructure, University of Vienna.

Extracurricular Activities

05/2009–05/2013	Student representative at the Faculty of Mathematics, University of Vienna.
05/2009–05/2011	Chairman of the students representatives at the Institute of Mathematics, University of Vienna.
06/2007–02/2011	Volunteer as a ambulance man/driver and instructor, Red Cross Steyr.

Additional Information

- Training in didactics for higher education (“Basisausbildung Lehre”) in the focus:lehre framework of the TU Wien.
- Languages: German (native), English (fluent), Spanish (basic).
- Software proficiency: Python (NGsolve, Tensorflow, OpenCV,...), Matlab, Mathematica, Ruby, Java, L^AT_EX, Linux, Microsoft Office.